From the Max Planck Institute of Psychiatry

Dissertation

zum Erwerb des Doctor of Philosophy (Ph.D.)

an der Medizinischen Fakultät der

Ludwig-Maximilians-Universität zu München

Unravelling the Role of Altered Genes in Human Periventricular Heterotopia

vorgelegt von:

Ane Cristina Ayo Martín

aus:

Bilbao, Baskenland, Spanien

Jahr:

2021

First supervisor: Prof. Dr. Moritz Rossner

Second supervisor: Dr. Silvia Cappello

Dean: Prof. Dr. med. dent. Reinhard Hickel

Datum der Verteidigung: 17. März 2021

A mis padres,

por su apoyo y amor incondicional

TABLE OF CONTENTS

ABSTRACT

The development of the human cortex is a very sophisticated process and any small disturbance will lead to a range of different cortical malformations. There are two main ways to study how the cortex develops. One is by studying different genes, pathways or mechanism that are essential for its correct functioning. The other way is by looking at the genes that are mutated and responsible for different neurodevelopmental disorders.

Using this last approach, we discovered mutations in two genes (*DCHS1* and *FAT4*) that are causative of Van Maldergem Syndrome and its associated phenotype, Periventricular Heterotopia. In these patients, there is a cluster of neurons unable to reach their correct position in the cortex. DCHS1 and FAT4 are two protocadherins that interact with each other and mutations in these proteins or their downregulation induce changes in the number of different types of progenitors in mice and alter neuronal migratory dynamics in humans. Additionally, in human-derived cerebral organoids with mutations in these two genes, there is a cluster of neurons with an altered neuronal state that we believe are the neurons with migratory defects that are not able to reach their correct place in the cortex. This subpopulation of altered neurons contains a different transcriptomic signature, being *GNG5* the most differentially dysregulated gene. Furthermore, those neurons also contain altered genes crucial for proper neuronal migration, axon guidance and synapse formation.

In this thesis, using this knowledge as a starting point, I have investigated different aspects of human cortical development using embryonic mice brains and human-derived cerebral organoids as model systems.

On the one hand, I have proven the importance of GNG5 for the control of the proper number of different types of neural progenitors and correct neuronal migration. *GNG5* is highly upregulated in neural progenitors and is downregulated during neuronal differentiation, however, in the altered cluster of neurons, it is still highly upregulated. Interestingly, the phenotypes observed in mouse and human with mutations in *DCHS1* and *FAT4* or its downregulation are very similar to the phenotypes observed after the overexpression of *GNG5* in those two model systems. The results indicate that GNG5, DCHS1 and FAT4 are part of the same pathway or have a similar role during cortical development.

On the other hand, I have investigated the usefulness of cerebral organoids as a model system to study neuronal activity and functionality. For one of the very first times, we have shown functional differences in a 3D *in vitro* system derived from patient cells. Moreover, I have characterized those aged cerebral organoids and looked at their transcriptomic differences which have given some insights

into the mechanism and pathways that are disrupted and may be responsible for those functional differences.

Finally, I have also investigated the role of DCHS1 in modern human brain development. After the full genome of the Neanderthals was sequenced, it was possible to identify 78 proteins that were different between modern humans and Neanderthals. Remarkably, DCHS1 was one of those proteins where modern humans present a different form, while Neanderthals kept the ancestral one. Preliminary data has shown that this unique amino acid change specific to humans, may have induced an increased number of progenitor cells and may have altered migratory dynamics in the developing modern human brain.

Thanks to these three projects I have investigated some unknown details of human cortical development increasing the comprehension for future treatments. This knowledge will be very useful to improve the quality of life of patients suffering from different types of cortical malformations.

CHAPTER 1: INTRODUCTION

1.1 DEVELOPMENT OF THE CORTEX

The brain is the most complex organ in the human body, yet the least understood. In particular, the cerebral cortex, and more concretely the neocortex, is the most and lastly developed area in the human brain. It is the brain region responsible for higher cognitive abilities. The human cerebral neocortex is the area involved in the integration of sensory and motor information, intelligence, consciousness, decision making and personality. In summary, it makes humans what we are (Diaz and Gleeson, 2009; Pirozzi et al., 2018; Rakic, 2009).

The development of the human cerebral cortex is a very well-structured process, and any small disturbance will lead to a range of different cortical malformations. Tackling the causes of these disorders can help to identify new central players and understand the complexity of human cortex development with a final aim of finding new and better treatments for patients.

1.1.1 How does the cortex develop?

During the very early stages of mammalian embryonic development, three main layers are produced: the *endoderm*, the *mesoderm* and the *ectoderm*. The nervous system will be generated from this last layer. The *ectoderm* will give rise to the neural crest and neural tube. While the neurons that are part of the peripheral nervous system will be generated from the neural crest, the neural tube will produce the entire central nervous system. During the differentiation of the neural tube, three different areas can be distinguished in the very rostral part: the *prosencephalon* also known as the forebrain, the *mesencephalon* or midbrain and the *rhombencephalon* or hindbrain. Once the forebrain continues developing, we start to distinguish different structures in it: the telencephalon, the diencephalon and the optic vesicles. It is the telencephalon that will finally give rise to the two cerebral hemispheres, where the cerebral cortex is found (Bear et al., 2007).

In mammals, the development of the cerebral cortex is a very intricated process that consists mainly of four significant steps: Neurogenesis (Götz and Huttner, 2005), neuronal migration, neuronal differentiation, neuronal maturation and circuit formation (Komuro and Rakic, 1998; Kriegstein et al., 2006; Taverna et al., 2014).

1.1.1.1 Neurogenesis

The term neurogenesis refers to the generation of neurons from neural stem cells (NSCs) and neural progenitor cells (NPCs). There is a wide variety of precursor cells that will give rise to all the neurons populating the cerebral cortex (Götz and Huttner, 2005). In the next pages, I will explain the characteristics of each of these types of progenitor and how they are generated.

Neuroepithelial cells

The neural tube, where the cerebral cortex is generated from, is mainly populated by neuroepithelial cells (NECs). These are stem cells that will continue to divide in a symmetric proliferative way (producing two daughter cells identical to the mother cell) during the early stages of the generation of the embryonic brain, increasing the pool of progenitor cells (Götz and Huttner, 2005; Rakic, 1995). NECs are polarised cells that present epithelial cell features which form a single layer of pseudostratified cells along the neural tube: their nuclei can be apically or basally located (Götz and Huttner, 2005; Rakic, 2009; Wodarz and Huttner, 2003). This structure is generated by the way these cells divide through interkinetic nuclear migration (INM): during mitosis, the cell bodies remain in the apical part of the neural tube, and during the G1-phase the nuclei move towards the basal part. The S-phase occurs in this basal position, and during G2-phase, the nuclei migrate back apically on the neural tube (Sauer, 1935; Taverna and Huttner, 2010). Just before the beginning of neurogenesis, NECs change the way they divide. They will start diving asymmetrically, generating two types of daughter cells: (a) a new NEC or a different kind of progenitor cells such as apical radial glia cells (aRGs) and (b) another type of NPC such as an apical intermediate progenitor (aIP), a subapical progenitor (SAP), a basal progenitor (BP) or a postmitotic neuron (Florio and Huttner, 2014; Götz and Huttner, 2005; Taverna et al., 2014).

Apical radial glial cells

At the start of neurogenesis and with the change to asymmetric division of NECs, these also change their morphology and will give raise to aRGs (Götz and Huttner, 2005; Rakic, 2009). These cells keep their polarity, but their epithelial markers become weaker and acquire astroglial markers such as GFAP (glial fibrillary acidic protein) in humans, GLAST (astrocyte-specific glutamate transporter), or BLBP (brain-lipid-binding protein) (Campbell and Götz, 2002; Götz and Huttner, 2005). They also upregulate transcription factors such as Pax6 (Götz et al., 1998). aRGs are the leading players in this complex process (Rakic, 1971). These cells are elongated cells with their two processes directed apically to the ventricular zone and basally to the basement membrane (Arai and Taverna, 2017; Bentivoglio and Mazzarello, 1999; Rakic, 2003).

They will be the scaffold for the later generated neurons to migrate to their correct place in the cortex (Lui et al., 2011; Rakic, 1972; Stiles and Jernigan, 2010). aRGs are the cells that will give rise to almost all the cells populating the cerebral cortex: neurons and glial cells (Götz and Huttner, 2005). aRGs can divide symmetrically or asymmetrically through INM, similarly to NECs. With the symmetric proliferative cell division, new aRGs that will increase the number of progenitor cells are generated. Consequently, the size of the area of the cortex where they are located, known as the ventricular zone (VZ), will be increased. Whereas with the asymmetric differentiative division, they will produce two different types of daughter cells, one with the identity of the mother cell and another with a new identity (Florio and Huttner, 2014; Götz and Huttner, 2005; Taverna et al., 2014). Once the pool of aRGs cells has increased and neurogenesis continues, aRGs start diving asymmetrically more often, producing other types of NPCs or neurons that will crowd the upper layers of the developed cortex (Florio and Huttner, 2014; Molyneaux et al., 2007; Noctor et al., 2004).

Apical intermediate progenitors

These NPCs, also known as short neural precursors (SNP), are essential to increase the production of neurons as they will only undergo one round of symmetric neurogenic division through INM. They have similar features to aRGs; they are bipolar cells with two processes. However, the basal processes of aIPs do not reach the pia surface. They express Pax6 as a marker (Arai and Taverna, 2017; Florio and Huttner, 2014; Gal et al., 2006; Kowalczyk et al., 2009; Tyler and Haydar, 2013).

Basal progenitors

The rest of the progenitors generated from NECs or aRGs will populate the zone basal to the VZ, the subventricular zone (SVZ) (Bystron et al., 2008). There are two types of BPs: Basal intermediate progenitors (bIPs) and basal radial glia cells (bRGs) (Arai and Taverna, 2017; Götz and Huttner, 2005). In contrast to NECs and aRGs, these BPs will not continue to divide through INM (Götz and Huttner, 2005).

Basal intermediate progenitors

These progenitors are generated from aRGs or NECs that delaminate and populate the SVZ. As the name indicates these progenitors divide basally in the SVZ, and unlike aRGs, they will only produce neurons (Götz and Huttner, 2005; Haubensak et al., 2004; Kriegstein et al., 2006; Miyata et al., 2004; Noctor et al., 2004). They lose the polarity specific of aRGs and start downregulating markers such as Pax6 and upregulate other markers such as Tbr2 (Englund et al., 2005). bIPs behave differently among different species. In lissencephalic animals such as mice, most bIPs

undergo symmetric neurogenic division giving raise directly to neurons (Florio and Huttner, 2014; Haubensak et al., 2004; Miyata et al., 2004; Noctor et al., 2004). On the contrary, in gyrencephalic species, bIPs can undergo more rounds of proliferative symmetric divisions to increase the number of bIPs before diving and producing neurons (Fietz et al., 2012; Florio and Huttner, 2014; Lui et al., 2011). These type of proliferative bIPs still retain the expression of Pax6 (Fietz et al., 2010). In summary, the central role of bIPs is to increase the number of neurons that are generated during the entire neurogenesis of the cerebral cortex (Götz and Huttner, 2005; Smart, 2002).

Basal radial glial progenitors

bRGs are a type of progenitors that are mainly found in gyrencephalic species such as ferrets and primates (Borrell and Reillo, 2012; Fietz et al., 2010). They are a very heterogeneous group of neural progenitors (Betizeau et al., 2013).

bRGs were discovered a few years ago (Betizeau et al., 2013; Borrell and Reillo, 2012; Fietz et al., 2010; Hansen et al., 2010; Reillo et al., 2011). Unlike bIPs, bRGs keep radial features such as the expression of astroglial markers (Florio and Huttner, 2014). Most of the bRGs keep expressing Pax6, while some of them also express Tbr2 (Betizeau et al., 2013; Florio et al., 2017; Florio and Huttner, 2014). In contrast to aRGs, they lose their epithelial features such as the presence of apical junctions (AJs) that keep aRGs attached to the ventricular surfaces (Borrell and Götz, 2014; Cappello et al., 2012; Fish et al., 2008; Götz and Huttner, 2005). In consequence, bRGs delaminate and populate the SVZ. They are monopolar cells with a basal process that keeps them attached to the pial surface of the cortex (Arai and Taverna, 2017; Fietz et al., 2010; Nowakowski et al., 2016).

The polarity of these cells and the type of processes that they have are essential for the kind of division they undergo. The presence of this type of cells in gyrencephalic species, and their abundance in species like primates and humans is relevant for brain folding, expansion and evolution (Borrell and Götz, 2014; Borrell and Reillo, 2012; Nonaka-Kinoshita et al., 2013; Reillo et al., 2011). Later in this introduction, I will explain more in depth the characteristics of this unique group of progenitors and their role in the evolution and structure of the human brain.

Subapical progenitors

SAPs are one of the least understood progenitors in the developing cortex. They were recently found by (Pilz et al., 2013) and they are highly enriched in the dorsal telencephalon of gyrified species (Pilz et al., 2013) and the ganglionic eminences (GE) of the ventral telencephalon in the mouse. As their name indicates, they divide in subapical locations of the developing cortex, that

is, in the SVZ and they keep an apical process. Their primary role during development is still not completely understood, however, they may be necessary to increase the number of progenitor cells (Arai and Taverna, 2017; Florio and Huttner, 2014; Pilz et al., 2013).

Truncated radial glial cells

Finally, a recently found type of radial glial cell, the truncated radial glial cell (tRG), seems to be important especially for human cortical development. These cells are in contact with the ventricles and extend a basal process to the pia membrane, however, this process is "truncated" and only extends until the SVZ. tRGs seem to appear in the developing cortex after gestational week (GW) 16.5 indicating an important role in human mid neurogenesis (Nowakowski et al., 2016).

1.1.1.2 Neuronal migration

The adult mammalian cortex consists of six layers of cells and is generated in an inside-out pattern, meaning that the neurons generated last will be colonising the upper layers of the cortex (Berry and Rogers, 1965; Rakic, 1974).

Excitatory cells in the cortex which are generated in the proliferative zones of the dorsal telencephalon must migrate radially to reach their correct laminar place in the cerebral cortex. In contrast, inhibitory interneurons are produced in the lateral and medial ganglionic eminences (LGE and MGE), which are part of the ventral telencephalon (Parnavelas, 2000). These cells migrate tangentially to reach the developing cortex where they are integrated and change their migration to radial migration to reach their final position in the corresponding layer of the cerebral cortex (Costa and Müller, 2015; Rakic, 1978; Silbereis et al., 2016; Sultan et al., 2013) (**Fig 1.1**).

In the previous pages, I have explained how excitatory neurons are generated. In the next paragraphs, I will mainly focus on the migration of these excitatory neurons and briefly mention the generation and migration of inhibitory neurons.

Radial migration

As it has been previously explained, NPCs located in the VZ and SVZ and the neurons generated from these progenitors will migrate radially creating the upper layers of the cortex (**Fig 1.1**). There are two different types of radial neuronal migration: somal translocation and glial-guided locomotion with an intermediate state called multipolar migration (Cooper et al., 2004; Nadarajah et al., 2001; Nadarajah and Parnavelas, 2002; Tabata and Nakajima, 2003).

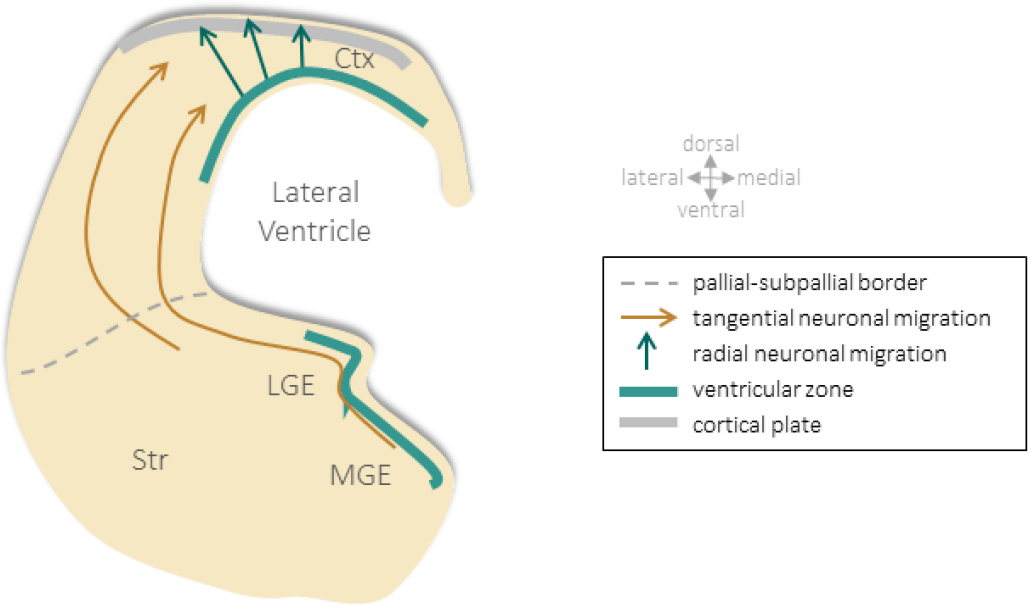

Figure 1.1: Excitatory and inhibitory neuronal migration in the mouse telencephalon.
Representative illustration of excitatory and inhibitory neuronal migration. Green straight arrows represent the radial migration that excitatory neurons follow from the VZ and SVZ to the CP in the cerebral cortex. The migratory trajectories that inhibitory neurons follow from the MGE and LGE until the reach the cortex and change to radial migration (green arrows) are represented in brown. Abbreviations: Ctx, cerebral cortex; LGE, lateral ganglionic eminence; MGE, medial ganglionic eminence; Str, Striatum. Figure adapted from (Buchsbaum and Cappello, 2019).

During the very early stages of development and when the cortex is still not very thick, neurons will mainly migrate by somal translocation. These neurons are attached basally to the pia surface of the cortex by a basal process. Upon migration, the process becomes shorter as the entire cell body moves upwards pulling itself (Miyata et al., 2001; Nadarajah et al., 2001; Tabata and Nakajima, 2003). The cells that migrate by somal translocation also have another trailing process directed to the VZ (Nadarajah et al., 2001).

When the cortex is thicker, neurons can switch to another type of migration or intermediate stage, called multipolar migration which is a radial glia independent movement (Tabata and Nakajima, 2003). Many of the neurons, located in the upper part of the SVZ and the lower half of the intermediate zone (IZ) of the developing cortex, migrate using this system (Cooper et al., 2004; Tabata and Nakajima, 2003). The IZ is the area of the cortex located between the SVZ and the CP (Bystron et al., 2008). This type of migration is much slower than somal translocation. Neurons do not follow a specific direction, and they extend and retract their processes to migrate even tangentially. This type of movement is limited to the SVZ and IZ. Once these neurons approach the upper parts of the IZ and the CP, they change their morphology to bipolar shape and their mode of migration to radial glia dependent locomotion (Cooper et al., 2004; Tabata and Nakajima, 2003). Some neurons may use multipolar migration to find the

environmental cues that will lead them to their correct path. It also implies that environmental factors such as secreted proteins and elements of the extracellular matrix (ECM) may have critical roles during neuronal migration (Kriegstein and Noctor, 2004; Tabata and Nakajima, 2003). One example of the importance of secreted proteins for the correct neuronal migration is Reelin. Reelin is secreted by Cajal Retzius cells located in the MZ. In mice lacking this protein (Reeler mice), the layering of the cortex is disrupted (D'Arcangelo et al., 1995; Lambert de Rouvroit and Goffinet, 2001, 1998).

Radial glia dependent locomotion is the second mode of migration (Nadarajah et al., 2001; Nadarajah and Parnavelas, 2002). In this type of movement, neurons use radial glial cells, whose processes extend from the apical part of the cortex to the pia surface, as their scaffold to move upwards (Rakic, 1972). During locomotion, neurons acquire a bipolar-like shape with one short process directed to the pia surface with a short growth cone-like structure on the tip but without being attached to it and a short trailing process (Nadarajah et al., 2001). In contrast to neurons that migrate via somal translocation, where the movement of the cell body is quite smooth, neurons that migrate via locomotion move with saltatory movements. Due to this type of action, the migration of these neurons takes longer (Nadarajah et al., 2001; Nadarajah and Parnavelas, 2002). Once the neurons that migrate via locomotion reach the marginal zone (MZ), that is, the uppermost layer of the cortex, above the CP, they can change the way of migration. They will undergo a terminal translocation that is very similar to somal translocation and find their final position in the cortex (Nadarajah et al., 2001; Nadarajah and Parnavelas, 2002; Sekine et al., 2011).

Even though somal translocation and locomotion are two independent processes regulated by a group of cytoskeletal proteins such as actin, microtubules and associated proteins, some steps are shared and consistent. Due to the saltatory movement of neurons during locomotion, these steps happen cyclically. In contrast, in somal translocation, this procedure only occurs once. Upon migration, the leading process of the neurons becomes shorter, pulling up the nucleus (Nadarajah and Parnavelas, 2002). This movement of the nucleus is called nucleokinesis (Lambert de Rouvroit and Goffinet, 2001). It is characterised by microtubules moving the nuclei upwards making the trailing process look longer (Morris et al., 1998). Finally, the trailing process becomes short again, and the cycle starts again until neurons reach their final position (Nadarajah and Parnavelas, 2002).

Tangential migration

Inhibitory GABAergic neurons generated in the GE (mainly from the MGE) of the ventral telencephalon follow tangential routes, that is, orthogonal to radial migration, to reach the dorsal cortex and integrate into the cortex (Anderson et al., 2002; Marin, 2003; Parnavelas, 2000).

Contrary to excitatory neurons, interneurons have a leading process that has many branches important for sensing the environment and the extracellular cues that will guide their directionality (Marin, 2013; Martini et al., 2009). The different types of interneurons are quite similar in terms of the mechanism they use to migrate, but the extracellular cues that they differently sense with specific receptors will guide them to the correct place in the cortex (Marin, 2013; Nobrega-Pereira and Marin, 2009).

Interneurons follow two main streams of migration to find the correct place in the cortex. In the first one, interneurons travel from the MGE through the MZ, and in the second one, they go a bit deeper in the cortex and travel from the MGE through the SVZ (Marin, 2013; Wichterle et al., 2001). There is a small fraction of interneurons that travels from the MGE to the subplate (SP), the region just above the IZ (Bystron et al., 2008; Marín, 2013) (**Fig 1.1**).

The reason why interneurons migrate through these specific areas in the cortex before changing to radial migration is the type of chemokines the cells populating these layers express (López-Bendito et al., 2008; Marin, 2013). Once the interneurons reach the cortex, they change their migration mode to radial glial migration and find their final position in the cortex (Costa and Müller, 2015; Silbereis et al., 2016; Sultan et al., 2013).

1.1.2 Differences between human and mouse brain development

The human brain is different in size and structure compared to other species and is much more complex. If we compare the human and mouse brains, we can see that it is much bigger, and it is folded (**Fig 1.2**). The human cerebral cortex contains approximately 16 billion neurons and 61 billion non-neuronal cells. That is more than 1000 times the number of cells in the cerebral cortex of mice (Azevedo et al., 2009; Herculano-Houzel et al., 2006; Hodge et al., 2019) but only two times more compared to chimpanzees, our closet living relative (Mora-Bermúdez et al., 2016).

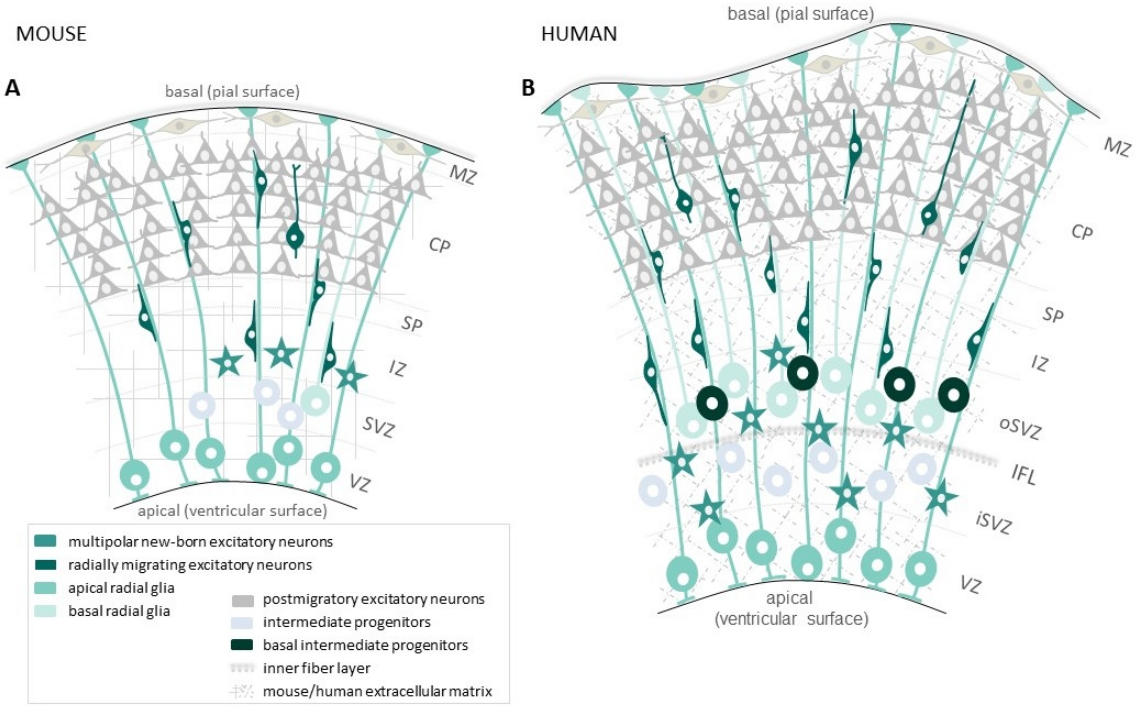

Figure 1.2: Mouse vs Human cortical development.
Representative illustration of the mouse (A) and human (B) developing cortex. In mice where the cortex is lissencephalic, aRGs will generate IPs or neurons directly. These neurons will use radial glia cells as a scaffold to migrate towards the CP. In humans, aRGs will generate more IPs and another type of progenitor not so abundant in mice, bRGs. The increased amount of BP in humans will create a new layer in the developing cortex, the oSVZ. The increased number of progenitors will result in an increased number of neurons. The increased number of progenitors and neurons, together with a more complex extracellular matrix will induce the formation of folds in the human brain. Abbreviations: aRG, apical radial glia; bIPs, basal intermediate progenitors; BP, basal progenitor; bRG, basal radial glia; CP, cortical plate; IFL, inner fiber layer; IPs, intermediate progenitors; iSVZ, inner subventricular zone; IZ, intermediate zone; MZ, marginal zone; oSVZ, outer subventricular zone; SP, subplate; SVZ, subventricular zone, VZ, ventricular zone. Figure adapted from (Buchsbaum and Cappello, 2019).

In this part of the introduction, I will focus on the specific characteristics that make the human brain so unique and in **Chapter 3,** I will focus on the distinct differences between the brain of modern humans, the brain of the *Homo sapiens neanderthalensis* (our closest extinct relatives), and the brain of our last common ancestor, to have a better overview of human brain evolution and development. It is essential to mention that the basis of neurogenesis and neuronal migration previously explained shares many common steps in rodent (e.g. mice) and primate (e.g. human) brain development. Nevertheless, there are two reasons why the human brain is bigger compared to rodents and non-human primates. One is the length of the neurogenic period (Lewitus et al., 2014; Wilsch-Bräuninger et al., 2016) by which more progenitors and, in consequence, more neurons can be generated. In mice, embryonic cortical neurogenesis starts at embryonic day 11 (E11) and continues until approximately E17-18 (Stagni et al., 2015; Takahashi et al., 1996; Van den Ameele et al., 2014). In humans, this period is much more

extended, starting at GW7-8 and continuing almost until birth (Stagni et al., 2015; Toma et al., 2016; Van den Ameele et al., 2014). The other one is the number of neural progenitor cells and the corresponding amount of neurons that can be generated from them by unit time (Borrell and Reillo, 2012; Haubensak et al., 2004; Rakic, 1995; Wilsch-Bräuninger et al., 2016). There are three different ways to increase the number of NPCs: (a) increase the pool of a specific type of NPCs (b) shorten the length of the cell cycle of progenitors and (c) change the type of division from neurogenic asymmetric to proliferative symmetric, so instead of generating two different cell types (neurons and progenitors), two progenitors will be created (Wilsch-Bräuninger et al., 2016). Among all the kinds of progenitors, I will focus on bRGs, which are highly abundant in gyrified primates including humans (Fietz et al., 2010; Reillo et al., 2011).

Lissencephalic species such as mice contain a low number of bRGs (Dehay et al., 2015; Shitamukai et al., 2011; Wang et al., 2011). On the contrary, they are very abundant in gyrencephalic species such as primates (Betizeau et al., 2013; Fietz et al., 2010; Hansen et al., 2010; Reillo et al., 2011). bRGs can go through more rounds of proliferative symmetric division or asymmetric divisions (Betizeau et al., 2013; Penisson et al., 2019). Through proliferative symmetric division, they can generate two bRGs. In contrast, through asymmetric divisions, they will create two different types of cells: one bRGs and one neuron or neurogenic bIP (Florio and Huttner, 2014; Taverna et al., 2014). In contrast to other progenitor cells in mice that increase the length of the cell cycle in later stages of neurogenesis, in primates, the cell cycle of bRGs is reduced (Betizeau et al., 2013; Kornack and Rakic, 1998; Penisson et al., 2019).

It is also believed that bRG proliferation can be controlled by ECM molecules which can produce a microenvironment around the bRGs (Fietz et al., 2012, 2010; Penisson et al., 2019; Pollen et al., 2015). Both through symmetric and asymmetric division, the pool of bRGs will be expanded. The increased number of bRGs together with other BPs in the SVZ will produce a new predominant area in the developing cerebral cortex in gyrencephalic species (Borrell and Reillo, 2012; Dehay and Kennedy, 2007; Smart, 2002). This new layer is the outer subventricular zone (oSVZ) and as its name indicates, it is generated above the subventricular zone. In species with an oSVZ, the SVZ is renamed to inner subventricular zona (iSVZ) (Fietz et al., 2010; Reillo et al., 2011; Smart, 2002). The iSVZ and oSVZ contain 85% of the cells in the developing cortex in humans while in rodents the SVZ will only contain 15-30% of the cells (Borrell and Reillo, 2012; Dehay and Kennedy, 2007; Reillo et al., 2011). It is important to mention that the presence of iSVZ and oSVZ with an increased number of bRGs is not unique to primates, but they are also present in other gyrified species such as the ferret (Borrell and Reillo, 2012).

The fact that bRGs are so abundant in gyrified species may implicate a role in the generation of folds (Borrell and Reillo, 2012). Still, they are not the only mechanism or reason behind the folding in gyrified species. For example, the marmoset monkey, which belongs to the taxonomic order of primates and has an abundant number of bRGs, has a lissencephalic brain (Borrell and Götz, 2014; Kelava et al., 2012). Another study in ferret where they overexpressed *CyclinD1* and *Cdk4* in bRGs allowing the overproliferation of these cells, resulted in an increased number of folds (Nonaka-Kinoshita et al., 2013). These studies show that the mere presence of a higher number of bRGs may not be enough for the formation of folds. Nevertheless, several different factors will induce the creation of folds in the cerebral cortex in different species (Borrell and Götz, 2014). The different components of the ECM are some of those factors (Fietz et al., 2012).

The ECM encompasses all the non-cellular components that are part of the tissue. It is the scaffold of the cells and essential for many processes, like proliferation, differentiation, migration, survival, polarity and homeostasis of the cell (Frantz et al., 2010; Hynes, 2009). It is composed of water, proteins and polysaccharides. Among the different components, it includes macromolecules that are important for cell adhesion and signalling (integrins and syndecans) or proteins essential for keeping the structure of the tissue (laminins, fibronectin, elastins or tenascins) among many others (Frantz et al., 2010; Hynes, 2009). The ECM is therefore essential for the correct development of the brain (Long and Huttner, 2019). It is important to mention that human ECM is much more complex than that of other species such as mice (Fietz et al., 2012; Long and Huttner, 2019). Distinct sets of collagens, laminins, proteoglycans, and integrins are expressed in higher levels in the germinal zone of the human developing neocortex compared to mice, possibly allowing a higher self-renewing capacity of human progenitor cells.

It has recently been shown that some ECM components (HAPLIN1, Lumican, and Collagen I) can induce folding of the developing neocortex (Long et al., 2018). The candidates were selected based on their high expression in the human foetal cortical plate. Only 19 hours after adding the three different components together to the human foetal neocortex, folds were generated. This study shows the importance of ECM components in brain development and their possible role in the formation of folds in gyrified species. Moreover, it also shows that these components alter the stiffness of the tissue and that this change in the physical structure of the brain may be necessary for the formation of folds.

Another factor to take into consideration in the generation of folds is the existence of genes with evolutionary changes that are implicated in brain development and evolution. There are some genes highly enriched in primates, including humans, compared to rodents, and that may

have a role in the higher expression of bRGs in the brain and the formation of folds. Some of the most relevant will be explained in the next lines.

ARHGAP11B

A study conducted by (Florio et al., 2015) studied genes that were found highly enriched in apical and bRGs in humans and for which there were no orthologs in mice. Among the 56 candidates, *ARHGAP11B* was the top gene due to its high enrichment in radial glia cells. *ARHGAP11B* was generated from the duplication of *ARHGAP11A* more than 5 million years ago. Interestingly, when overexpressing this new variant in the mouse cortex, the number of basal progenitors was increased, the mouse brain was expanded and the presence of gyri was noticeable (Florio et al., 2015). This study demonstrates that evolutionary changes in existing genes may have had a significant role in the evolution, expansion and gyrification of the human cortex (Florio et al., 2015).

TBC1D3

The hominoid-specific gene TBC1D3 is an interesting gene with a unique expression in primates (Ju et al., 2016; Penisson et al., 2019). Interestingly, in chimpanzees, it appears as a single copy while in humans, it has multiple copies (Ju et al., 2016; Penisson et al., 2019). Overexpression of this gene in the cortex of mice induced the delamination of aRGs and increased the number of BPs, especially bRGs, and the presence of folds in the electroporated area. Moreover, the downregulation of *TBC1D3* in human brain slices reduces the number of bRGs (Florio et al., 2017; Ju et al., 2016; Penisson et al., 2019).

TMEM14B

In this study (Liu et al., 2017) researchers investigated the role of genes that were enriched in human foetal bRGs using single-cell RNA sequencing (scRNA-seq). One of the genes they found is TMEM*14B,* a primate-specific gene. After performing *in utero* electroporation (IUE) to transiently overexpress the gene in the developing mouse cortex and generating a conditional knock-in (cKI) mice model, they show how important this gene is for brain development. The induced expression of *TMEM14B* promotes an increase in the number of BPs localised in the SVZ, an increased number of upper-layer neurons. It also induces an increased number of deep-layer neurons only in a cKI mouse model and a mild cortical folding (Liu et al., 2017; Penisson et al., 2019).

NOTCH2NL

In this study (Suzuki et al., 2018) human-specific duplicated genes in the human foetal cortex were studied. Among 35 candidate genes, they focused on *NOTCH2NL* (*NOTCH2* receptor paralog) due to its known role in progenitor pool maintenance. After overexpression of the gene in mice, there was an expansion in the pool of progenitors, mainly RGs, and a consequently increased number of neurons *in vitro* and *in vivo* (Suzuki et al., 2018). Even though there is not a direct implication of bRGs in this study, it implies that gene duplication during evolution may have a crucial role in the development of the human brain (Florio et al., 2018).

Adhesion molecules: FLRTS

Apart from the importance of genes that are highly enriched in neural progenitors and have a critical role in the expansion and gyrification of the human cortex, other elements are also essential in the folding of the human cortex. In a recent study by (Del Toro et al., 2017) it was revealed that the adhesion molecules FLRT1 and FLRT3 are essential for intercellular adhesion, cell migration and consequent clustering of neurons in their correct place with the creation of gyri and sulci in the brain as a result (Del Toro et al., 2017).

Finally, in **Chapter 4**, I will talk about a new possible candidate gene (*GNG5,* G protein subunit gamma 5*)*, highly enriched in basal radial glia cells and with a potential role in proliferation and migration. With a final aim of increasing the still not wholly known intricated process of cortical development.

1.2 CORTICAL MALFORMATIONS

It is clear after understanding the complex and well-orchestrated process behind the generation of the human cortex that any disturbance may lead to a range of different developmental problems. Malformations of cortical development (MCDs) encompass a wide variety of disorders that can be generated if any of the processes previously mentioned does not go as expected. Many of the children carrying genetic mutations that lead to cortical malformations have intellectual disability, developmental delay and epilepsy (Lee, 2017). Interestingly, 40% of patients suffer from seizures that are not treatable (Kuzniecky, 1994; Lee, 2017). In **Chapter 5,** I will focus more on the reasons behind the defects at functional or circuit levels in these patients and the different ways we have to study it in humans.

Many factors can induce a poor development of the human cortex and consequent MCDs (Buchsbaum and Cappello, 2019; Gaitanis and Tarui, 2018; Ishii and Hashimoto-Torii, 2015; Martens and van Loo, 2007; Pang et al., 2008). On the one hand, environmental aspects such us alcohol intake during pregnancy (Hashimoto-Torii et al., 2014; Hendrickson et al., 2017; Mattson and Riley, 1998; Wass et al., 2001) or drug consumption (Gressens et al., 1992; Thompson et al., 2009), maternal seizures (Hashimoto-Torii et al., 2014), exposure to heavy metals during pregnancy (Hashimoto-Torii et al., 2014), hypoxia (Golan et al., 2009; Ortega et al., 2017; Vasilev et al., 2016), perinatal infections such as Zika virus (Nunes et al., 2016; Oliveira Melo et al., 2016; Qian et al., 2016; Shao et al., 2016; Van Den Pol et al., 2017), vascular events during development (Lee, 2017) or radiation (Ferrer et al., 1993) can lead to MCDs. The severity, timing and degree of this environmental influences will determine the level of disorder these kids will suffer from (Pang et al., 2008). On the other hand, genetic factors play a very important role in the development of these disorders (Buchsbaum and Cappello, 2019; Guerrini and Dobyns, 2014; Hu et al., 2014; Pang et al., 2008; Romero et al., 2018), and this is the topic I will explain in detail in the next pages.

I will focus on the most important and well-studied MCDs, the genetic changes that lead to their formation as well as the machinery that is affected and leading to the incorrect development of the cerebral cortex. It is important to emphasise that MCDs and the genetic variants that lead to these disorders are very difficult to classify. There is not a unique gene that causes one specific disease nor is there one disorder caused by a unique disruption in a gene. The reason behind MCDs is much more complex and multifactorial. MCDs are genetically and clinically very heterogeneous. One way of classifying the disorders is by looking at the type of cells and the steps in the development of the cortex that are disrupted: malformations due to (a) abnormal

cell proliferation or apoptosis (b) abnormal cell migration or (c) abnormal post-migrational development (Barkovich et al., 2012; Desikan and Barkovich, 2016; Hu et al., 2014).

1.2.1 MCDs due to abnormal cell proliferation or apoptosis

In this type of disorders, there is a reduced proliferation and increased apoptosis (microcephaly), increased proliferation and decreased apoptosis (megalencephaly) or disrupted proliferation (dysplastic malformations) of progenitors (Barkovich et al., 2012; Desikan and Barkovich, 2016). Microcephaly is one of the most studied MCDs in this category. As its name implies, the patients suffering from this disorder have a smaller brain (circumference of the brain more than three standard deviations below healthy population) (Gilmore and Walsh, 2013). Since primary recessive microcephaly (MCPH) was first studied, at least eighteen loci associated with this disease have been identified (Okamoto et al., 2018). Interestingly, most of the genes found to be mutated and associated with the disorder are essential for neurogenesis and cell proliferation (Desikan and Barkovich, 2016). One of the most studied genes is *ASPM* and is the cause for almost 40% of all the MCPH cases (Bond et al., 2002; Létard et al., 2018; Nicholas et al., 2009). This gene, as many of the genes causative of MCPH, code for centrosomal and pericentriolar proteins or proteins essential for correct chromosomal segregation and consequent accurate cell division (Barkovich et al., 2012; Hu et al., 2014). Some examples are: cell cycle and checkpoint regulators (*microcephalin* (Jackson et al., 2002; Zhong et al., 2006)*, CENPJ* (Hung et al., 2000)*, CDK5RAP2* (Megraw et al., 2011; Thornton and Woods, 2009))*;* mitotic spindle formation and orientation (*WDR62* (Chen et al., 2014)*, ASPM* (Bond et al., 2002; Létard et al., 2018; Nicholas et al., 2009; Thornton and Woods, 2009), *STIL* (Tang et al., 2011)); centrosome duplication and maturation (*CDK5RAP2* (Megraw et al., 2011))*;* or centriole duplication (*CEP152* (Nikola S. Dzhindzhev et al., 2010)) among others (Desikan and Barkovich, 2016). The discovery of all the causative genes associated with MCHP highlights the importance of genetics in MCDs.

Megalencephaly results from an overgrowth of the brain (weight of the brain more than 2-3 standard deviations above average population (DeMyer, 1986; Pirozzi et al., 2018). Numerous patients suffering from this disorder have associated syndromes such as polymicrogyria (PMG) (Barkovich et al., 2012; Leventer et al., 2010). Several genes have been associated and believed to be causative of the disorder. Among these, the intracellular signalling phosphatidylinositol-3-kinase (PI3K)-AKT-MTOR pathway has been one of the most studied due to its role in controlling cell growth and homeostasis (Desikan and Barkovich, 2016; Laplante and Sabatini, 2012). Recently, mutations in some of the genes involved in the mTOR pathway have been identified such as *AKT3*, *PIK3CA*, and *PIK3R2* (Desikan and Barkovich, 2016; Mirzaa et al., 2016; Rivière et al., 2013). Mutations in those genes have also been associated with focal cortical dysplasia (FCD)

(D'Gama et al., 2015; Desikan and Barkovich, 2016), periventricular nodular heterotopia (PVNH) or PMG (Alcantara et al., 2017). This is just one example highlighting the complexity of the different MCDs. Interestingly, some of these mutations usually are not inherited but appear "de novo", and some only affect a subset of cells (mosaicism) (Desikan and Barkovich, 2016). The degree, severity and phenotype of patients suffering from different types of megalencephaly varies a lot due to the presence of the mosaicism and somatic mutation (Desikan and Barkovich, 2016). For example, in some types of megalencephaly, such as dysplastic megalencephaly, formerly known as hemimegalencephaly, the problem only affects 8-35% of the cells. In consequence, the disorder only appears in a part of one of the hemisphere, even though it can also affect the entire hemisphere and sometimes even the cerebellum (Desikan and Barkovich, 2016; Nakahashi et al., 2009).

1.2.2 MCDs due to abnormal neuronal migration

The most important neuronal migration disorders (NMDs) are: periventricular heterotopia (PH) (problems in the initiation of migration) (**Fig 1.3, 3**); subcortical band heterotopia (SBH) (localised neuronal migrational problems) (**Fig 1.3, 2**); 'cobblestone' malformations (abnormal terminal migration of neurons) (**Fig 1.3, 4**) and lissencephaly (general migration problems) (Desikan and Barkovich, 2016; Lee, 2017) (**Fig 1.3, 1**).

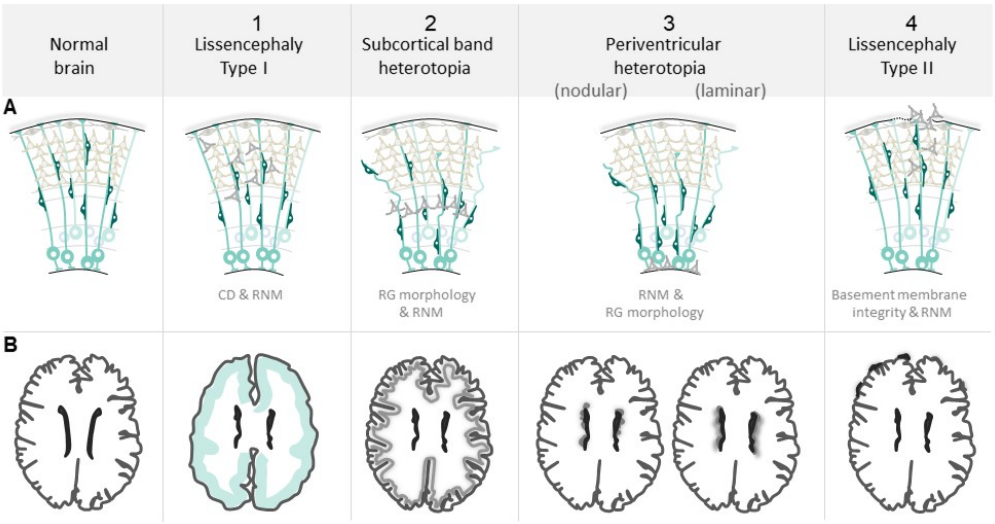

Figure 1.3: Cellular and morphological heterogeneity of neural migration disorders.
(A) Representative illustration of the different cell types affected in each type of NDM and (B) representative pictures of the most characteristic morphological features found in these patients. (1) Lissencephaly type I in which patients have a thicker cortex due to abnormal cell division and neuronal migration. (2) Subcortical band heterotopia where there is an extra layer of neurons between the cortex and the ventricular zone due to abnormal neuronal migration and radial glia morphology. (3) Periventricular heterotopia characterized by the presence of ectopic clusters of neurons in nodules (nodular) or as a sheets (laminar) lining the ventricles also due to abnormal neuronal migration and erratic radial glia morphology. (4) Lissencephaly type II in which neurons over migrate due to problems of the basement integrity and radial migration. Abbreviations: CD, cell division; RG, radial glia; RNM, radial neuronal migration. Figure adapted from (Buchsbaum and Cappello, 2019).

The meaning of heterotopia is "out of place" and encompasses a group of disorders in which ectopic neurons are found outside the cortex (Barkovich et al., 2012; Desikan and Barkovich, 2016; Gaitanis and Tarui, 2018; Ishii et al., 2015). The localisation and shape of these ectopic neurons will determine the type and degree of the heterotopia (Barkovich et al., 2012; Desikan and Barkovich, 2016) (**Fig 1.3, 3**). PVNH is characterised by the presence of nodules of neurons lining the ventricles (Barkovich et al., 2012; Barkovich and Kuzniecky, 2000). PVNH is the most common type of heterotopia (Barkovich et al., 2012) and represents around 31% of NMDs (Broix et al., 2016). Patients suffering from PH do not always suffer from intellectual disability (Dubeau et al., 1995; Pang et al., 2008). However, about 90% of the patients have epilepsy which usually appears during adolescence (Dubeau et al., 1995; Gaitanis and Tarui, 2018; Pang et al., 2008). The seizures in these patients localise to the clusters of ectopic neurons (Scherer et al., 2005) and the surrounding cortex (Desikan and Barkovich, 2016; Tassi et al., 2005). Interestingly, even though most of the times, PVNH is classified among NMDs, it has been shown that it may not only be due to an inherent neuronal-motility problem per se (Barkovich et al., 2012). Instead, there are two main reasons why there is a specific cluster of neurons next to the ventricles that is not able to reach the cortex in patients with PH: inherent problems in neuronal motility or loss of the neuroependymal integrity and altered morphology of aRGs with a consequent disruption for the neurons to migrate correctly during the development of the cortex (Desikan and Barkovich, 2016; Ferland et al., 2009; Klaus et al., 2019).

FLNA is one of the most common mutations found in patients with PVNH (Ekşioğlu et al., 1996; Fox et al., 1998; Parrini et al., 2006). Located in chromosome X, *FLNA* encodes for the actin-binding protein filamin A that is involved in remodelling the cellular cytoskeleton by interacting with integrins and different transmembrane receptors (Fox et al., 1998). In consequence, alterations in this protein can alter RGs and neuronal polarity and can cause difficulties for the neurons to migrate properly (Carabalona et al., 2012).

Another significant mutation known to be causative of a PVNH is *ARFGEF2*. It encodes for the protein brefeldin-inhibited GEF2 (BIG2) (De Wit et al., 2009; Sheen et al., 2004). It appears as an autosomal recessive mutation, and patients carrying this mutation often suffer from other features, normally microcephaly (Sheen et al., 2004). This protein is vital for vesicle trafficking from the trans-Golgi network and intracellular communication (Desikan and Barkovich, 2016; Ferland et al., 2009). *ARFGEF2* is also essential for the traffic of *FLNA* to the cell surface (Pang et al., 2008). Both *FLNA* and *ARFGEF2* are highly expressed in the neuroepithelium and have a role in maintaining the neuroependymal integrity (Pang et al., 2008).

Mutations in *FAT4* and *DCHS1* have also been associated with PH (Badouel et al., 2015; Cappello et al., 2013). These two genes encode for two protocadherins that interact with each other and have a role in cell migration, planar cell polarity and cell proliferation (Cappello et al., 2013; Ishiuchi et al., 2009; Klaus et al., 2019). These two proteins, and especially DCHS1, are the main actors of this thesis, and I will explain their role in human cortical development in much more detail in **Chapter 2.** *MOB2,* which is part of the Hippo pathway, same as *FAT4* and *DCHS1*, has also been associated with PH. The protein is necessary for *FLNA* phosphorylation, linking two different pathways involved in the formation of PH (Adam C O'Neill et al., 2018).

In patients with SBH, also known as "double cortex", there is a band of grey matter between the ventricle and the cerebral cortex (Gleeson et al., 1999; Lee, 2017; Pang et al., 2008) (**Fig 1.3, 2**). Mutations in the microtubule-associated gene, doublecortin (*DCX*) are associated with almost 85% of sporadic cases of SBH (Gleeson et al., 1999; Matsumoto et al., 2001). Due to this mutation, neurons are not able to migrate to their destination in the cortex. Germline mutations in *DCX,* which is X-linked, mainly leads to SBH in females, and many of the patients have intractable epilepsy (Lerche et al., 2001). Disruptions in radial glia themselves have also been shown to be causative of SBH. The conditional inactivation of the gene that codes for the small GTPase RhoA in the developing mouse cortex showed that the loss of scaffolding for neuronal migration also causes this type of MDC. The protein is necessary for the correct stabilisation of the cytoskeleton (Cappello et al., 2012).

Mutations in the gene EML1 have also been associated with the presence of ectopic neurons in the brain. Patients with mutations in this gene present a ribbon-like SBH. Mouse models for the disorder have properly recapitulated the human phenotype. The gene codes for a microtubule-associated protein (MAB) and is vital for correct spindle orientation (Bizzotto et al., 2017; Kielar et al., 2014).

DCX mutations also cause one of the most common NMDs, lissencephaly type I. However, while mutations in DCX cause SBH in females (Lerche et al., 2001), in males, mutations in *DCX* usually produce lissencephaly (Hu et al., 2014). In these patients, there is an increase in brain thickness due to the loss of the gyral patterning (Hu et al., 2014). The standard lamination of the cortex is lost due to abnormal neuronal migration (**Fig 1.3, 1**) (Dobyns et al., 1996; Wynshaw-Boris et al., 2010). Together with *DCX*, mutations in the gene *LIS1* are responsible for most of the cases of lissencephaly type I (Pilz, 1998). *LIS1* encodes for another MAP. Both *DCX* and *LIS1* have an essential role during neuronal migration as they interact with dynein to mediate nuclear to centrosomal coupling during neuronal migration (Tanaka et al., 2004). *LIS1* is also essential for correct neuroepithelial cell proliferation due to its role in spindle orientation and symmetric cell

division (Yingling et al., 2008). Mutations in *LIS1* are the cause of Miller-Dieker Syndrome (MDS), and interestingly these patients commonly have a smaller brain (Dobyns and Das, 1993).

De novo mutations in *TUBA1A,* which encodes a neuronal alpha-tubulin, have also been associated with lissencephaly. This again shows the critical role of cytoskeletal proteins in correct progenitor motility and neuronal migration (Keays et al., 2007). Mutations in this gene affect the folding of tubulin heterodimers and their interaction with other MAPs such as *LIS1* and *DCX* (Moores et al., 2004). The clinical features of patients with mutations in *TUBA1A* are very variable, and most of them also suffer from microcephaly, PMG, mental retardation or developmental (Bahi-Buisson et al., 2008; Barkovich et al., 2012; Jansen et al., 2011). Mutations in *Reelin* (*RELN)* which encodes for a secreted extracellular matrix protein have also been associated with lissencephaly (Hong et al., 2000).

The last type of the main MCDs in this group is cobblestone lissencephaly (COB-LYS) or lissencephaly type II. It is characterised by over migration of neurons at the pial surface (Bizzotto and Francis, 2015) (**Fig 1.3, 4**). It is often associated with other disorders such as congenital muscular dystrophy and eye abnormalities (Gaitanis and Tarui, 2018). One of the causes behind the formation of this type of malformation is the difficulty for the basal process of radial glia cells to attach to the basal membrane (BM) due to its disruption (Bizzotto and Francis, 2015; Francis et al., 2006). Consequently, the endfeet of RGs do not attach properly to the BM and neurons continue migrating. It is therefore not surprising that mutations in components of the ECM, essential for the maintenance of the BM, or other proteins necessary for preserving its integrity, cause this disorder. Different mutations are causative of the disorder: *POMT1, POMT2, FKTN, FKRP, LARGE* and *POMGnT1,* encoding for different glycosyltransferases (Bizzotto and Francis, 2015; Brockington, 2001; Buchsbaum and Cappello, 2019; De Bernabé et al., 2002; Mercuri et al., 2009; Van Reeuwijk et al., 2005; Vuillaumier-Barrot et al., 2011; Yamamoto et al., 2004). Glycotransferases are important for the glycosylation of α-dystroglycan a component of the dystrophin-associated glycoprotein complex essential for the correct attachment of cells to the BM (Francis et al., 2006; Grewal and Hewitt, 2003). Mutations in *LAMB1* and *COL4A1* which code for elements of the ECM have also been associated with the disorder, showing the previously explained importance of the ECM in correct neuronal development (Labelle-Dumais et al., 2011; Radmanesh et al., 2013). Finally, mutations in the genes that code for *GPR56* a G protein-coupled receptor (GPCR) have also been associated to cobblestone-like human cortical dysgenesis (Bahi-Buisson et al., 2010; Desikan and Barkovich, 2016; Luo et al., 2011) and with other MCDs such as bilateral frontoparietal polymicrogyria (BFPP) (Bahi-Buisson et al., 2010; Fujii et al., 2014). This protein is localised in the basal processes of progenitors and it is crucial

for correct cortical patterning and BM integrity due to its role binding ECM proteins (Li et al., 2008; Luo et al., 2011). The discovery of mutations in a G protein-coupled receptor highlights the relevance of G proteins and coupled receptors in cortical development (Bae et al., 2014; Li et al., 2008; Luo et al., 2011) In **Chapter 4** I will talk about the importance of this large family of proteins and especially of one of its members in neurogenesis and neuronal migration.

1.2.3 MCDs due to abnormal post-migrational development

Two are the primary disorders found in this group: PMG and schizencephaly.

PMG is characterised by overfolding and abnormal cortical layering (Desikan and Barkovich, 2016; Leventer et al., 2010; Stutterd and Leventer, 2014). As mentioned before the intracellular signalling phosphatidylinositol-3-kinase (PI3K)-AKT-MTOR pathway has been associated with this disorder in patients suffering also from megalencephaly (Alcantara et al., 2017). Mutations in members of the tubulin family, such as *TUBA1* previously mentioned, can also induce PMG in some patients (Jansen et al., 2011; Stutterd and Leventer, 2014).

Schizencephaly is characterised by a cleft full of fluid between the ventricles and the cortex usually lined by a polymicrogyric cortex (Barkovich and Kjos, 1992; Buchsbaum and Cappello, 2019; Pang et al., 2008). It is also considered as a very severe case of PMG. It is typically caused by environmental factors such as young maternal age, alcohol intake during pregnancy or inadequate prenatal care (Barkovich et al., 2012; Dies et al., 2013; Kuzniecky and Barkovich, 2015).

All the mutations previously explained are just some of the most known and studied inherited or “de novo” mutations that have been associated with the wide variety of MDCs. I hope this information clarified the complexity of MCDs and the importance of a correct regulation in all the steps of human cortical development. Not only that but the importance of continuous research in the field to tackle all the mechanisms behind these astonishing well-organised processes necessary for proper human brain development. In the next and final part of the introduction of this thesis, I would like to explain how we can study it.

1.3 MODEL SYSTEMS TO STUDY THE DEVELOPMENT OF THE CORTEX

The brain is a very complicated organ to study, not only due to its complexity but also due to limited human material availability. The only human material accessible to study its development, such as *post-mortem* tissue or biopsies, is not often available, or well-preserved. Moreover, getting tissue from specific patients with a particular disorder is even more challenging. Different models can be used in neuroscience to tackle this problem. In the next lines, I will explain the most common *in vivo* and *in vitro* models that we have nowadays.

1.3.1 *In vivo* models: Rodents

Rodents, and especially mice, are the most common animal model used to study cortical neurodevelopment and cortical malformations. The advances in human genetics to find mutations causative of different MCDs and the knowledge acquired in animal transgenesis have been very useful for scientists studying the development of the human cortex.

By generating specific knockouts (KO) of the genes known to be causative of cortical malformations, it has been possible to better understand the role of these genes and the pathways in which they are involved. Unfortunately, few mouse models have successfully replicated the complete phenotype found in patients with MCDs. The KO for *Eml1* is an excellent example. As previously explained this gene is mutated in patients with ribbon-like SBH. The mouse model is characterised by the presence of bilateral SBH, recapitulating the human phenotype (Bizzotto et al., 2017; Kielar et al., 2014). Another example is the *Gpr56* KO mouse model, in which there is an over migration of neurons due to the disruption of the BM integrity, recapitulating a cobblestone-like cortex found in patients with mutations in this gene (Bahi-Buisson et al., 2010; Li et al., 2008). In this case, it is only a partial recapitulation of the phenotype as patients with *GPR56* mutations also suffer from polymicrogyria and generalised seizures (Bahi-Buisson et al., 2010).

Unfortunately, in most of the studies in which the genes associated with MCDs in humans are knocked out, mice do not show the characteristic malformations of the cortex found in patients. That is the case of the *Dcx* mouse model in which KO mice do not show any sign of cortical disruption, but mainly hippocampal defects (Bazelot et al., 2012; Corbo et al., 2002). The absence of a prominent phenotype in mice probably implicates the presence of other genes with similar or compensatory roles (Deuel et al., 2006), (Romero et al., 2018). Interestingly, the knockdown (KD) of *Dcx* in rats does induce SBH like phenotype, indicating specifies-specific phenotypes (Ramos et al., 2006).

Another example is the mouse model for *Lis1*. Homozygous KO of the gene is lethal while the heterozygous model presents hippocampal abnormalities with 5% of the embryos also suffering from epilepsy (Hirotsune et al., 1998). Only when genetically manipulating and reducing the expression levels of *Lis1* is when the phenotype in mice starts to be slightly similar to what we see in human patients (Hirotsune et al., 1998). There is a disorganisation of the cortex due to delayed neuronal migration (Hirotsune et al., 1998; Romero et al., 2018). Same as with *Dcx*, KD of *Lis1* in rats induces an SBH-like phenotype (Tsai et al., 2005). The homozygous KO model for *Arfgef2* is also lethal, while heterozygous mice are healthy with no sign of cortical malformations. Another animal model to study PH is the KO model of *Flna* which also results in embryonic lethality (Feng et al., 2006). However, the conditional knockout in neural progenitors results in a PH-like phenotype (Feng et al., 2006).

In a similar situation, the KO of *Fat4* does not present the PH phenotype found in patients, and the KO mouse model for *Dchs1* induces neonatal lethality (Badouel et al., 2015; Buchsbaum and Cappello, 2019; Romero et al., 2018). However, when reducing the levels of these genes by acutely knocking them down, there is the increased proliferation and reduced neuronal differentiation (Cappello et al., 2013). Finally, using the mouse as a model system, it has been possible to study genes important for cortical development for which human mutations have not been described yet. These experiments show the importance of using mice to understand in detail different mechanisms underlying cortical malformation. Some examples are *E-catenin* (Schmid et al., 2014), Ccdc85C (Mori et al., 2012), *Rapgef2/Rapgef6* (Maeta et al., 2016), *Afadin* (Yamamoto et al., 2013) and the already mentioned *RhoA* (Cappello et al., 2012). When these genes are manually downregulated it is possible to induce phenotypes similar to PH and SBH (Romero et al., 2018). It reveals the importance of apical junctions and the cytoskeleton for radial glial cell integrity and correct neuronal migration (Buchsbaum and Cappello, 2019).

These are just examples of some of the most studied genes related to human cortical malformations and the mouse models we have to study them. We have obtained very insightful information using this system. However, due to the differences between the brain of mice humans, we cannot study all aspects of human cortical development with them. Characteristics such as the lower number of progenitor cells, the shorter neurogenic period or the lissencephalic nature of the mouse brain do not allow us to study all the aspects that cause human cortical malformation in mice. To overcome this problem scientists have used different models which have more similarities with the human brain. That is the case of ferrets and non-human primates.

Ferret (*Mustela putorius furo*) a mammal from the carnivore order is a species with a larger brain, which is gyrified. It is one of the most used non-rodent models to study brain development (Fietz et al., 2010; Pinson et al., 2019). An increased number of NPCs, the presence of the oSVZ, an increased number of bRG compared to rodents, and discrete domains of gene expressions (Borrell and Reillo, 2012; De Juan Romero and Borrell, 2015; Fietz et al., 2010; Reillo et al., 2011) make them an optimal model to study corticogenesis. Moreover, it is possible to manipulate them genetically by IUE (Kawasaki et al., 2013), CRISPR-Cas9 (Kou et al., 2015) or by the generation of transgenic ferrets (Johnson et al., 2018). This technology allows us to study the role of specific genes in the developing brain, and it has been possible to recapitulate human cortical malformation phenotypes in this system. As previously mentioned, *Aspm* is one of the genes associated with MCPH. By knocking out this gene in ferrets, scientists were able to not only partially recapitulate the human phenotype but to show the importance of this gene in maintaining the ratio of aRGs in the VZ (Johnson et al., 2018). These studies reflect the importance of moving towards animal models that are more similar to humans due to the possibility of recapitulating human phenotypes that are very difficult to obtain in mice (Pinson et al., 2019). Of course, there are some limitations for this to happen more effectively: longer gestational time, the lack of genetically homologous inbreed lines and the absence of a full genome annotation are some of them (Pinson et al., 2019)

Non-human primates are the closest living organism we can use to study the human brain. Rhesus monkey (*Macaca mulatta*) and marmosets (*Callithrix jacchus*) are the most widely used in the field of cortical development. By studying the foetal brain of macaques, it has been possible to get more insights into the morphology and function of bRGs (Betizeau et al., 2013). Marmosets are lissencephalic, but in their brain, there is a clear oSVZ. Studying these animals has been advantageous for understanding that the mere presence of that layer and the consequent increase in the number of progenitors and bRGs are not enough to induce gyrification (Kelava et al., 2012). Finally, it has been possible to generate transgenic macaques and marmosets, which have been proven as a potent tool to mimic human brain malformations (Heide et al., 2020; Sasaki et al., 2009; Shi et al., 2019).

1.3.2 *In vitro* models

Even though the knowledge gained by using different animal models to study brain development has increased over time, we still lack the perfect tool to study the human brain. Non-invasive human studies and *post-mortem* tissue are few of the resources we have to study the intact entire human brain. However, the use of animal models is not a powerful enough technique to understand the immense complexity of the human brain and associated brain malformations.

Fortunately, scientists have developed a wide variety of protocols to study some of the aspects of the developing human brain *in vitro*.

There is a wide variety of protocols in which stem cells can be differentiated to neural precursor cells, neurons and glial cells that can be cultured as a monolayer or two dimensions (2D). Additionally, in the last few years, there has been significant progress in the development of three dimensional (3D) cultures named brain organoids. Finally, thanks to the establishment of effective reprogramming protocols, it is now possible to get different human cells such as fibroblast or peripheral blood mononuclear cells and bring them to a stem cell state. These induced pluripotent stem cells (iPSCs) can be converted to any type of cell (Staerk et al., 2010; Takahashi and Yamanaka, 2006; Yu et al., 2007). All this technology allows us to study some of the features of the healthy and unhealthy human brain in a dish.

The 2D neuronal cultures are the most simplistic systems to study neurons *in vitro*. Most of the protocols are based on the intrinsic ability of NPCs, which still have neuroepithelial features, to self-organise forming rosettes (Elkabetz et al., 2008; Shi et al., 2012a, 2012b). The cells keep their apicobasal cell polarity as it happens in the brain (Shi et al., 2012b). These NPC cultures that are generated from human embryonic stem cells (hESCs) or iPSCs can be further expanded and differentiated into different neuronal types (Boyer et al., 2012; Brennand et al., 2011; Chambers et al., 2009; Gunhanlar et al., 2017; Shi et al., 2012a, 2012b). It is also possible to generate neuronal cultures directly from hESCs/iPSCs or fibroblast by direct reprogramming with specific small molecules or by forced expression of neurogenin-2. With these two methods it is possible to get fully mature neurons in a significantly shorter time and in a more robust, efficient and direct way (Vierbuchen et al., 2010; Zhang et al., 2013). The advantage of these cultures is the generation of a more homogeneous population of the neuronal type to be studied and the possibility to explore the morphological and functional characteristics of each cell individually such as gene expression, neuronal migration, neuronal maturation and synapse formation (Brennand et al., 2011; Buchsbaum and Cappello, 2019; Gunhanlar et al., 2017). However, in this system, the cells lose their external context and the ability to grow and maintain the characteristic spatiotemporal pattern and neuronal connectivity found in the brain. By taking advantage of the ability of cells to self-organize during organogenesis, scientists have developed 3D brain organoids in which the problems encountered in the 2D system are largely overcome.

Spheroids were first established 12 years ago and are the predecessors of brain organoids (Eiraku et al., 2008; Kadoshima et al., 2013). In this system, cells are grown in suspension; they self-organise forming polarised embryoid bodies (EBs). This semispherical structure consists of a multi-layered structure resembling the layers in the developing human cortex (Eiraku et al.,

2008; Kadoshima et al., 2013). These protocols were improved by adding a scaffold (normally Matrigel) to the EBs so they could self-assemble and develop further and in a more sophisticated way. That is how the first brain organoids were generated (Lancaster et al., 2013; Lancaster and Knoblich, 2014). As in the case of spheroids, brain organoids are characterised by VZ-like structures where progenitor cells are located. Around this structure, there is an area mainly populated by IPs and bRGs like the iSVZ and oSVZ in the human brain. Finally, there is a CP-like zone in which neurons from the different neuronal layers are located (Lancaster et al., 2013; Lancaster and Knoblich, 2014; Qian et al., 2016).

There are two primary types of protocols to generate COs: non-patterning and patterning protocols (Kyrousi and Cappello, 2019). The first one is based on the intrinsic ability of cells to further develop in specific areas of the brain recapitulating some of the aspects that happen in the developing human foetal brain (Camp et al., 2015; Lancaster et al., 2013; Lancaster and Knoblich, 2014; Quadrato et al., 2017). Consequently, in this type of brain organoids, we can find discrete brain regions resembling the dorsal or ventral cortex, hippocampus, retina, choroid plexus as well as the retina. The advantage of this type of protocols is the option to study human brain development and disease in a more comprehensive way including different regions and more cell types that are affected (Kyrousi and Cappello, 2019).

Patterning protocols are based on extrinsic factors that will induce the differentiation to specific brain regions in a controlled way. Until now it has been possible to generate brain organoids from the forebrain, midbrain, hypothalamic regions or cerebellum (Krefft et al., 2018; Muguruma et al., 2015; Qian et al., 2018, 2016; Sakaguchi et al., 2015; Watanabe et al., 2017). These types of protocols allow us to study specific brain regions. However, it is important to mention that these 3D systems also have some limitations (Jabaudon and Lancaster, 2018; Velasco et al., 2019): (1) Reproducibility: even though scientists are trying to optimise protocols for a homogenous generation of brain organoids there is still a batch to batch variability between brain organoids (Krefft et al., 2018; Velasco et al., 2019); (2) Size: brain organoids can only grow up to a point due to the lack of nutrients and oxygen going inside the brain organoids; the lack of a vascularisation seems to be the main reason. That is why scientists are trying to find a way to implement a vascular system for them (Cakir et al., 2019; Mansour et al., 2018). (3) Gyrification: even though human brain organoids contain a significant amount of bRGs, there is no presence of gyri. As mentioned above, the mere presence of bRGs and an increased number of other NPCs do not necessarily lead to the gyrification of the brain. However, the lack of wrinkling in the brain organoids limits the possibilities of studying cortical malformations such as lissencephalic

or PMG. Scientists have tried to solve this by inducing the folding by growing the brain organoids in a microfabricated compartment to study (Karzbrun et al., 2018). (4) Lack of a full brain picture: the brain consists of many different regions that correctly interact with each other. However, with the patterned brain organoids, we are only able to grow independent brain regions. Assembloids or fused brain organoids are a fantastic alternative in which brain organoids from two different brain regions are merged, and their interaction can be studied (Bagley et al., 2017; Birey et al., 2017; Sloan et al., 2018). For example, by fusing dorsal and ventral telencephalon brain organoids, it has been possible to study radial and tangential migration of excitatory and inhibitory neurons, respectively. The migration of interneurons from the ventral to the dorsal region can also be studied in this system (Bagley et al., 2017; Birey et al., 2017).

1.3.2.1 Functional studies in organoids

Cerebral organoids (COs) which mainly refer to brain organoids recapitulating the forebrain are a potent tool to study brain evolution, development and cortical malformations. And there are a wide variety of techniques we can use on them to explore that.

COs can be permanently or acutely modified genetically (Kyrousi and Cappello, 2019). CRISPR/Cas9 technology has allowed us to generate mutations in specific genes as well as the generation of KO (Ran et al., 2013). Moreover, the possibility of getting isogenic lines, with the same genetic background, allows us to have the perfect controls for our experiments. Many scientists have used the CRISPR/Cas9 technique to obtain COs with a specific genetic background to study brain disorders such as autism (Wang et al., 2017), gangliosidosis, a neurodegenerative disorder (Latour et al., 2019), lissencephaly (Karzbrun et al., 2018) and PH (Buchsbaum et al., 2020). Same as in mice or ferret, COs can be acutely manipulated employing electroporation (Kyrousi and Cappello, 2019). By targeting the cavities resembling the ventricles, we can manipulate a specific subset of cells. This technique allows spatial and temporal control of desired genes (Kyrousi and Cappello, 2019). This technology has been beneficial to study the role of different genes involved in cortical malformations (Buchsbaum et al., 2020; Klaus et al., 2019; Lancaster et al., 2013; Di Matteo et al., 2020; O'Neill et al., 2018b, 2018a).

Single-cell RNA sequencing (scRNA-seq) and analysis have been a potent tool to study the transcriptomic signatures that are similar between the foetal brain and COs indicating the validity of this new technology for the study of the developing brain (Camp et al., 2015). scRNA-seq in COs from different species have also been very useful to study brain evolution (Kanton et al., 2019; Mora-Bermúdez et al., 2016; Otani et al., 2016). These studies indicated the power of using COs for evolutionary studies. In **Chapter 3**, in collaboration with the group of Dr Svante

Pääbo at the Max Planck Institute of Evolutionary Anthropology, we will use the technology of CRISPR/Cas9 to study the characteristics of COs from an evolutionary perspective, carrying one of the gene variants between humans and the last common ancestor with the Neanderthals.

By using scRNA-seq and fluorescence-activated cell sorting (FACS), it has also been possible to study the COs derived from patients with cortical malformations (Kyrousi and Cappello, 2019). By looking at the entire transcriptome/proteome that is altered, it has been possible to understand the mechanism and pathways that are affected (Bershteyn et al., 2017; Klaus et al., 2019).

It is also possible to look at the functionality of the matured neurons in these COs by looking at different electrophysiological properties. In **Chapter 5**, I will explain this in more detail, but in summary, it is possible to do whole COs extracellular cell recordings (Quadrato et al., 2017). They can also be pharmacologically treated to understand the electrical nature of the neurones that form the COs.

Using a combination of different techniques, it has been possible to study different MCDs and the steps essential for correct brain development. Some examples are: PVNH (Buchsbaum et al., 2020; Klaus et al., 2019; Adam C O'Neill et al., 2018), lissencephaly (Bershteyn et al., 2017; Iefremova et al., 2017) and microcephaly (Lancaster et al., 2013; Li et al., 2017). Moreover, it has also been possible to find human-specific mechanisms that were not possible to identify in mice. This is the case of the COs model for MDS the most severe case of classical lissencephaly with a deletion in 17p13.3, which includes the gene *LIS1*. As previously mentioned, mouse models of lissencephaly do not completely recapitulate the human phenotype. In this study, scientists were able to identify among other problems, mitotic defects in oRGs, something that was not possible in mice due to the almost complete absence of this type of cells (Bershteyn et al., 2017).

In conclusion, the development of the cortex is a very complicated process, and unfortunately, we still do not have access to the perfect technique to study all the steps. It is therefore essential to use a combination of in *vivo* and *in vitro* systems, to investigate the molecular and cellular mechanisms underlying the defects and consequently understand much better the underlying biological processes of corticogenesis.

CHAPTER 2: DCHS1 AND FAT4 AND THE SCOPE OF THIS THESIS

2.1 MUTATIONS IN DCHS1 AND FAT4 CAUSE CORTICAL MALFORMATIONS

FAT4 and *DCHS1* code for two non-classic cadherins or protocadherins that heterophilically interact with each other (Ishiuchi et al., 2009; Rock et al., 2005). They are the homologues of *dachsous (ds)* and *fat (ft)* in *Drosophila* (Rock et al., 2005). In humans, FAT4 is a 542 kDa protein, and DCHS1 is 342 kDa (Cappello et al., 2013). In mice, both are highly expressed during embryogenesis and the developing central nervous system (Badouel et al., 2015; Ishiuchi et al., 2009). More concretely, they are highly expressed in the apical portion of neuronal progenitor cells (Ishiuchi et al., 2009). They are essential for different functions such as planar cell polarity and correct organ development (Ishiuchi et al., 2009; Rock et al., 2005).

Mutations in these two genes have been associated with the autosomal recessive disorder Van Maldergem syndrome (VMS) (Cappello et al., 2013). Patients with this syndrome have a variety of clinical features such as skeletal dysplasia, limb malformations, intellectual disability and the presence of ectopic neurons lining the ventricles indicating a neuronal migration disorder resembling PH (Maldergem et al., 2008; Mansour et al., 2012; Neuhann et al., 2012).

Mouse mutants for *Dchs1* and *Fat4* show similar phenotypes indicating their interaction as ligand-receptor during embryogenesis (Mao et al., 2011). Both mutants present kidney, ear, skeleton, heart and lung problems (Mao et al., 2011; Saburi et al., 2008). However, *Fat4*−/− and *Dchs1*−/− mouse embryos do not show any neuronal migration or cortical malformation phenotypes similar to those observed in VMS patients. Moreover, due to the neonatal lethality of these mouse models, it is difficult to carry out further analysis (Mao et al., 2011; Saburi et al., 2008). Fortunately, spatio-temporal controlled downregulation of these genes has been a useful technique to understand their role in rodent cortical development. After acute downregulation of *Dchs1* and *Fat4,* there was an apparent reduction of the cells that reached the CP in mice.

The lower number of neurons was due to the reduced ability of Pax6+ progenitor cells to further differentiate in Tbr2+ intermediate progenitor and a consequent reduction of Tbr1+ neuron generation (Cappello et al., 2013).

In this study, it was also possible to confirm that these alterations in the development of the cortex of these mice were due to the disrupted Hippo pathway. The effector Yap in this pathway acts downstream of Fat4 and Dchs1 and has a role in the maintenance of the pool of progenitors and correct differentiation during cortical development (Cappello et al., 2013).

We have also studied the role of *DCHS1* and *FAT4* in humans, and interestingly there may be a species-specific role of the proteins. Taking advantage of the iPSCs technology and 3D culturing systems, we were able to generate COs from patients with mutations in *DCHS1* and *FAT4.* Interestingly, the COs from these patients show the presence of ectopic clusters of neurons next to the ventricles recapitulating partially, in contrast to mouse models, the human phenotype (Klaus et al., 2019). As explained in the introduction, there are two main reasons why neurons are not able to migrate to the correct place during cortical development and therefore produce PH. The first one is the disruption of the scaffold that neurons need to migrate; that is, radial glial cells. In the COs derived from patients, radial glial cells present a disrupted morphology. Moreover, data obtained from scRNA-seq showed that patient COs had a higher number of cells belonging to the iSVZ and oSVZ as well as the CP at the expense of the cells in the VZ (**Fig 2.1**). The disruption of radial glia cells shown in patient COs is probably due to premature delamination from the apical belt which may induce an early differentiation of progenitors and problems for the generated neurons to migrate to the correct place.

The second known reason for the generation of the ectopic cluster of neurons is inherent problems in those cells. After performing live imaging of patient neurons, it was possible to identify a group of neurons with an altered neuronal migration dynamic. These neurons were slower and did not show a straight trajectory, typical of excitatory neurons. Additionally, sc-RNA seq confirm the presence of a subpopulation of neurons with an altered neuronal state. From the transcriptomic data, it was possible to identify neurons from *DCHS1* and *FAT4* COs that did not follow a "correct" differentiation trajectory (**Fig 2.2b**) but instead took an alternative path. This alternative trajectory is characterised by the different regulation of some genes (**Fig2.2c**).

Interestingly, most of the genes that were upregulated are essential for basic neurodevelopmental processes such as neuronal migration (*NDNF*), axon guidance (*ROBO3, DCC*, *EFNA3*, *EPHB3*, *CNTN2*), patterning (*HOX*) or progenitor pool maintenance (*GNG5*). The genes that were downregulated are also essential for other developmental steps such as synapse formation (*GRIA2*), cytoskeleton (*SNCA*, *MAPT*, *MAP1B*, *SPTAN1*) or axon guidance (*FLRT2*). Moreover, some of the genes already mentioned have been associated with epilepsy and seizures and even PH (*MAPT*, *MAP1B*, *STAN1*) (Heinzen et al., 2018; Klaus et al., 2019).

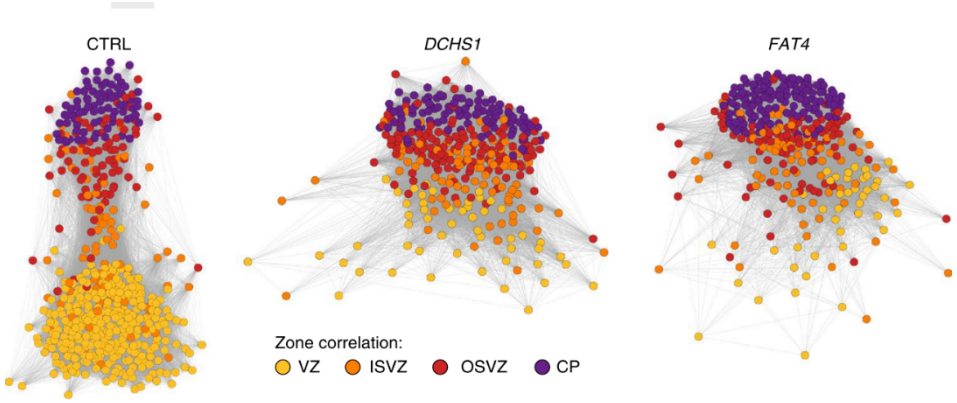

Figure 2.1: Pairwise correlation network.
Single-cell RNA sequencing data from *DCHS1* and *FAT4* mutant COs reveal a different distribution of individual cells in the different areas of the developing COs. Most of the cells in *FAT4* and *DCHS1* COs belong to the iSVZ, oSVZ and CP while in control COs there is a clear cluster of cells belonging to the VZ, lost in patients COs. Abbreviations: VZ: ventricular zone; iSVZ: inner subventricular zone; oSVZ: outer subventricular zone; CP: cortical plate. (Klaus et al., 2019).

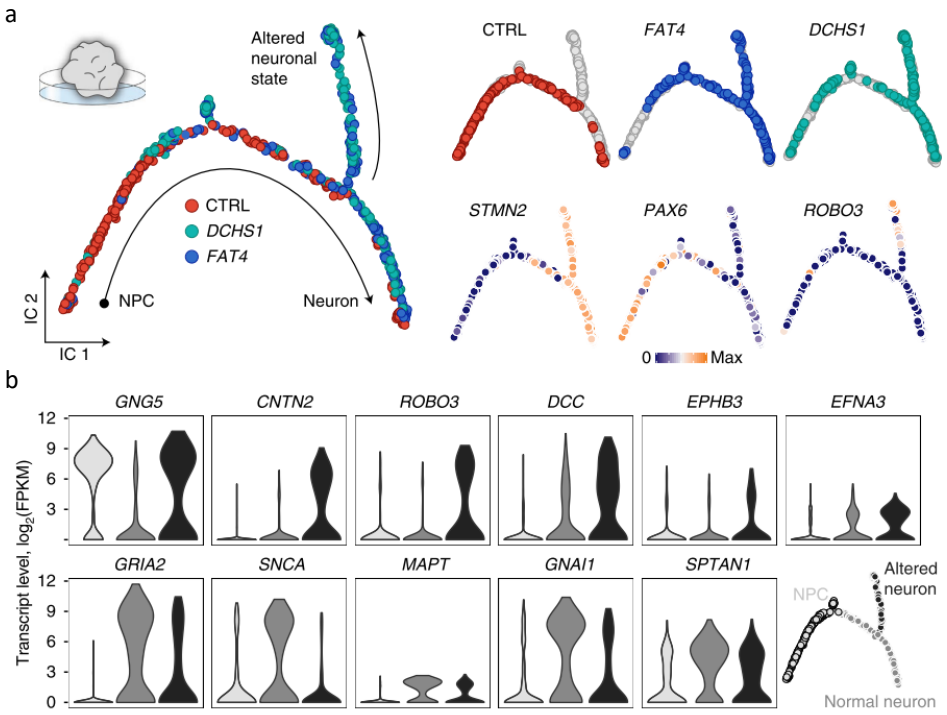

Figure 2.2: scRNA-seq reveals a cluster of neurons with an altered neuronal state.
(a) Monocle2 lineage reconstruction of all single cells from all three organoid using the genes identified by PCA. The results reveal an altered group of neurons in the mutant COs that have a different differentiation trajectory. The three top panels indicate the NPC-Neuron differentiation trajectory of all the cells in control, *FAT4* or *DCHS1* COs. The three bottom right panels show the expression levels of example genes for neurons (STMN2), NPCs (PAX6) and the altered neuronal state (ROBO3) during the NPC-Neuron differentiation trajectory. (b) Violin plots show the expression levels of some of the genes that are upregulated (top) or downregulated (bottom) in the altered neuronal population (black) compared with healthy neurons (dark grey) and NPCs (light grey) (Klaus et al., 2019).

2.2 SCOPE OF THIS THESIS

All these studies have highlighted the importance of DCHS1 and FAT4 during cortical development. Moreover, it has also been possible to identify a subset of neurons with an altered neuronal state that resembles what we see in humans with PH in which only some neurons do not reach their destination in the developing cortex.

Among the genes, *GNG5* is the top differentially regulated gene. *GNG5* is highly expressed in neuronal precursor cells and is downregulated when they differentiate to neurons. However, the altered subpopulation of neurons keeps expressing this gene. The results indicate a possible role of GNG5 in correct cortical development. In **Chapter 4**, I will investigate the function of this gene during the development of the cortex.

Patients with PH frequently have intractable epilepsy. Analysis of *DCHS1* and *FAT4* mutant COs revealed that many of the genes differentially regulated in the altered subpopulation of neurons are essential for axon guidance and synapse formation. This data suggests that mutations in *DCHS1* and *FAT4* may alter the correct function of neurons in patients. In **Chapter 5,** I will characterise *DCHS1* and *FAT4* COs at later time points when they are functionally mature. By looking at the RNA and electrophysiological properties of the COs, it will be possible to better understand the functional role of DCHS1 and FAT4 in these patients.

Finally, as explained during the introduction, looking at evolutionary changes in genes among different species has allowed us to understand in more detail how the human brain develops as it does. However, our closest living relative, the chimpanzee, and our ancestors diverged 6 million years ago (Fiddes et al., 2018) and the information we can get evolutionarily speaking is limited. Fortunately, researchers from the Max Planck Institute of Evolutionary Anthropology were able to sequence the genome of our closest extinct relative, the *Homo neanderthalensis* (Green et al., 2010). Interestingly, when comparing their genome to the human genome, only 78 proteins were found to be different between humans and the Neanderthals, who kept the ancestral form of the proteins. Fascinatingly, DCHS1 was one of those proteins. In **Chapter 3**, I will investigate the possible role of DCHS1 in human brain evolution using COs carrying the “neanderthalized” *DCHS1* mutation.

In summary, after combining the data obtained from these three different projects, I will show the importance of DCHS1, FAT4 and GNG5 in human brain evolution and development with the final aim to bring knowledge to the field of cortical development and help in the future design of treatments for these patients.

In **Chapter 3**, I will show the results of the project:

The role of DCHS1 in human brain evolution

This project has been done in collaboration with Stefan Riesenberg in the group of Prof. Dr Svante Pääbo at the Max Planck Institute of Evolutionary Biology.

Stefan Riesenberg generated the CRISPR/Cas9 cells used in the experiments that were performed by me.

CHAPTER 3: THE ROLE OF DCHS1 IN HUMAN BRAIN EVOLUTION

3.1 HUMAN BRAIN EVOLUTION

The expansion of the brain and more precisely the neocortex and concretely the prefrontal cortex has been associated with increased intellectual, cognitive, emotional and social abilities in humans (Cikili-Uytun, 2018; Fuster, 2002; Pirozzi et al., 2018; Roth and Dicke, 2005). Understanding which are the evolutionary changes behind these differences will help us to comprehend the complex process behind human brain development and the characteristics that make it so exceptional.

As mentioned in **Chapter 1** of this thesis, there are many reasons behind the differences between the brain of humans and other species in terms of development, including changes in the proportion of progenitor cells, the presence of a more complex extracellular material and the expression of genes that are specific to primates or humans are some of them. The only way for scientists to find these differences and understand the evolutionary changes that have driven human brain development has been to compare it to the brain of different animals. While the information collected has widely increased the knowledge of human brain development, it still does not allow us to appreciate the full image of human brain evolution. An alternative method to study human brain evolution has been to study the remains of our extinct ancestors. The access to soft tissue such as the brain is, of course, impossible. However, access to the endocasts or fossils has helped researchers to understand the differences with the brain of our ancestors. These studies have given scientists a better idea of the small changes that allowed the human brain to acquire higher cognitive and intellectual abilities and made us interact with the world as we do.

In the next part, I will explain the essential discoveries that have been made regarding the differences between modern human and the *Homo sapiens neanderthalensis* or Neanderthals, our closest extinct relative. Modern humans and Neanderthals shared the same common ancestor.

3.1.1 What do we know about the differences of the *Homo sapiens neanderthalensis* and *Homo sapiens sapiens* brain?

Neanderthals lived in Europe and western Asia between 300.000 and 30.000 years ago and partially coexisted with modern humans. Scientists have stipulated that the gene divergence between modern humans and Neanderthals is between 550 and 789 million years ago (MYA) (**Fig 3.1**) (Beerli and Edwards, 2003; Krings et al., 1997). Since the discovery of the first Neanderthal fossils, anthropologists have tried to find the most noticeable differences with the modern human.

Some scientists indicated that the average adult brain size of Neanderthals is similar or slightly larger than that of the modern humans (Holloway, 1981; Pereira-Pedro et al., 2020; Ponce De León et al.,

2008) while at birth, the brain size was comparable (Ponce De León et al., 2008). Additionally, it has been found that full brain growth in Neanderthals was delayed in comparison to modern humans (Rosas et al., 2017). This data could indicate an extended developmental period which may result in a larger brain (Ponce De León et al., 2008). However, it is very difficult to state the truthfulness of these data due to the limited amount of material to be studied. Moreover, it is still unclear if the extended brain growth could be due to an intrinsic difference in the growth rate or due to energetic constraints (Ponce De León et al., 2008; Rosas et al., 2017).

Studies comparing the endocranial space between modern humans and Neanderthals have also shown differences in brain shape (De Sousa and Cunha, 2012; Gunz et al., 2010; Neubauer et al., 2018; Pereira-Pedro et al., 2020), the visual cortex (Pearce et al., 2013) and the cerebellum (Kochiyama et al., 2018). The Neanderthal brain is elongated while the modern human brain has a globular structure (De Sousa and Cunha, 2012; Gunz et al., 2010; Neubauer et al., 2018; Pereira-Pedro et al., 2020). The globularization phase that happens after birth is believed to be a characteristic specific to the modern human brain. This phase may have been essential for brain reorganization, which induces associated cognitive abilities and helped in the positive selection of modern humans (Gunz et al., 2012). In 2019 scientists integrated palaeoanthropology, comparative genomics, neuroimaging, and gene expression to shed light on this question (Gunz et al., 2019) and they found that some Neanderthal alleles could be involved in generating a more elongated brain shape. These alleles influence genes essential for neurogenesis and could induce a reduced proliferation which may lower the overall globularity (Gunz et al., 2019). The authenticity of this theory is, however, under debate. In 2016 (Ponce de León et al., 2016) found opposite results after studying an extended sample of Neanderthal infants. They claimed that Neanderthal and the modern human at birth had different endocranial morphology but shared a similar postnatal model of endocranial development, indicating that maybe modern human and Neanderthal cognitive capacities were the same or at least similar. The question if this developmental feature was already found in their last common ancestor or it developed in parallel in both species remains elusive (Ponce de León et al., 2016).

In summary, endocast studies have partially answered questions regarding the size, growth length or shape of the Neanderthal brain and similarities with the modern human brain. However, the possibility to access soft tissue limits a lot what we can know about the evolutionary differences between Neanderthals, modern humans and our last common ancestor and many questions remain to be answered. Which are the changes that made the development of the modern human brain possible? Are our intellectual and cognitive abilities specific to modern humans? Or did the Neanderthals and our last common ancestor have those abilities? These questions will be, of course,

complicated to answer, but progress in technology will help us to improve our methodology and start answering some of those questions.

Thanks to the advances in human genetics, it has been possible to look at the genome of the *Homo sapiens neanderthalensis*, our closest evolutionary relative (Green et al., 2010). Modern humans and Neanderthals have the same common ancestor. In consequence, by looking at the genomic difference with Neanderthals, it has been possible to identify the genetic variations that give rise to the modern human. In this study, scientists were able to identify 78 nucleotide changes that altered the protein-coding capacity of genes in modern humans and differ with the ones found in the Neanderthal genome that carry the ancestral form (Green et al., 2010). By studying these changes, we could have a better understanding of the role of these proteins, and how through evolution they have allowed the modern human brain to become what it is now. Interestingly DCHS1 (or PCD16; Protocadherin-16) is one of the proteins with a substitution in the amino acid at the position 777. The change from the ancient aspartic acid (N) that is present in Neanderthals to the modern asparagine (D) that is present in humans (N777D) (**Fig 3.2**), indicates a human-specific change in the DCHS1 protein. DCHS1 has a critical role in correct cortical development, as described previously (Cappello et al., 2013; Klaus et al., 2019). In this chapter, I will investigate its developmental role in the modern human brain through the context of evolution, by studying the human and ancient variants.

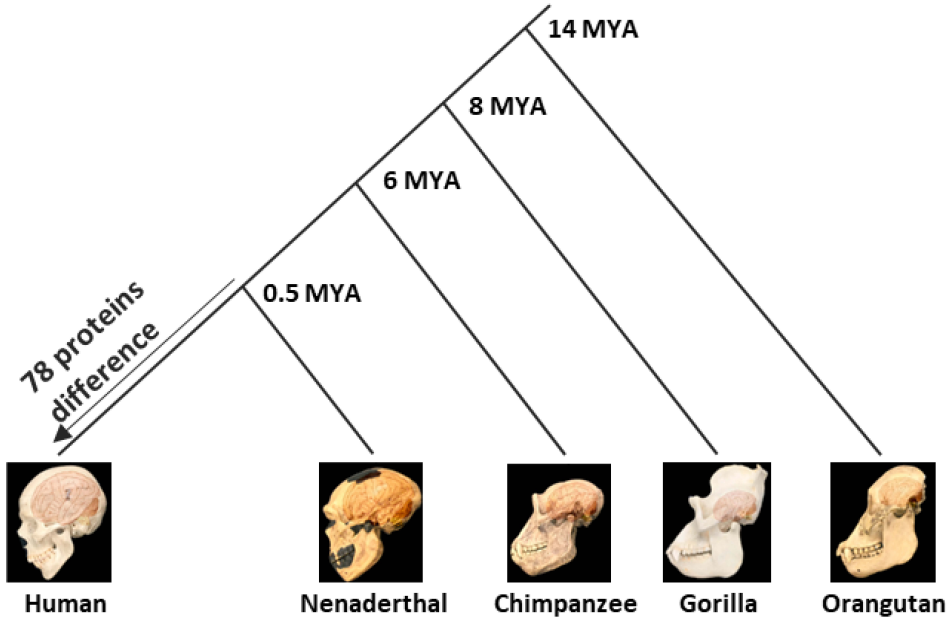

Figure 3.1: Primate phylogenetic tree.
Phylogenetic tree including some of the most representative primates. In its branch we can see how many years ago the two species diverged. In the genomes of modern humans and Neanderthals there only 78 loci with nucleotide substitutions in which Neanderthals keep the ancestral form. It is also possible to distinguish the difference elongation pattern of the Neanderthal and the human brain. Figure adapted from (Fiddes et al, 2018).

3.1.2 How can we study human brain evolution in the laboratory?

In collaboration with the group of Svante Pääbo in the Max Planck Institute of Evolutionary (MPI EVA) Biology, we have been able to study "DCHS1 neanderthalized COs" that contain the ancestral form of the protein. Thanks to the CRISPR/Cas9 technology our collaborator Stephan Riesengberg in the MPI EVA generated human iPSCs with the ancestral mutation D777N (asparagine (D) in modern humans and aspartic acid (N) in Neanderthals), that is present in the Neanderthals and not in modern humans (**Fig 3.2**). DCHS1 has a critical role in mouse and human brain development, by regulating progenitor pool maintenance and neuronal migration. Therefore, we believe it is an excellent candidate to have an essential role in human brain evolution. Using the "neanderthalized COs", we have investigated the changes that D777N may have induced in the cell cycle and neuronal migration that could explain some of the differences between the human brain and the brain of our last common ancestor with the Neanderthals.

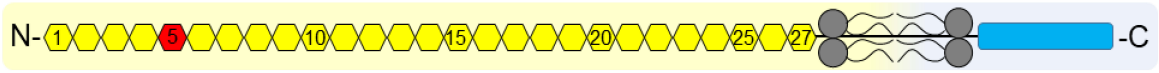

Figure 3.2: Schematic representation of DCHS1 protein.
This figure illustrates the structure of the Human and Neanderthal protocadherin. DCHS1 has 27 (hexagons) cadherin repeats. In red is represented the cadherin where the human and Neanderthal variation is located. In blue is the intracellular region of the protein. Figure adapted from (Klaus et al., 2019), courtesy of Melina Vaki.

3.2 RESULTS

3.2.1 The N777D change is specific to modern humans

N777D is an amino acid change that is present in humans but not in our closest extinct relative the Neanderthals. More concretely, while Neanderthals kept the ancestral form of the protein, modern humans acquired a different amino acid at position 777. To confirm that this change in the sequence was human-specific we aligned the FASTA sequences of DCHS1 obtained from NCBI from different primates including the one of modern humans, together with the Neanderthal sequence, changed manually according to (Green et al., 2010; Prüfer et al., 2014). Interestingly, the alignment obtained with the MAFFT program on UniPro UGENE confirmed that the specific change from asparagine (N) to aspartic acid (D) only happened in humans (**Fig 3.3**).

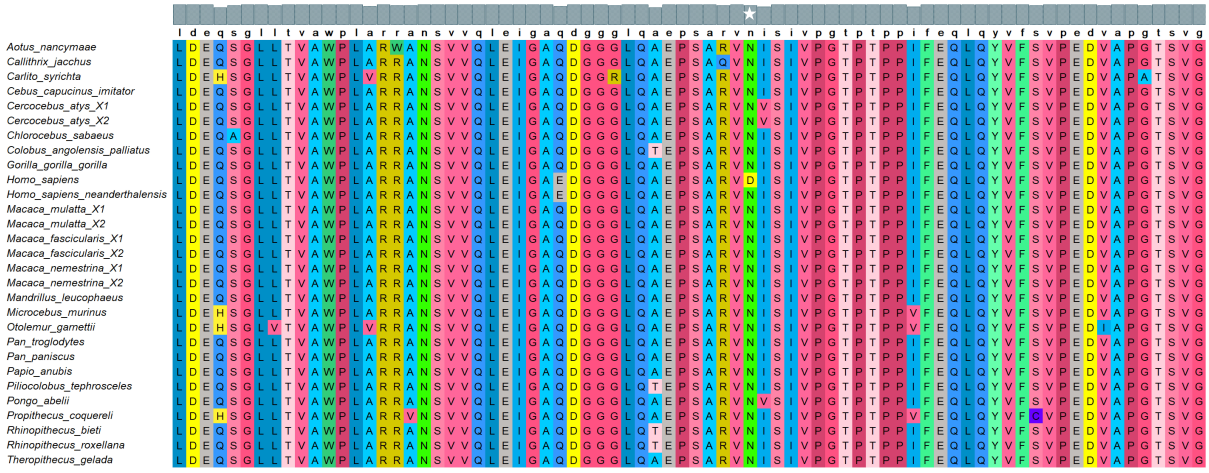

Figure 3.3: N777D is a unique change that only happens in modern humans.
Screenshot of the MAFFT alignment of the primate DCHS1 protein. The sequence of DCHS1 primate proteins were obtained with the Unipro UGENE program. The alignment shown in the pictures corresponds to the 735-810 amino acids according to the human coordinates. The species' names are on the left and are shown in alphabetical order. The consensus sequence for DCHS1 is shown on top and the grey bars indicate the frequency of the consensus amino acid. The position 777 is marked with a white star.

3.2.2 The N777D change may have induced a loss of an N-glycosylation site in modern humans

To investigate what changes the N777D substitution could induce in the human DCHS1 protein, we looked at different aspects of the structure and post-translational modifications of the protein. Interestingly, we found a difference in one type of post-translational modifications. We used the online platform NetNglyc which predicts the likelihood of glycosylation of the asparagine (N) amino acids in a protein sequence (Gupta et al., 2004). Interestingly, the asparagine (N) at position 777 is predicted to be glycosylated, meaning that the modern DCHS1 + loses an N-glycosylation site since aspartic acid (D) cannot be glycosylated (**Fig 3.4**). How this loss alters the function of the modern DCHS1 compared to the ancient one remains elusive and is something we would like to further investigate.

Position	Potential	Jury agreement	N-Glyc result	Position	Potential	Jury agreement	N-Glyc result
217 NRSH	0.5949	(6/9)	+	217 NRSH	0.5949	(6/9)	+
256 NQSR	0.6041	(8/9)	+	256 NQSR	0.6041	(8/9)	+
402 NVSL	0.7107	(9/9)	++	402 NVSL	0.7107	(9/9)	++
584 NASL	0.5574	(5/9)	+	584 NASL	0.5574	(5/9)	+
777 NISI	0.5959	(8/9)	+				
1249 NGTI	0.5482	(7/9)	+	1249 NGTI	0.5482	(7/9)	+
1521 NASR	0.4224	(8/9)	-	1521 NASR	0.4224	(8/9)	-
1718 NLTV	0.5936	(8/9)	+	1718 NLTV	0.5936	(8/9)	+
1996 NASI	0.3501	(8/9)	-	1996 NASI	0.3502	(8/9)	-
2361 NLTV	0.7066	(9/9)	++	2361 NLTV	0.7066	(9/9)	++
2428 NGTL	0.5511	(7/9)	+	2428 NGTL	0.5511	(7/9)	+

Figure 3.4: Modern DCHS1 may have lost an N-glycosylation site at position 777.
Results from the NetNglyc online platform for the ancient (left) and modern (right) variants of DCHS1. A result is considered as positive above 0.5 threshold. The arrow indicates the "lost" N-glycosylation site.

3.2.3 The D777N change may induce a reduced progenitor pool in the "neanderthalized" COs

To understand how the modern aspartic acid (D) in position 777 of the DCHS1 protein that is only present in modern humans may have altered the structure or development of the human brain, I generated COs (control) with the human sequence and COs with the ancient asparagine (N) in position 777. From now on this "neanderthalized" COs that contain the ancient asparagine (N) will be called D777N COs.

It was clear from the very beginning that even though there are only 78 loci that differ between modern humans and our closest extinct relatives, studying only one of those altered proteins would make it difficult to find a distinct phenotype or major differences between the control and the D777N COs. Therefore, we focused our efforts on doing a full characterization of the COs to have a good overview of possible differences.

First, I decided to investigate any possible differences in the number or identity of NPCs in the COs as they will give rise to the rest of the cells. I looked at the levels of PAX6+ progenitor via FACS at two different time points, at 30 days when COs are still young and start presenting a germinal zone-like area (GZL) and a cortical plate-like area (CPL) and at 60 days in which both structures are clearly distinguished. The number of PAX6+ cells was significantly reduced in the D777N COs both at 30 and 60 days (**Fig 3.5 A-E**). These data indicate that D777N COs contain a lower number of PAX6 dorsal progenitors. I also examined the thickness of the GZL identified by PAX6 staining. I analysed different ventricular-like cavities (VLs) surrounded by clear PAX6+ GZL in different control and D777N COs at 3 different time points: 30, 60 and 75 days. More concretely I measured the thickness of the PAX6+ GZL. In the D777N COs, the PAX6+ GZL was significantly thinner than in controls at 30 and 60 days (**Fig 3.5 F-I, L**). However, at 75 days the thickness was more similar, still with a tendency for thinner GZL in the D777N COs (**Fig 3.5 F, G, J, L**). By looking at the trajectory of the PAX6 thickness at the 3 different time points normalized to the thickness at day 30, while the increase in the thickness over time is quite stable in control COs, D777N COs show a faster increase indicating that in D777N COs they may reach the same GZL thickness but that they need more time (**Fig 3.5 K**).

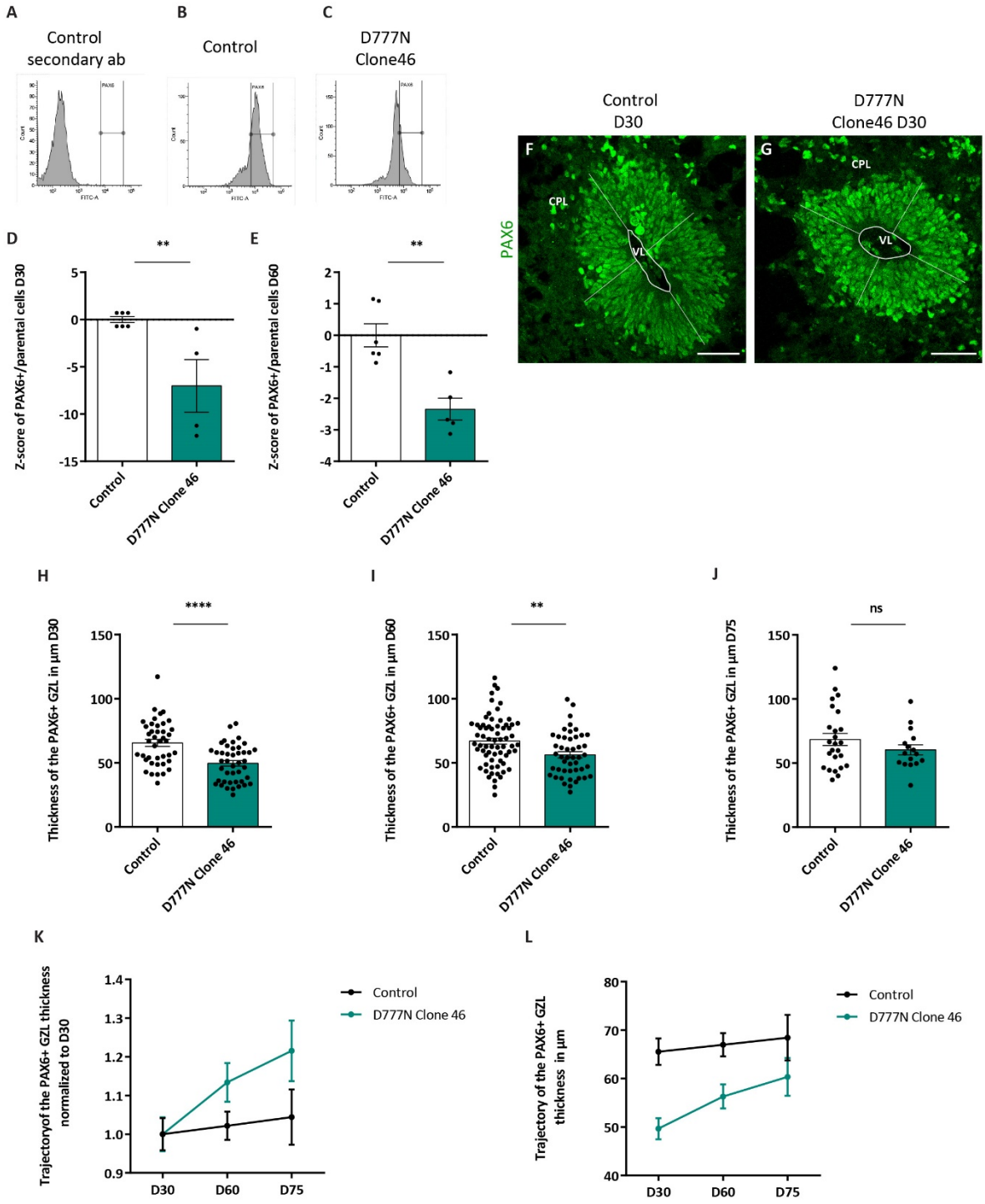

Figure 3. 5: D777N COs present a thinner GZL.

(A-C) Representative pictures of the FACS strategy used to select the PAX6+ cells. (A) Secondary control without any PAX6+ cells detected. (B, C) Control and D777N COs with PAX6+ cells. (D, E) Z-scores of the PAX6+ cells per parental cell at (D) 30 days and (E) 60 days. (F, G) Representative pictures of PAX6+ GZL in (F) control and (G) D777N. The lines show the way how the width of the GZL was measured. (H-J) Quantification of the thickness of the PAX6+ GZL of different VLs at (H) 30 days, (I) 60 days and (J) 75 days. (K) Graph representing the trajectory of the PAX6+ GZL thickness normalized to day 30 in control and D777N COs. (L) Graph showing the thickness of the PAX6+ GZL in the control and D777N VLs at the 3 different time points in µm. FACS and PAX6 thickness statistical analysis were based on Mann-Whitney U-test, **** $p<0.0001$ and ** $p < 0.01$. FACS PAX6+ 30 days: Control batches (b)=3, COs (o)=18; D777N b=2, o=12 and 60 days Control b=3, o=18; D777N b=2, o=15. PAX6+ thickness 30 days b=2, o=10, ventricles (v)= 41; D777N b=2, o=9, v= 43 and 60 days Control: b=2, o=16, v=67; D777N b=2, o=13, v=47 and 75 days Control: b=1, o=6, v= 25; D777N b=1, o=7, v=16. Data shown as mean ± SEM. Scale bars: (F, G) 50µm. Abbreviations: CPL: cortical plate-like area, GZL: germinal zone-like area ns: no significant, VL: ventricle-like cavities.

3.2.4 D777N COs do not show a reduced proliferative capacity of progenitors

To determine if the reduced number of PAX6+ cells and the thinner PAX6+ GZL found in the D777N COs could be due to a reduction of the proliferative capacity of the progenitors in the D777N COs, I looked at two different parameters: the length of the apical belt and the number of apical dividing cells stained with the mitotic marker phospho-histone H3 (PH3) at 30, 60 days and 75 days.
The length of the apical belt was similar both in control and D777N COs at the 3 time points (**Fig3.6 A-E, G**). This data indicates that the decrease in the number of PAX6+ cells does not induce a general reduction of the GZL, but only a reduction of the thickness of the GZL. Interestingly, when I looked at the trajectory of the length of the apical belt normalized to day 30, it seems that while in controls the apical belt length stops growing at day 75, in D777N COs the length of the apical belt was still growing (**Fig 3.6 F**). It is well known that COs stop growing after a few weeks in culture. This is the time when neurons start maturing and neuronal networks start developing. This data could indicate that the GZLs of the D777N COs could continue expanding for a longer period while control COs stop.

The number of PH3+ cells in the apical belt that indicates the number of dividing aRGs was also the same in control and D777N COs at the 3 different time points (**Fig 3.7 A-E, G**). This data indicates that the reduced number of PAX6+ cells in D777N and the reduction in the thickness of the PAX6+ GZL was not due to a reduction in the proliferative capacity of the aRGs. Finally, in contrast to what I saw with the trajectory of the length of the apical belt, the number of apical PH3+ cells was reduced over time in the same way in control and D777N COs (**Fig 3.7 F**), indicating that again that the number of apical PH3+ cells was not only the same between controls and D777N but that the reduction over time of mitotic cells had the same tendency.

Why the number of apically diving cells was the same, but the thickness of the GZL was reduced in the D777N COs could be explained by the way those aRGs divide. Vertical or symmetrical division gives rise to the same daughter cells, if the division is proliferative the cells will have the same identity as the mother cell and if the division in consumptive or neurogenic the daughter cells will be different. The horizontal and oblique division also known as the asymmetric division will produce two daughter cells with a different identity. If the asymmetric division is self-renewing one of the daughter cells will have the same identity as the mother cell while if it is consumptive both daughter cells will have an identity different to the mother cell (Taverna et al., 2014).

By looking at the way the cells divide apically we can therefore hypothesise the reason behind the reduced number of PAX6+ and thinner GZL but the same number of dividing cells.

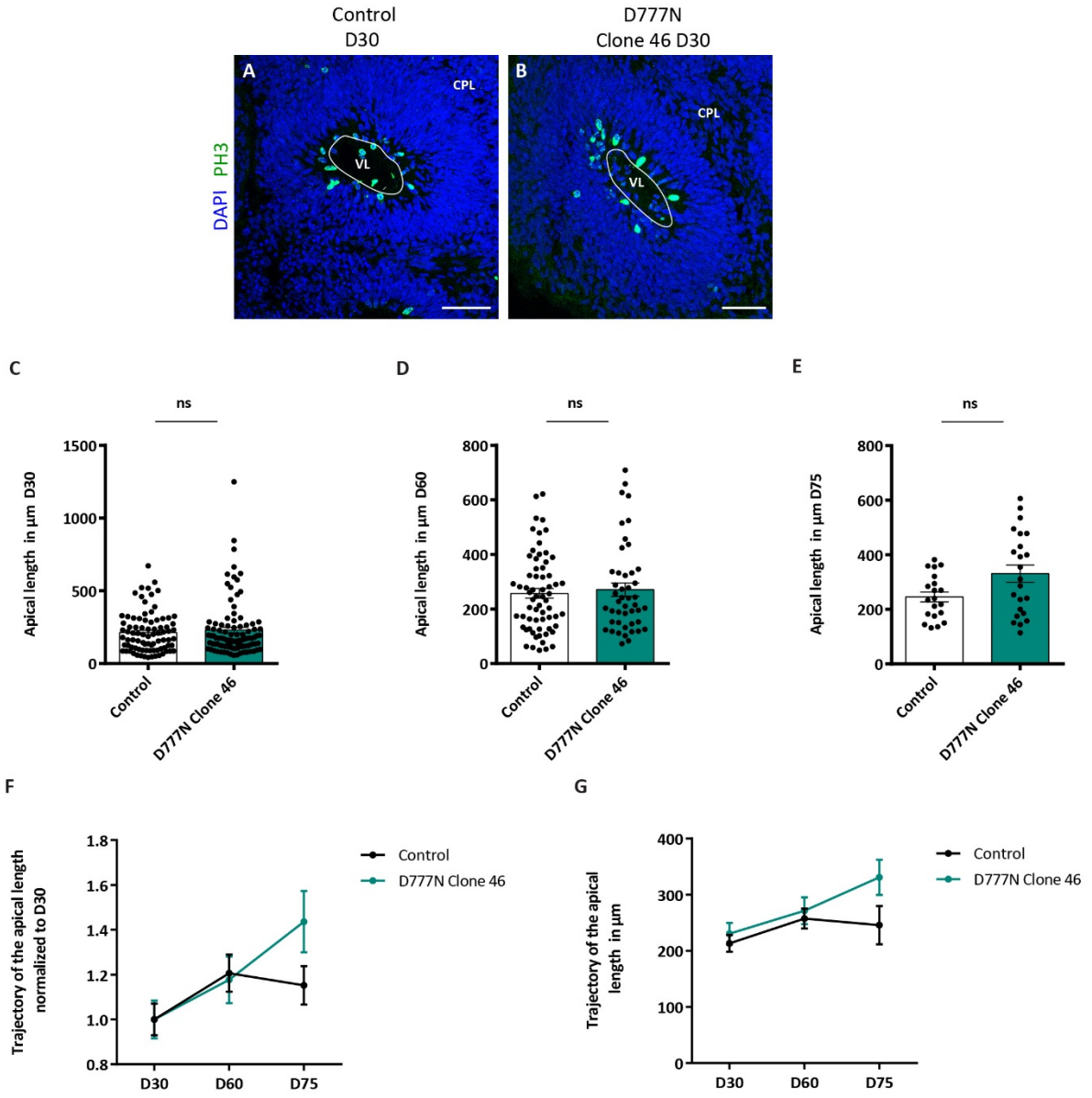

Figure 3. 6: Control and D777N COs have the same apical belt length.

(A, B) Control and D777N COs stained with the PH3 marker. The line above the VL represents the line used to measure the length of the apical belt. (C-E) Quantification of the length of the apical belt at (C) 30 days, (D) 60 days and (E) 75 days of different VLs. (F) Graph representing the trajectory of the length of the apical belt normalized to day 30 in control and D777N COs. (G) Graph showing the length of the apical belt in control and D777N COs at the 3 different time points in µm. Statistical analysis was based on Mann-Whitney U-test. Apical length: 30 days b=2, o=16, v= 84; D777N b=2, o=16, v= 99 and 60 days Control: b=2, o=16, v=65; D777N b=2, o=12, v=46 and 75 days Control: b=1, o=5, v= 20; D777N b=1, o=10, v= 23. Data shown as mean ± SEM. Scale bars: (A, B) 50µm. Abbreviations: CPL: cortical plate-like area, GZL: germinal zone-like area ns: no significant, VL: ventricle-like cavities.

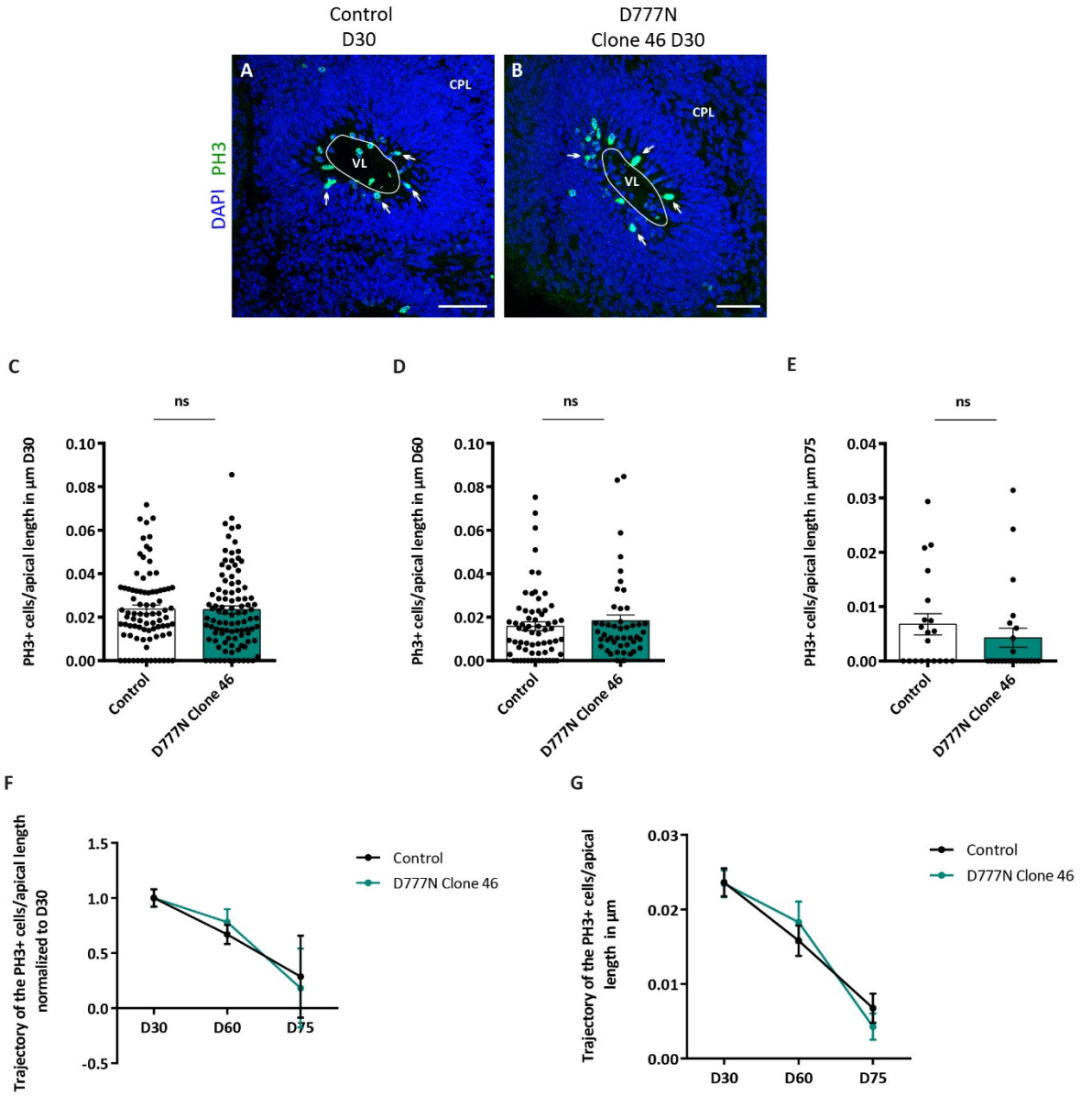

Figure 3. 7: Control and D777N COs have the same number of apically diving cells.

(A, B) Control and D777N COs stained with the PH3 marker. The line above the VL represents the line used to measure the length of the apical belt and the arrows indicate the PH3+ cells (C-E) Quantification of the number of PH3+ cells divided by the length of the apical belt at (C) 30 days, (D) 60 days and (E) 75 days of different VLs. (F) Graph representing the trajectory of the of the number of PH3+ cells divided by the length of the apical belt normalized to day 30 in control and D777N COs. (G) Graph showing the length of the number of PH3+ cells divided by the length of the apical belt in control and D777N COs at the 3 different time points in µm. Statistical analysis was based on Mann-Whitney U-test. PH3+ cells: 30 days b=2, o=16, v= 84; D777N b=2, o=16, v=99 and 60 days Control: b=2, o=16, v=65; D777N b=2, o=12, v=46 and 75 days Control: b=1, o=5, v=20; D777N b=1, o=10, v=23. Data shown as mean ± SEM. Scale bars: (A, B) 50µm. Abbreviations: CPL: cortical plate-like area, GZL: germinal zone-like area ns: no significant, VL: ventricle-like cavities.

3.2.5 D777N COs contain more vertically diving cells

To determine the way cells divide I looked at the spindle orientation of the dividing cells. By looking at the cells in telophase by PH3 and DAPI staining it was possible to determine the angle of division of the proliferative cells in the apical belt. If the angle of the dividing cell with the apical belt was between 0 and 60°C it was judged as horizontal-oblique division while if the angle was between 60 and 90° the division was considered vertical. This way of measuring was adapted from (Iefremova et al., 2017). The results indicated that D777N COs contain a higher number of vertically or symmetrically diving apical cells both at 30 and 60 days. The difference is significant at 30 days and it has the same tendency at 60 days (**Fig 3.8**). This data indicates that in D777N COs more cells are dividing symmetrically in the apical site. Considering the reduced number of PAX6+ cells and the thinner PAX6+ GZL it could be that there is an increased consumptive symmetrical division.

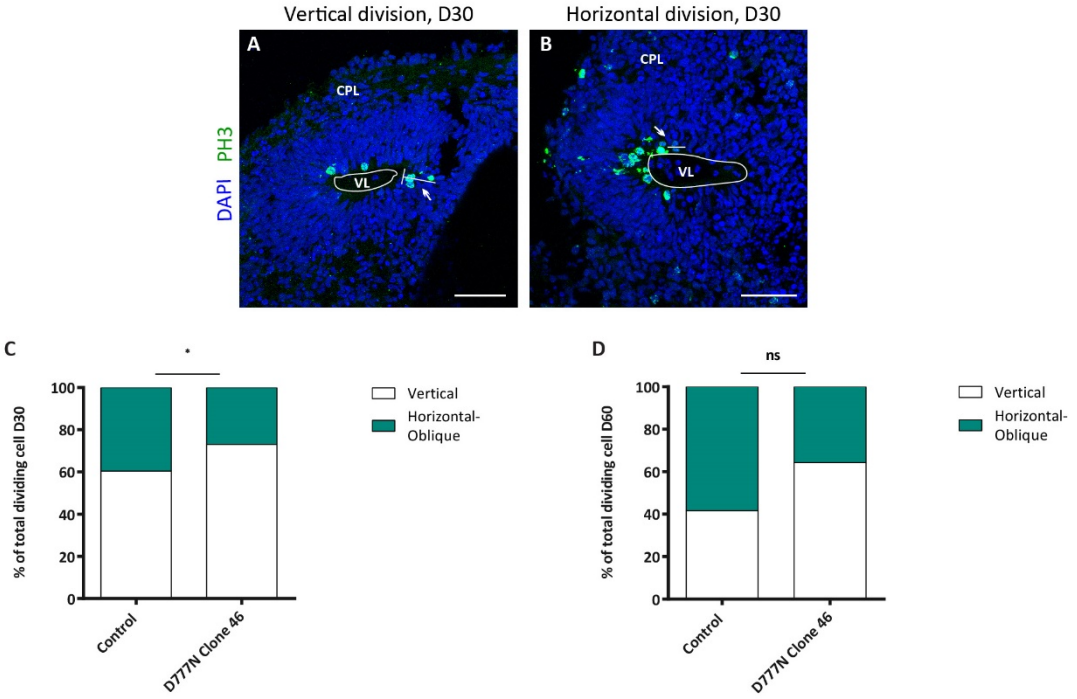

Figure 3.8: D777N COs contain more vertically diving cells in the apical belt.
(A, B) Control and D777N COs stained with the PH3 marker. The line above the VL represents the line used to measure the length of the apical belt and the arrows and thinner lines indicate the plane of the cell division. (C, D) Percentage of the number of PH3+ cells dividing vertically or horizontal-obliquely at (C) 30 days and (D) 60 days. Statistical analysis was based on exact binomial test, * $p<0.05$. Cell division: 30 days b=2, o=18, v= 36, cells (c)= 53; D777N b=2, o=19, v=58, c=85 and 60 days Control: b=2, o=12, v=20, c=24; D777N b=2, o=11, v=12, c=14. Scale bars: (A, B) 50µm. Abbreviations: CPL: cortical plate-like area, ns: no significant, VL: ventricle-like cavities.

3.2.6 D777N COs do not contain fewer IPs

An increased number of IPs could be the consequence of consumptive symmetrical division. Therefore, using the IP marker TBR2, we looked at the number of TBR2+ cells per GZL area in control

and D777N COs at 30 and 60 days (**Fig 3.9**). The results indicated that at 30 days there is a reduced number of TBR2+ cells in the D777N COs while at 60 days there is a tendency for the same result. Surprisingly, all together, these data are in contrast with the more vertical or symmetric division as we observed a general reduction in progenitors, both PAX6+ cells and TBR2+ cells and a thinner GZL in D777N COs.

Therefore, to shed new light on the mechanism underlying the phenotype, I also looked at the neuronal migration and maturation on the control and D777N COs.

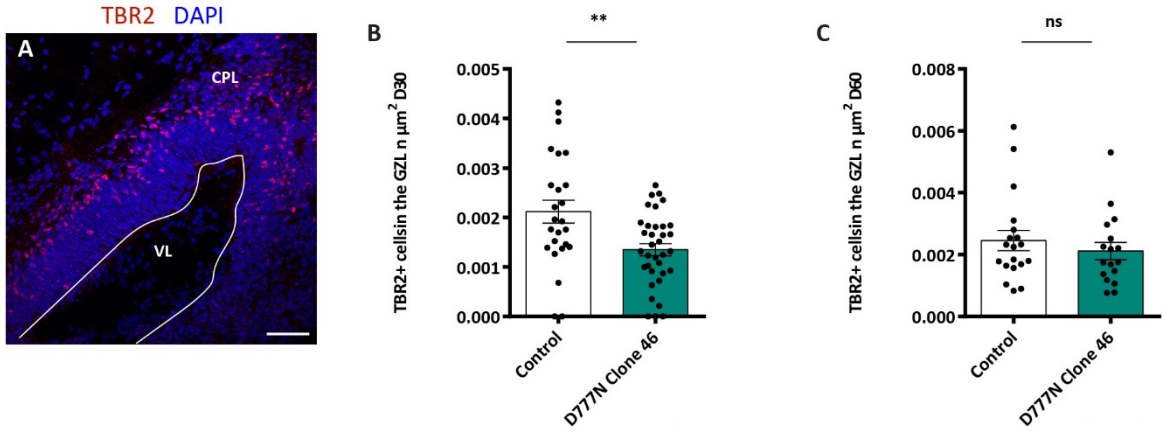

Figure 3.9: D777N COs do not contain fewer IPs.

(A) Representative picture of a CO stained with the IP marker TBR2. (B, C) Quantification of the number of TBR2+ cells in the GZL at (B) 30 days and (C) 60 days. Statistical analysis was based on Mann-Whitney U-test, ** p<0.01. TBR2+ cells: 30 days b=2, o=5, v= 25; D777N b=2, o=6, v=35 and 60 days Control: b=1, o=4, v=19:; D777N b=1, o=3, v= 17. Scale bars: (A) 50µm. Abbreviations: CPL: cortical plate-like area, GZL: germinal zone-like area, IP: intermediate progenitor, ns: no significant, VL: ventricle-like cavities.

3.2.7 The D777N change may induce neuronal migration defects

To study the possible differences between neurons and/or neuronal migration between control and D777N I performed different types of analysis. Through FACS I analysed the total number of early-born neurons using the appropriate marker DCX at 30 and 60 days (**Fig 3.10 A-E**). While at 30 days the number or level of DCX+ cells were not significantly reduced in D777N COs (**Fig 3.10 D**) at day 60 there was a clear reduction (**Fig 3.10 E**). A reduced number of PAX6+ cells and TBR2+ cells in the D777N COs could easily explain these results. If there is a lower number of progenitors, it is also expected to see a reduction in the number of neurons.

Apart from quantifying the total number of neurons I also examined the migration dynamics of those cells. At 30 and 60 COs contain differentiated GZL and CPL areas. By using the DCX marker I looked at the number of VLs with a clear (**Fig 3.10 F**) GZL or with processes (**Fig 3.10 G**) and cell bodies (**Fig 3.10 H**) inside the GZL. While at 30 days we can expect some migrating neurons, at 60 days most of the neurons should have reached the CPL. The results indicate that at 30 days control and D777N COs present a similar percentage of VLs with the presence of DCX+ processes and cell bodies in the GZL

(**Fig 3.10 I**). However, at 60 days while in controls the percentage of VLs with either processes or neuronal cell bodies was reduced, in D777N it increased, especially the percentage of VLs with neuronal DCX+ cell bodies in the GZL (**Fig 3.10 J**). This data indicates that at 60 days not only there was a total reduction in the number of DCX+ cells or a reduced expression of DCX by these cells, but that those neurons also have some migratory alterations.

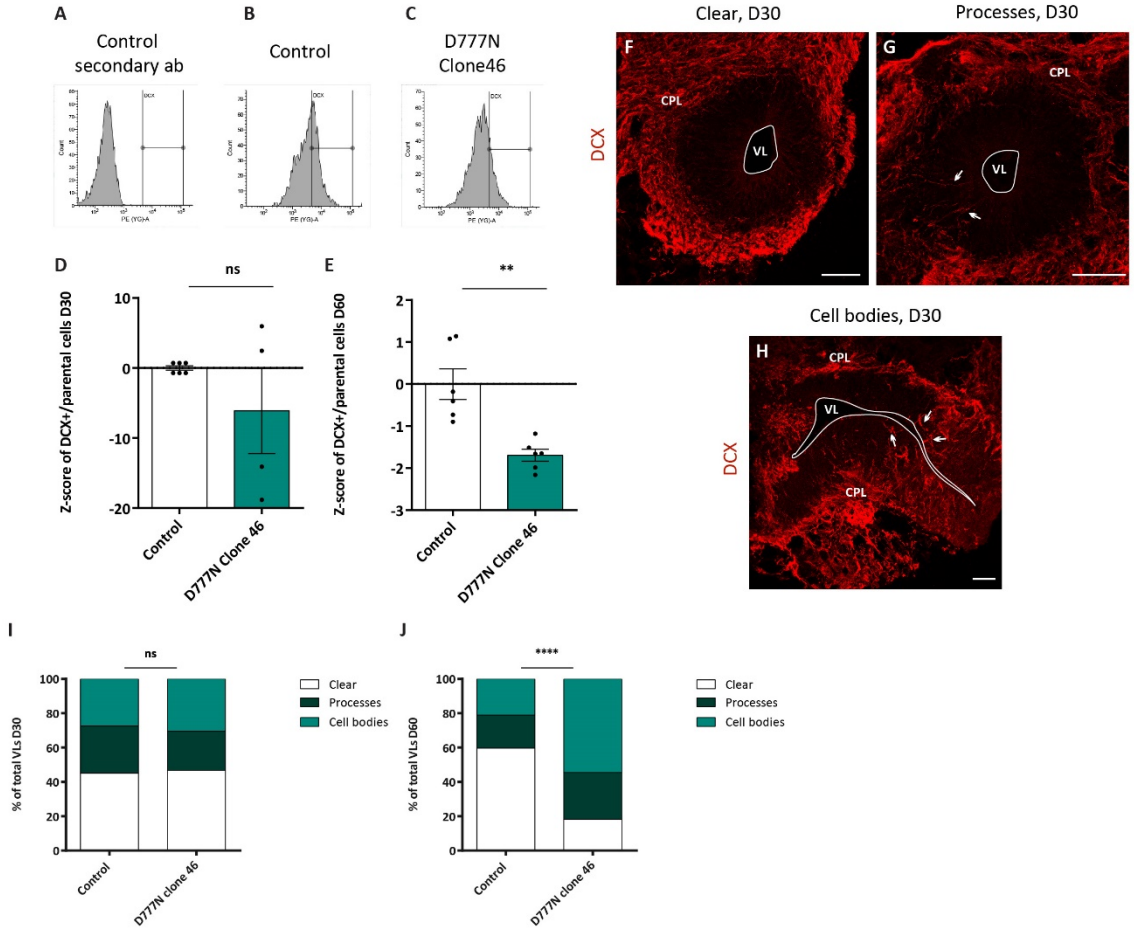

Figure 3. 10: D777N COs present neuronal migration problems.

(A-C) Representative pictures of the FACS strategy used to select the DCX+ cells. (A) Secondary control without any DCX+ cells detected. (B, C) Control and D777N COs with DCX+ cells. (D, E) Z-scores of the DCX+ cells per parental cell at (D) 30 days and (E) 60 days. (F-H) Representative pictures of DCX+ COS with (F) a clear GZL, (G) ectopic processes in the GZL and (H) ectopic cells bodies. Arrows indicate the incidence of ectopic processes and cell bodies. (I-J) Percentage of VLs with clear, ectopic processes or ectopic cell bodies at (I) 30 days and (J) 60 days. FACS statistical analysis was based on Mann-Whitney U-test. DCX intrusion statistical analysis was based on the multinomial Chi-Square goodness of fit test, ****$p < 0.0001$ and **$p < 0.01$. FACS DCX+ 30 days: Control batches b=3, o=18; D777N b=2, o=12 and FACS DCX+ 60 days Control b=3, o=18; D777N b=2, o=18. DCX intrusions 30 days Control: b=2, o=18, v=80; D777N b=2, o=13, v=105 and 60 days Control: b=2, o=16, v= 52; D777N b=2, o=10, v=33. Data shown as mean ± SEM. Scale bars: (F-H) 50µm. Abbreviations: CPL: cortical plate-like area, GZL: germinal zone-like area, ns: no significant, VL: ventricle-like cavities.

3.2.8 There are no changes in the radial glial process neither in the apical belt integrity

The neuronal migration defects could be due to two main reasons, intrinsic problems in the neurons that do not allow the cells to migrate properly and morphological or delamination problems in the scaffold (RGs) the neurons use to migrate (Cappello et al., 2012; Klaus et al., 2019). To understand if the neuronal migration phenotype found in the D777N COs was due to morphological alteration in the RGs I analysed their structure with the RG marker NESTIN (**Fig 3.11 A, B**). Thanks to these markers it is possible to identify the RG processes. After analysing the tortuosity of the processes, which indicates how straight a process is, I did not see any differences between the RGs of control and D777N COs at 30 and 60 days (**Fig 3.11 C, D**). I also looked at the integrity of the apical membrane in the VLs of control and D777N COs at 30 days by looking at the fraction of actin contained in fibres (F-ACTIN) by PHALLODIN immunostaining (**Fig 3.12 A, B**). Areas with an intact DAPI staining but with a PHALLOIDIN staining could indicate a disruption of the apical belt and possible premature delamination of progenitor cells. The results indicated that there were no differences between the percentages of VLs with an intact or disrupted apical belt between control and D777N COs (**Fig 3.12 c**). All these data suggest that the neuronal changes could be due to changes in the neurons themselves.

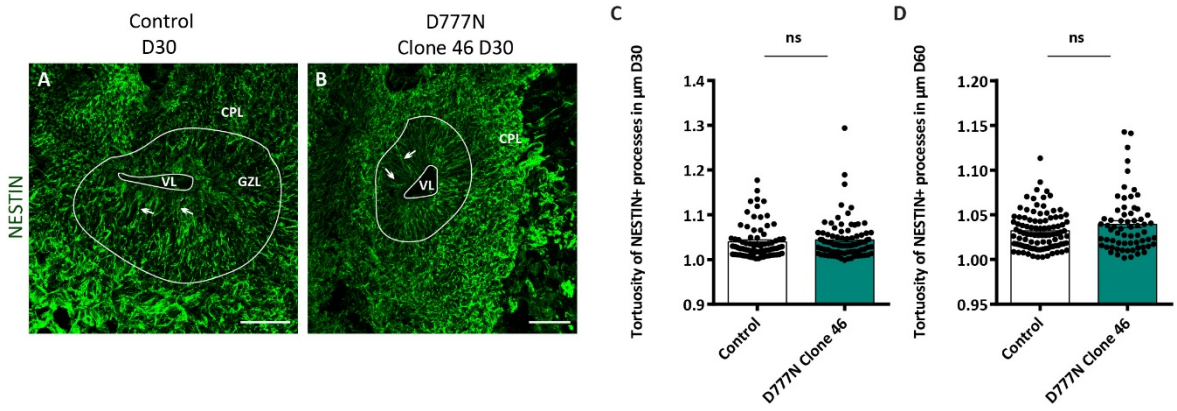

Figure 3.11: The neuronal migration defects in D777N COs are not due to disrupted RG morphology.
(A, B) Representative pictures of a COs stained with the RG marker, arrows indicate different processes. NESTIN. (C) Quantification of the tortuosity of the RG processes in control and D777N COs at (C) 30 day and (D) 60 days. Statistical analysis was based on Mann-Whitney U-test. NESTIN: 30 days b=1, o=3, v=16, processes (p)=90; D777N b=1, o=3, v= 18, p=80 and 60 days b=1, o=3, v=20, p= 100; D777N b=1, o=3, v=13, p=65. Scale bars: (A, B) 50µm. Abbreviations: CPL: cortical plate-like area, ns: no significant, VL: ventricle-like cavities.

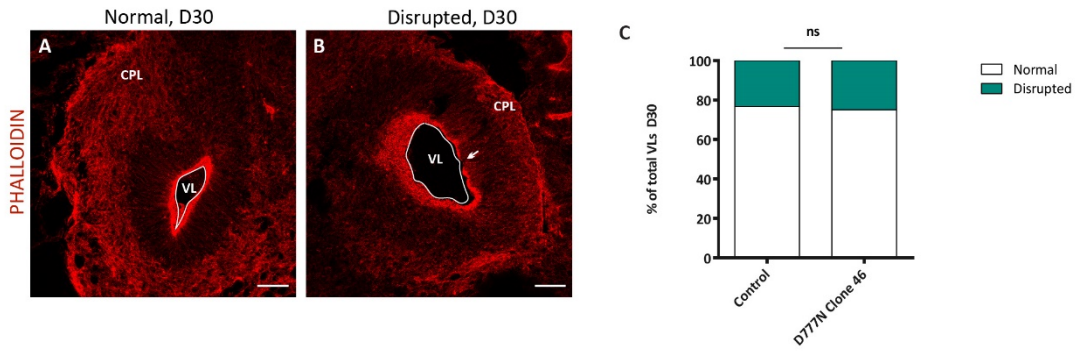

Figure 3.12: The neuronal migration defects in D777N COs are not due to premature delamination.
(A, B) Representative pictures of a COs stained with the apical belt marker, PHALLOIDIN. (C) Percentage of the number of VLs with an apical belt disruption at 30 days Statistical analysis was based on exact binomial test. PHALLOIDIN: b=1, o=7, v= 43; D777N b=1, o=6, v=37. Scale bars: (A, B) 50µm. Abbreviations: CPL: cortical plate-like area, ns: no significant, VL: ventricle-like cavities.

3.2.9 D777N COs present an increased number of upper-layer neurons and reduced number of deep-layer neurons

Finally, I investigated neuronal subtypes using different neuronal markers and quantifying the number of those cells in the CPL. I focused on the deep layer neurons that can be identified by the CTIP2 marker (**Fig 3.13 A**) and the upper layer neurons by the SATB2 marker (**Fig 3.13 D**). During cortical development, deep layer neurons are born before the upper-layer neurons. The results indicate that in control COs there are significantly less deep-layer neurons both at 30 and 60 days compared to D777N (**Fig 3.13 B, C**) while there is a significant increase in the number of upper-layer neurons at 30 days and a tendency at 60 days in D777N COs (**Fig 3.13 E, F**).

This complementary data could indicate a possible premature differentiation of the progenitor cells in D777N COs or a shift in the generations of upper vs deep layer neurons. However, this is very preliminary data and many more experiments and analyses need to be done to prove this.

In summary, D777N COs present some differences compared to controls. On the one hand, they contain a reduced number of PAX6+ and a thinner GZL that is stable over time. They also contain less amount of TBR2+ cells at early time points. However, there are more cells with a vertical division. The reduced number of PAX6+ and TBR2+ and the same levels of proliferative capacity could potentially mean that this type of symmetric division is potentially consumptive, however, this hypothesis should be further studied. On the other hand, D777N COs also present a reduced number of neurons or reduce expression of the DCX marker at later time points and migration defects that seem to be due to intrinsic neuronal problems. Additionally, there seems to be a difference in the number of deep and upper-layer neurons.

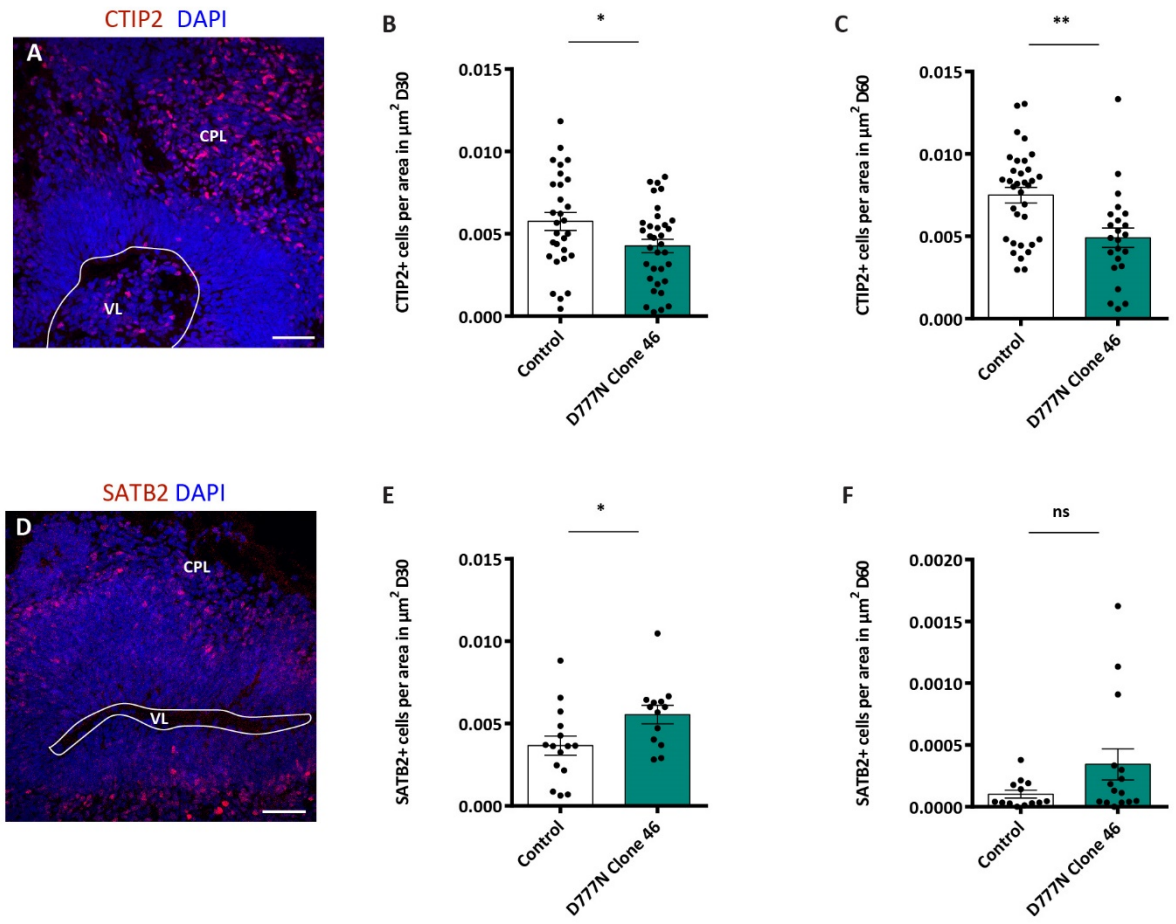

Figure 3.13: D777N COs contain less CTIP2 and more SATB2 neurons.

(A) Representative picture of a CO stained with the deep neuronal layer marker, CTIP2. (B, C) Quantification of the number of CTIP2+ cells per area in the CPL at (B) 30 days and (C) 60 days. (D) Representative picture of a CO stained with the upper neuronal layer marker, SATB2. (E, F) Quantification of the number of SATB2+ cells per area in the CPL at (E) 30 days and (F) 60 days. Statistical analysis was based on Mann-Whitney U-test, ** $p<0.01$, * $p<0.05$. CTIP2+ cells: 30 days b=2, o=8, v=29; D777N b=2, o=8, v=34 and 60 days Control: b=1, o=7, v= 34:; D777N b=1, o=4, v= 18. SATB2+ cells: 30 days b=1, o=3, v= 15; D777N b=1, o=3, v=13 and 60 days Control: b=1, o=8, v= 12:; D777N b=1, o=4, v=10. Scale bars: (A, D) 50µm. Abbreviations: CPL: cortical plate-like area, ns: no significant, VL: ventricle-like cavities.

In **Chapter 4**, I will show the results of the manuscript that is published in the journal Frontiers in Molecular Bioscience:

GNG5 controls the number of apical and basal progenitors and alters neuronal migration during cortical development

Ane Cristina Ayo-Martin, Christina Kyrousi, Rossella Di Giaimo, Silvia Cappello

The work presented in this project contains all original work done by me. Data not included in the manuscript is also presented. Some of the figures, figure legends and results in this chapter are adapted from the manuscript with the permission of the Journal under the copyright:

CHAPTER 4: GNG5 CONTROLS THE NUMBER OF APICAL AND BASAL PROGENITORS AND ALTERS NEURONAL MIGRATION DURING CORTICAL DEVELOPMENT

4.1 GNG5 AND THE G-COUPLED PROTEINS FAMILY

GNG5 codes for the G protein subunit gamma 5 (Gγ5). GNG5 is member of the G protein family. G proteins, together with their transmembrane partners, GPCRs, play significant roles inside and outside the cell (Gilman, 1987). In combination with the α and β subunits, the γ subunits form a heterotrimeric protein complex. On the cell membrane, they interact with the GPCRs by which they can transduce signals intracellularly (Clapham and Neer, 1997; Gilman, 1987; McCudden et al., 2005; Smrcka, 2008). In resting condition, the α subunit, which contains a guanine nucleotide-binding site occupied by GDP, and the βγ subunits form the heterotrimeric complex and are attached to the membrane (Pimplikar and Simons, 1993). When a ligand binds to the GPCRs, the α subunit becomes free, which induces the exchange of GDP to GTP and a consequent release of the βγ subunits from the membrane into the intracellular lumen (Bomsel and Mostov, 1992). Once the α subunit and βγ subunits are free, they will take part in a wide variety of intracellular pathways (Clapham and Neer, 1997, 1993; Hewavitharana and Wedegaertner, 2012; Smrcka, 2008; Wedegaertner et al., 1995).

In humans, there are at least 16 genes that code for 23 different α subunit proteins. These subunits have a range of size from 35-49 kDa (Im et al., 1988; McCudden et al., 2005). α subunits have been implicated in a variety of processes and interact with a variety of effectors such as adenylyl cyclase, retinal phosphodiesterase, phospholipase C, and ion channels (Gilman, 1987; Tang and Gilman G., 1991). In contrast, there are only 5 genes that code for different β subunits and 12 genes that code for the γ subunits (McCudden et al., 2005). These last two proteins are smaller in a size range around 36-40 kDa and 7.5-8 kDa, respectively (McIntire, 2009). βγ subunits are non-covalently bound to each other and always work together under physiological conditions (Spiegel and Weinstein, 2004). All γ subunits are prenylated post-synthetically in the C-terminal. This post-translational modification is essential for the localization of the βγ dimer to the membrane (McCudden et al., 2005). βγ subunits are necessary for different pathways such as MAP Kinase cascade or vesicular trafficking (Clapham and Neer, 1997, 1993; Hewavitharana and Wedegaertner, 2012; Smrcka, 2008; Wedegaertner et al., 1995). Having such a large number of different subunits allows an incredible amount of different possible combinations. Scientists have been trying to understand which are the possible combinations that can be seen *in vivo* and which have important physiological roles in cellular pathways (McCudden et al., 2005; Schwindinger et al., 2004). Moreover, different combinations of heterotrimeric proteins

can be coupled to the same receptor. Interestingly, only a few of a large number of possible combinations have been detected experimentally (Giulietti et al., 2014). Besides being essential for the localization in the membrane and the activation of effectors in various pathways, G protein γ subunits may be necessary for the specificity of the hundreds of known receptors (Lim et al., 2001; Schwindinger et al., 2004). It is therefore important to understand the specific role of each subunit and to identify the pathways they are involved in.

GNG5 was firstly discovered in 1992 by (Cali et al., 1992) and was found to be highly expressed in brain tissue (Betke et al., 2014; Kim et al., 2014). *Gng5* KO is lethal in mice and they die at embryonic day 10.5 (E10.5) due to defects both in the heart and the brain. One of the main reasons behind this is the reduction of cell proliferation in the absence of Gng5 (Moon et al., 2014). Furthermore, *Gng5* is highly expressed in the NPCs of the embryonic and adult mouse brain (Asano et al., 2001; Morishita et al., 1999; Telley et al., 2019). Additionally, in humans, it is highly expressed in a different type of progenitors especially on those located in the oSVZ, during development. Finally, in human-derived COs, *GNG5* is mainly expressed in different types of NPCs and especially enriched in bRGs (Kanton et al., 2019; Polioudakis et al., 2019; Pollen et al., 2016). As explained in **Chapter 1**, these type of progenitors are highly abundant in gyrified species and are believed to be important for brain expansion and gyrification (Fietz et al., 2010; Florio and Huttner, 2014; Kelava et al., 2012; Penisson et al., 2019).

Considering that in *DCHS1* and *FAT4* COs the transcript for *GNG5* remains highly upregulated in the neurons with the altered state (Klaus et al., 2019) makes us believe that it could be one of the main responsible genes in these neurons not to behave as they should. We believe that these neurons may be the ones that form the heterotopia in patients with VMS and its associated PH. Understanding the role of GNG5 could thus help understand better what goes wrong during the development of the brain of these patients and will aid to elucidate a mechanism necessary for brain development that has not been studied before. The main aim of this chapter is to understand better how GNG5 is essential for brain development and more concretely how its upregulation in a subpopulation of neurons derived from VMS patients could be affecting the proper migration and localisation of new-born neurons in the brain. For this purpose, we have used two different approaches: An *in vivo* system using the developing mouse brain to understand the role of GNG5 in a real environment and a human 3D *in vitro* system (iPSCs-derived COs) to understand the species-specific role that GNG5 may have in human brain development.

4.2 RESULTS

4.2.1 *GNG5* is highly expressed in different types of progenitor cells in different model systems

Our data from human COs showed that in control COs *GNG5* is highly expressed in progenitor cells and is subsequently downregulated during neuronal differentiation. However, in the altered cluster of neurons in *DCHS1* and *FAT4* COs, *GNG5* continues to be upregulated (**Fig 4.1**).

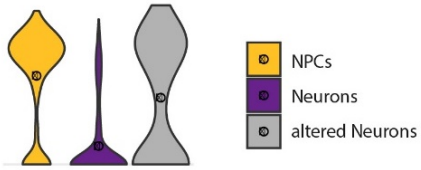

Figure 4. 1: *GNG5* is highly expressed in NPCs and in the altered population of neurons while being downregulated in control neurons.
Violin plot representing the expression levels of GNG5 in NPCs (yellow), neurons (purple) and the altered population of neurons (grey) in *DCHS1* and *FAT4* mutant COs. Abbreviations: NPCs: Neuronal precursor cells. Figure adapted from (Klaus et al., 2019).

Therefore, I examined the gene expression of *GNG5* in different databases of mouse and human brain development. In mice, *Gng5* is highly enriched in progenitor cells mainly in the first stages of development (**Fig 4.2 A-D**) while in humans its expression is high in all progenitors, with an important enrichment in bRGs (**Fig 4.2 E-G**). Moreover, if we look at the expression of *GNG5* especially in human-derived COs, it is also highly expressed in a different type of progenitors including bRGs (**Fig 4.3**).

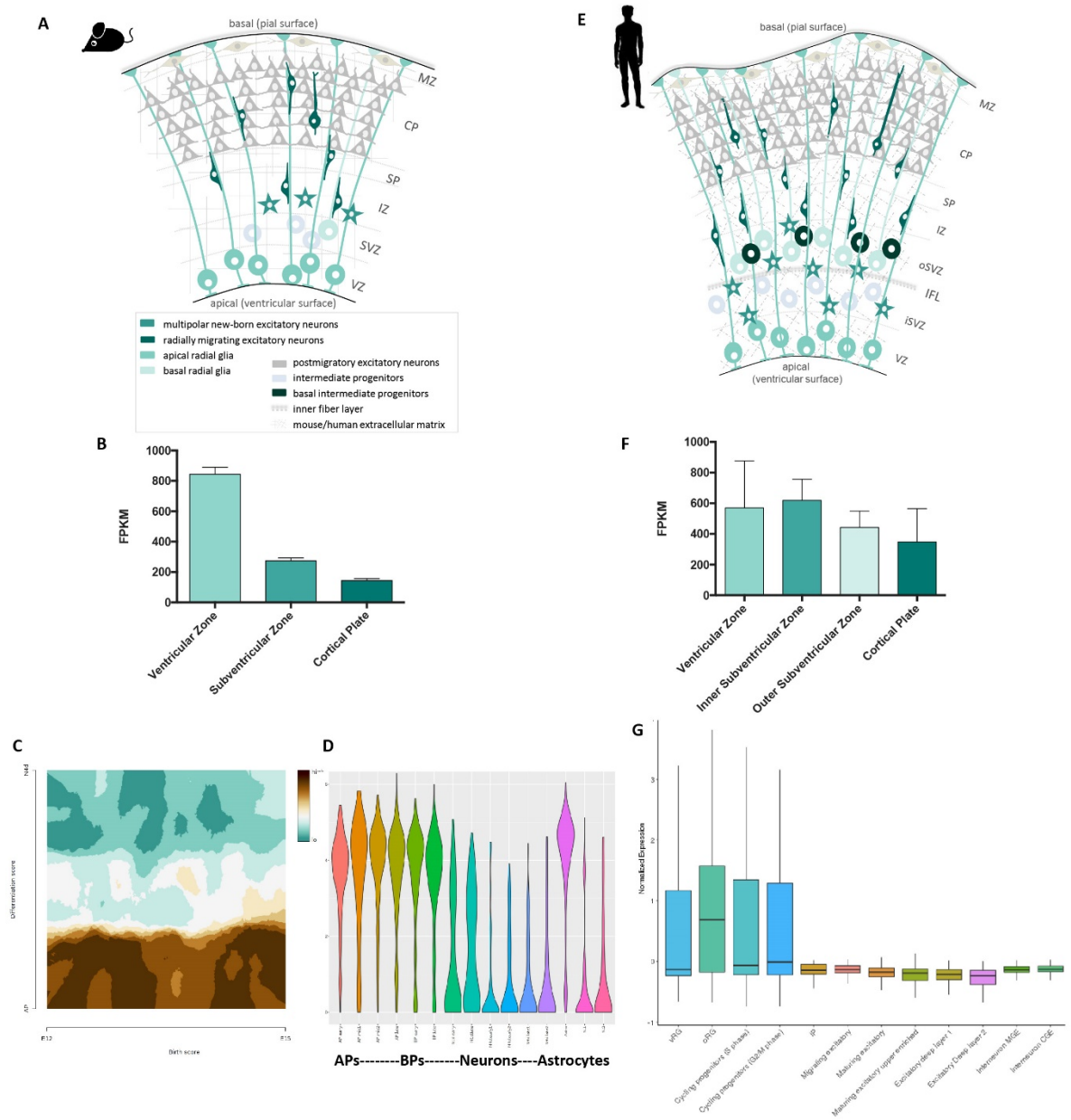

Figure 4. 2: *GNG5* expression levels in mice and humans.

Schematic of the (A) mouse developing cortex. Figure adapted from (Buchsbaum et al., 2019). (B) *GNG5* expression in the different areas of the developing mouse cortex adapted from (Fietz et al, 2012). (C, D) The level of *Gng5* expression and the expression landscape in different cellular groups of the developing mouse cortex at E12-E15 (Telley et al., 2019). (E) Schematic of the human developing cortex. Figure adapted from (Buchsbaum et al., 2019). (F) *GNG5* expression in the different areas of the developing human cortex adapted from (Fietz et al, 2012). (G) *GNG5* expression in the different type of cells of the human developing neocortex (Polioudakis et al., 2019). Abbreviations: AP: apical progenitor, BP: Basal progenitor, CP: cortical plate, FPKM: fragments per kilobase of exon model per million reads mapped, IP: intermediate progenitor, iSVZ: inner subventricular zone, IZ: intermediate zone, MZ: marginal zone, N4D: differentiated neurons, oSVZ: outer subventricular zone, RG: radial glia (v=ventral, o=outer), SP: subplate, VZ: ventricular zone.

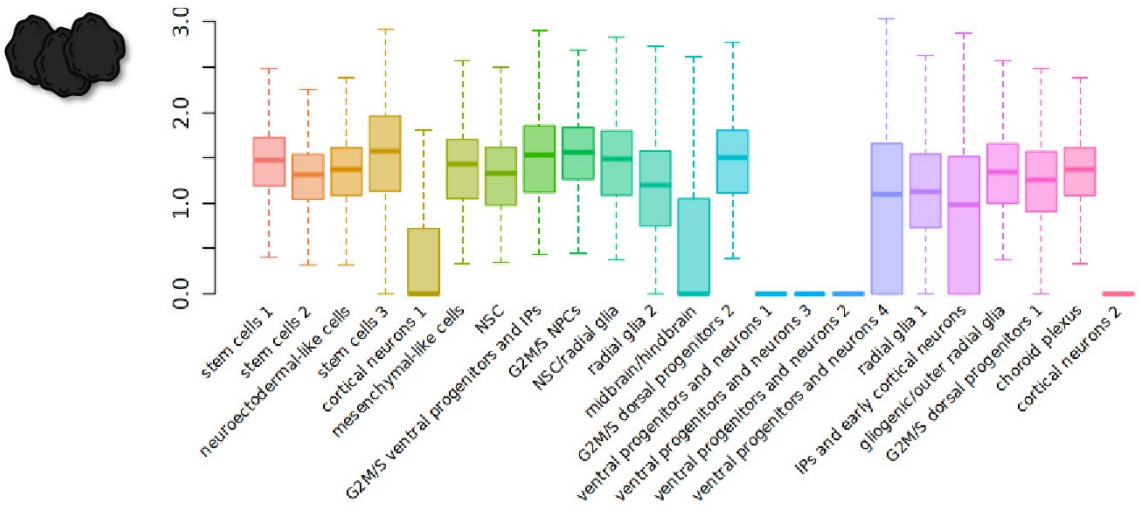

Figure 4. 3: *GNG5* expression levels in human-derived COs.
Data from scRNA-seq data in human-derived COs and the expression of *GNG5* in the different cellular clusters identified (Kanton et al, 2020). Abbreviations: NPCs: neural precursor cells, NSC: neural stem cells.

4.2.2 Acute overexpression of *GNG5* alters the morphology and distribution of electroporated cells in human-derived COs

A good way to study the role of different candidate genes in COs is to electroporate the gene of interest in VLs structures and study how its overexpression or downregulation alters the morphology and the surroundings of the electroporated cells. Therefore, to understand the role of *GNG5* in early stages of development and corticogenesis, I overexpressed *GNG5* by the electroporation of the *pCAG-GNG5-IRES-GFP* plasmid into the VLs of COs at an early and a later timepoint: at day 20 and day 35. At day 20, most of the cells in CO ventricles are progenitor cells and neurons are in the very early stages of development/differentiation and migration, while at 35 days, a more mature stage is reached in which progenitors and neurons are organized into clear GZL and CPL areas. COs were analysed 7 days post electroporation (dpe) for both time points. **Fig 4.4** illustrates the electroporation chamber used (**Fig 4.4 A**) and shows the picture of an electroporated organoid; in green electroporated cells can be distinguished (**Fig 4.4 B**).

To be able to better visualize the cell profile and better detect the morphology of the cells, I also co-electroporated the COs with a plasmid that codes for *GAP43-GFP*. This fused protein labels the cell membrane (Attardo et al., 2008).

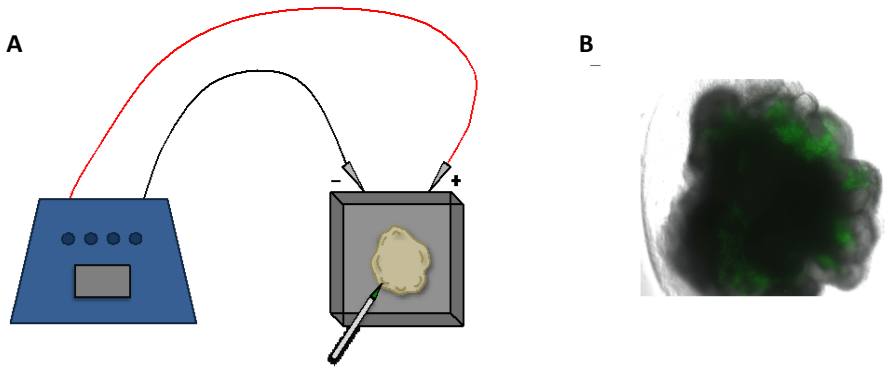

Figure 4.4: Electroporation of a CO and the electroporation chamber.
(A) Representation of the organoid electroporation chamber. (B) Representative image of an organoid after electroporation. In green, electroporated cells can be distinguished, most of which are localized inside the VZ of the COs.

At 20+7 days, after the acute overexpression (OX) of *GNG5,* the electroporated cells in the COs show an altered morphology. The cells contain less process and the few processes that stay are less straight compared to controls (**Fig 4.5 A-B'**).

Moreover, not only the morphology of the cells looks different, but the distribution of the GFP+ cells in the GZL area was different. To analyse the distribution of the GFP+ cells in the COs, I divided the GZL area into two equal Bins. At day 20, 7 days after acute OX of *GNG5*, electroporated GFP+ cells stay closer to the VL (BinA), while in the COs electroporated with the control plasmid GFP+ cells migrate further to the upper parts of the GZL (BinB) (**Fig 4.5 C-E**).

4.2.3 Forced overexpression of *GNG5* induces neuronal migration defects in COs

Besides a possible intrinsic problem in neurons, neuronal migration problems have also been shown to be a consequence of faulty RG morphology (Cappello et al., 2013, 2012; Klaus et al., 2019). Therefore, I examined the position of MAP2+ neurons by counting the number of VLs with neuronal cell bodies or processes in the GZL of electroporated COs (**Fig 4.6 A-C'**). An increased number of any of the parameters could indicate neuronal migration defects.

At 20+7 days, there was already an increased percentage of VLs with MAP2+ neuronal cell bodies in the GZL consequence of the forced expression of *GNG5*, in contrast to the COs in which the control plasmid was electroporated and where most neurons migrated properly (*GNG5* OX 45% of the VLs with MAP2+ neuronal cell bodies in the GZL and controls 21%; *GNG5* OX 30% of the VLs with neuronal processes in the GZL and controls 39%) (**Fig 4.6 D**). The neuronal migration phenotype was also significantly different at 35+7 days (*GNG5* OX 33% of the VLs with MAP2+ neuronal cell bodes in the GZL and controls 5%; *GNG5* OX 39% of the VLs with neuronal processes in the GZL and controls 33%) (**Fig 4.6 E**).

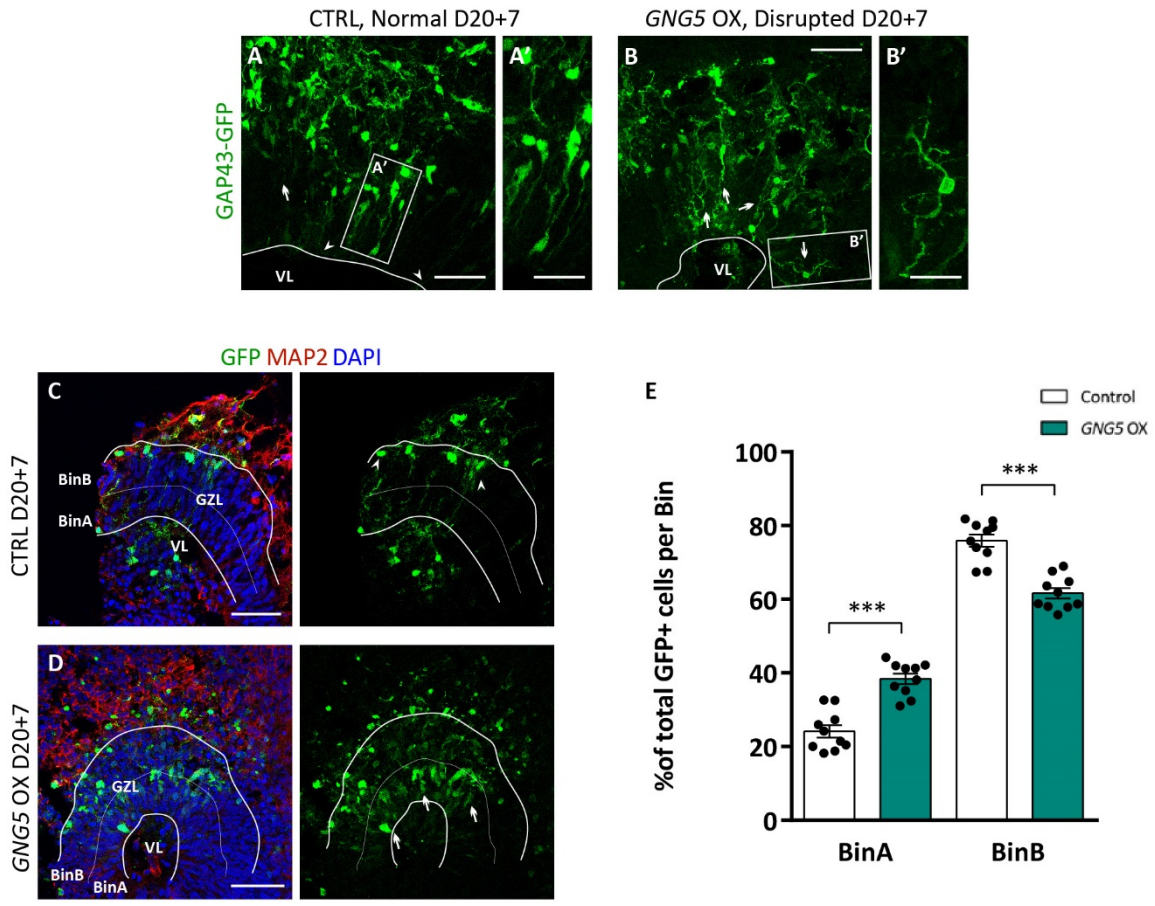

Figure 4. 5: Force expression of *GNG5* alters the morphology of cells and the distribution of the electroporated cells in COs.

(A-B') Representative pictures of cells from COs in which the *GNG5* OX or control plasmids were co-electroporated with the *GAP43-GFP* plasmid. Arrows show disrupted or delaminated RGs and arrowheads intact cells. (C, D) Representative pictures of cells from COs in which the *GNG5* OX or control plasmids are co-electroporated with the *GAP43-GFP* plasmid. The GZL is divided into two equal Bins and the GFP+ cells localize in each Bin are counted. Arrows indicate apically located GFP+ cells (BinA) and arrowheads point at basally located GFP+ cells (BinB). The statistical analysis was based on Mann-Whitney U-test, ***p < 0.001. CTRL b=1, o=4, v=10; *GNG5* OX b=1, o=3, v=10. Data shown as mean ± SEM. Scale bars: (A', B') 20 µm, (A-D) 50 µm. Abbreviations: CTRL: control, GZL: Germinal zone-like area; OX: Overexpression, VL: ventricle-like cavities.

The presence of MAP2+ neuronal processes in GZLs, which is more abundant during the first stages of developmental, is representative of the neurons that are migrating and that start to become more mature and start expressing the corresponding markers. In control conditions, this proportion was reduced at later time points (**Fig 4.6 D, E**). Remarkably, the percentage of clear GZLs in *GNG5* OX COs was the same in the two-time points, which indicates a delay in neuronal migration (**Fig 4.6 D, E**).

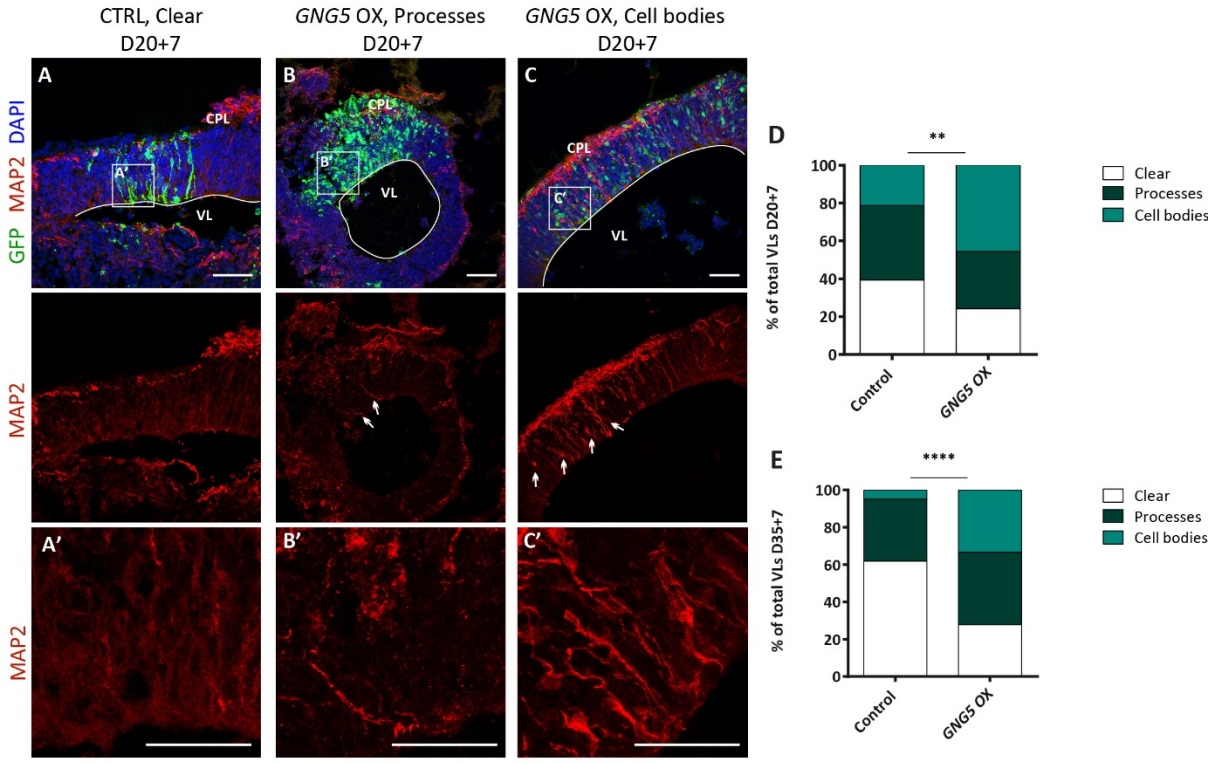

Figure 4. 6: Forced expression of *GNG5* promotes neuronal migration defects in COs.
(A, A') Representative image of a clear GZL area at 20+7 days in control electroporated COs. (B) Representative picture of a GZL area with the presence of neuronal processes upon *GNG5* OX. (C, C') Representative picture of a GZL in which neurons do not migrate properly and there are neuronal bodies in GZL upon *GNG5* OX. Arrows show the presence of processes or neuronal cell bodies in the GZL. (D, E) Percentage of VLs without any MAP2 staining in the GZL (clear), MAP2+ processes in the GZL or MAP2+ neuronal cell bodies in the GZL in control and *GNG5* OX COs (D) at 20+7 and (E) at 35+7 days. MAP2 statistical analysis was based on the multinomial Chi-Square goodness of fit test, **p < 0.01, ****p < 0.0001. D20+7: CTRL b=2, o=11, v=61; *GNG5* OX b=2, o=11, v=33 and 35+7 CTRL b=2, o=8, v=21; *GNG5* OX b=2, o=9, v=18. Scale bars: (A'-C') 30 µm and (A-C) 50 µm. Abbreviations: CPL: cortical plate-like area, CTRL: control, GZL: germinal zone-like areas OX: Overexpression, VL: ventricle-like cavities. Figure adapted from (Ayo-Martin et al., 2020) with permission from Frontiers in Molecular Biosciences.

To confirm the migration problem in COs at 20+7 days and 35+7 days, I also stained for the general neuronal nuclear marker NEUN. Same as the results obtained with the MAP2 staining in which there was an increased number of ectopic neuronal processes and neuronal cell bodies in the *GNG5* OX COs, there was an increased number of NEUN+ neuronal cell bodies in the GZL of *GNG5* OX COs (**Fig 4.7**). At day 20+7, the proportion of VLs with the presence of NEUN+ cells in the GZL was significantly higher in *GNG5* OX COs (more than 60% of VLs with ectopic NEUN+ neuronal nuclei in *GNG5* OX compared to 22% in control) (**Fig 4.7 A-C**). At the later time point, the tendency was still there, but the results were not significant (**Fig 4.7 D**). These data are in line with previously presented findings and indicate a delay in neuronal migration upon acute *GNG5* OX.

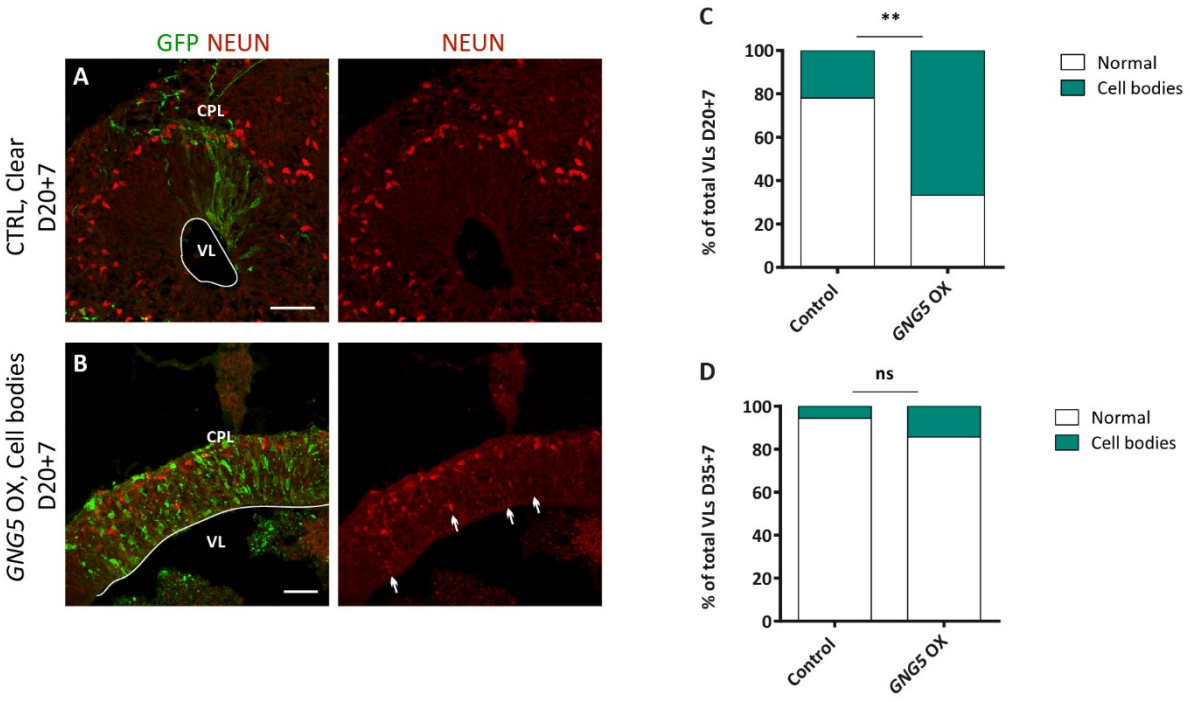

Figure 4. 7: Forced expression of *GNG5* promotes neuronal migration defects in COs.
(A, B). Representative figures of COs stained with the neuronal nuclear marker NEUN after the electroporation of the control or the *GNG5* OX plasmid. (A) Representative picture of a VL in which there are no NEUN+ cell bodies in the GZL (clear). (B) Representative picture of a VL in which there are few NEUN+ cell bodies in the GZL (cell bodies). Arrows indicate the location of the ectopic NEUN+ cell bodies. NEUN statistical analysis was based on exact binomial test **p < 0.01. NEUN: 20+7 CTRL b=2, o=6, v=32; *GNG5* OX b=2, o=4, v=9 and 35+7 CTRL b=2, o=8, v=18; *GNG5* OX b=2, o=5, v=7. Scale bars: (A, B) 50 µm. Abbreviations: CPL: cortical plate-like area, CTRL: control, GZL: germinal zone-like areas, ns: no significant, OX: Overexpression, VL: ventricle-like cavities. Figure adapted from (Ayo-Martin et al., 2020) with permission from Frontiers in Molecular Biosciences.

4.2.4 Forced expression of *GNG5* promotes apical belt disruptions in COs

As previously reported in *DCHS1* and *FAT4* mutant COs (Klaus et al., 2019), the disrupted morphology in RGs, as well as defects in neuronal migration, might be induced by premature delamination of RGs. Normally, the delamination of aRGs happens together with the disruption of the apical junctions, that is why I examined the integrity of the apical membrane by looking at the fraction of actin contained in fibres (F-ACTIN) by PHALLODIN immunostaining (**Fig 4.8 A-B'**). Areas with PHALLOIDIN- patches in the apical belt were distinguished as a consequence of the forced expression of *GNG5* at the 2-time points. Approximately, 40% of the VLs at 20+7 days and 27% of the VLs at 35+7 days presented a defective apical membrane upon *GNG5* OX while in controls only 11% and 9% of VLs presented a defective apical membrane respectively (**Fig 4.8 C-D**).

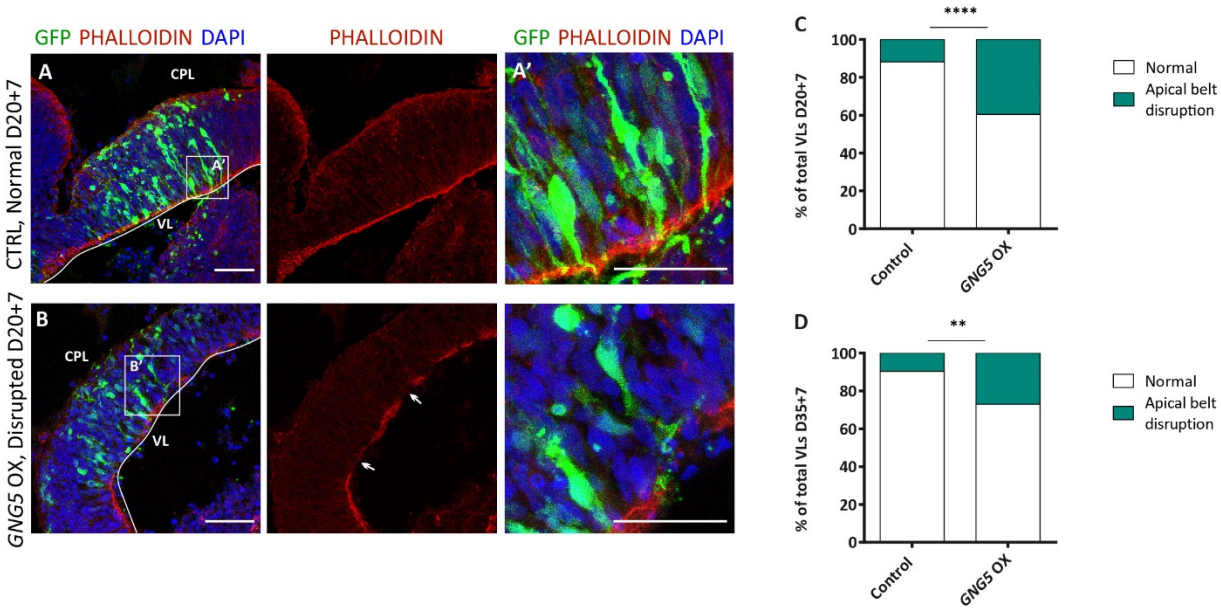

Figure 4. 8: Forced expression of *GNG5* promotes premature aRG delamination in COs.
(A). Representative images of a control CO with an intact apical belt visualized with the PHALLOIDIN antibody and (B) disrupted apical membrane after *GNG5* OX. Arrows show the area of the apical belt that is disrupted. (C) Percentage of VLs in which the apical belt is intact or disrupted at 20+7 days and (D) 35+7 days. PHALLOIDIN statistical analysis was based on exact binomial test **p < 0.01, ****p < 0.0001. PHALLOIDIN: 20+7 CTRL b=2, o=11, v=68; *GNG5* OX b=2, o=10, v=43 and 35+7 CTRL b=2, o=5, v=21; *GNG5* OX b=2, o=7, v=26. Scale bars: (A', B') 20 µm, and (A, B) 50 µm. Abbreviations: CPL: cortical plate-like area, CTRL: control, OX: Overexpression, VL: ventricle-like cavities. Figure adapted from (Ayo-Martin et al., 2020) with permission from Frontiers in Molecular Biosciences.

4.2.5 Acute overexpression of *GNG5* does not induce any significant changes in the number of progenitor cells in COs

Finally, due to the increased number of GFP+ cells in the apical part of the GZL after forced expression of *GNG5*, I also looked at the number of proliferative cells to detect a possible increase in the proliferative capacity due to the *GNG5* OX. Interestingly, there was not a significant increase in the total number of the 3 progenitor markers I looked at, phospho-VIMENTIN (pVIMENTIN) **Fig 4.9**, PH3 or KI67, indicating that *GNG5* OX does not induce an increase in the proliferative capacity of neural progenitor cells in human-derived COs.

In summary, the data obtained after the overexpression of *GNG5* in COs suggest that it promotes morphological changes that induce the premature delamination and alteration in the position of the electroporated aRGs in the GZL. Since neurons need a proper RG scaffold for their radial migration, alterations in the morphology and/or distribution of RGs may induce defective neuronal migration to the CPL Remarkably, the phenotypes observed in *DCHS1* and *FAT4* mutant COs in which RGs also have a disrupted morphology and neurons present migratory problems are evocative of the data obtained in COs after *GNG5* OX.

Since the expression of *GNG5* was significantly altered in *DCHS1* and *FAT4* mutant COs, we theorized that alterations in the expression levels of *GNG5* could be the reason behind the changes identified in those COs (Klaus et al., 2019), indicating that GNG5 may have a crucial role in RG function and morphology.

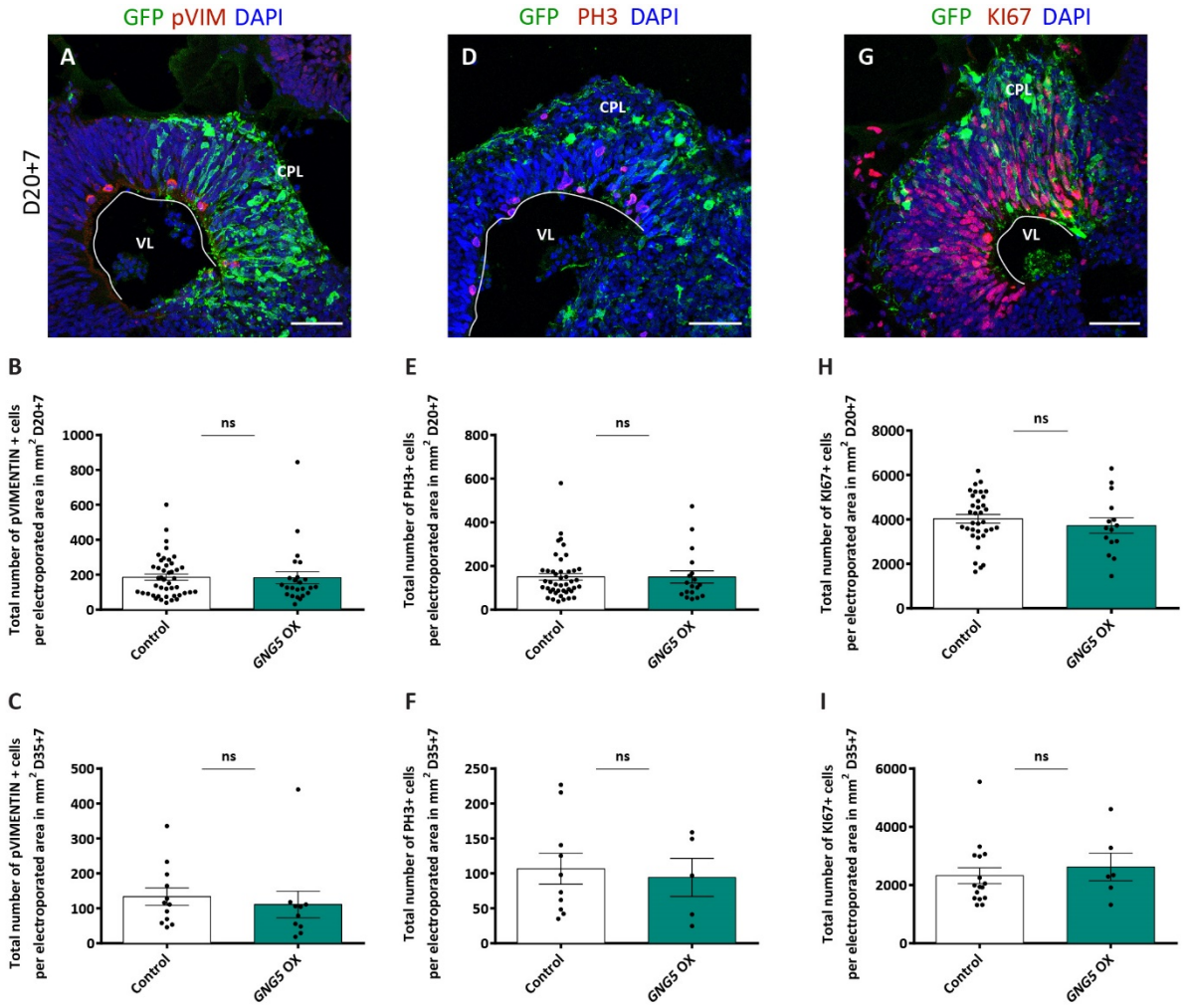

Figure 4.9: Forced expression of *GNG5* does not alter the levels of proliferative cells in COs.

(A) Representative images of VL structured stained for the proliferative marker pVIMENTIN after control electroporation. (B) Quantification of the total number of pVIMENTIN+ cells per electroporated area at 20+7 and (C) 35+7 days. (D) Representative picture of VL structured stained for the proliferative marker PH3. (E) Quantification of the total number of PH3+ cells per electroporated area at 20+7 and (F) 35+7 days. (G) Representative image of VL structured stained for the proliferative marker KI67. (H) Quantification of the total number of KI67+ cells per electroporated area at 20+7 and (I) 35+7 days. The statistical analysis was based on Mann-Whitney U-test. pVIMENTIN: 20+7 CTRL b=2, o=10, v=44; *GNG5* OX b=2, o=7, v=24 and 35+7 CTRL b=1, o=6, v=11; *GNG5* OX b=1, o=6, v=10; PH3: 20+7 CTRL b=2, o=9, v=44; *GNG5* OX b=2, o=8, v=18 and 35+7 CTRL b=2, o=6, v=10; *GNG5* OX b=2, o=4, v=5; KI67: 20+7 CTRL b=2, o=8, v=35; *GNG5* OX b=2, o=4, v=15 and 35+7 CTRL b=2, o=4, v=16; *GNG5* OX b=2, o=4, v=6. Data shown as mean ± SEM. Scale bars: (A, D, G) 50 µm. Abbreviations: CPL: cortical plate-like area, CTRL: control, ns: no significant, OX: Overexpression, VL: ventricle-like cavities.

4.2.6 Acute overexpression of *GNG5* promotes alterations in the morphology of RGs and the distribution of electroporated cells *in vivo* 1 dpe

After the results obtained *in vitro* in human-derived COs, I decided to examine the role of GNG5 in cortical development *in vivo*. For that purpose, I overexpressed *GNG5* by acute IUE in the cortex of the developing mouse at embryonic day 13 (E13) and examined 1, 3 and 6 dpe.

1 dpe, it was already possible to see alterations in the location/distribution of the cells overexpressing *GNG5*. These results could indicate possible alterations in their fate and/or migration (**Fig 4.10**). To better examine the position of the mislocalized GFP+ cells, I subdivided the cortex into five equally sized bins starting from apical belt until the basement membrane (**Fig 4.10 A, B**). On the one hand, most of the GFP+ cells in control embryos were mainly positioned between BinA and BinB, the areas roughly corresponding to the VZ and SVZ, respectively (**Fig 4.10 A, C**). On the other hand, in the brain of embryos overexpressing *GNG5*, most GFP+ cells accumulated between BinB and BinC with a smaller proportion of cells in upper Bins (BinD) (**Fig 4.10 B, C**).

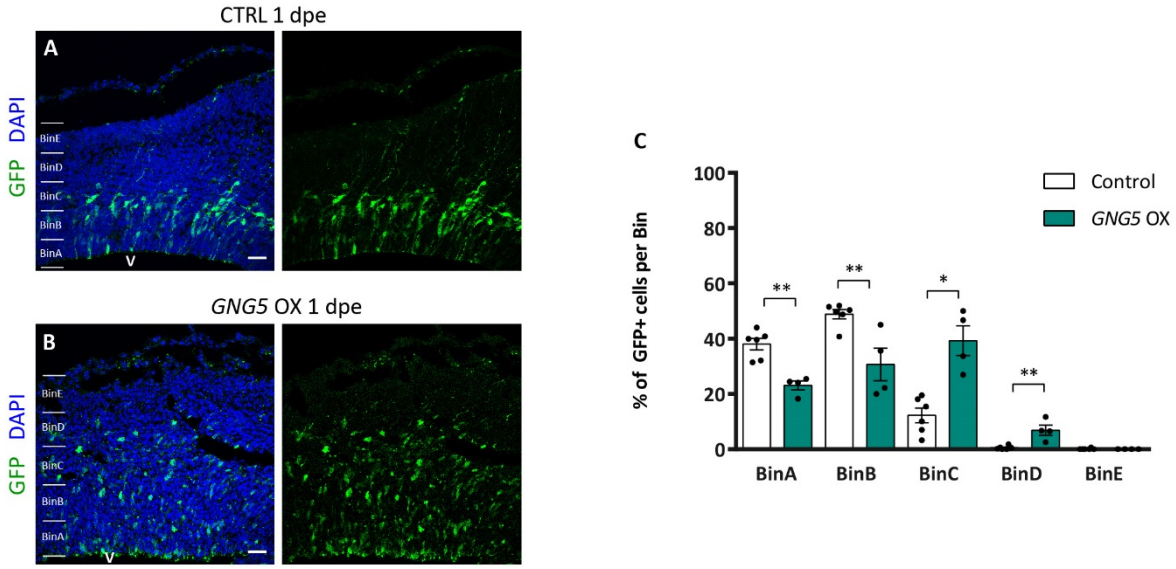

Figure 4.10: Forced expression of *GNG5* in mouse embryos at E13 changes the distribution of electroporated cells 1 dpe. (A, B) Pictures of the electroporated lateral cortex of mouse brain sections stained with the GFP antibody. Sections were divided into five equal bins for quantification. (A) The GFP+ cells of the brain of embryos electroporated with a control plasmid localized to BinA and BinB while in (B) the embryos electroporated with the *GNG5* OX plasmid, GFP+ cells localized to BinB, BinC and to a less extend in BinD. (C) Graph showing the proportion of GFP+ cells per bin in control and *GNG5* OX mice at E13-E14. Statistical analysis was based on Mann-Whitney U test *p<0.05 and **p < 0.01. Control n=6 and *GNG5* OX n=4 brains. Data shown as mean ± SEM. Scale bars: (A, B) 30 µm. Abbreviations: CTRL: control, dpe: day post electroporation , OX: Overexpression, V: ventricle. Figure adapted from (Ayo-Martin et al., 2020) with permission from Frontiers in Molecular Biosciences.

These results, together with the *in vitro* data obtained from COs, suggest that the mislocalization of the cells electroporated with *GNG5* OX could be the consequence of disrupted morphology and premature delamination or differentiation of aRGs to IPs. To answer the first hypothesis, I co-electroporated the *GNG5* plasmid with the control *pCAG-GFP* plasmid, that has a stronger GFP signal

and it is useful to visualize the entire cell morphology. Notably, upon *GNG5* overexpression, most of the GFP+ cells presented a disrupted cell morphology compared to controls, with less or missing radial processes and with a star-like shape, characteristic of IPs (**Fig 4.11**). Considering the star-like shape and to answer if the presence of GFP+ cells in upper bins could be due to premature differentiation, I counted the number of Tbr2+ IPs. Nevertheless, the distribution and the total number of Tbr2+ cells were quite consistent between control and *GNG5* OX mice. There was only a small predisposition for Tbr2+ cells to accumulate in the upper Bins (BinC and BinD) in *GNG5* OX brains (**Fig 4.12**).

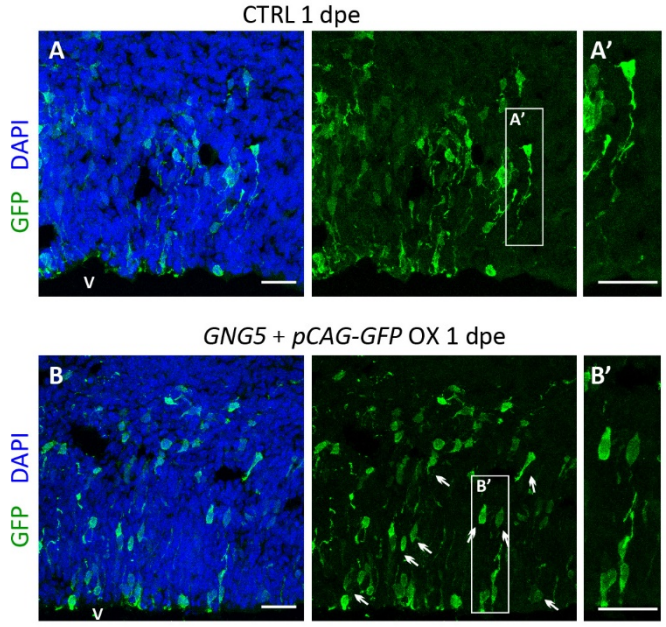

Figure 4.11: Forced expression of *GNG5* in mouse embryos at E13 changes the morphology of electroporated cells 1 dpe. (A-B') Representative images of brain sections from embryos electroporated with a (A, A') control or (B, B') *GNG5* OX plasmid with the *pCAG-GFP*. Cells electroporated with the *GNG5* OX plasmid show an altered morphology with a lower number or the absent of processes. Arrows point at examples of electroporated cells with a non-radial morphology. Scale bars: (A, B) 30 µm. Abbreviations: CTRL: control, dpe: day post electroporation, OX: Overexpression, V: ventricle. Figure adapted from (Ayo-Martin et al., 2020) with permission from Frontiers in Molecular Biosciences.

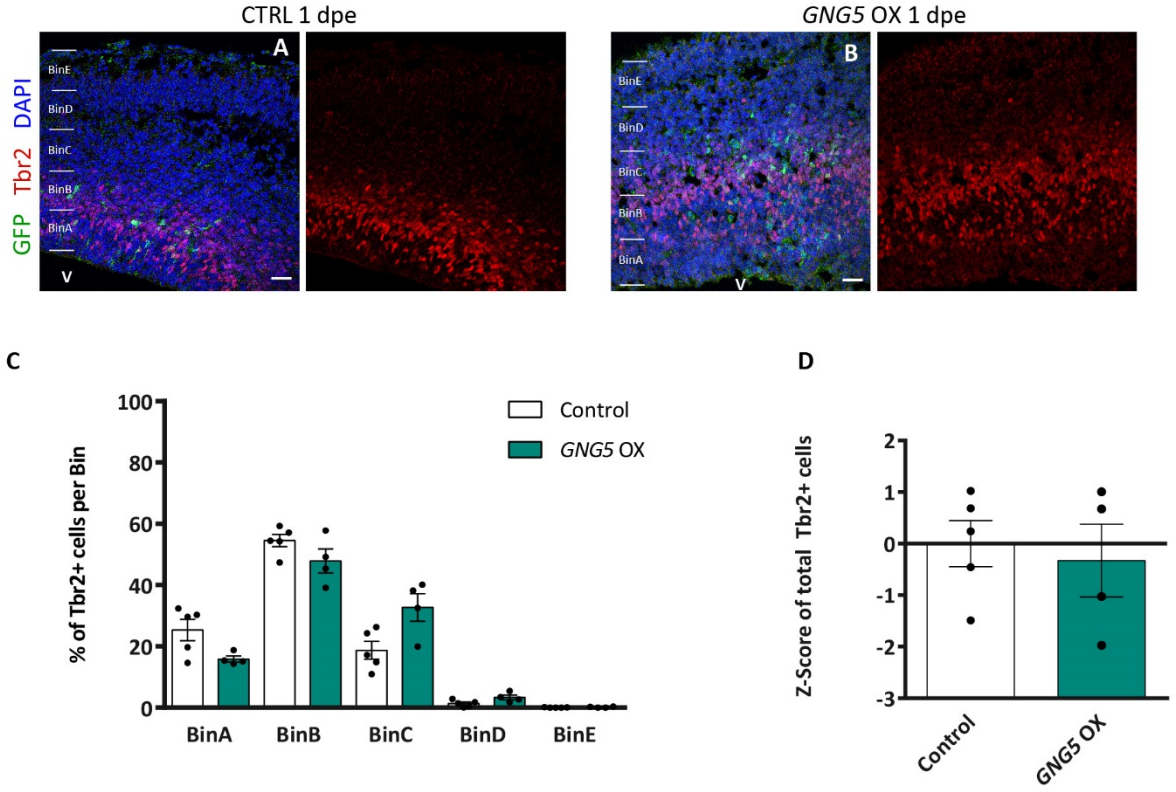

Figure 4.12: Forced expression of *GNG5* does not change the distribution or number of IPs 1 dpe.
(A, B) Pictures of the electroporated lateral cortex of mouse brain sections electroporated at E13 and analysed 1 day after stained with the Tbr2 antibody. Sections were divided into five equal bins for quantification. (C) Graph showing the proportion of Tbr2+ cells per bin in control and *GNG5* OX mice at E13-E14. (D) The total number of Tbr2+ IPs in the lateral cortex per embryonic brain shown as z-scores. There is no significant difference in the distribution between control and *GNG5* OX mice. Statistical analysis was based on Mann-Whitney U test. Tbr2: Control n=5 and *GNG5* OX n=4 brains. Data are presented as mean ± SEM. Scale bars: (A, B) 30 µm. Abbreviations: CTRL: control dpe; day post electroporation, IPs: intermediate progenitors, OX: Overexpression, V: ventricle. Figure adapted from (Ayo-Martin et al., 2020) with permission from Frontiers in Molecular Biosciences.

4.2.7 Acute overexpression of *GNG5* promotes changes in the distribution of electroporated cells in *vivo* 3 dpe

Just 1 dpe the forced electroporation of *GNG5* in brains of mouse embryos it was possible to visualize small but substantial changes in the location and morphology of the GFP+ cells. I thus hypothesized that overexpressing *GNG5* in progenitor cells for a longer time could induce a more pronounced phenotype (**Fig 4.13-15**). 3 days dpe (E13-E16), there was an accumulation of GFP+ cells in BinB and BinC which correspond approximately to the SVZ and IZ in the brains overexpressing *GNG5*. In control embryos, however, a larger proportion of GFP+ cells migrated to the basal part of the cortex (**Fig 4.13**).

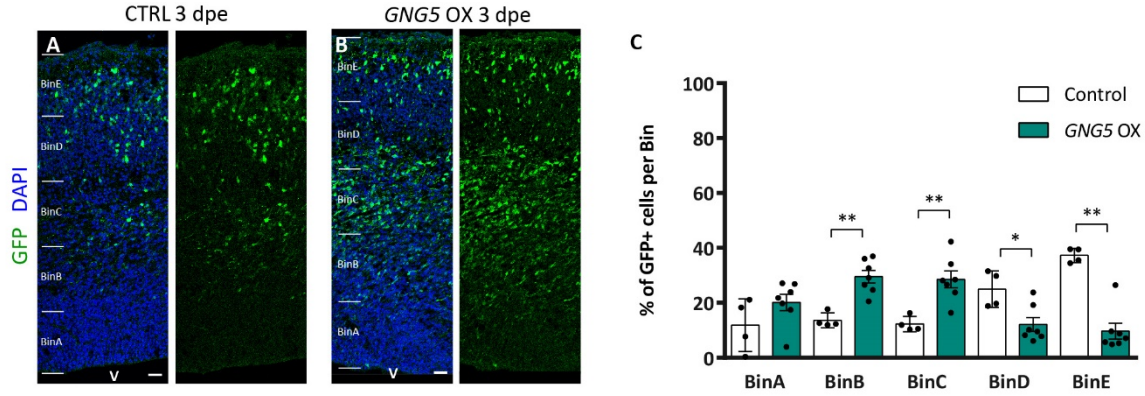

Figure 4.13: Forced expression of *GNG5* in mouse embryos at E13 changes the distribution of electroporated cells 3 dpe. (A, B) Pictures of the electroporated lateral cortex of mouse brain sections electroporated at E13 with (A) control or (B) *GNG5* OX plasmid and analysed 3 dpe after, stained with the GFP antibody. Sections were divided into five equal bins for quantification. (C) Graph showing the proportion of GFP+ cells per bin. In the brain of embryos in which the control plasmid was electroporated, GFP+ cells were spread throughout all bins with an increased amount in BinD and BinE. In *GNG5* OX mice, GFP+ cells were significantly enriched in BinB and BinC. Statistical analysis was based on Mann-Whitney U test *p<0.05 and **p < 0.01. Control n=4 and *GNG5* OX n=7 brains. Data are presented as mean ± SEM. Scale bars: (A, B) 30 µm. Abbreviations: CTRL: control, dpe: day post electroporation, OX: Overexpression, V: ventricle. Figure adapted from (Ayo-Martin et al., 2020) with permission from Frontiers in Molecular Biosciences.

4.2.8 Acute overexpression of *GNG5* induces alterations the proportion of basal progenitor cells *in vivo* 3 dpe

As an increase in the number of GFP+ cells in BinB and BinC could be due to an increased proliferative capacity of the *GNG5* OX cells, I examined the number of dividing cells using the mitotic marker PH3. Interestingly, there was an increase in the proportion of PH3+ cells in BinB and a slight but not significant increase in BinC at the expense of BinA in *GNG5* OX compared to control embryos (**Fig 4.14**). Moreover, there was also a general increase in the number of PH3+ cells in *GNG5* OX brains (**Fig 4.14 D**).

The increase in GFP+ cells in intermediate areas of the cortex and a higher number of proliferative cells in BinB and BinC could indicate an increased number of progenitor cells due to the overexpression of *GNG5*. Moreover, considering the enrichment of GNG5 in BPs (and especially in bRGs in humans), which mainly localize in BinB and BinC, I wanted to investigate further the possible BP identity of the cells accumulating in that area in which *GNG5* OX cells accumulated. Hence, I performed different immunohistochemical analyses using several BP markers. In humans, HOPX is mainly expressed in bRGs (Pollen et al., 2016) while in mice, its expression is similar to Pax6, which is mainly expressed in aRGs since bRGs cells are infrequent (Telley et al., 2019; Wang et al., 2011) (**Fig 4.15 G**). The analysis of the distribution of the number of Hopx+ cells after forced expression of *GNG5 in vivo* showed an accumulation of Hopx+ cells in BinB and BinC which, as I mentioned before, correspond to the SVZ and IZ approximately, and which normally do not contain RGs in the mouse brain (**Fig 4.15 A-C**). Interestingly, while the total number of apical Hopx+ cells (total number of Hopx+ cells in BinA and

BinB) was not different between *GNG5* OX and control (**Figure 4.15 G**), the total number of basal Hopx+ cells (total number of Hopx+ cells in BinC-BinE) was different. These results indicate a possible cellular transition from aRGs to bRG (**Fig 4.15 H**). I also analysed the distribution and number of IPs by Tbr2 immunohistochemistry, paralleling the analysis at 1 dpe. While the total number of Tbr2+ IPs was also increased by 3 dpe (**Fig 4.15 I**), the distribution of Tbr2+ IPs was the same in control and *GNG5* OX. As Tbr2+ are normally basally located, this indicates an overall increase of Tbr2 in the Bins in which IPs can usually be found (**Fig 4.15 D-F**).

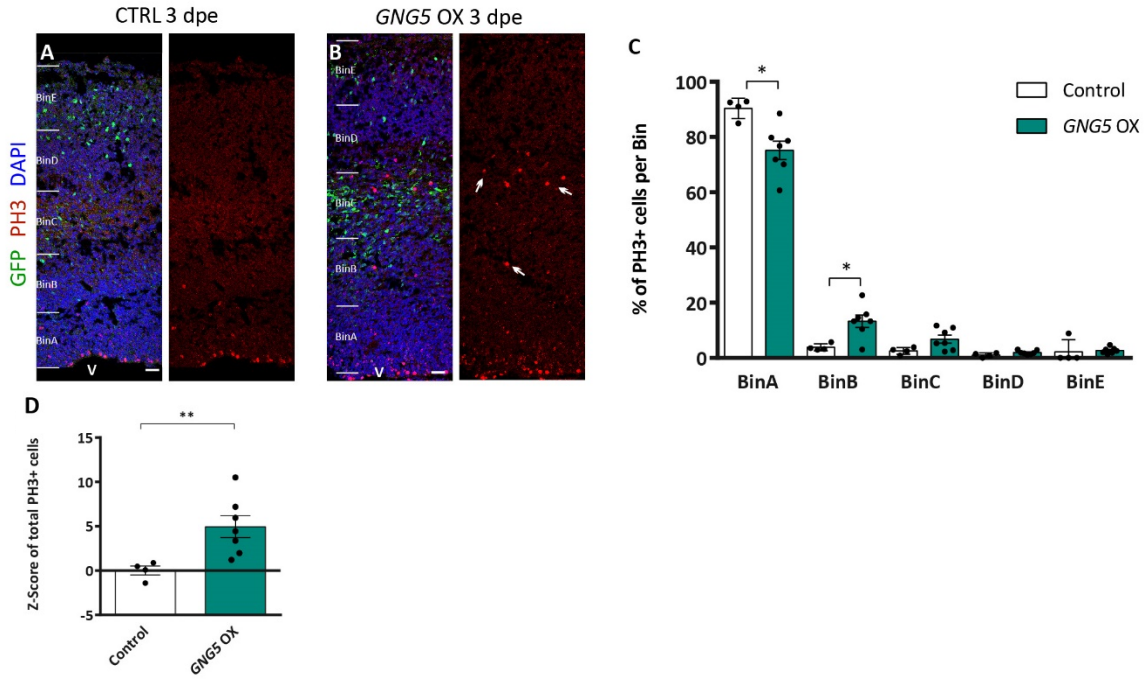

Figure 4.14: Forced expression of *GNG5* in mouse embryos at E13 changes the distribution and number of proliferative cells 3 dpe.

(A, B) Pictures of the electroporated lateral cortex of mouse brain sections electroporated at E13 and analysed 3 days later after stained with the PH3 antibody. Sections were divided into five equal bins for quantification. (C) Graph showing the proportion of PH3+ cells per bin. In the brain of embryos in which the control plasmid was electroporated, PH3+ cells were mainly located in the apical part of the cortex (BinA) while in *GNG5* OX there was an increased number of PH3+ cells in BinB and few in BinC. (D) The total number of PH3 + cells per brain shown as z-scores. Statistical analysis was based on Mann-Whitney U test *p<0.05 and **p < 0.01. Control n=4 and *GNG5* OX n=7. Data are represented as mean ± SEM. Scale bars: (A, B) 30 µm. Abbreviations: CTRL: control, dpe: day post electroporation, OX: Overexpression, V: ventricle. Figure adapted from (Ayo-Martin et al., 2020) with permission from Frontiers in Molecular Biosciences.

These results indicate that forced expression of *GNG5* enhances the capacity of progenitor cells to proliferate, especially of the cells located in more basal positions including IPs and bRGs. The results also suggest that in mice, forced expression of *GNG5* induces the transition from aRGs to bRGs, a type of cells that are rare in the mouse brain. Remarkably, the analysis of the GFP expression level of the PH3+, Hopx+ or Tbr2+ quantified cells revealed that most of them did not show any green labelling. This indicates that GFP may either be quickly downregulated after electroporation or a that GNG5 has cell non-autonomous function.

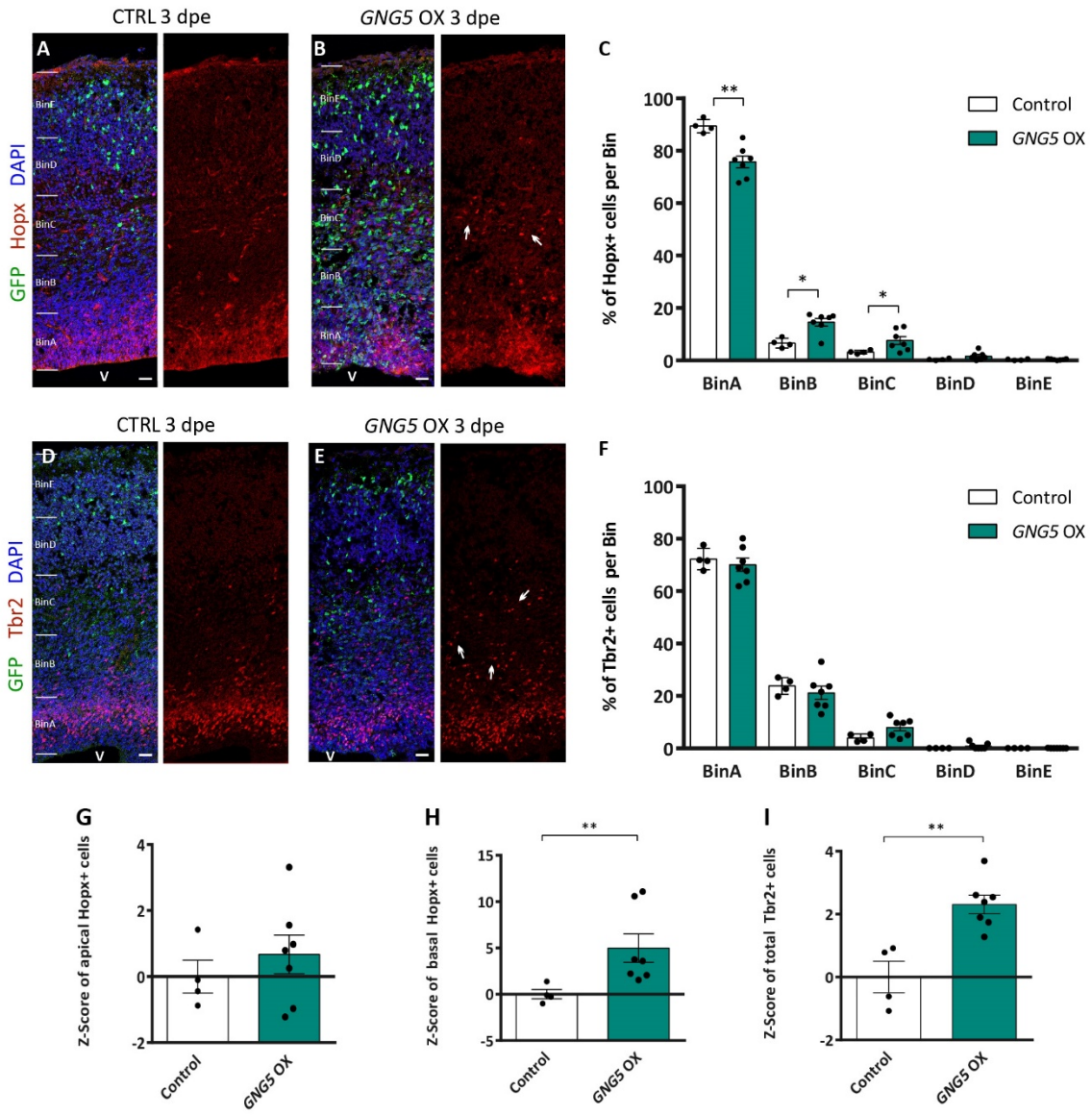

Figure 4.15: Forced expression of *GNG5* in mouse embryos at E13 changes the distribution and number of basal progenitor cells 3 dpe.

(A, B) Pictures of the electroporated lateral cortex of mouse brain sections electroporated at E13 and analysed 3 dpe after stained with the Hopx antibody. Sections were divided into five equal bins for quantification. (C) Graph presenting the proportion of Hopx+ cells per bin. In the brain of embryos in which the control plasmid was electroporated, Hopx+ cells were mainly located in the apical part of the cortex (BinA), while upon *GNG5* OX there was an increased proportion of Hopx+ cells in BinB and BinC. (D, E) Images of the electroporated lateral cortex of mouse brain sections electroporated at E13 and analysed 3 dpe after stained with the Tbr2 antibody. (F) Graph representing the distribution of Tbr2+ cells per bin. In the brain of embryos in which the control plasmid was electroporated, Tbr2+ cells were mainly located in the apical part of the cortex, (BinA and BinB), while in *GNG5* OX even if not significant there was a tendency for an increased proportion of Tbr2+ cells in BinC. The total number of BPs per section per brain shown as Z-scores for: (G) apically located Hopx+ cells; (H) basally located Hopx cells and (I) Tbr2+ cells. Statistical analysis was based on Mann-Whitney U test *$p<0.05$ and **$p < 0.01$. Control n=4 and *GNG5* OX n=7 brains. Data shown as mean ± SEM. Scale bars: (A, B, D, E) 30 µm. Abbreviations: CTRL: control, dpe: day post electroporation, OX: Overexpression, V: ventricle. Figure adapted from (Ayo-Martin et al., 2020) with permission from Frontiers in Molecular Biosciences.

Finally, I also compared the role that GNG5 has in progenitors in mouse and human by examining the integrity of the apical belt using the β-catenin antibody. In contrast to the results *in vitro*, in which the integrity of the apical belt was affected, in mice, it was mostly comparable between *GNG5* OX and control. Only 2 out of the 7 analysed embryos presented disruptions of the apical belt, which indicates a weaker penetrance of *GNG5* in mice compared to human RGs, a reduced fraction of transfected cells between COs and mice. I can also be because the brain is a more stable structure and the disruption of the apical belt is less likely to happen in mice compared to COs. (**Fig 4.16**).

Previous data from the acute downregulation of *Dchs1* and *Fat4* in mice showed comparable changes in the distribution and number of progenitor cells (Cappello et al., 2013). Taken together, a comparison of the phenotypes suggests that overexpression of *GNG5* and downregulation of *DCHS1* and *FAT4* could produce comparable effects both *in vivo* and *in vitro*.

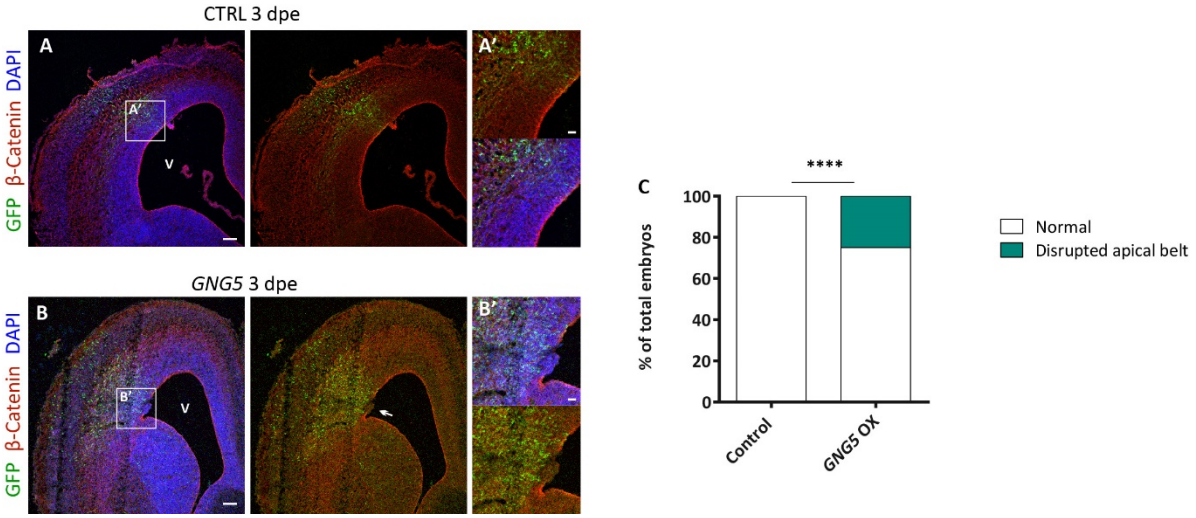

Figure 4.16: Acute overexpression of *GNG5* induces small changes in the apical belt integrity 3 dpe.
(A, B) Pictures of the electroporated lateral cortex of mouse brain sections electroporated at E13 and analysed 3 dpe after stained with the β-Catenin antibody. The arrow indicates the disrupted apical belt in *GNG5* OX. (C') Representative pictures of mouse embryos electroporated at E13 and analysed 3 dpe and stained with the β-Catenin marker. Percentage of embryos with alteration in the integrity of the apical membrane. Statistical analysis was based on exact binomial test ****$p < 0.0001$. β-Catenin: Control n=6 and *GNG5* OX n=8 brains. Scale bars: (A, B, C', D') 30 µm and (C, D) 100 µm. Abbreviations: CTRL: control, dpe: day post electroporation, OX: Overexpression, V: ventricle. Figure adapted from (Ayo-Martin et al., 2020) with permission from Frontiers in Molecular Biosciences.

4.2.9 Forced expression of *GNG5* affects the distribution of neurons *in vivo* 3 and 6 days dpe

One of the reasons behind the expansion and folding of the human cortex is believed to be the increased number of progenitors at basal locations. Interestingly, mutant *DCHS1* and *FAT4* COs contain a population of neurons with an altered transcriptome profile in neurons that also show alterations in their migratory dynamics (Klaus et al., 2019). Taking all this information into consideration, I examined the position of neurons upon overexpression of *GNG5* in mouse embryos. I analysed 2 different time points (3 and 6 dpe) in which the migration of neurons can be analysed properly (**Fig 4.17** and **Fig**

4.18). Remarkably, the forced expression of *GNG5* induced different neuronal alterations even at 3 dpe. More concretely, forced expression of *GNG5* induced diverse forms of neuronal mispositioning (**Fig 4.17 A-D**) in 62.5% of the analysed embryos (**Fig 4.17 E**). Among the different neuronal phenotypes, we can distinguish: disrupted neuronal layering which was present in 25% of the embryos (**Fig 4.17 A, B, B', F**); the presence of ectopic neurons at apical locations which was found in 25% of embryos and resembles the human PH phenotype (**Fig 4.17 A, C, C', G**); and the presence of basally located neurons which occurred in 50% of the embryos. These basally located clusters of neurons sometimes resembled the formation of a small cobblestone (**Fig 4.17 A, D, D', H**). I also performed the analysis at a later timepoint (6 dpe) and this confirmed the phenotypes found at 3 dpe (**Fig 4.18 A-C**). Interestingly, the neuronal phenotypes were more visible. For example, the clusters of apically located ectopic neurons were more pronounced (**Fig 4.18 A-B'**). The same happened with basally located ectopic neurons which generated formations that could be described as rudimental folds (**Fig 4.18 A, C, C'**). In total, 75% of the embryos had some type of neuronal migratory defect at 6dpe (**Fig 4.18 D**). By Laminin immunohistochemistry, I could also confirm that the basement membrane was not totally destroyed, indicating that the formation of the clusters of basally located neurons was a consequence of the overexpression of *GNG5* (**Fig 4.19**). All these results suggest that during the development of the mouse cortex, proper expression levels of *GNG5* are essential for correct neuronal migration and neuronal layering.

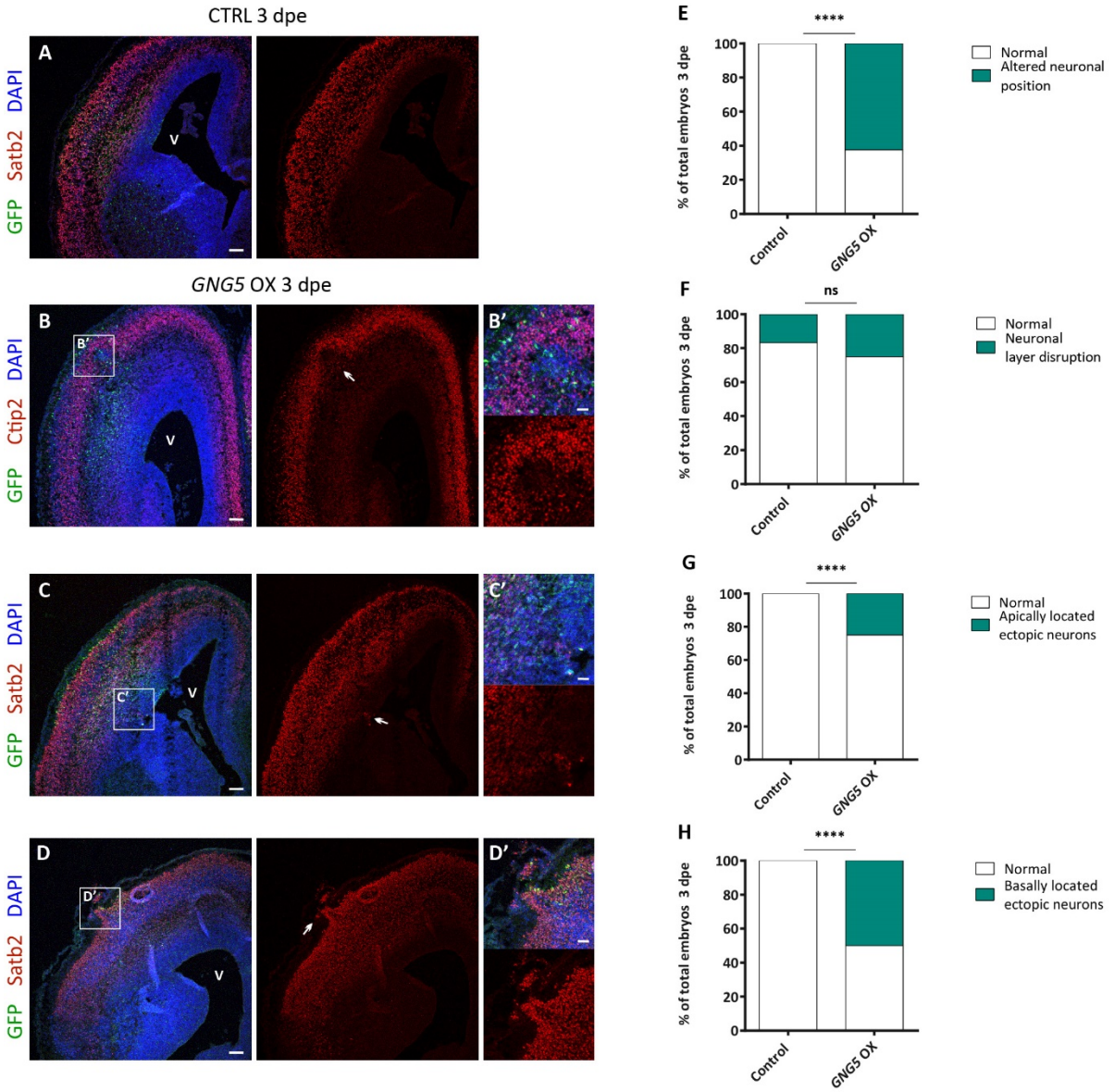

Figure 4.17: Forced expression of *GNG5* promotes migration alterations in mice 3 dpe.

(A) Pictures of the electroporated lateral cortex of a control mouse brain section electroporated at E13 and analysed 3 dpe with a proper neuronal layer marker. (B-D') Representative pictures of brain sections after *GNG5* OX with different neuronal migratory alterations: (B, B') disruption in the neuronal layer; (C, C') apically located ectopic neurons or (D, D') basally located ectopic neurons. (E-H) Percentage of brains from different embryos with a neuronal migratory alteration 3 dpe. Statistical analysis was based on exact binomial test ****$p < 0.0001$. Scale bars: (B'-D') 30 µm, (A-D) 100 µm. E13-E16 Control n=6 and *GNG5* OX n=8 brains. Abbreviations: CTRL: control, dpe: day post electroporation, OX: Overexpression, V: ventricle. Figure adapted from (Ayo-Martin et al., 2020) with permission from Frontiers in Molecular Biosciences.

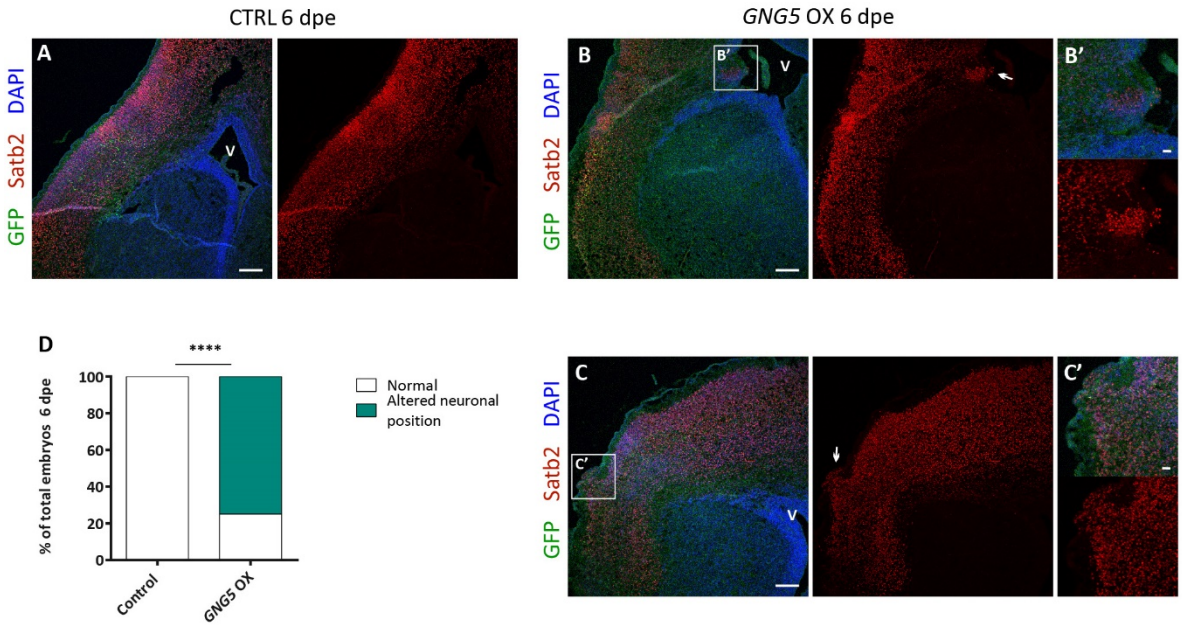

Figure 4. 18: Forced expression of *GNG5* promotes migration alterations in mice 6 dpe.

(A) Pictures of the electroporated lateral cortex of a control mouse brain section electroporated at E13 and analysed 6 days later with a proper neuronal layer marker. (B-C') Representative pictures of brain sections after *GNG5* OX with different neuronal migratory alterations: (B, B') apically located ectopic neurons or (C, C') basally located ectopic neurons. (D) Percentage of brains from different embryos with a neuronal migratory alteration 6 dpe. Statistical analysis was based on exact binomial test ****p < 0.0001. Scale bars: (B'-C') and (A-C) 150 µm. E13-E19 Control n=3 and *GNG5* OX n=8 brains. Abbreviations: CTRL: control, dpe: day post electroporation, OX: Overexpression, V: ventricle. Figure adapted from (Ayo-Martin et al., 2020) with permission from Frontiers in Molecular Biosciences.

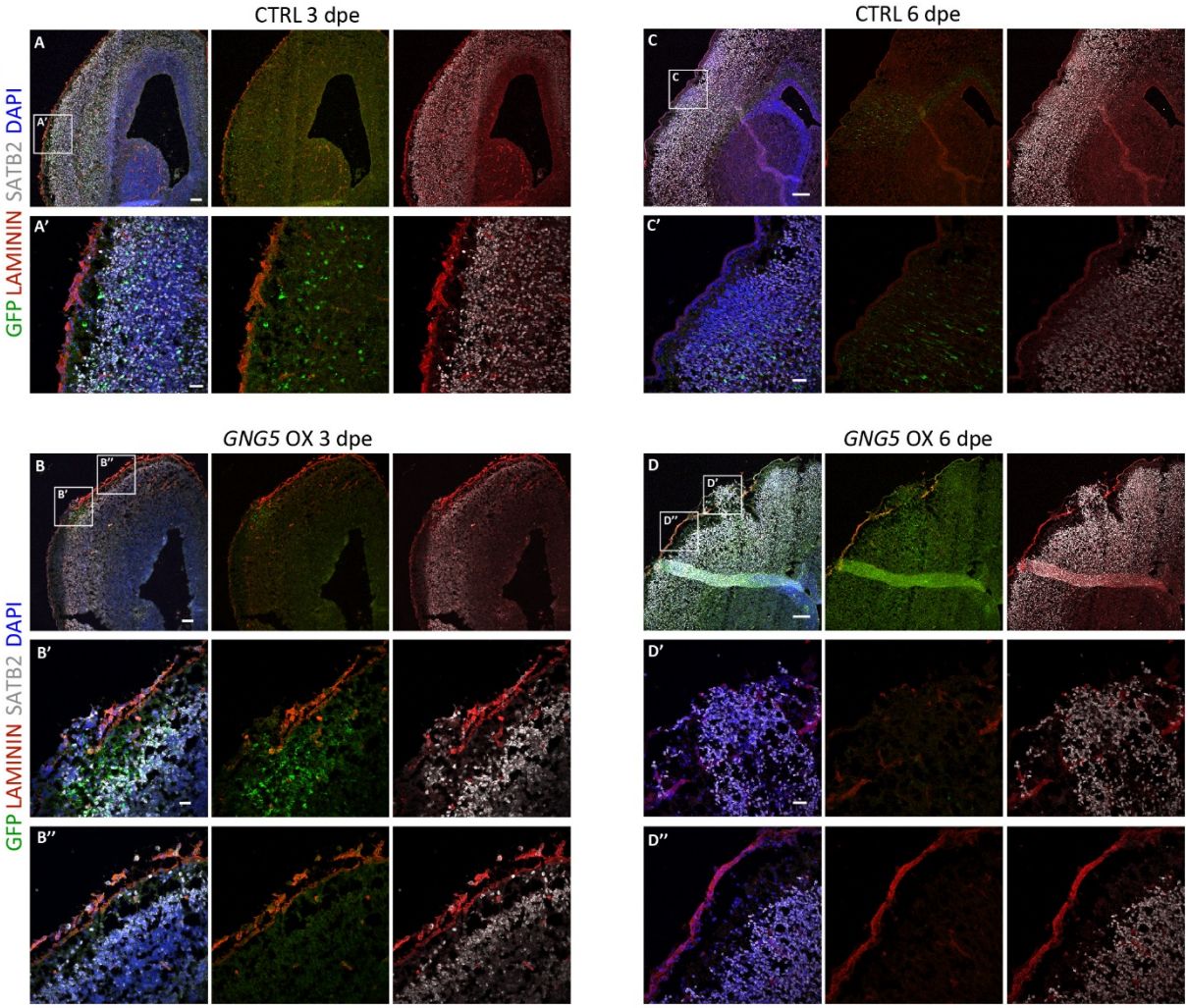

Figure 4.19: Forced expression of *GNG5* induces basally located neurons but does not lead to a disruption of the basal membrane.

Pictures of the electroporated lateral cortex of mouse brain sections electroporated with the control or the *GNG5* OX plasmid at E13 and analysed 3 and 6 dpe. (A, A') Laminin staining 3 dpe indicates the intact basal membrane in control embryos at E13-E16 and (C, C') at E13-E19. (B, B', B'') The forced expression of *GNG5* induces the accumulation of basally located ectopic neurons, but the basal membrane stays intact in (C, C') E13-E16 and (D, D', D'') only slightly altered at E13-E19. Scale bars: (A', B', B'', C', D', D'') 30 µm, (A, B) 100 µm and (C, D) 150 µm. Abbreviations: CTRL: control, dpe: day post electroporation, OX: Overexpression, V: ventricle. Figure adapted from (Ayo-Martin et al., 2020) with permission from Frontiers in Molecular Biosciences.

In **Chapter 5**, I will show the results of the project:

Functional characterization of mature *FAT4* and *DCHS1* mutant cerebral organoids and astroglial cells

Part of this project has been done in collaboration with:

1) Francesco di Matteo and Dr Matthias Eder at the Electrophysiology core facility of the Max Planck Institute of Psychiatry who performed the Silicon probe recording and data analysis
2) Dr Cristiana Cruceanu, Anthi Krontira, Susann Sauer, Maik Ködel and Dr Darina Czamara from the group of Dr Prof. Elisabeth Binder who helped me in the preparation of the libraries and analysis for the bulk RNA sequencing of the astroglial cells.
3) Dr Tobias Straub from the Biomedical Center in Munich performed the analysis of the bulk-RNA sequencing of PAX6+ and NEUN+ extracted nuclei
4) Dr Filippo Cernilogar from the Biomedical Center in Munich helped me with the differential expression analysis of the astroglial cells

CHAPTER 5. FUNCTIONAL CHARACTERIZATION OF MATURE DCHS1 AND FAT4 MUTANT CEREBRAL ORGANOIDS AND ASTROGLIAL CELLS

5.1 PERIVENTRICULAR HETEROTOPIA AND SEIZURES

Patients with Van Maldegem Syndrome suffer from intellectual disability, craniofacial malformations, auditory problems, skeletal anomalies, and the presence of ectopic neurons resembling PH-like phenotype (Maldergem et al., 2008; Mansour et al., 2012). Mutations in the two protocadherins DCHS1 and FAT4 are causative of this syndrome (Cappello et al., 2013). Many patients with any type of PH have seizures and epilepsy. It is, indeed, the presence of seizures in patients that precedes the MRI-supported diagnosis of PH in many cases (Lerche et al., 2001).

A seizure is defined as an incorrect neuronal activity in which neurons are hypersynchronized and overactive. Epilepsy is defined as the recurrent presence of seizures and it is one of the neurological conditions that mostly complicate the daily life of patients and make "normal life" almost impossible (Stafstrom and Carmant, 2015). It is therefore essential to understand and investigate the machinery that is important to maintain the synchronicity and the right level of neuronal activity for the correct function of the brain.

Interestingly, if we look at our scRNA-seq data from Van Maldergem patient cells, we can detect that in the altered cluster of neurons, there are genes essential for synapse formation, axon guidance and the generation of ion channels that are differentially regulated in comparison to control cells (Klaus et al., 2019) (**Fig 5.1**). This knowledge on dysregulated genes related with neuronal activity suggests that mutations in *DCHS1* and *FAT4,* apart from interfering with the correct neuronal progenitor pool preservation and neuronal migration, may also interfere with the maintenance of a correct neuronal activity.

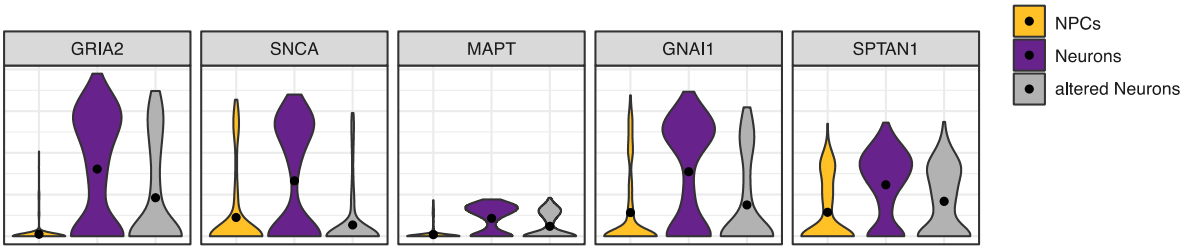

Figure 5.1: scRNA-seq reveals a cluster of neurons with an altered neuronal state.
Violin plots show the expression levels of some example genes that are upregulated in the altered neuronal population (grey) compared with normal neurons (purple) and NPCs (yellow) (adapted from Klaus et al., 2019). Most of these genes are important for synapse and circuit formation. Figure adapted from (Klaus et al., 2019).

On the one hand, in this project, we have tried to understand if the mutations in these two protocadherins could be responsible for the disrupted neuronal activity found in patients with mutations in *DCHS1* and *FAT4.* On the other hand, we tried to understand if the use of COs and novel techniques for their electrophysiological characterization, could be good systems to study functional neuronal activity in a dish.

For that purpose, we have analysed and characterised mature (more than 8-9 months old) control, *DCHS1* and *FAT4* COs at different levels by looking at different features. These COs contain functional neurons with a defined neuronal activity and neurons are found together with other important players for proper neuronal functioning such as astroglial cells.

First, we have examined the transcriptome of mature COs from which we isolated different types of nuclei. Second, in collaboration with Dr Matthias Eder and Francesco di Matteo at the MPI of Psychiatry, we have established a 3D extracellular recording system (Silicon probes) to study aged COs at functional levels. Finally, I have established a protocol to generate astroglia from mature COs. The generation of astroglial cells from control and *DCHS1* and *FAT4* COs has been useful for two different aspects of this project. On the one hand, to understand if the astroglial cells in *DCHS1* and *FAT4* COs differ from controls and may, in consequence, contribute to the phenotypes found in these patients. On the other hand, the generation of astroglial cells from control and mutant COs is an important technology to improve the quality of intracellular electrophysiological recordings, which has not been successful in our hands in previous approaches.

5.2 RESULTS

5.2.1 Mature COs contain most of the cell types expected in mature COs and present characteristics of functional neurons

The COs generated with the protocol in this thesis (Lancaster and Knoblich, 2014) can be maintained in culture for over a year. However, since very few scientists have examined COs that have been in culture for several months, it was important to characterize and look at the cell types present in control COs at this stage. Our analysis revealed that COs contain cells that are dividing or in an active cell cycle shown by different types of proliferative markers such as KI67. The presence of the progenitor markers PAX6, SOX2, NESTIN and TBR2 indicated the presence of aRGs and IPs; and the different astroglial markers such as GFAP or S100β indicated the presence of astrocytes (**Fig 5.2**).

I also examined the different types of neuronal cells present in control COs at this stage and looked at different synaptic markers which could indicate a sign of maturity and network formation. 8-9 months old COs presented general neuronal markers such as MAP2, DCX and NEUN at a similar level as they do at earlier time points. However, it is important to mention that the organization is lost and that the presence of clear GZL and CPL zones disappears with time. COs also presented markers of the different neuronal layers: the deep neuronal layer markers TBR1 and CTIP2, as well as the upper neuronal layer maker SATB2, could be clearly distinguished (**Fig 5.3**).

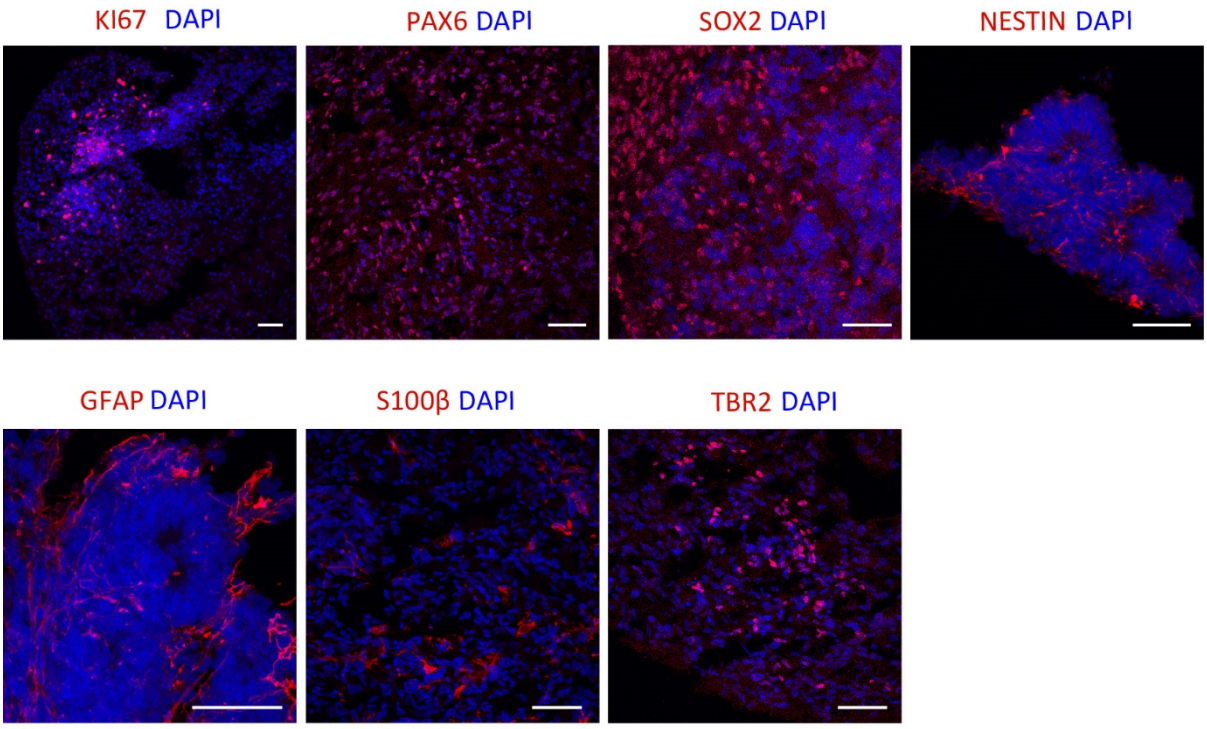

Figure 5.2: Mature COs contain different progenitor and astroglial markers.
Representative pictures of COs at 8-9 months. COs contain different markers of proliferating cells, KI67 and makers for different types of NPCs: PAX6, SOX2 and NESTIN as markers of aRGs and TBR2 as a maker of IPs. COs also contain astroglia cells that can be detected by GFAP and S100β stainings. Scale bars: 50µm. Abbreviations: aRGs: apical radial glial cells; COs: cerebral organoids and IPs: intermediate progenitors.

Moreover, aged COs also presented a significant amount of different synaptic markers: presynaptic vesicles of excitatory neurons were detected by VGLUT1, VGLUT2, SYNAPSIN1 and SYNAPTOPSHYSIN1 immunohistochemistry and the postsynaptic vesicles of excitatory neurons were detected by PSD95 (**Fig 5.3**).

Finally, since the COs obtained with this protocol are unpatterned, I also detected the presence of inhibitory neurons indicated by the GAD67 marker, as well as the presence of synapses of inhibitory neurons detected with the GABAergic marker VGAT (**Fig 5.3**).

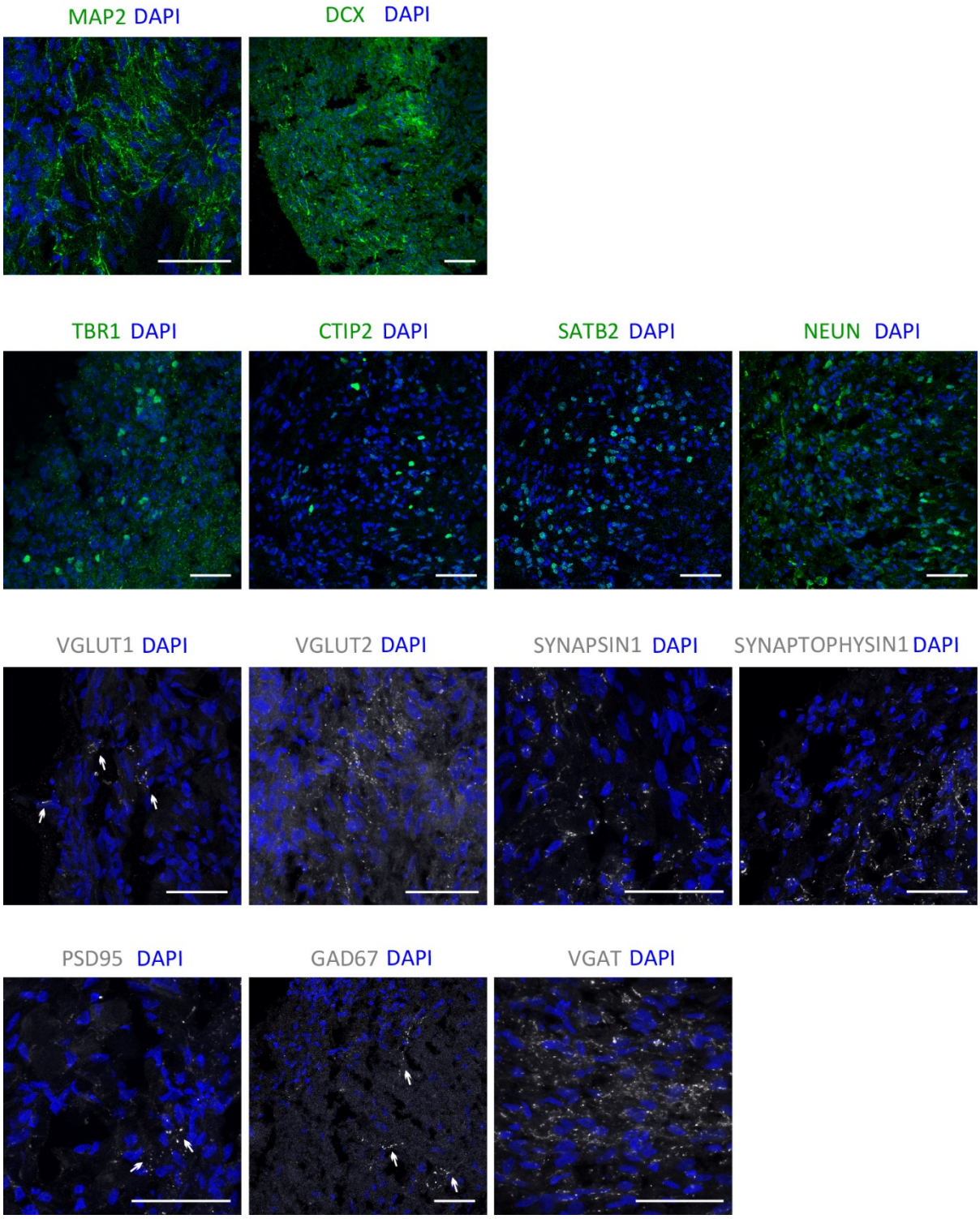

Figure 5.3: Mature COs contain different neuronal and synaptic markers.
Representative pictures of COs at 8-9 months. COs contained both immature and mature neurons, stained by DCX and MAP2. Aged COs also presented markers of the different neuronal layer such as deep layer neurons stained by CTIP2 and TBR1, or upper layer neurons stained by SATB2. COs also contained more general mature neuronal nuclei markers such as NEUN. A sign of maturity in neurons is the presence of pre- and postsynaptic densities. 8-9 months COs contained both presynaptic vesicles stained by VGLUT1, VGLUT2, SYNAPSIN1 and SYNAPTOPHYSIN 1 as well as post-synaptic vesicles stained by PSD95. Finally, COs also presented a small fraction of inhibitory neurons detected by GAD67 staining, which also contained presynaptic vesicles of inhibitory neurons detected by VGAT staining. Scale bars: 50 µm. Abbreviations: COs: cerebral organoids.

5.2.2 Nuclear extraction protocol and the validation of sorted nuclei by quantitative PCR

We have already examined the differences between *DCHS1* and *FAT4* mutant COs at early stages of development and we found interesting differences in the transcriptome of the different mutant COs (Klaus et al., 2019). Once aged COs were characterized and I detected signs of maturity at 8-9 months, we also wanted to examine the transcriptome of control, *DCHS1* and *FAT4* mutant COs at this later time point. Knowing that in early stages of development there are already differences in the expression of genes important for synapse formation and axon guidance in a proportion of neurons in the mutant COs, we expected these differences to be more significant once COs have reached maturity. For that purpose, we designed an experiment that can be visualized in **Fig 5.4**.

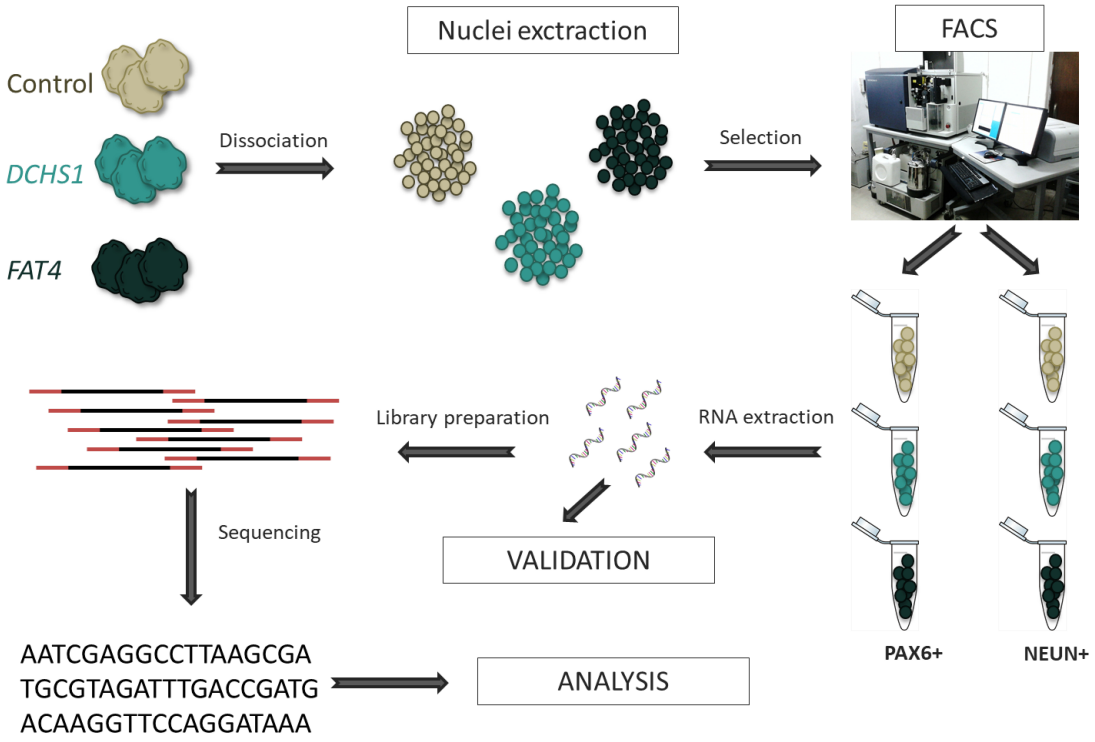

Figure 5.4: Visual summary for the transcriptome analysis of aged COs.
Control, *DCHS1* and *FAT4* COs were dissociated, nuclei isolated and PAX6+ and NEUN+ nuclei separated via FACS. The RNA from the nuclei was obtained and validated before preparing the samples for RNA sequencing. The obtained sequences were analysed with the help of Dr Tobias Straub.

I collected COs from control, *DCHS1* and *FAT4* mutant COs at 4 and 8-9 months, isolated the nuclei and sorted into progenitor cells (PAX6+) or neurons (NEUN+). After the RNA extraction, I validated the quality and the identity of the 4 months old control COs, by qPCR before continuing with the library preparation and RNA sequencing. This step was essential to understand if the protocol for sorting the nuclei was correct and powerful enough. The results (**Fig 5.5**) indicate that indeed this was the case. NEUN+ cells showed an increased relative expression of neuronal markers such as NEUN (significant) and DCX and TUBB3 (not significant but with a clear tendency), compared to PAX6+ nuclei. On the contrary PAX6+ nuclei show and increase expression of PAX6 and NESTIN which are progenitor markers. Finally, I also examined the expression of GNG5 and even if not significant its relative expression was higher in PAX6+ nuclei compared to NEUN+ as expected due to its high expression in progenitor cells (**Fig 5.5**).

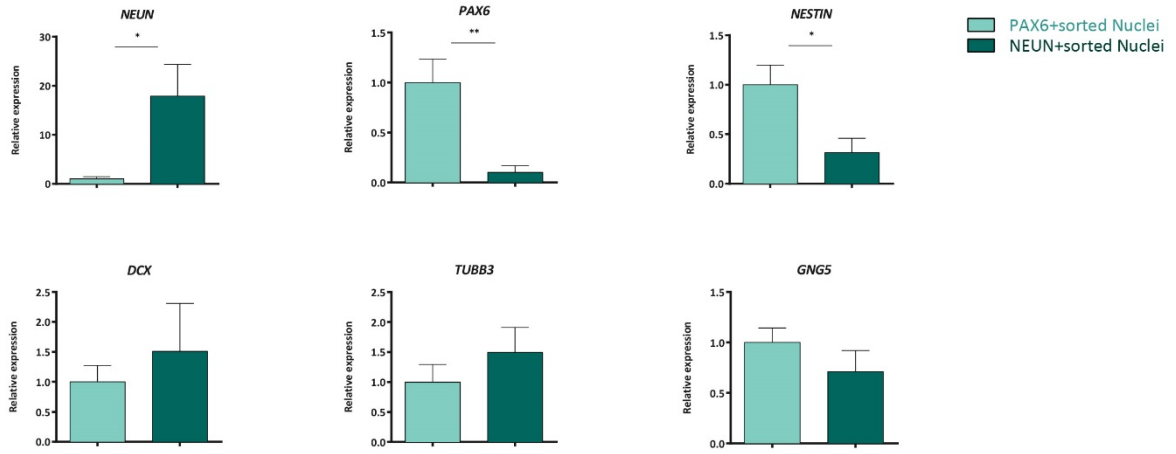

Figure 5.5: PAX6+ and NEUN+ nuclei present characteristics or progenitor and neuronal cells respectively.
Real-time qPCR results from control COs at 4 months for the level of expression of *PAX6, NEUN, NESTIN, DCX*, *TUBB3* and *GNG5*. The results are from PAX6+ and NEUN+ FACS selected nuclei. Statistical significance was based on Student's t-test *p< 0.05, **p< 0.01. Data are represented as mean ± SEM. For *NEUN*, *NESTIN*, and *GNG5*, 9 COs were examined as biological replicates: 5 for PAX6+ nuclei and 4 for *NEUN*+ nuclei. For PAX6, *DCX* and *TUBB3* 10 COs were analyses as biological replicates: 5 for *PAX6*+ nuclei and 5 for *NEUN*+ nuclei. Abbreviations: COs: cerebral organoids. Part of this data was also published in (Di Matteo et al., 2020).

5.2.3 Transcriptome analysis of nuclei extracted from mutant *DCHS1* and *FAT4* aged COs

Once I validated that the PAX6+ nuclei and NEUN+ nuclei contain characteristics of progenitor and neuronal cells respectively we sequence the RNA of 8-9 months old COs-derived nuclei. The sequencing results were analysed with the help of Dr Tobias Straub. Preliminary results from NEUN+ nuclei, that is, from neurons isolated from *DCHS1* and *FAT4* mutant COs at 8-9 months showed very interesting results. We compared the list of differentially regulated genes from this nuclei to the genes that were altered in neurons in the mutant *DCHS1* and *FAT4* COs at 60 days (Klaus et al., 2019). Interestingly, many genes that were dysregulated at that stage were still differentially expressed. At a later time point- A GO term analysis carried in STRING.db (Szklarczyk et al., 2017) showed that the proteins these genes code for are involved in a different subset of processes essential for proper neuronal communication and maturation. On the one side, we see that 19 of these proteins are important for neuronal differentiation, 14 are necessary for proper axon development and 8 for proper axon guidance among many other processes. On the other side, some proteins are implicated in different types of brain disorders such as autism (AUTS2, CNTNAP2) and proper excitatory (SEZ6, NPTX1, NSMF) or inhibitory (LAMB5, JAKMIP1) synapse connectivity. All these results confirmed our hypothesis that in mutant *DCHS1* and *FAT4* COs there are neurons with altered neuronal differentiation and maturation abilities. Therefore, we focused on establishing a method to study neuronal functionally in this *in vitro* system.

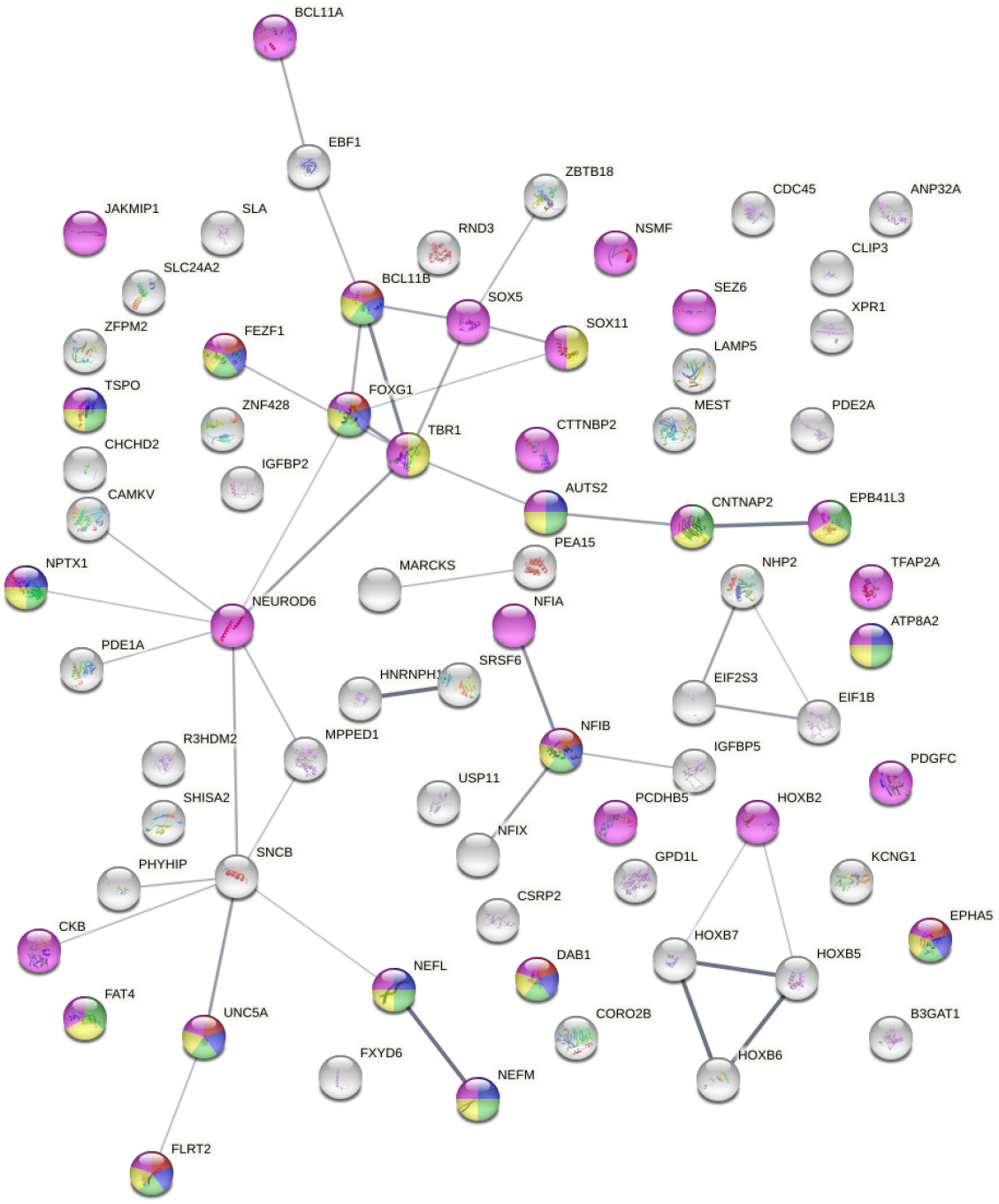

Figure 5.6: GO term analysis of proteins differentially regulated in NEUN+ *DCHS1* and *FAT4* mutant nuclei and in *DCHS1* and *FAT4* mutant neurons at 60 days old COs.

GO term analysis was carried out in STRING.db. Many of the proteins found to be dysregulated in 60 days old neurons from *DCHS1* and *FAT4* mutant COs are still differentially regulated in NEUN+ nuclei from *DCHS1* and *FAT4* aged COs at 8 months. Different colours represent the biological process in which those proteins are involved. (Yellow) neuron differentiation, (Pink) nervous system development, (Green) neuron projection development, (Blue) axon development and (Red) axon guidance.

5.2.4 Aged COs have functional excitatory and inhibitory activity

Knowing the implication of mutation in *DCHS1* and *FAT4* in PH and that patients suffering from this disorder are affected with seizures and epilepsy it is important to know the possible implication of these mutations in the presence of aberrant neuronal activity. Moreover, we know that these two mutations affect the expression of genes important for synapse formation. Since COs at 8-9 months present characteristics of maturity, we also examined their extracellular activity with the help of Dr Matthias Eder and Francesco di Matteo.

With the use of a Silicon probe (**Fig 5.7**), it was possible to look at the activity of neurons in different areas of control, *DCHS1* and *FAT4* mutant COs.

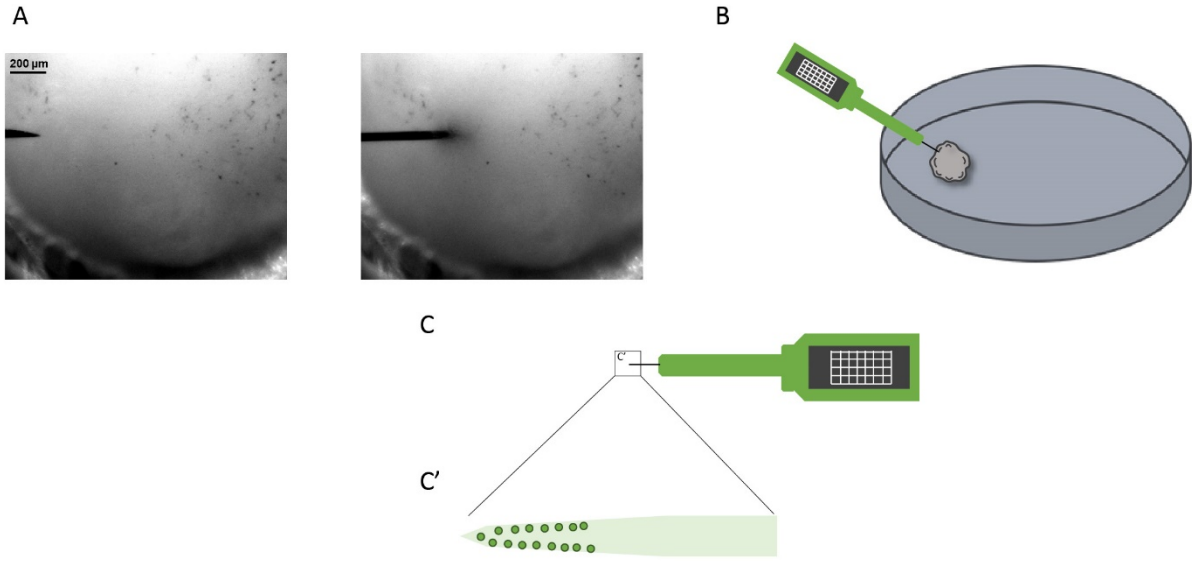

Figure 5.7: Silicon probe recording of spike activity in COs.
(A) Representative photo of a Silicon probe inserted in a COs. Photos are courtesy of Dr Matthias Eder. (B) Representative scheme of figure A in which the CO and the Silicon probe can be distinguished. (C) Illustration of the appearance of the 16 channel acute silicon probe and (C') magnified image of the tip of the probe containing the 16 electrodes. Figures B and C are adapted from Cambridge Neurotech Company´s booklet.

The first thing we examined was the presence of spontaneous neuronal activity (**Fig 5.8**). We confirmed that this activity was real by adding KCl which increased the frequency of that spontaneous activity (**Fig 5.8 A**) and by adding Tetrodotoxin (TTX) a toxin which blocks the sodium channels and stops any kind of specific neuronal activity (**Fig 5.8 B**). Since the mere presence of presynaptic and postsynaptic vesicles does not necessarily indicate the existence of functional synapse and proper neuronal communication, we also added agonist and antagonist of excitatory and inhibitory neurotransmitters. By adding NMDA, an agonist of NMDA excitatory receptors, we showed a reduction of neuronal activity, but when we added the antagonist, D-AP5 the activity came back indicating the presence of functional excitatory neurons (**Fig 5.8 C**). The same happened when we

added GABA, an agonist of GABA inhibitory receptors and its antagonist Bicuculline, also indicating the presence of functional inhibitory neurons (**Fig 5.8 D**).

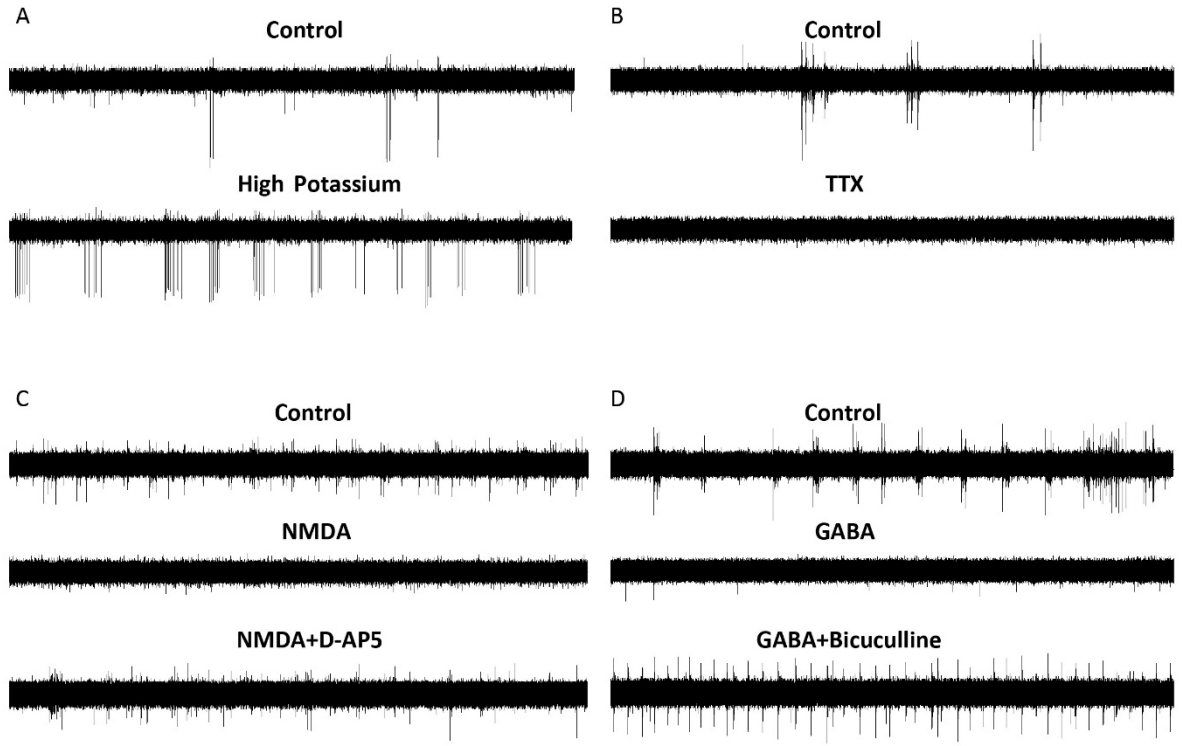

Figure 5.8: Mature COs contain functional excitatory and inhibitory activity.
Pharmacological treatment in mature control COs at 8-9 months. COs have functionally active neurons. (A) COs are reactive to high levels of KCl and (B) are reactive to the TTX toxin. (C) COs are reactive to the excitatory agonist NMDA and (D) the inhibitory agonist GABA. (C) Adding the antagonist of NMDA (D-AP5) and (D) the antagonist of GABA (Bicuculline) inverts the activity, suggesting the presence of active excitatory and inhibitory neurons. Figure is a courtesy of Dr Matthias Eder.

5.2.5 *DCHS1* and *FAT4* mutant COs present higher frequency of spontaneous activity

Once the extracellular recordings with the use of the Silicon probes were validated and the presence of functional excitatory and inhibitory neurons confirmed we focused on examining the frequency of spontaneous activity in control, *DCHS1* and *FAT4* mutant COs. Interestingly, even if the number of spikes recorded in a fixed amount of time (5 minutes) was not different between control and mutant COs (**Fig 5.9 B, D, F**) the percentage of high-frequency spikes (less than 200 milliseconds between each spike) was significantly different between control and mutant COs (**Fig 5.9 A, C, E**). Both *DCHS1* and *FAT4* mutant COs presented and increased the percentage of high-frequency activity. Remarkably, when comparing *DCHS1* and *FAT4* mutant COs we also saw differences in the frequency of spikes, *DCHS1* mutant COs showed a more active neuronal activity which could indicate a more severe phenotype (**Fig 5.9 E**).

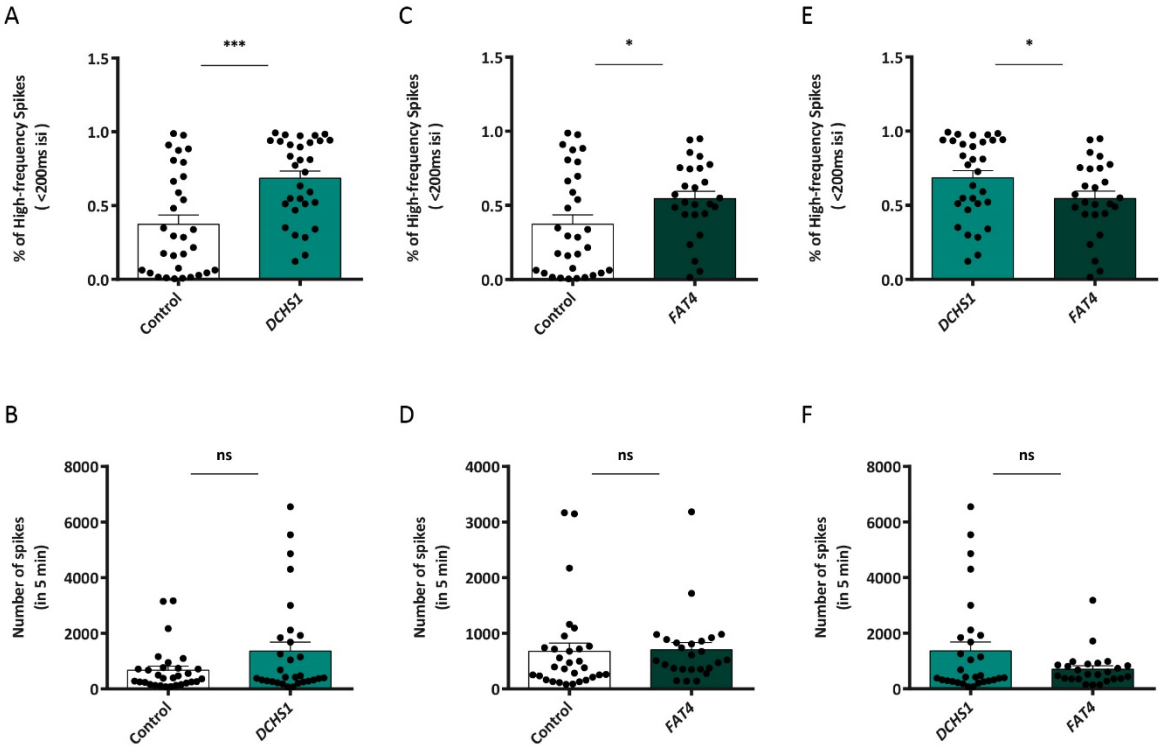

Figure 5.9: Recording of spontaneous activity in mature COs suggest an increased high-frequency activity in *DCHS1* and *FAT4* COs.

(A) *DCHS1* and (C) *FAT4* mutant COs contain a higher number of spikes with increased frequency compared to control COs. (E) The increase in the frequency is also higher in *DCHS1* compared to *FAT4* COs. (B, D, F) The total number of spikes is the same in control, *DCHS1* and *FAT4* COs. Statistical significance was based on Mann-Whitney test *p<0.05 and ***p < 0.001. CTRL b=1, o=6-8, n=31; *DCHS1* b=1, o=6-8, n=31 and *FAT4* b=1, o=6-8, n=24 . n= number of records spots in the COs**.** Data are represented as mean ± SEM. Abbreviations: COs: cerebral organoids; min: minutes; ms: milliseconds; ns: no significant. Results obtained by Francesco di Matteo.

These results even if preliminary and basic, give us two important conclusions: (a) COs are a valid model to study basic functional activity in a 3D system and the silicon probes are a valid tool to examine their extracellular activity; and (b) we have detected differences at a functional level between control, *DCHS1* and *FAT4* mutant COs. The increased high-frequency activity could be an indication of different neuronal behaviour between mutant and control neurons. These results, of course, need to be further investigated to conclude more concrete alterations. Additionally, intracellular recordings of *DCHS1* and *FAT4* mutant COs or neurons will be essential to find the reasons behind the differences in the frequency of this spontaneous activity.

5.2.6 Astroglial cell generation and characterization obtained from aged COs

In the last part of this project, I focused on the generation of astroglial cells from mature COs. Even if many times are forgotten, it is well known that astroglial cells play an important role in neuronal communication. Additionally, the presence of astrocytes is essential for the correct maturation of neurons and proper intracellular recordings *in vitro*. That is the reason why I established a protocol to generate astroglial cells from mature COs. Most of the protocols for the generation of astrocytes are

long and tedious or do not recapitulate all the qualities and characteristics of human astrocytes (Dezonne et al., 2017; Krencik et al., 2011; Li et al., 2018; Palm et al., 2015; Pasca et al., 2015; Roybon et al., 2013; Shaltouki et al., 2013; Sloan et al., 2017; Zhou et al., 2016). The protocol I established also requires the generation of mature COs (over 8 months), however, it is an interesting protocol to use when generating COs for experiments that also require long-term cultures such as functional activity essays. Moreover, it has also been shown that the astrocytes grown for long-term in a 3D system, are one of the most similar to the astrocytes to human mature astrocytes (Sloan et al., 2017). In **Fig 5.10** there is the visual representation for the generation and validation of these astroglial cells. I collected control, *DCHS1* and *FAT4* mutant COs at 8-9 months, dissociated them and plated the cells. After some days in culture, the surviving cells presented and astroglial cell morphology which was validated by different astroglial markers such as the transcription factors SOX9 and NFIA and the marker S100β (Fig (**Fig 5.11**). Additionally, the lack of MAP2 staining which is a marker for neurons indicated the only presence of astroglial cells in these *in vitro* cultures (**Fig 5.11**). It is important to mention that the astroglial cells generated from mature COs thought this protocol do not express well-known astrocytes markers such as GFAP. The reason behind this result, however, could be due to the stage of the cells. It is possible that after the dissociation they acquire a less mature identity and express a different set of astroglial markers.

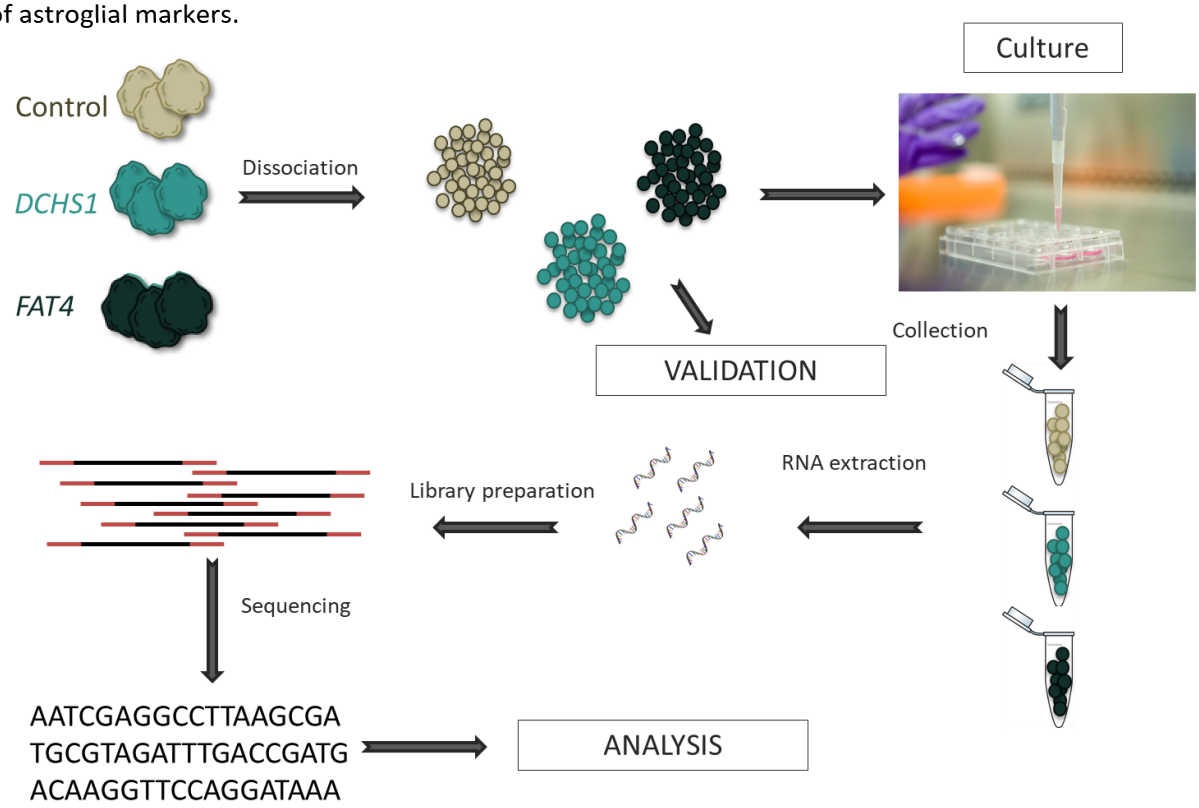

Figure 5.10: Visual summary for the characterization of astroglial cells and their transcriptome analysis.
Control, *DCHS1* and *FAT4* COs were dissociated, and single cells plate for the generation of astroglial cells. The RNA from the nuclei was obtained and the samples prepared for BULK RNA sequencing with the help of Dr Cristiana Cruceanu, Ani Krontira, Susann Sauer and Maik Ködel. In parallel astroglial cells were characterized by immunohistochemistry. The obtained sequences were analysed with the help of Dr Filippo Cernilogar and Dr Darina Czamara.

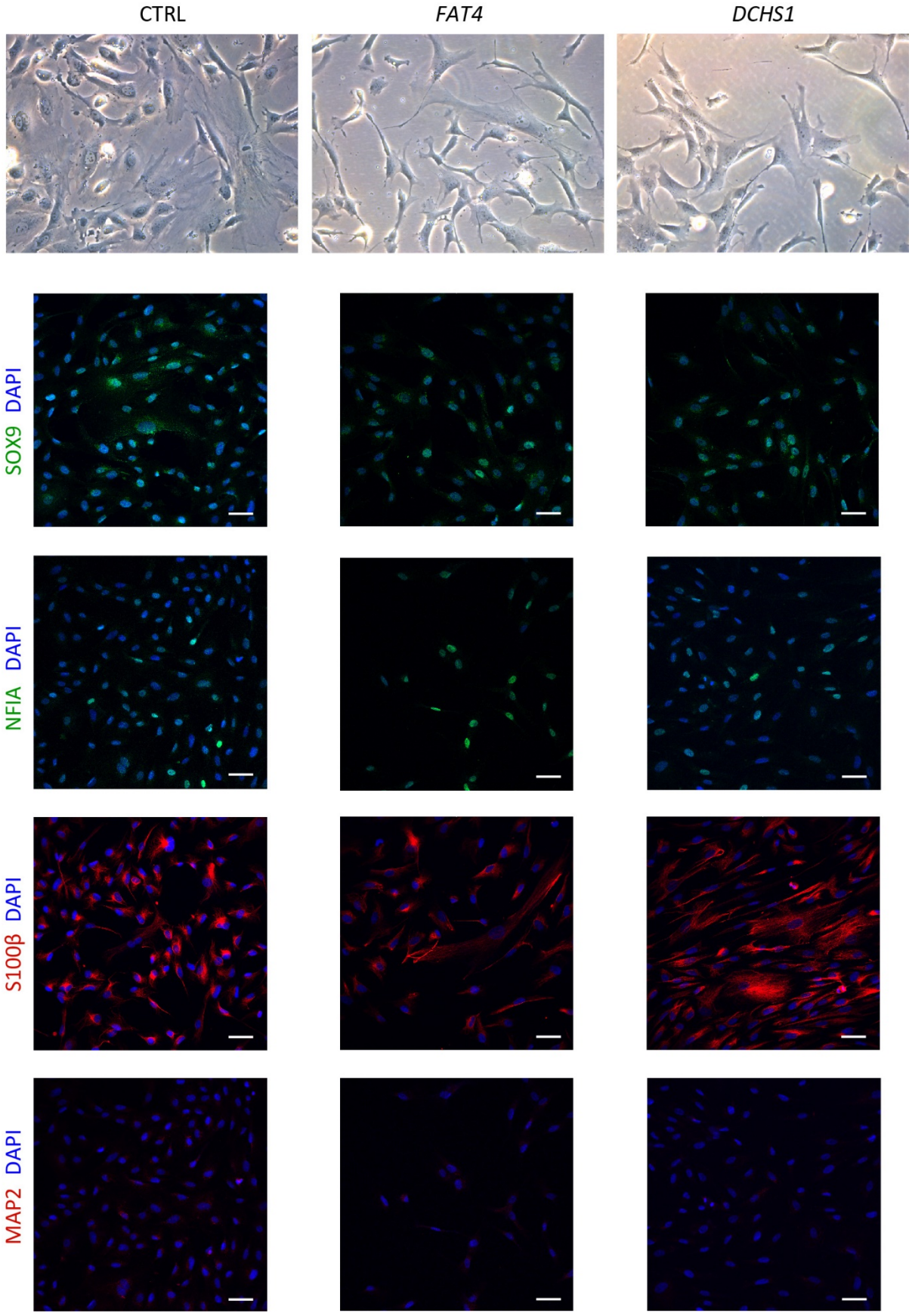
CTRL
FAT4
DCHS1
SOX9 DAPI
NFIA DAPI
S100β DAPI
MAP2 DAPI

Figure 5.11: Astroglial cells obtained from mature COs express different astroglial markers.
Representative pictures of astroglial cells obtained from COs at 8-9 months. Control, *DCHS1* and *FAT4* astroglial cells express different astrocytic markers like SOX9, NFIA and S100β. On the contrary they do not express neuronal markers such as MAP2. Scale bars: 50µm. Abbreviations: COs: cerebral organoids.

However, to confirm the identity of the generated cells and also to examine a possible difference in the transcriptome of astroglial cells in *DCHS1* and *FAT4* mutant COs with the help of members from the group of Prof. Dr Elisabeth Binder and the help of Dr Filippo Cernilogar we sequence and analyse the transcriptome of the cells (**Fig 5.11**).

5.2.7 *DCHS1* and *FAT4* astroglial cells are not very different from controls

The transcriptome data indicates that the cells mainly expressed genes that are compatible with the known genes expressed by astrocytes, bRGs (also known as oRGs) and radial glial cells in general and not of early developed neurons (**Fig 5.12, A**). These data, therefore, confirms the astroglial identity of the cells and validates the protocol for future use.

The results obtained when comparing control, *DCHS1* and *FAT4* astroglial cells however were not so interesting. Very few genes were differentially regulated in *DCHS1* and *FAT4* mutant astroglial cells (42 and 14 respectively) (**Fig 5.12, B**). After examining the genes that were differentially regulated and doing a GO term analysis using the STRING.db database, none of them seemed to be part of the same pathway, there were no significantly enriched biological processes or cellular component. In addition, none of the genes seemed to be important for any processed relevant for the type of research we perform, such us, neurogenesis, differentiation, cell migration… (**Fig 5.12, C** and **Fig 5.13**). Interestingly, when we looked at the expression of *DCHS1* and *FAT4* in astroglial cells derived from COs, the results indicated that the expression of the two protocadherins is very limited (Kanton et al., 2019). Therefore, the expression of *DCHS1* and *FAT4* in astroglial cells could be the reason for not seeing a big difference in the transcriptome of mutant *DCHS1* and *FAT4* astroglial cells compared to controls or they may not have a specific function in this type of cells.

In summary in this project, we have characterized 8-9 months COs at different levels. We have found differences in the transcriptome and at the functional level of *DCHS1* and *FAT4* mutant COs compared to controls. Finally, we have established a protocol for the generation of astroglial cells which could be very useful to further investigate the defective neuronal activity found in mature *DCHS1* and *FAT4* mutant COs.

A

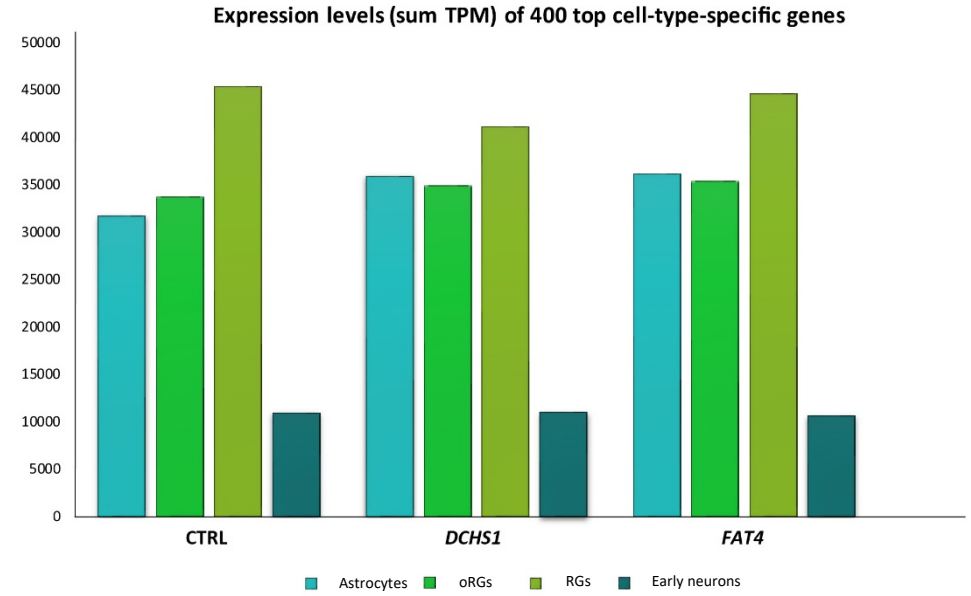

B

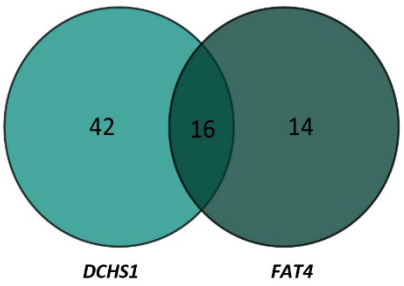

C

Names	total	elements
DCHS1 FAT4	16	CRYZ SLC15A4 PEG3 NAP1L5 LINC00839 PLN MMP1 HSPA12B CADPS2 TYW3 ZNF558 NLRP2 AJAP1 CDA SLC24A3 CHCHD2
DCHS1	42	UNC13A DDX3Y KDM5D LYNX1 ZNF667-AS1 TXLNGY ZNF667 UVSSA LOC441666 USP9Y ZNF528-AS1 PRPH2 ZNF229 UBE2NL EIF1AY PRKY DLSTP1 APOBEC3B CTHRC1 UTY ZNF880 MEDAG ZNF528 NKX3-2 PCDHA6 GAS8 SETD9 PARP8 LDOC1 FAM19A5 DFNB59 ZNF471 MFSD6 SLC2A14 TTTY15 CRIPAK PNMAL1 VSTM2L ZFY NLGN4Y TYW1B LOC389831
FAT4	14	TWIST2 ZNF518B FKBP1AP1 CTSF THEM6 LOC284581 HLA-L NAP1L2 EPGN THNSL2 ESPNL PLBD1 TMEM132B IRX2

Figure 5.12: Transcriptome analysis of the astroglial cells generated from mature COs.

(A) The expression level of the most highly expressed genes in control and *DCHS1* and *FAT4* mutant cells indicate that they have characteristics of astrocytes and astroglial cells.

(B) *DCHS1* and *FAT4* mutant astroglial cells contain 42 and 14 genes respectively that are differentially regulated from controls and 16 genes that are also differentially regulated in *DCHS1* and *FAT4* mutant astroglial cells together. (C) The list of genes that are differentially regulated. Abbreviations: COs: cerebral organoids, oRGs: outer radial glial cell, RG: radial glial cell. Analysis done by Dr Filippo Cernilogar.

A Functional enrichment in the dysregulated proteins in ***DCHS1*** mutant derived astroglial cells

local STRING network cluster

cluster	*description*	*count in gene set*	*false discovery rate*
CL:29369	mostly uncharacterized, incl. Putative golgin subfamily A mem...	3 of 47	0.0296
CL:29374	mixed, incl. Retrotransposon gag protein , and Neuronatin	2 of 12	0.0347
CL:29180	mostly uncharacterized, incl. CCDC144C protein coiled-coil re...	4 of 159	0.0347
CL:33927	mixed, incl. LDOC1-related, and Paraneoplastic antigen Ma	2 of 23	0.0375

PFAM Protein Domains

domain	*description*	*count in gene set*	*false discovery rate*
PF13912	C2H2-type zinc finger	7 of 452	0.0029
PF06292	Domain of Unknown Function (DUF1041)	2 of 5	0.0029
PF01352	KRAB box	6 of 382	0.0032
PF00096	Zinc finger, C2H2 type	7 of 664	0.0075
PF07690	Major Facilitator Superfamily	3 of 117	0.0235

INTERPRO Protein Domains and Features

domain	*description*	*count in gene set*	*false discovery rate*
IPR036051	KRAB domain superfamily	6 of 370	0.0105
IPR016192	APOBEC/CMP deaminase, zinc-binding	2 of 13	0.0105
IPR014770	Munc13 homology 1	2 of 7	0.0105
IPR010439	Calcium-dependent secretion activator domain	2 of 5	0.0105
IPR001909	Krueppel-associated box	6 of 375	0.0105
			(more ...)

SMART Protein Domains

domain	*description*	*count in gene set*	*false discovery rate*
SM01145	Domain of Unknown Function (DUF1041)	2 of 5	0.0017
SM00349	krueppel associated box	6 of 396	0.0020
SM00355	zinc finger	7 of 813	0.0107

B Functional enrichment in the dysregulated proteins in ***FAT4*** mutant derived astroglial cells

local STRING network cluster

cluster	*description*	*count in gene set*	*false discovery rate*
CL:29371	mostly uncharacterized, incl. Retrotransposon gag protein , an...	3 of 32	0.0014
CL:29374	mixed, incl. Retrotransposon gag protein , and Neuronatin	2 of 12	0.0040

PFAM Protein Domains

domain	*description*	*count in gene set*	*false discovery rate*
PF00956	Nucleosome assembly protein (NAP)	2 of 13	0.0069

INTERPRO Protein Domains and Features

domain	*description*	*count in gene set*	*false discovery rate*
IPR037231	NAP-like superfamily	2 of 13	0.0141
IPR002164	Nucleosome assembly protein (NAP)	2 of 13	0.0141

Figure 5.13: GO term analysis of *DCHS1* and *FAT4* mutant astroglial cells.

(A) Functional enrichment of *DCHS1* and (B) *FAT4* mutant derived astroglial cells. The list of dysregulated genes both in *DCHS1* and *FAT4* astroglial cells do not show enrichment for any biological process or cellular component. Network analysis was performed in STRING.db.

CHAPTER 6. DISCUSSION

6.1 GENERAL DISCUSSION

The development of the human cortex is a very complex process and scientists have been trying for decades to understand the machinery that allows it to happen. The function, pathways and mechanism of many genes have been completely understood; however, the majority remain elusive. I believe there are two major paths we can follow to study and understand the processes of cortical formation. On the one hand, we can look at different genes, pathways and mechanisms that have been associated and analyse each of the components in depth. On the other hand, we can look at the wide variety of known neurodevelopmental disorders and look for the genetic cause behind them. By finding the genes that are mutated or dysregulated, we can find key players in corticogenesis. This last approach has been the starting point of the thesis.

I have concretely focused on a neuronal migration disorder, PH, and the genes that have been associated with this disorder: *GNG5*, *DCHS1* and *FAT4*. Thanks to this tactic it has not only been possible to better understand how PH happens and in consequence, increase the future knowledge for finding new treatments for this disorder, but it has also been possible to study and understand the role of key players in correct cortical development that were not well known before or not so well understood. Additionally, thanks to previous studies and collaborative work I have also studied the role of DCHS1 in modern human brain evolution.

This thesis contains new information important for understanding human cortical development from three different perspectives:

1) From an evolutionary point of view: *DCHS1,* one of the genes found to be mutated in patients with PH, has also been shown to be one of the 78 loci that differ between modern humans and its last common ancestor with Neanderthals (Green et al., 2010). In **Chapter 3** I have analysed the alterations that this change from the ancestral form of DCHS1 to the one of modern humans may have induced in human brain evolution using COs.
2) From a developmental point of view: Mutant *DCHS1* and *FAT4* Cos, which have recapitulated some of the features patients with PH have, contain a subset of neurons with an altered neuronal state. The gene that is mostly dysregulated in those neurons is *GNG5* (Klaus et al., 2019). In **Chapter 4** I have studied the role GNG5 has in neurogenesis and neuronal migration.
3) From a functional point of view: Patients with PH normally suffer from seizures. Until now it has not been possible to study the role that *DCHS1* and *FAT4*, the genes associated with VMS and PH, may have in neuronal activity and maturation. In **Chapter 5** I have suggested that COs

could be a good model to study neuronal functionality *in vitro* and I have shown preliminary results that suggest that DCHS1 and FAT4 are important for proper neuronal communication.

6.2 UNDERSTANDING HUMAN CORTICAL DEVELOPMENT BY LOOKING AT EVOLUTIONARY DIFFERENCES

In **Chapter 3** I have analysed the possible alteration of an amino acid substitution in position 777 of DCHS1 protein in modern human brain evolution. Thanks to the full sequence of the Neanderthal genome it was possible to find 78 nucleotide substitutions that were fixed in the genome of modern humans while Neanderthals kept the ancestral form (Green et al., 2010). Modern *DCHS1* was one of the few genes that showed a different sequence compared to the ancestral form. Interestingly, modern humans are the only primates that contain this amino acid substitution (**Fig 3.3**). In this project, I have therefore tried to understand how just one amino acid change in position 777 of DCHS1 protein, in which Neanderthals kept the ancestral form and modern humans acquired a new amino acid substitution, may have induced important evolutionary changes in modern human's brain development.

Unfortunately, access to living Neanderthal material is impossible for obvious reasons. However, due to the advances in genome edition, as well as *in vitro* cellular cultures, it is now possible to design cell lines with the desired genome alteration, convert it to the desired cell type and grow tissue from specific organs. Thanks to this technology and the collaboration with Prof. Dr Svante Pääbo and Stephan Riesenberg at the MPI EVA, it has been possible to grow COs with the ancestral DCHS1 protein and examine the contribution of the modern human change in brain development.

It is important to remember that we are studying one of the 78 changes that were found, which is just one of the amino acid substitutions. Right now, it is not possible to generate a cell line that contains all the amino acid substitutions. Moreover, this is an *in vitro* system and the information that can be obtained is limited. Thus, the changes or alterations found are not conclusive. Additionally, all the results explained in the thesis are from 1 iPSCs clone and to make those results stronger, the obtained data should be replicated in at least one other clone. However, the results, although difficult to interpret, are very interesting and could give us some insights into the role of the modern DCHS1 compared to its ancestral form.

6.2.1 D777N COs show small differences in the developmental trajectory

On the one side, we have seen a total reduction in the number of PAX6+ progenitors in the COs with the ancestral form of DCHS1, D777N. The reduction was specific to the width of the GZL areas (**Fig 3.5**). However, the length of the apical belt and the number of mitotic cells was the same in control

and D777N COs (**Fig 3.6** and **Fig 3.7**). Moreover, the size of the COs was also the same. This set of results indicates that the general growing speed and size of D777N COs are the same as controls but the size of the GZL is different. It is essential to remember that a CO does not recapitulate a unique "brain" or "brain region" but that inside a CO there are different VLs with their corresponding GZL and CP that represent independent developing brain areas. Since the COs I have grown are unpatterned, different brain regions could develop from them, though there is a general tendency for the formation of cortical-like regions identifiable by the progenitor marker PAX6 which stains aRGs. A smaller PAX6+ GZL in the D777N COs could indicate a smaller proliferative cortical-like structure. There is no material from the last common ancestor between the Neanderthals and modern humans and it is therefore very difficult to understand what are the differences that arise that made modern humans and Neanderthals so different. However, we can compare material from Neanderthals and modern humans to understand the most important evolutionary changes. Reconstruction studies from Neanderthal brain differ from one another, but most recent studies did not show a significant difference between the total size of the modern human and Neanderthal brain. However, most of the studies claim that the shape was different as well as the size of specific regions (Gunz et al., 2012, 2010; Neubauer et al., 2018; Pereira-Pedro et al., 2020). That is the case of the visual cortex or the cerebellum for example (Kochiyama et al., 2018; Pearce et al., 2013). The areas we are interested in, that is, the cortex and more concretely, the prefrontal cortex, responsible for the increased intellectual, cognitive, emotional and social abilities in humans (Cikili-Uytun, 2018; Fuster, 2002; Pirozzi et al., 2018; Roth and Dicke, 2005) has also shown some differences. Even though the general size of the frontal lobe does not differ between Neanderthals and modern humans, areas of the prefrontal cortex appear to be different (Gunz et al., 2019). For example, the orbitofrontal cortex, important for decision making, seems to be smaller (Pearce et al., 2013). If this is true or what this means evolutionarily speaking, is complicated to say. Unfortunately, there is no soft tissue that we could study to prove that parts of the frontal cortex of Neanderthals were different. All the analyses are based on the shape and size of very few endocasts. However, considering the importance of the different regions of the prefrontal cortex regarding cognitive abilities, differences in the size or morphology of any of the regions would be something interesting to examine.

The presence of a smaller PAX6+ GZL could also be due to a delayed developmental program. Especially when looking at the trajectory of the widening of the PAX6+ GZL over time from 30 to 75 day (**Fig 3.5K**), the slope for the D777N COs is more pronounced than the one in controls. Which could indicate that while control COs have a stable growing tendency, the growth of the D777N COs is more substantial between 30 and 60 days. Besides, there is an increased number of symmetric divisions at earlier stages of development of the D777N COs compared to controls measured by the angle of

division of mitotic cells in the telophase stage (**Fig 3.8**). The spindle orientation has been previously used as a guidance to understand which type of division a progenitor is going through. A cell will be dividing asymmetrically when the spindle is between 0-60° while in the symmetric division it is between 60-90° (Iefremova et al., 2017). However, this type of analysis does not give us information regarding the type of symmetric or asymmetric division as they can either be proliferative when the mother and at least one of the daughter cells are the same or consumptive when none of the daughter cells is the same as the mother cell (Taverna et al., 2014). An increased number of proliferative symmetric divisions together with the increased size of the PAX6+ GZL width over time could indicate as previously mentioned a delayed developmental program in D777N COs. Interestingly, few paleontological studies have hypothesized about delayed development in the brain of Neanderthals infants compared to modern humans. By studying the endocast of a juvenile Neanderthal skeleton they found that the brain growth was not completed by the time when in modern humans it would have been finalised. The difference in the growth length was assumed to be due to energetic constraints Neanderthals had to grow a slightly larger body and brain (Rosas et al., 2017).

However, according to the generally reduced number of PAX6+ progenitors a consumptive division could make more sense. This would mean that in D777N COs, PAX6+ progenitors divide symmetrically but instead of producing more aRGs they will give raise to IPs. Nevertheless, the reduced number of TBR2+ IPs at 30 days in the D777N COs may be in contrast with this hypothesis (**Fig 3.9**). Unless there is a very rapid generation of neurons from these IPs that could be reflected in the increased number of SATB2+ cells and reduced number of CTIP2+ in D777N COs, marking upper and deep layer neurons respectively (**Fig 3.13**). An increased number of upper-layer neurons could be reflective of the faster developmental program as this type of neurons, colonising the upper cortical layers, are produced later in time. Interestingly, it has been shown that in chimpanzees, even if there is no difference in the spindle orientation of progenitor cells, there is a reduced proliferative capacity of aRGs (Mora-Bermúdez et al., 2016).

It is important to remember that all these are preliminary data and difficult to interpret. Life imaging studies would be very useful to understand which type of symmetric division is the one happening in D777N COs. Additionally, by studying earlier time points we could also have some insights into the speed of the development program in D777N COs. Finally, it would also be interesting to see if there are differences in the length of the cell cycle of progenitor cells as it has also been shown that humans have a longer prometaphase-metaphase compared to chimpanzees (Mora-Bermúdez et al., 2016).

6.2.2 D777N COs show small alterations in neuronal migration

On the other side, there are also differences in the neuronal population in D777N COs. First, there is a general reduction of DCX+ neurons at 60 days (**Fig 3.11**). DCX is a maker for young neurons, therefore these data could indicate a general reduction of the number of neurons expressing this marker or just a reduced expression of this protein, due to the reduced number of PAX6+ or the production of more mature neurons. Secondly, at 60 days, many neurons seem to have migratory alterations in D777N COs. There is an increased number of neuronal processes and cell bodies in the GZL of the D777N COs (**Fig 3.11**). Neuronal migration alterations during cortical development could be due to different reasons: (a) alterations in the morphology of RGs or (b) intrinsic neuronal problems (Klaus et al., 2019). The correct morphology of the RGs and the intact apical belt in D777N COs indicated that the neuronal migration alterations were not due to problems in the scaffold these neurons need to migrate to the correct place but due to intrinsic problems (**Fig 3.11** and **Fig 3.12**). The loss of the N-glycosylation could be the reason for neurons in modern humans to increase their migratory dynamics as this post-translational modification is important for neuronal development and neuronal migration (Medina-Cano et al., 2018; Scott and Panin, 2014). To prove that this is true and how it happens further experiments should be performed. By analysing neuronal dynamics, it would be possible to understand why these neurons migrate differently: if they are slower, they have differences in following a specific trajectory or they are just not able to reach their correct place in the CPL at the same time as modern human neurons. Analysing later time points could also allow us to understand if the neurons are not able to reach their destination or they just need more time. Additionally, proteomic and biochemistry analyses could be useful to study how the loss of the N-glycosylation site affects the different migration dynamics.

Even though many questions remain elusive and data must be replicated, this is one of the first studies in which an ancestral form of a protein that differs from modern humans and the last common ancestor is studied using COs. Thanks to this type of studies it will be possible to have more insights into human brain evolution and cortical development.

6.3 GNG5, A KEY PLAYER IN CORTICAL DEVELOPMENT?

In **Chapter 4** I have examined the role of GNG5 in the development of the mouse and human cortex. After the analysis of scRNA-seq data from *DCHS1* and *FAT4* mutant patient-derived COs, we found that in both types of COs there was a subset of neurons with a different transcriptional expression. Among the list of differentially regulated genes, *GNG5* was the top one. I, therefore, focused on mimicking what we found in *DCHS1* and *FAT4* mutant COs and if it was possible to recapitulate the phenotype

observed with mutations in *DCHS1* and *FAT4* or with their downregulation in mice and humans. It is important to remember that in this project I have only studied one of the dysregulated genes. However, many others could be very interesting to study due to their role in axon guidance or synapse formation, essential for proper neuronal migration and maturation (Klaus et al., 2019).

6.3.1 GNG5 controls the numbers of proliferative cells and is necessary for proper neuronal migration

Interestingly, the results indicate that by overexpressing *GNG5* we have alterations that resemble the phenotypes obtained in mutant *DCHS1* and *FAT4* COs or after the downregulation of those 2 genes in mice and COs.

On the one hand, the results indicate that in mice GNG5 has a clear role in controlling the number of different types of progenitors since after its overexpression we see an increased number of proliferative cells. More concretely there is a general increase of IPs and a specific increase of basally located Hopx cells+ (**Fig 4.14** and **Fig 4.15**). Moreover, there is also a change in the distribution of progenitor cells with an increased number of proliferative cells in higher parts of the cortex corresponding to the SVZ and IZ as well as an increased number of bRGs (**Fig 4.14** and **Fig 4.15**). *GNG5* is regulated by transcription factors essential for proper cortical development, for example, PAX6 and SOX2 (Lachmann et al., 2010; Matys et al., 2006, 2003). Additionally, it is highly expressed in a different type of progenitor cells but with a high incidence in bRGS (**Fig 4.2** and **Fig4.3**). This information made us believe that GNG5 is an essential gene in proper neurogenesis. It is therefore not surprising that after overexpressing it in mice we see alterations in these types of cells. Moreover, in mouse, the presence of bRGs is very reduced and Hopx+ mainly marks aRGs (Penisson et al., 2019; Wang et al., 2011). The presence of ectopic bRGs in bins corresponding to the SVZ and IZ, an area where there are no or very few bRGs in the mouse cortex could indicate that indeed GNG5 is important for the generation of this type of “primate enriched” cells. If it does so by switching the state of aRGs to bRGs or just increases the proliferative capacity of the very few existing bRGs in the mouse cortex remains elusive.

The increased number of bRGs in primates and specifically in humans is believed to be one of the reasons behind the gyrification of the cortex (Fietz et al., 2010; Florio and Huttner, 2014; Kelava et al., 2012; Penisson et al., 2019). Interestingly, acute overexpression of *GNG5* 3 dpe induces migratory alterations in mice (**Fig 4. 17**) and more concretely few of the brains show an increased number of basally located ectopic neurons which increases over time (at 6 dpe) (**Fig 4.18** and **4.19**). Those basally located ectopic neurons have the form of a very small fold or cobblestone-like formations. The increased number of bRGs produced after the overexpression of *GNG5* may be responsible for the generation of those “folds” or cobblestones. It is not the first time that a gene that is enriched in

human bRGs induces these types of phenotypes. That is the case of *ARHGAP11B,* a gene that appears uniquely in humans after a partial duplication of the gene *ARHGAP11A*, it has a radial glial specific signature and its overexpression induces not only an increased amount of bRGs but also expands the mouse cortex and induces its gyrification (Florio et al., 2015).

On the other side, the data obtained from COs also indicates that acute overexpression of *GNG5* in human induces neuronal migration defects (**Fig 4.6** and **4.7**) that may be induced by premature delamination of the RG observed by the disrupted apical belt upon GNG5 overexpression (**Fig 4.8**). Another reason for the neuronal migration defects found both in mice and COs could be due to the defective RG morphology (**Fig 4.5** and **4.11**). It has been previously stated that an alteration in the scaffold for the neurons to migrate to the CP, could induce migratory defects in these cells (Cappello et al., 2006; Klaus et al., 2019).

In contrast to the data obtained in mouse, in COs there was no significant change in the number of different types of progenitor cells (**Fig 4.9**). This could be due to a species-specific difference as we have also observed with the phenotypes obtained after the downregulation of *Dchs1* and *Fat4* in mice and the phenotype of mutant *DCHS1* and *FAT4* COs (Cappello et al., 2013; Klaus et al., 2019). After the acute overexpression of *GNG5* in mice, the downregulation of *Dchs1* and *Fat4* induces a change in the number and distribution of progenitors (Cappello et al., 2013). In mutant COs, on the contrary, there is a population of neurons with an altered neuronal migration dynamic and those are the cells that highly expressed *GNG5* (Klaus et al., 2019).

6.3.2 Hypothesis on the pathways GNG5 is involved

These data indicate that GNG5, DCHS1 and FAT4 may be part of the same pathways or somehow interconnected as the phenotypes obtained both in mice and humans are very similar. Unfortunately, I have not been able to find the answer to how these 3 genes are related. But it is possible to formulate different hypotheses on how they could be interconnected.

GNG5 is highly expressed in mitochondria (MitoCarta). One of our first hypothesis was that any alteration in genes that are important for cell metabolism could be behind the neuronal defects found in the mutant COs. Even if the brain is only 2% of the entire body weight it consumes 20% of the produced energy. In consequence, cell metabolism must be perfectly regulated in the different brain cells to obtain the required energy (Harris et al., 2012; Rolfe and Brown, 1997). The lack of energy that could be produced after defective mitochondrial functioning could be behind the slow migration found in the altered cluster of cells in *DCHS1* and *FAT4* mutant COs. Interestingly, the atypical cadherin Fat in Drosophila, that is the homologue of FAT4 in mammals, has been shown to have an important regulatory role in this subcellular compartment (Sing et al., 2014). The information not only shows the

possible role of GNG5 in cell metabolism but also indicates a possible connection between those two proteins (Ayo-Martin et al., 2020). *GNG5* is not the only gene that is highly expressed in bRGs to be found in mitochondria. ARHGAP11B, is also found in this subcellular organelle and as I explained before is essential for correct human brain development (Namba et al., 2020). . Additionally, it has been shown that mitochondria play a very important role in correct cortical development and cell fate decision (Iwata et al., 2020).

Another question that I was not able to answer is via which mechanism or pathway is GNG5 functioning. As explained in the introduction of this thesis, for the subunit βγ to be released and function in a different type of pathway, it is necessary that a ligand binds to a GPCRs (Gilman, 1987; McCudden et al., 2005). Unfortunately, until now it is not very clear to which GPCRs GNG5 is linked. Interestingly, when looking at the list of differentially regulated genes in *DCHS1* and *FAT4* COs, it was possible to distinguish a few candidates that are part of the G-protein family and could be related to GNG5 (Ayo-Martin et al., 2020; Klaus et al., 2019).

One of those genes is the G protein-coupled receptor 56 (*GPR56* or *ADGRG1*). Mutations in this gene in humans induce bilateral frontoparietal polymicrogyria with phenotypic features of cobblestone-like lissencephaly (Bahi-Buisson et al., 2010). These patients suffer from seizures. In mice mutations in the gene produce cobblestone-like formations due to an increased proliferative capacity of NPCs and an over migration that induces the disruption of the pia membrane (Bae et al., 2014; Li et al., 2008).

Another gene that is highly upregulated and concretely is part of the genes that were used to distinguish the altered population of neurons is the Endothelin receptor B (*EDNRB*) (Klaus et al., 2019) and it has an important role in the cerebellum controlling the proper proliferation of NPCs (Vidovic et al., 2008). ECE2 which has recently been shown to be essential for neuronal migration and progenitor proliferation during cortical development is necessary for the generation of biologically active EDNRB ligands. Manipulation of ECE2 induces cell fate alterations and neuronal mispositioning as well as premature cell delamination similar to what we see after the overexpression of *GNG5* in mice and COs (Buchsbaum et al., 2020).

Finally, as observed in most of the results and especially in the mouse data, most of the ectopic, altered or disrupted cells are GFP- which implies a possible cell non-autonomous role of GNG5. That GNG5 is being secreted and plays a role extracellularly could be one of the explanations for the phenotypes observed. This is a very important observation as until now there are no studies on the possible role GNG5 may have in intercellular communication. However, some proteomic analyses (also performed in the lab) have shown that GNG5 is being secreted through exosomes. Not only GNG5 but also DCHS1, FAT4 and GPR56 are secreted in this type of vesicles (Sharma et al., 2019). This means

that all these proteins may have an important role in cell to cell communication. The fact that the phenotypes observed after mutations or dysregulation of these genes are similar made us believe that they are part of similar secretory pathways. Understanding how all these proteins play a role through exosomes and modulate neurogenesis could help us answer the question on the pathways in which GNG5 is involved (Ayo-Martin et al., 2020).

In summary, in this project presented in **Chapter 4**, apart from studying the role of GNG5 in human and mouse cortical development I have validated a previous study in which this project is based on (Klaus et al., 2019). I have proven that GNG5, the top dysregulated gene in the altered population of neurons in *DCHS1* and *FAT4* COs is a good candidate and could be responsible for the phenotype found in the COs of patients with VMS.

6.4 STUDYING NEURONAL FUNCTIONALITY USING COS AS A MODEL SYSTEM

The project presented in **Chapter 5** has been a collaborative project. Thanks to the expertise in different areas of the people involved we have been able to characterize 8-9 month-old COs from different perspectives. Additionally, I have been able to establish a protocol to generate astroglia cells from those COs.

6.4.1 COs are a good *in vitro* system to study neuronal functionality

The generation of COs and their use in the study of corticogenesis and cortical malformations is a relatively new technology, which was firstly published in 2013 (Lancaster et al., 2013; Lancaster and Knoblich, 2014). It is therefore essential to better understand the limits of this technology and to implement new techniques that could be used on them to understand different aspects of cortical development.

It is well known that many patients with different cortical malformations suffer from seizures and epilepsy (Pang et al., 2008). A seizure is defined as a failure in proper neuronal communication, characterized by a hypersynchronous neuronal activity. Epilepsy is the condition where there are recurrent seizures (Stafstrom and Carmant, 2015). To study how this hypersynchronous activity happens as a consequence of malformations during the development of the cortex it is important to have good model systems. Animal models (Kandratavicius et al., 2014) and different *in vitro* systems such as the use of primary cultures (Dichter and Pollard, 2006) and organotypic slices (Wong, 2011) derived from animals have widely increased our knowledge in proper neuronal communication and functionality. The use of iPSCs and genome editing techniques have also contributed to a better understanding of specific disorders and the contribution of specific genes important for proper neuronal functionality (Hirose et al., 2020). However, new and better model systems are needed. COs

are a good alternative as they allow us to study the function of specific genes in a 3D system recapitulating some aspect of human brain development. Nevertheless, even if many studies have shown their usefulness for studying cortical malformations from a morphological and structural point of view, very few studies have shown their utility as a good model to study malformation of the cortex and their associated conditions such as epilepsy from a functional perspective. One of the very first studies in which they studied COs from a functional point of view was performed by the group of Paola Arlotta in 2017 where they grew retina-like brain organoids and performed extracellular recordings using a Silicon Probe. They found that the neurons were not only functional but also reactive to light (Quadrato et al., 2017). Another study by the group of Alysson Muotri also recorded functional activity in long term cultured COs using a multielectrode array system (MEA) (Trujillo et al., 2019). However, this system has been mainly established to study functionality in 2D *in vitro* systems and the benefits of having a 3D system are lost. The group of Sergiu Pașca developed patch-clamp recording techniques in slices of another 3D culture system, brain spheroids (Pasca et al., 2015). The group of Bennet Novitch also recorder neuronal activity in acute slices of 3 months old COs (Watanabe et al., 2017). Finally, the group of Guo Li Ming also recorder functional neuronal activity in acute slices of 80 days old COs grown in the so-called, mini reactors (Qian et al., 2016). Not only is the number of studies in which the neuronal maturity of COs is analysis reduced, but the studies in which patient-derived COs are used is almost inexistent to date. Moreover, from the studies explained above only one of them took advantage of studying the neuronal activity in an intact 3D system. For this reason, we believed it was essential to validate our *in vitro* system at different levels and probe that they are appropriate for functional studies. That is what we have done in the first part of the project explained in **Chapter 5**.

On the one side, we could confirm that COs grown for over 8 months in culture contain all the essential elements for proper neuronal functioning: progenitors, astrocytes, excitatory and inhibitory neurons and more importantly, pre- and post-synaptic excitatory and inhibitory vesicles, elements essential for proper neuronal communication and network formation (**Fig 5.2** and **Fig 5.3**). On the other side, we confirmed the presence of spontaneous and functional neuronal activity (**Fig 5.7**) as well as the existence of functional excitatory and inhibitory receptors (**Fig 5.8**).

But what makes our project so unique is that for the very first time, we have recorded neuronal activity in patient-derived COs with a neurodevelopmental disorder, more concretely, in COs carrying mutation in *DCHS1* or *FAT4*. As previously described, these COs contain an altered neuronal population with a subset of dysregulated genes among which we can find important players in axon guidance and synapse formation (Klaus et al., 2019) (**Fig 5.1**). Interestingly, we found differences in the number of high-frequency spikes over time both in *DCHS1* and *FAT4* COs compared to control (**Fig 5.9**). These

results are very preliminary data but give us two important take-home messages. Firstly, that COs cultured for a long period are very valid *in vitro* system to study neuronal activity for healthy and patient-derived iPSCs in a 3D system. Secondly, there are important functional differences in *DCHS1* and *FAT4* mutant COs.

Nevertheless, there are still many questions to be answered and experiments that could be performed to increase the knowledge on the usefulness of COs as an *in vitro* model to study functional neuronal activity and network formation. Moreover, more experiments should be performed to detect the reason behind the functional alterations in *DCHS1* a *FAT4* mutant COs. On the one side, we did not perform any pharmacological treatment in *DCHS1* and *FAT4* mutant COs while recording their activity. This type of experiments will give us more insights into which kind of activity is disrupted and which type of receptors are involved. On the other side, with the Silicon Probes, we are only looking at the extracellular activity. However, it would be very useful to establish patch-clamp techniques to record intracellular activity in our COs to also analyse the intrinsic properties of neurons grown in a 3D structure and have a full overview on the functional alteration in *DCHS1* and *FAT4* mutant COs. The group of Sergiu Pașca also developed techniques to dissociated brain spheroids as well as COs to performed patch-clamp to study the neuronal activity from COs. They used this technology to study neuronal activity from patients COs with the 22q11.2 deletion syndrome (22q11DS), causative of neuropsychiatric disorders (Khan et al., 2020). Similarly, in the lab, we have developed a protocol to grow neurons from COs in a monolayer with the idea of performing patch-clamp in them. Francesco di Matteo, a PhD student in the lab, is establishing this technique which would be a perfect complementary data to the extracellular recording already performed. A combination of pharmacology, extracellular and intracellular recordings will give us all the necessary information to understand which are the possible defects in *DCHS1* and *FAT4* mutant mature neurons. Additionally, we are also differentiation neurons from *DCHS1* and *FAT4* mutant NPCs, that is, a 2D system. By comparing the results obtained from the 2D and 3D systems we could have a better overview on the advantages of COs in disease modelling from a functional perspective as COs recapitulate better aspects of human brain development *in vivo*. Furthermore, as it has recently been shown, COs could also be transplanted in the mouse developing brain (Daviaud et al., 2018; Mansour et al., 2018). By doing so, COs could grow in a real environment with a proper vascular and immune system. It would therefore be possible to study human to human neuronal connectivity inside the COs in an *in vivo* system.

Finally, the question if the difference in neuronal activity in the mutant COs is caused by the altered population of neurons remains elusive. To be able to study the altered population of neurons we should be able to identify them in the COs and record their activity. One way to assess this question

could be by using one of the dysregulated genes that is found in the cell membrane such as *ROBO3*. ROBO3 is a transmembrane receptor important for commissural axon guidance (Friocourt and Chédotal, 2017). While ”normal” neurons do not express this receptor, the altered population of neurons does. Being a receptor, it would be easy to select the neurons that express it and in consequence, we could detect the altered population of neurons, label them and possibly record their intracellular activity.

6.4.2 The establishment of new technology to study the transcriptome of aged COs

Combining the recording and analysis of the functional neuronal activity of COs kept in culture for a long term with scRNA-seq data would be the perfect approach to have a full overview of the reason behind the pathology of any given neurological disorder in which there are alterations in neuronal activity, function and/or communication. Unfortunately, scRNA-seq may not be the most optimal technique due to its high cost and the actual difficulties of getting the proper material to perform this technique in aged COs (over 8-9 months). After keeping COs in culture for a very long period, the tissue is tight and getting single-cells sometimes is complicated. In **Chapter 5** I have developed a protocol for the isolation of neuronal (NEUN+) and progenitor (PAX6+) nuclei in COs adapted from (Krishnaswami et al., 2016) (**Fig 5.4**). By following this protocol, it is possible to isolate both neurons and progenitors from long-term cultured COs which can then be analysed as desired. We verified the suitability of the protocol by real-time qPCR confirming the high level of expression of NEUN and PAX6 in isolated neurons and progenitors respectively (**Fig 5.5**).

The preliminary data from the Bulk RNA sequencing of the neurons and progenitors from aged *DCHS1* and *FAT4* mutant COs gave us more insights into the possible alterations behind the phenotype found in patients with VMS from a functional perspective. Similarly to the neurons from *DCHS1* and *FAT4* mutant COs at 60 days (Klaus et al., 2019), aged *DCHS1* and *FAT4* mutant neurons (NEUN+) still contain some of the same dysregulated genes essential for proper neuronal differentiation (*BCL11B, TBR1, CNTNAP2, SOX11*…), axon development (*EPHA5, FLRT2, EPBA1L3*…) or axon guidance (*FLRT2, UNC5A, FEZF1*…), processes essential for proper neuronal maturation and connectivity (**Fig 5.6**). By looking closer to specific genes, we distinguished some that may be interesting for further study. That is the case of *SE6Z* which has been associated with febrile seizures and is necessary for the proper cell to cell signalling and arborization of cortical neuron dendrites as well as their proper excitability (Gunnersen et al., 2007; Mulley et al., 2011). *LAMP5* is another interesting gene, essential for proper GABAergic synaptic transmission (Tiveron et al., 2016). Another interesting gene is *CNTNAP2* which is necessary for cell to cell interaction in the nervous system. It has been associated with different developmental disorders such as autism or intellectual disability (Rodenas-Cuadrado et al., 2014). Mouse models of KO models of *Cntnap2* suffer from epilepsy and neuronal migration problems (Peñagarikano et al.,

2011). These are just some of the examples we could look at. By combining a further analysis of the dysregulated genes with proper functional studies it would be possible to shed light into the complete mechanisms and pathways that are disrupted in *DCHS1* and *FAT4* mutant COs and better understand the reason behind the malformation of the cortex in those patients.

6.4.3 Generation of astrocytes from aged COs

Astrocytes are a type of glial cells, one of the types of non-neuronal cells that populate the brain. Even if until now there is no clear data on the real amount of these cells populating the human brain, it has been clearly stated that they are essential for proper neuronal communication (Durkee and Araque, 2019).

The implementation of astrocytes in neuronal cultures to improve the quality of the neuronal recordings has been widely used in the past, however, most of the neuronal *in vitro* cultures were enriched with mouse or rat derived primary cultures of astrocytes (Sofie et al., 2012). This technique may not be the most appropriate one due to the species-specific differences. Many scientists have therefore tried to generate astrocytes from hESC or iPSCs. Most of the protocols are long and tedious, it takes between 2 to 6 months to get a mature astrocytic culture, and relies on the generation of progenitor cells for a further differentiation to astrocytes (Krencik et al., 2011; Palm et al., 2015; Roybon et al., 2013; Shaltouki et al., 2013). Fortunately, in recent years, scientists have developed protocols in which astrocytes can be obtained in up to 30 days (Emdad et al., 2012; Mormone et al., 2014; Zhou et al., 2016). However, those astrocytes have not been so well characterized and the quality regarding improving neuronal communication remains in most of the cases elusive. Other scientists have tried to accelerate the natural process of astrocyte generation by the expression of specific transcription factors (Li et al., 2018). Even if the quality and the function of these astrocytes has been properly validated, adding artificial factors for a certain type of experiments may not be ideal. Additionally, thanks to the development of 3D *in vitro* cultures such as the generation of spheroids or brain organoids, and the presence of astrocytes in these structures later during development, some researchers have also isolated and characterized astrocytes from these structures. In the case of brain spheroids astrocytes have been isolated at 17-20 months (Pasca et al., 2015; Sloan et al., 2017) while from COs at 45 days (Dezonne et al., 2017). Even though in both cases astrocytes showed signs of functionality and the expression of characteristic markers, it has been shown that by keeping astrocytes in culture over time they transition to a more mature state (Sloan et al., 2017).

In this **Chapter 5,** I have established a very similar and quick protocol to the one from Dezonne et al., 2017, but for the generation of astroglial cells from 8-9 month-old COs to obtain a more mature state of these cells (**Fig 5.10**).

Even though the astrocytes generated with this protocol have not been fully characterized in terms of improving the quality of neuronal activity and maturity, we have been able to show some characteristics that could make them good candidates for proper neuronal-astrocyte coculture. Immunostaining analysis indicates that they express astrocytic markers such as S100β, NFIA or SOX9 and do not express neuronal marker such as MAP2 (**Fig 5.11**). Moreover, the differential gene expression analysis performed in control astroglial cells indicates that they mainly express markers of astroglial identity (**Fig 5.12**).

Nevertheless, to claim that the astroglial cells generated from aged COs are functional more experiments should be performed. On the one hand, it is important to see if the co-culture of neurons with these astroglial cells improves the quality of the neuronal activity recordings. On the other hand, it is important to understand the maturity level of these astroglial cells. Even though they were grown for over 8 months in a 3D system, we do not know how the dissociation and replanting of the cells affected their maturity.

Finally, since our final aim is always to study the healthy and disease brain and look for possible dysregulated pathways with a final aim of understanding better brain development and maturation, we also analysed the astroglial cells derived from mutant *DCHS1* and *FAT4* COs. Unfortunately, and possibly due to the low expression of these two genes in astroglial cells (Kanton et al., 2019) we did not find any remarkable difference after the differential expression analysis (**Fig 5.13**).

6.5 CONCLUSIONS AND FUTURE PERSPECTIVES

This thesis contains the results of three different projects that are interconnected. All the three projects are based on previous studies carried out in the lab where mutations in the two protocadherins, DCHS1 and FAT4 have been associated with PH, a malformation of the cortex characterized by the failure of neurons to migrate (Cappello et al., 2013).

In **Chapter 3** I have investigated the role of DCHS1 in human brain evolution by studying D777N COs, that contain the ancient form of the protein. The unique amino acid change seems to have been important for the generation of the proper number of apical progenitors and may have induced a change in neuronal migration. The role of DCHS1 and FAT4 in proper progenitor pool maintenance and neuronal migration were previously shown (Cappello et al., 2013; Klaus et al., 2019). Interestingly, in COs derived from patient iPSCs with mutations in *DCHS1* and *FAT4,* it was possible to

identify a cluster of neurons with an altered neuronal state (Klaus et al., 2019). One of the signatures of these neurons was the upregulation of the progenitor marker GNG5. In **Chapter 4** I have shown that remarkably, the acute upregulation of *GNG5* also induces differences in the numbers of progenitors in mice and controls proper neuronal migration in mice and human. Taken together this data indicates that GNG5, DCHS1 and FAT4 may be part of the same pathway. Finally, in **Chapter 5**, apart from confirming the appropriateness of COs as a good *in vitro* model system for the study of neuronal activity, we have proved that mutations in *DCHS1* and *FAT4* induce neuronal activity changes.

Futures studies will try to understand how a unique amino acid change has induced the changes found in D777N COs. How the upregulation of *GNG5* induces similar results to the downregulation and or mutations of *DCHS1* and *FAT4,* may induce similar phenotypes and via which pathways and mechanism they are connected. Finally, how mutations in *DCHS1* and *FAT4* induce neuronal activity differences.

Even if many questions remain indefinable, that is the beauty of science. Trying to answer a question many others arise, however, I strongly believe that any small discovery is an open door for others to continue investigating, with a final aim of better understanding how the brain develops, how different disorders arise so to find better treatments and increase our quality of life.

CHAPTER 7: MATERIALS AND METHODS

7.1 TABLES FOR MATERIALS AND METHODS

Table 1: List of all the general components used in this thesis.

Compound	Catalogue #	Vendor
100 µm cell strainer	352360	Corning®, New York, USA
5-bromo-2'-deoxyuridine (BrdU)	B5002	Sigma Aldrich, St. Louis, MO, USA
AMPure XP beads	A63881	Beckman Coulter, California, USA
Aqua-Poly/Mount	18606-20	PolyScience, Illinois, USA
BD round bottom polystyrene test tubes with cell strainer snap cap	352235	Corning®, New York, USA
Boric acid (H_3BO_3)	6943.1	Carl Roth, Karlsruhe, Germany
Bovine serum albumin (BSA)	A4503-50G	Sigma Aldrich, St. Louis, MO, USA
Chloroform	102445	Millipore, Massachusetts, USA
microTUBE AFA Fiber Pre-Slit Snap-Cap 6x16mm	520045	Covaris, Chicago, USA
DH5 α subcloning efficiency competent bacteria	18265017	Thermo Fisher Scientific, Waltham, MA, USA
Dithiothreitol (DTT)	D0632	Sigma Aldrich, St. Louis, MO, USA
DNase I (RNAase free)	M0303	NEB, Massachusetts, USA
Ethanol (C_2H_5OH)	5054.3	Carl Roth, Karlsruhe, Germany
Fast Green FCF	F7252	Sigma Aldrich, St. Louis, MO, USA
Glass Micro pipets	5-000-1001-X10	Drummond Scientific, Broomall, PA, USA
Hydrochloric acid (HCl)	20 252 290	VWR chemicals, Radnor, PA, USA
Magnesium chloride ($MgCl_2$)	HN03.1	Carl Roth, Karlsruhe, Germany
Monopotassium phosphate (KH_2PO_4)	3904.1	Carl Roth, Karlsruhe, Germany
Normal goat serum (NGS)	S-1000	Vector Laboratories, CA, USA
OCT Compound	361603E	VWR chemicals, Radnor, PA, USA
Paraformaldehyde (PFA)	30525-89-4	Millipore, Massachusetts, USA
Potassium chloride (KCl)	6781.3	Carl Roth, Karlsruhe, Germany
Protease Inhibitor Cocktail	P2714	Sigma Aldrich, St. Louis, MO, USA
QIAzol® Lysis Reagent	79306	Qiagen, Hilden, Germany
Random primers	481900-11	Thermo Fisher Scientific, Waltham, MA, USA
Murine RNase inhibitor (RNAse IN)	M0314	NEB, Massachusetts, USA
Recombinant restriction enzymes: NheI & EcoRV	R0131 & R0195	NEB, Massachusetts, USA
Sodium chloride (NaCl)	3957.1	Carl Roth, Karlsruhe, Germany
Sodium citrate tribasic dihydrate ($C_6H_5Na_3O_7 \cdot 2 H_2O$)	4088.1	Carl Roth, Karlsruhe, Germany
Sodium phosphate dibasic (Na_2HPO_4)	10049-21-5	Millipore, Massachusetts, USA
Sucrose ($C_{12}H_{22}O_{11}$)	S7903-1KG	Sigma Aldrich, St. Louis, MO, USA
Tris ($C_4H_{11}NO_3$)	4855.2	Carl Roth, Karlsruhe, Germany
Triton ® X 100	3051.1	Carl Roth, Karlsruhe, Germany
Tween® 20	9127.1	Carl Roth, Karlsruhe, Germany

Table 2: List of all the cell culture components used in this thesis.

Compound	Catalogue #	Vendor
2-Mercaptoethanol (50 mM)	31350010	Thermo Fisher Scientific, Waltham, MA, USA
Accutase® solution	A6964	Sigma Aldrich, St. Louis, MO, USA
Antibiotic Antimycotic Solution (100X)	A5955	Sigma Aldrich, St. Louis, MO, USA
B-27™ Supplement (50X)	17504044	Thermo Fisher Scientific, Waltham, MA, USA
B-27™ Supplement (50X), minus vitamin A	12587010	Thermo Fisher Scientific, Waltham, MA, USA
basic fibroblast growth factor (bFGF)	100-18B	Peprotech, Rocky Hill, NJ, USA
DMEM/F-12, HEPES	11330032	Sigma Aldrich, St. Louis, MO, USA
DMEM/F-12+GlutaMAX™ Supplement	10565018	Thermo Fisher Scientific, Waltham, MA, USA
Dimethyl Sulfoxide (DMSO)	D2650	Sigma Aldrich, St. Louis, MO, USA
Dulbecco's Phosphate Buffered Saline (DPBS)	D8537	Sigma Aldrich, St. Louis, MO, USA
GlutaMAX™ Supplement	35050061	Thermo Fisher Scientific, Waltham, MA, USA
Heparin	H3149	Thermo Fisher Scientific, Waltham, MA, USA
hESC-quality Fetal Bovine Serum (FBS)	10270106	Thermo Fisher Scientific, Waltham, MA, USA
Insulin	I9278	Sigma Aldrich, St. Louis, MO, USA
KnockOut™ Serum Replacement	10828028	Thermo Fisher Scientific, Waltham, MA, USA
Matrigel® Basement Membrane Matrix, LDEV-free	354234	Corning®, New York, USA
MEM Non-Essential Amino Acids Solution (100X)	11140035	Thermo Fisher Scientific, Waltham, MA, USA
mTESR1 medium and supplement	85850	Stem Cell Technologies, Vancouver, Canada
N2™-Supplement (100X)	17502048	Thermo Fisher Scientific, Waltham, MA, USA
Neurobasal™ Medium	21103049	Thermo Fisher Scientific, Waltham, MA, USA
Rock inhibitor Y-27632(2HCl)	72304	Stem Cell Technologies, Vancouver, Canada
0.5% trypsin-EDTA no phenol red	15400054	Thermo Fisher Scientific, Waltham, MA, USA
Round bottom Ultra-Low Attachment 24-Well Plates	CLS3473	Corning®, New York, USA
Ultra-Low Attachment 96-Well Plates	CLS7007	Corning®, New York, USA

Table 3: List of all the antibodies used for immunostaining in this thesis.

Antigen	Dilution	Species	Vendor	Catalogue #
Alexa Fluor® secondary antibodies	1:1000	Many	Thermo Fisher Scientific, Waltham, MA, USA	Different #s
CTIP2	1:500	Rat	Abcam, Cambridge, UK	AB18465
4,6-diamidino-2 phenylindole (DAPI)	1:1000	-	Sigma Aldrich, St. Louis, MO, USA	D9542
DCX	1:2000	Guinea P.	Millipore, Massachusetts, USA	AB2253
GAD67	1:800	Mouse	Millipore, Massachusetts, USA	MAB5406
GFAP	1:500	Rabbit	Dako, Agilent Technologies, California, USA	Z0334
GFP	1:1000	Chicken	Aves Lab, Oregon, USA	GFP-1020
Isotype control	1:200	Rabbit	Abcam, Cambridge, UK	27478
KI67 (1)	1:500	Mouse	Dako, Agilent Technologies, California, USA	M7248
KI67 (2)	1:500	Rabbit	Abcam, Cambridge, UK	AB15580
LAMININ	1:500	Rabbit	Millipore, Massachusetts, USA	AB2034
MAP2	1:500	Mouse	Sigma Aldrich, St. Louis, MO, USA	M4403
NESTIN	1:200	Mouse	Millipore, Massachusetts, USA	MAB5326
NEUN	1:500	Mouse	Millipore, Massachusetts, USA	MAB377
NFIA	1:500	Rabbit	Novus Biologicals, Colorado, USA	NBP1-81406
PAX6 (1) (human)	1:500	Rabbit	BioLegend, California, USA	PRB-278p
PAX6 (2) (mouse)	1:500	Rabbit	Millipore, Massachusetts, USA	AB2237
PH3	1:500	Rabbit	Millipore, Massachusetts, USA	6570
PHALLOIDIN (Conjugated-546)	1:40	-	Thermo Fisher Scientific, Waltham, MA, USA	A12381
PSD95	1:200	Rabbit	Thermo Fisher Scientific, Waltham, MA, USA	516900
PVIMENTIN	1:2000	Mouse	Abcam, Cambridge, UK	ab22651
S100β	1:250	Mouse	Millipore, Massachusetts, USA	S2532
SATB2	1:500	Mouse	Abcam, Cambridge, UK	AB51502
SOX2	1:500	Rabbit	Cell Signalling, Massachusetts, USA	2748
SOX9	1:500	Rabbit	Millipore, Massachusetts, USA	AB5535
SYNAPSIN1	1:500	Mouse	Synaptic Systems, Göttingen, Germany	106 001
SYNAPTOPHYSIN1	1:200	Rabbit	Millipore, Massachusetts, USA	AB9272
TBR1	1:500	Rabbit	Abcam, Cambridge, UK	AB31940
TBR2	1:500	Rabbit	Abcam, Cambridge, UK	AB23345
VGAT	1:500	Mouse	Synaptic Systems, Göttingen, Germany	131011
VGLUT1	1:500	Rabbit	Synaptic Systems, Göttingen, Germany	135303
VGLUT2	1:500	Rabbit	Synaptic Systems, Göttingen, Germany	135403
β-CATENIN	1:500	Mouse	BD Biosciences, New Jersey, USA	610154

Table 4: List of all the primers used in this thesis.

Gene	Forward Primer (5'-3')	Reverse Primer (5'-3')	Reference
DCX	TCCCGGATGAATGGGTTGC	GCGTACACAATCCCCTTGAAGTA	(Di Matteo, et al, 2020
GAPDH	AATCCCATCACCATCTTCCAGGA	TGGACTCCACGACGTACTCAG	(Di Matteo, et al, 2020
GNG5	GCTCAACATGACCCTCTGCT	GGAGTGGTTTGGGAAACCTTTG	-
NEUN	CCAAGCGGCTACACGTCT	GCTCGGTCAGCATCTGAG	(Di Matteo, et al, 2020
PAX6	ACCCATTATCCAGATGTGTTTGC	ATGGTGAAGCTGGGCATAGG	(Di Matteo, et al, 2020

Table 5: List of all the kits used in this thesis.

Kits	Catalogue #	Vendor
5 µM PCR_SMARTer II A	634925	Takara, California, USA
Agilent DNA 1000 kit	5067-1505	Agilent Technologies, California, USA
Agilent RNA 6000 Pico kit	5067-1513	Agilent Technologies, California, USA
AllPrep DNA/RNA Micro kit	80284	Qiagen, Hilden, Germany
Clean & Concentrator Kit	R1013	Zymo Research, California, USA
EndoFree Plasmid Maxi Kit	12362	Qiagen, Hilden, Germany
LightCycler® 480 SYBR Green I Master	4707516001	Roche, Basel, Switzerland
Microplex Library preparation kit v2	C05010012	Diagenode, Liege, Belgium
NEBNext Poly(A) mRNA Magnetic Isolation Module	E7490	NEB, Massachusetts, USA
NEBNext Ultra II Directional Library Prep kit for Illumina	E7765/L 96R	NEB, Massachusetts, USA
RNA Clean & Concentrator Kit	R1013	Zymo Research, California, USA
Qiagen Plasmid Mini Kit	12123	Qiagen, Hilden, Germany
Qubit™ dsDNA HS Assay kit	Q32851	Thermo Fisher Scientific, Waltham, MA, USA
SMARTer® PCR cDNA Synthesis Kit	634925	Takara, California, USA
SMART-Seq® v4 Ultra® Low Input RNA Kit for Sequencing	634888	Takara, California, USA
SuperScript III reverse transcriptase	18080-044	Thermo Fisher Scientific, Waltham, MA, USA

7.2 COMMON TECHNIQUES

7.2.1 Maintenance, splitting and freezing of iPSCs

HPS0076 cells used in Chapters 3 and 4 were generated from human fibroblasts and obtained from the RIKEN Bioresource Center, Japan and generated according to the protocol in (Okita et al., 2011). Control, *DCHS1* and *FAT4* mutant iPSCs used in Chapter 5 were generated from patients' fibroblast. They were produced by Ejona Rusha, at the Helmholtz-Center Munich, before the start of this PhD project. The detailed protocol can be found in (Klaus et al., 2019).

For the general maintenance, iPSCs were kept in the incubator at 37 °C, 5% CO2 and ambient oxygen level and were grown in Matrigel® Basement Membrane Matrix, LDEV-free coated plates. Matrigel® coated plates were used in the 2 weeks after preparing them to keep the cells in the best possible condition. Cells were cultured with mTESR1 medium supplemented with 1x mTESR1 supplement. The medium change was performed every day. For passaging, cells were first washed off with DPBS and treated with Accutase® solution diluted 1:4 in DPBS at 37 °C for 5 min. Detached colonies were washed with off DMEM/F-12, HEPES, and centrifuged at 300 g for 5 min to collect the pellet. Colonies were then resuspended in mTESR1 with 1x mTESR1 supplement and 10 µM Rock inhibitor Y-27632(2HCl) and diluted as needed to the desired density. Dilution was never over 1/6 to avoid the differentiation of the colonies due to the low number of cells. For freezing, cells were washed with DPBS and detached from the plate with Accutase® solution diluted 1:4 in DPBS at 37 °C for 5 min. Detached colonies were washed with DMEM/F-12, HEPES, and centrifuged at 300 g for 5 min to collect the pellet. 1 ml of freezing medium (50% DMEM/F-12, HEPES, 40% hESC-quality FBS and 10% DMSO) was added to the collected cells. Afterwards, iPSCs were directly moved to a freezing vial which was kept at -80 °C for at least 24 hours before being moved to the liquid nitrogen tank.

7.2.2 COs generation

COs were generated following the protocol published in (Ayo-Martin et al., 2020; Klaus et al., 2019; Lancaster and Knoblich, 2014). During the whole CO generation, they were kept at 37°C, 5% CO2 and ambient oxygen level. iPSCs were washed once in DPBS and detached with Accutase® solution at 37 °C for 5 min to obtain single cells. 9000 cells per well were plated in Round Bottom Ultra-Low Attachment 96-Well Plates with *hES medium* (DMEM/F12+Glutamax supplemented with 20% KnockOut™ Serum Replacement, 3% hESC-quality FBS, 0.1 mM 2-Mercaptoethanol (50 mM), 1% MEM Non-Essential Amino Acids Solution (100X) and freshly added 4 ng/ml bFGF, and 50 µM Rock inhibitor Y-27632(2HCl)). Cells were maintained in *hES* medium for 6 days until EBs were generated, adding Rock inhibitor and bFGF only for the first 4 days. After day 6, EBs (two EBs per well) were moved to Ultra-Low Attachment 24-Well Plates with *NIM medium* (DMEM/F12+Glutamax supplemented with

1:100 N2™-Supplement (100X), 1% MEM Non-Essential Amino Acids Solution (100X) and 5 µg/ml Heparin) and kept in culture for 6 additional days. EBs were embedded in Matrigel® Basement Membrane Matrix, LDEV-free on day 12 and moved to a 10 cm dish (30 EBs per plate) with *NDM-A medium* (DMEM/F12+Glutamax and Neurobasal™ Medium in a 1:1 ratio supplemented with 1:200 N2™-Supplement (100X), 1:100 B-27™ Supplement (50X) minus vitamin A, 0.5% MEM Non-Essential Amino Acids Solution (100X), 0.5% GlutaMAX™ Supplement, 50 µM 2-Mercaptoethanol (50 mM), 1:100 Antibiotic Antimycotic Solution (100X) and 2.5 µg/ml Insulin). For embedding, each EB was transferred to a parafilm sheet with 30 small moulds using a cut p200 pipette. The medium was removed and a drop of Matrigel® was added to each single EB. The parafilm sheet was then transferred to a 10 cm dish and kept at 37 °C for 30 min for the solidification of the matrix. Then *NDM-A medium* was added to the plate, washing embedded EBs off the parafilm. After 4 days in *NDM-A medium,* COs were cultured with *NDM+A medium* (DMEM/F12+Glutamax and Neurobasal™ Medium in a 1:1 ratio supplemented with 1:200 N2™-Supplement (100X), 1:100 B-27™ Supplement (50X), 0.5% MEM Non-Essential Amino Acids Solution (100X), 0.5% GlutaMAX™ Supplement, 50 µM 2-Mercaptoethanol (50 mM), Antibiotic Antimycotic Solution (100X) and 2.5 µg/ml Insulin) and put over an orbital shaker rotating at 55 rpm. *NDM+A medium* was changed every 3 days.

7.2.3 Buffers for Immunostaining

Phosphate-Buffered Saline (PBS)

- 137 mM NaCl
- 2.7 mM KCl
- 10 mM Na_2HPO_4
- 1.8 mM KH_2PO_4
- pH = 7.4

Citric buffer

- 0.01 M $C_6H_5Na_3O_7 \cdot 2\ H_2O$
- pH = 6

Boric buffer

- 0.1 M H_3BO_3
- pH = 8.5

Blocking solution

- 0.1% Tween® 20
- 3% BSA
- 10% NGS

7.4.3 Fixation and cryosectioning of COs and mouse brains

When the desired moment arrived COs and mouse brain were washed with 1X DPBS, fixed in 4% PFA for 1-2 hours for the COs to overnight for the mouse brains. Next, for cryopreservation, they were moved to 30% sucrose in 1X PBS overnight. COs and mouse brains were frozen in OCT Compound and stored at -20°C. For immunohistochemistry, COs were cut in sections of 14 µm while mouse brains in sections of 12 µm with the help of a cryostat.

7.2.4 Immunostaining

The preparation of frozen mouse brain and COs sections for immunostaining was done by thawing them for 20 min at room temperature (RT) and rehydration with 1X PBS for 5 min.

Antigen retrieval with fresh citric buffer (0.01 M, pH = 6) was used for the exposure of nuclei antigen. Sections were incubated for 1 min at 720 W and 10 min at 120 W in the citric buffer. Afterwards, sections were kept at RT for 20 min. To completely cool down the sections half of the citric buffer was removed, and water added for another 10 min. Finally, sections were washed once with 1X PBS for 5 min and then the staining was continued with the standard immunostaining protocol.

After the complete antigen retrieval procedure, sections were fixed for 10 min with 4% PFA. Next, sections were washed twice with PBS and permeabilized with 0.3% Triton ® X 100 in 1X PBS for 5 min. At that point, sections were washed 3 times with PBS for 5 min before performing the blocking of the antigens with blocking solution (10% NGS, 1% BSA in 0.1% Tween® 20 in 1X PBS) for 1 hour at RT. Subsequently, the primary antibody was diluted in blocking solution in the desired concentration and sections were incubated in this mix at 4°C overnight (see list of antibodies in Table 3). Next, several washes with 0.01% Tween in 1X PBS were performed and sections were incubated for 1 hour at RT with AlexaFluor-conjugated secondary antibody of the desired species and fluorophore at 1:1000 dilution together with 0.1 µg/ml DAPI to detect nuclei. For the detection of F-ACTIN, sections were incubated with Alexa Fluor 546-conjugated PHALLOIDIN together with the secondary antibodies. Finally, after several washes with 0.01% Tween in 1X PBS, sections were mounted with Aqua-Poly/Mount and left to dry in the dark before confocal imaging.

Astroglial cells were cultured in 24-well plates with coverslips. Once the desired confluency was obtained, they were fixed at RT for 15 min with 4% PFA. Finally, the immunostaining protocol was followed precisely as for mouse brain and COs sections.

7.2.5 Confocal imaging

Mouse brain and COs sections, as well as astroglial cells, were visualised using a Leica SP8 confocal laser-scanning microscope with 10x, 25x and 40x objectives. For mouse brain sections and COs sections, Z-projections were taken to obtain the full 3D image, while for astroglial cells only a single plane was taken.

7.3 TECHNIQUES SPECIFIC TO CHAPTER 3

7.3.1 Generation of the Dataset

The reference for the *DCHS1* human variant (NCBI RefSeq NP_003728.1) and all the primate protein sequences were found on the NCBI Protein Basic Logical Alignment Search Tool (pBLAST) and downloaded as FASTA files. The *DCHS1* Neanderthal sequence was manually generated by altering the FASTA file and including the aspartic acid (D) to asparagine (N) change in position 777.

7.3.2 Protein Alignments

For the alignment of the DCHS1 protein in different species, the Unipro UGENE programme was used (Okonechnikov et al., 2012) as it contains different sequence alignment methods. The MAFFT program was used to align the different human and primate DCHS1 proteins (Pais et al., 2014) using the following parameters: gap opening penalty=1.53, offset=0.123 and number of iterative refinement=1000 (Long et al., 2016).

7.3.3 Post-Translational Modification Investigation

The server NetNglyc was used to predict N-glycosylation sites in the modern and ancient DCHS1 variants (Gupta et al., 2004).

7.3.4 CRISPR-CAS9

The genetically modified human iPSCs were generated in collaboration with the Max Planck Institute of Evolutionary Anthropology in Leipzig by Stephan Riesenberg in the group of Prof Dr Svante Pääbo. In short, 409-B2 human iPSCs were edited using the CRISPR Cas9 system to modify *DCHS1* to express asparagine (N) at position 777 instead of aspartic acid (D). The full protocol can be found in (Riesenberg and Maricic, 2018).

The sequence for the donor DNA is (DCHS1_N777D):

AAAAAACATACTGTAGTTGCTCAAATATGGGTGGTGTGGGGGTTCCAGGCACGATGCTGATGTTCACTCGGG
CACTGGGTTCTGCTTGTAGGCCACCTCCGTCCTCAGCCCCGATCTCCAGCTGCACCACAGAATT

7.3.5 FACS analysis

COs were analysed by FACS at day 30 and day 60. For each condition, 3 COs were mixed, and all the procedures were done in triplicates or quadruplets (i.e. using 3 x 3 or 3 x 4 COs). COs were washed once with 1X DPBS and incubated in Accutase® solution at 37°C for 10 min and then manually dissociated by pipetting 10 times using a p1000. If required, this incubation and manual dissociation was repeated maximally 2 times. Resulting dissociated cells were washed with 1X DPBS and centrifuged for 5 min at 12000 rpm. Cells were resuspended in 1 ml of DPBS and filtered with a 100

µm cell strainer. Cells were mixed with 5 ml of 70% ice-cold ethanol while vortexing and kept at -20°C for 1 hour for fixation. Subsequently, the mixture was centrifuged for 30 minutes at 4°C and 2000 rpm, the supernatant was discarded, and the pellet was washed with the blocking solution (1% FBS in 1X DPBS). The mixture was centrifuged again for 30 min at 4°C and 2000 rpm and the pellets were resuspended in 100 µl of the leftover blocking solution. Primary antibodies were diluted in blocking solution and incubated with the cells for 30 minutes on ice (PAX6 1:200; TBR2 and DCX 1:500; PH3 1:300). Cells were washed with blocking solution and centrifuged for 30 min at 4°C at 2000 rpm. Cells were then resuspended and incubated with a secondary antibody (1:1000) on ice and in the dark for 30 min. Finally, cells were washed with blocking solution and centrifuged for 30 min at 4°C and 2000 rpm. Cells were then resuspended in DPBS and transferred to FACS tubes. For the FACS analysis, a FACS Melody TM cell sorter (BD) was used. Samples were analysed in BD FACS Flow TM medium. The nozzle had a diameter of 100 µm. Forward scatter and sideward scatter were used to gate out the cell debris and aggregates. For the gating of fluorophores samples stained with an isotype control (IC) or a secondary antibody only were used.

7.3.6 Image analysis, quantification, and statistical analysis

The cell quantification and analysis of the electroporated COs was performed in Fiji (Schindelin et al., 2012). Data were obtained from the analysis of several COs per condition. Data are shown with n=number of analysed VLs structures except for the angle of division in which n=number of cells and NESTIN staining in which n=number of processes. The exact number of VLs, COs and batches analysed per experiment and condition are indicated in the corresponding figure legend.

The number of apically dividing cells was assessed by PH3 staining. For each VL, one z-stack was used and only the PH3+ cells found on the apical side of the ventricle were counted. The number of PH3+ cells was normalized to the apical length of each GZL which was measured using the DAPI staining and looking at the morphology of the GZL.

The angle of the division was assessed by the morphology of dividing cells in the apical part of the VLs. Division angles were classified as horizontal-oblique (0-60°) or vertical (60-90°) following similar rules as in (Iefremova et al., 2017). The apical belt of the COs was used as a baseline and the angle of the division was measure in relation to this baseline.

The neuronal migration phenotype was assessed by DCX+ stainings and VLs were classified into different categories depending on their phenotype. On the one hand, if there were three or more DCX+ processes inside the GZL, VLs were included in the *processes* category. On the other hand, if there was a DCX+ cell body in the apical site of the GZL or two or more DCX+ cell bodies in the GZL, VLs were included in the *cell bodies* category.

The tortuosity of the RG processes was identified by NESTIN staining. The straightness of the processes was measured by tracing the total length of the process which was divided by the straight distance from the apical part to the basal part of the process. Five processes per ventricle were measured.

The disruption of the apical belt was analysed with PHALLOIDIN immunohistochemistry. If a VL contained areas of the apical belt without PHALLOIDIN staining, but with intact DAPI staining, it was included in the *disrupted apical belt* category.

The number of TBR2+, CTIP2+ and SATB2+ cells was assessed by measuring the number of cells in the GZL areas for TBR2, and in CPL areas for CTIP2 and SATB2 in different COs and the number of positive cells was normalized to the area in which those cells were located.

Finally, for the trajectory of the width of the PAX6+ GZL, the length of the apical length and the number of PH3+ cell per apical length, as well as the PAX6 FACS results, all independent values in control and D777N COs for each time point were normalized to the mean of the data obtained at day 30 in controls and D777N respectively.

Statistical analysis and data representation were completed with GraphPad Prism® version 6.01. The statistical test performed for each analysis is explained in each figure legend

7.4 TECHNIQUES SPECIFIC TO CHAPTER 4

7.4.1 Cloning

The generation of the *pCAG-GFP-IRES-GNG5* plasmid was done by cloning the open reading frame (ORF) of the human *GNG5* gene (Ensemble ENST00000370645.9) into a *pCAGGS* plasmid containing a GFP sequence (Cappello et al., 2013) following standard cloning methods. To gain the ORF of human *GNG5*, cDNA from neuroblastoma (SH-SY5Y) cells was used and amplified using the following primers:

- Forward: 3' – TCCTCTTCAGACCCCCTCTT – 5'
- Reverse: 5' – ATTGTATGCTGCTGCCAGTG – 3'

The primers for the amplification of the ORF and the introduction of the restriction sites (5' NheI and 3'EcoRV) to clone the ORF into the *pCAGGS-GFP* vector were as follow:

- Forward with NheI restriction enzyme: 3' – AAAGCTAGCATGTCTGGCTCCTCCAGC – 5'
- Reverse with EcorV restriction enzyme: 5' – ATAGATATCCTACAAAAAGGAACAGACTTTCTGGGG – 3'

The *pCAG-GFP-IRES-GNG5* overexpression plasmid and the control empty *pCAG-GFP* plasmid were electroporated in COs and embryonic mouse brains at different time points which are explained later in the section. For the analysis of the cell profile and membrane, COs were co-electroporated with the *pCAG-GAP43-GFP* plasmid (Attardo et al., 2008; Cappello et al., 2006; Klaus et al., 2019). On the contrary, mice were co-electroporated with the *pCAG-GFP-IRES-GNG5* and the *pCAG-GFP*.

7.4.2 Plasmid preparation

DH5α strains of competent bacteria were transformed with 1 µg/µl plasmid DNA. Bacteria were incubated with the plasmid DNA on ice 30 min and for the transformation, a heat shock at 42°C for 45 seconds was performed. Afterwards, the bacteria were left on ice for 5 min and then incubated for 30 min to 1 hour in 1 ml in LB-medium warmed to 37°C while shaking. Subsequently, 100 ml of bacteria were spread on an Agar plate with the corresponding antibiotic.

For the generation of small-scale plasmids, independent colonies were picked and grown in 5 ml of LB-medium with the corresponding antibiotic. Colonies were grown overnight at 37°C on the shaker at 180 rpm. The day after, with the help of the Qiagen Plasmid Mini Kit and following the manufacturer´s protocol the plasmid DNA was extracted.

For the generation of large-scale plasmid, independent colonies were picked and grown in 250 ml of LB-medium with the corresponding antibiotic. Colonies were grown overnight at 37° on the shaker at 180 rpm. The day after, with the help of the endotoxin-free, Endofree Qiagen Plasmid Maxi Kit and following the manufacturer´s protocol the plasmid DNA was extracted.

7.4.3 Electroporation, fixation and cryosectioning of COs

COs were electroporated at day 20 and day 35 after the start of the CO generation. During the entire procedure, COs were maintained in *NDM+A* medium without Antibiotic Antimycotic solution and placed into an electroporation chamber (Harvard Apparatus, Holliston, MA, USA). With the help of a stereoscope, the VLs were localized. To visualize the plasmid DNA, it was mixed with 0.1% Fast-Green FCF. 1-2 µl of the respective plasmid (*pCAG-GFP*, *pCAG-GFP-IRES-GNG5*, 2/3 of *pCAG-GFP* + 1/3 of *pCAG-GAP43-GFP* or 2/3 of *pCAG-GFP-IRES-GNG5* + 1/3 of *pCAG-GAP43-GFP*) at a final concentration of 1µg/µl were injected into each VL using Glass Micropipets. After DNA injection and to enable the entry of the plasmid from the VLs into the neighbouring cells, five pulses were applied at 80 mV for 50 ms each at intervals of 500 ms (ECM830, Harvard Apparatus). 24 hours after electroporation new *NDM+A medium* with Antibiotic Antimycotic solution was added to the COs and they were kept in culture for 7 additional days. COs were then washed with 1X DPBS, fixed in 4% PFA for 1-2 hours, and for cryopreservation moved to 30% sucrose in 1X PBS overnight. Finally, COs were frozen in OCT Compound and stored at -20°C. For immunohistochemistry, COs were cut in sections of 14 µm with the help of a cryostat.

7.4.4 *In Utero* Electroporation in mice

IUEs were performed in pregnant C57BL/6 mice under the license number 55.2-1-54-2532-79-2016 approved by the Government of Upper Bavaria. Animals were anaesthetized with an intraperitoneal injection in which a saline solution was mixed with the following combination of drugs: fentanyl (0.05 mg per kg body weight), midazolam (5 mg per kg body weight) and medetomidine (0.5 mg per kg body weight) (Btm license number 4518395). Embryos were always electroporated at E13 and the protocol used was based on the paper by (Saito, 2006). In short, the uterus was exposed and with the help of a lamp, the brain and the ventricles of each embryo were localized. To visualize the plasmid DNA, it was mixed with 0.1% Fast-Green FCF. 1-2 µl of each plasmid (*pCAG-GFP*, *pCAG-GFP-IRES-GNG5* or 2/3 of *pCAG-GFP-IRES-GNG5* + 1/3 of *pCAG-GFP*) at a final concentration of 1 µg/µl were injected into the lateral ventricles using Glass Micropipets. After the electroporation, anaesthesia was finalised by an intraperitoneal injection in which a saline solution was mixed with the following combination of drugs: buprenorphine (0.1 mg per kg body weight), atipamezole (2.5 mg per kg body weight) and flumazenil (0.5 mg per kg body weight). Brains were fixed in 4% PFA at 1 dpe, 3 dpe or 6 dpe for 4 hours (1 dpe) or overnight (3 and 6 dpe). For cryopreservation, brains were kept in 30% sucrose in PBS overnight. Finally, brains were frozen in OCT Compound and stored at -20°C. For immunohistochemistry, brains were cut in sections of 12 µm with the help of a cryostat.

7.4.5 Image analysis, quantification, and statistical analysis

For the cell quantification and analysis of the *in vivo* experiments after IUE, Adobe Photoshop CS6 was used. Brain sections were divided into five equally divided bins for the binning or distribution analysis. At least 2 sections were analysed per brain. At E13-E14 6 controls and 4 *GNG5* OX for GFP quantification and 5 controls and 4 *GNG5* OX for Tbr2 quantification, while at E13-E16 4 controls and 7 *GNG5* OX brains were counted. The neuronal disruption phenotype was analysed at E13-E16 in 6 controls and 8 *GNG5* OX brains and at E13-E19 in 3 controls and 8 *GNG5* OX brains. The integrity of the apical belt was analysed at E13-E16 in 6 controls and 8 *GNG5* OX brains. All brains were obtained from mouse embryos electroporated in at least two independent experiments. The exact number of analysed brains are indicated in the corresponding figure legend.

The cell quantification and analysis of the electroporated COs was performed in Fiji (Schindelin et al., 2012). Data were obtained from 2 independent batches of COs generation from which several COs were analysed (except for the GPF+ cell distribution and the pVIMENTIN quantification at day 35+7, in which only 1 batch was analysed). Data are represented with n=number of analysed VLs structures (see figure legends). The exact number of VL, COs and batches analysed per experiment and condition are indicated in the corresponding figure legend.

The distribution of GFP+ cells in COs was passed by diving the GZL in two equal bins (Bina and BinB). GFP+ cells in each bin were counted and the percentage of GFP+ cells per bin calculated.

The neuronal migration phenotype was assessed by MAP2+ stainings and VLs were classified into different categories depending on their phenotype. On the one hand, if there were three or more MAP2+ processes inside the GZL, VLs were included in the *processes* category. On the other hand, if there was a MAP2+ cell body in the apical site of the GZL or two or more MAP2+ cell bodies in the GZL, VLs were included in the *cell bodies* category.

Migration defects were also analysed by NEUN+ staining. VLs were categorised as showing neuronal migration defects whenever there were two or more NEUN+ cell bodies in the GZL of the electroporated VLs.

The integrity of the apical belt in COs was examined by PHALLOIDIN immunohistochemistry and in mice by β-CATENIN staining. A VL or brain section was classified as *disrupted apical belt* whenever the DAPI staining was intact and there were patches without the corresponding marker in an electroporated area.

The number of progenitor cells (KI67, PH3 and pVIMENTIN) was examined by counting the positive cells for each marker and normalizing it to the electroporated area.

Statistical analysis and data representation were completed with GraphPad Prism® version 6.01. The statistical test performed for each analysis is explained in each figure legend.

7.5 TECHNIQUES SPECIFIC TO CHAPTER 5

7.5.1 Buffers for Nuclei extraction

Nuclei Isolation Medium 1 (NIM1)

- 250 mM Sucrose
- 25 mM KCL
- 5 mM $MgCl_2$
- 10 mM Tris, pH=8
- Nuclease free H2O

Nuclei Isolation Medium 2 (NIM 2)

- NIM1
- 0.5M DTT
- 1:10 Protease Inhibitor Cocktail

Homogenization Buffer

- NIM1
- 20% Triton ® X 100
- 1:1000 DAPI
- 0.4 units/µL RNaseIN
- 1units/µl DNaseI

Blocking buffer

- DPBS
- 2% BSA
- 0.2unita/µL RNaseIN

7.3.2 Nuclei extraction and FACS sorting

Nuclei from 4 and 8-9 months old COs were isolated following the protocol from (Krishnaswami et al., 2016) with small modifications (Di Matteo, et al, 2020). For each condition, 2 to 3 COs were used, and all the procedure was done in triplicates. In short, COs were washed with 1X DPBS and dissociated by Dounce homogenization in homogenization buffer (5 strokes of the loose pestle and 10 strokes of the tight pestle). Dissociated cells were filtered with BD Falcon tubes with a cell strainer cap to get single cells and were collected by centrifugation at 1000 g for 8 min at 4˚C. The pellet of cells was then resuspended in blocking buffer for 15 minutes at 4˚C. Primary antibodies for PAX6 and NEUN were added to the blocking buffer solution containing the single cells in 1:2500 dilution and 1:1000, respectively, and incubated under rotation for 30 min at 4˚C. Cells were washed with blocking solution and collected by centrifugation at 500 g for 30 min at 4˚C. Secondary antibodies goat anti-rabbit-Alexa

Fluor® 488 and Alexa Fluor® 546 Goat Anti-Mouse IgG1 (γ1) were used in 1:2500 dilution in blocking solution and cells were incubated under rotation for 30 min at 4˚C. DAPI (0.5 mg/ml) was added in the last 10 min of incubation of the secondary antibody. Cells were collected by centrifugation at 500 g for 30 min at 4˚C and resuspended in DPBS containing RNAse inhibitor (0.2 units/µl). For the FACS analysis, a FACS Melody TM cell sorter (BD) was used. Samples were analyzed in BD FACS Flow TM medium. The nozzle had a diameter of 100 µm. Forward scatter and sideward scatter were used to gate out the cell debris and aggregates. For the gating of single cells, FSC-W/FSC-A was used. For the gating of fluorophores samples stained with a secondary antibody only were used (as isotype control). Sorted cells were collected in DPBS containing RNAse inhibitor (0.2 units/µl) and 1ml QIAzol® Lysis Reagent was added to the mix and kept in -80°C until further analysis.

7.6.3 RNA extraction, cDNA synthesis and Real-Time-qPCR

The FACS sorted *NEUN+* and *PAX6+* nuclei were lysed in QIAzol® Lysis Reagent. Nuclear RNA was isolated using the RNA Clean & Concentrator Kit following the manufacturer's protocol and cDNA was synthesised with the SuperScript III reverse transcriptase with random primers according to the manufacturer's protocol. Afterwards, qPCR was performed in triplicates on a LightCycler® 480 II (Roche, Basel, Switzerland) with the LightCycler® 480 SYBR Green I Master mix. qPCR was done according to the following protocol: denaturation at 95 °C for 10 min, 45 cycles of 95 °C 10 s, 60 °C 10 s and 72 °C 10 s). qPCR primer information can be found in **Table 4**. Relative gene expression (E) was calculated using the $\Delta\Delta C_p$ method: $E = 2^{\wedge -\Delta\Delta Cp}$. ΔΔCp represents the difference between the Cp value of the gene of interest and the Cp value of the housekeeper (*GAPDH*) for PAX6+ and NEUN+ nuclei.

Statistical analysis and data representation were completed with GraphPad Prism® version 6.01. The statistical test performed is explained in the respective figure legend.

7.6.4 cDNA amplification library preparation and data analysis

All the steps for the library preparation from the RNA extracted from the PAX6+ and NEUN+ were done according to (Ramsköld et al., 2012). First, the integrity of the extracted RNA was analyzed at the Bioanalyzer by using the Agilent RNA 6000 pico kit following the manufacturer's protocol.
First-Strand cDNA synthesis and cDNA amplification were done with the SMART-Seq® v4 Ultra® Low Input RNA Kit for Sequencing following the manufacturer´s protocol. For the cDNA amplification, we performed a range of PCR cycles.

To determine the optimal number of PCR cycles of amplification for each sample, we performed a real time-PCR (RT-PCR) reaction on an aliquot of 5 µl of cDNA produced after the 4th cycle of the PCR reaction according to the manufacturer´s protocol. The RT-PCR was performed in a final volume of 15 µl containing 1 µl of 5 µM PCR_SMARTer II A primer, 7.5 µl 2x PCR Master Mix SensiMix from the

SMARTer® PCR cDNA Synthesis Kit. The amplification protocol was as follows: 95°C for 10 min; 20 X 98°C for 10 sec, 65°C for 30 sec, 68°C for 3 min; 72°C for 10 min; 4°C forever. Once the optimal number of cycles was established, the normal PCR reaction was continued accordingly.

The amplified cDNA was purified with AMPure XP beads. In short, one volume of AMPure XP beads was added to each sample, the mix was transferred into 1.5 ml low binding tube and mixed by pipetting the entire volume up and down at least 10 times. Samples were incubated for 10 min at RT to let the cDNA bind to the beads in a magnetic separation device. The supernatant was discarded and 200 µl of freshly prepared 80% ethanol were added to each sample twice. The leftover ethanol was removed, and the samples were dried at RT for 5 min. Finally, the beads were resuspended in 17 µl Elution Buffer (10 mM Tris pH = 8) for 5 min at RT. The beads were removed from the mixture by placing them in the magnetic separation device. The clean (15 µl) supernatant was collected and its concentration was measured with the Qubit DNA HS kit following the manufacturer´s protocol. The concentration was ranging between 0.5-2 ng/µl.

The cDNA shearing was performed using the S220 Covaris with AFA technology (Covaris, Chicago, USA) and the library was prepared with Microplex Library preparation kit v2 following the manufacturer's protocol. In short, the shearing protocol was as followed: 106 µl Elution Buffer (10mM Tris pH=8) was added to each purified cDNA and transferred to Covaris microtubes (microTUBE AFA Fiber Pre-Slit Snap-Cap 6 X 16 mm). After the shearing was complete, 80 µl Elution Buffer (10 mM Tris pH = 8) were added to the sheared cDNA. After the Covaris treatment, the resulting cDNA was in 200–500 bp size range. For DNA precipitation, 8 µl 5 M NaCl, 30 µg glycogen and 600 µl ethanol were added and incubated for 30 min at -80°C. The cDNA was collected by centrifugation at 16000 g for 30 min at 4°C, washed with 70% ethanol and centrifuged again. The pellet was resuspended in 11 µl Elution buffer. Finally, the concentration was measured with the Qubit DNA HS kit. The final concentration was 0,5-2 ng/ul (10-20 ng in total). After the library amplification steps with the Microplex Library preparation kit v2 following the manufacturer's, the DNA concentration was measured with the Qubit DNA HS Kit. The concentration of the DNA was between 5-6 ng/µl. The library was purified using the AMPure XP beads and the concentration was checked with Qubit HS DNA kit again, revealing a final concentration between 2-6 ng. Finally, the quality and molarity of the library were also analyzed with the Agilent DNA 1000 kit.

The prepared libraries were sequenced at LAFUGA Genomics, Genzentrum, Universität München (LMU). The analysis of the sequenced results and the differential expression analysis were performed by Dr Tobias Straub at the Biomedical Center in Munich.

7.6.5 Astroglial cells generation and characterization

Astroglial cells were generated from COs that were between 375-445 days old. 2 to 3 COs were collected per condition. COs were washed with 1X DPBS and dissociated by pipetting 5 times using a p1000. Then, COs were incubated in Accutase® solution at 37°C for 10 min and manually dissociated again by pipetting 5 times using a p1000. Cells were washed with 1X DPBS and centrifuged for 3 min at 300 g. Cells were resuspended in *NDM+A* medium and distributed in four wells of a 12 well plate previously coated with Matrigel® Basement Membrane Matrix, LDEV-free. The following day, cells were refreshed with *Astrocyte medium* (90% DMEM/F12+Glutamax, 10% of hESC-quality FBS and 1% of Antibiotic Antimycotic Solution (100X)). The medium was changed every 2-3 days. For splitting, astroglial cells were washed with DPBS and dissociated with 0.05% trypsin-EDTA without phenol red for 5 min at 37°C. Cells were centrifuged for 3 min at 300 g and plated in Matrigel coated plates at the desired concentration. Astroglial cells were analysed at passage 3 for immunostaining and Bulk RNA sequencing as already explained in section 7.6.6.

7.6.6 RNA extraction of astroglial cells, library preparation and data analysis

The transcriptome analysis of the astroglial cells was done in collaboration with members of the group of Prof. Dr Elisabeth Binder at the Max Planck Institute of Psychiatry. The RNA and DNA extraction were performed by Dr Cristiana Cruceanu and Anthi Krontira. The library preparation was done with the support of Susann Sauer and Maik Ködel. In short, RNA and DNA were extracted from 84 samples using the AllPrep DNA/RNA Micro kit, nucleic acid concentration and quality were assessed with an Epoch plate reader. The mean 260/280 ratio for the RNA of all samples was 2.093 (minimum 1.831 and maximum 2.270). RNA sequencing library preparation was done with the NEBNext Ultra II Directional Library Prep kit for Illumina using the NEBNext Poly(A) mRNA Magnetic Isolation Module. Libraries were pooled according to their concentration and the pooling was assessed and re-calibrated with a test run in a MiSeq. The pool was sequenced in 3 lanes of the HiSeq4000 with paired-end 75 bp run type and we acquired an average of 13,5 million reads per library. The samples were randomized in the library preparation plate taking into consideration their cell type origin, treatment group, RNA quality and cell culturing user to reduce as much as possible any technical batch effects.

The libraries were sent to the sequencing core facility at the Max Planck for Molecular Genetics in Berlin for sequencing. Finally, the analysis of the sequence results and the differential expression analysis was performed by Dr Darina Czamara from the group of Prof Dr Elisabeth Binder and by Dr Filippo Cernilogar at the Biomedical Center in Munich.

7.6.7 GO term analysis

The GO term analysis and protein interaction of the dysregulated proteins in mutant *DCHS1* and *FAT4* NEUN+ nuclei and astroglial cells was performed using the STRING database. The functional enrichment of each network was considered significant when the false discovery rate (FDR) was <0.05 (Szklarczyk et al., 2017).

7.6.8 Silicon probe recording

The extracellular recordings in the COs were performed by Francesco di Mateo and Dr Matthias Eder. The Silicon probes (ASSY1 E-1) were purchased from Cambridge NeuroTech company.

CHAPTER 8: REFERENCES

Alcantara, D., Timms, A.E., Gripp, K., Baker, L., Park, K., Collins, S., Cheng, C., Stewart, F., Mehta, S.G., Saggar, A., Sztriha, L., Zombor, M., Caluseriu, O., Mesterman, R., Van Allen, M.I., Jacquinet, A., Ygberg, S., Bernstein, J.A., Wenger, A.M., Guturu, H., Bejerano, G., Gomez-Ospina, N., Lehman, A., Alfei, E., Pantaleoni, C., Conti, V., Guerrini, R., Moog, U., Graham, J.M., Hevner, R., Dobyns, W.B., O'Driscoll, M., Mirzaa, G.M., 2017. Mutations of AKT3 are associated with a wide spectrum of developmental disorders including extreme megalencephaly. Brain 140, 2610–2622.

Anderson, S.A., Kaznowski, C.E., Horn, C., Rubenstein, J.L.R., Mcconnell, S.K., Lasdon, R., Ave, Y., 2002. Distinct Origins of Neocortical Projection Neurons and Interneurons In Vivo. Cereb. Cortex 12, 702–709.

Arai, Y., Taverna, E., 2017. Neural progenitor cell polarity and cortical development. Front. Cell. Neurosci. 11, 1–11.

Asano, T., Shinohara, H., Morishita, R., Ueda, H., Kawamura, N., Katoh-Semba, R., Kishikawa, M., Kato, K., 2001. Selective localization of G protein γ5 subunit in the subventricular zone of the lateral ventricle and rostral migratory stream of the adult rat brain. J. Neurochem. 79, 1129–1135.

Attardo, A., Calegari, F., Haubensak, W., Wilsch-Bräuninger, M., Huttner, W.B., 2008. Live imaging at the onset of cortical neurogenesis reveals differential appearance of the neuronal phenotype in apical versus basal progenitor progeny. PLoS One 3, e2388.

Ayo-Martin, A.C., Kyrousi, C., Di Giaimo, R., Cappello, S., 2020. GNG5 Controls the number of apical and basal progenitors and alters neuronal migration during cortical development. Front. Mol. Biosci. 7, 1–14.

Azevedo, F.A.C., Carvalho, L.R.B., Grinberg, L.T., Farfel, J.M., Ferretti, R.E.L., Leite, R.E.P., Filho, W.J., Lent, R., Herculano-Houzel, S., 2009. Equal numbers of neuronal and nonneuronal cells make the human brain an isometrically scaled-up primate brain. J. Comp. Neurol. 513, 532–541.

Badouel, C., Zander, M.A., Liscio, N., Bagherie-Lachidan, M., Sopko, R., Coyaud, E., Raught, B., Miller, F.D., McNeill, H., 2015. Fat1 interacts with Fat4 to regulate neural tube closure, neural progenitor proliferation and apical constriction during mouse brain development. Development 142, 2781–2791.

Bae, B. Il, Tietjen, I., Atabay, K.D., Evrony, G.D., Johnson, M.B., Asare, E., Wang, P.P., Murayama, A.Y., Im, K., Lisgo, S.N., Overman, L., Šestan, N., Chang, B.S., Barkovich, A.J., Grant, P.E., Topçu, M., Politsky, J., Okano, H., Piao, X., Walsh, C.A., 2014. Evolutionarily dynamic alternative splicing of GPR56 Regulates regional cerebral cortical patterning. Science 343, 764–768.

Bagley, J.A., Reumann, D., Bian, S., Lévi-Strauss, J., Knoblich, J.A., 2017. Fused dorsal-ventral cerebral organoids model complex interactions between diverse brain regions. Nat. Methods 14, 743–751.

Bahi-Buisson, N., Poirier, K., Boddaert, N., Fallet-Bianco, C., Specchio, N., Bertini, E., Caglayan, O., Lascelles, K., Elie, C., Rambaud, J., Baulac, M., An, I., Dias, P., Des Portes, V., Moutard, M.L., Soufflet, C., El Maleh, M., Beldjord, C., Villard, L., Chelly, J., 2010. GPR56-related bilateral frontoparietal polymicrogyria: Further evidence for an overlap with the cobblestone complex. Brain 133, 3194–3209.

Bahi-Buisson, N., Poirier, K., Boddaert, N., Saillour, Y., Castelnau, L., Philip, N., Buyse, G., Villard, L., Joriot, S., Marret, S., Bourgeois, M., Van Esch, H., Lagae, L., Amiel, J., Hertz-Pannier, L., Roubertie, A., Rivier, F., Pinard, J.M., Beldjord, C., Chelly, J., 2008. Refinement of cortical dysgeneses spectrum associated with TUBA1A mutations. J. Med. Genet. 45, 647–653.

Barkovich, A.J., Guerrini, R., Kuzniecky, R.I., Jackson, G.D., Dobyns, W.B., 2012. A developmental and genetic classification for malformations of cortical development: Update 2012. Brain 135, 1348–1369.

Barkovich, A.J., Kjos, B.O., 1992. Schizencephaly: Correlation of clinical findings with MR characteristics. Am. J. Neuroradiol. 13, 85–94.

Barkovich, A.J., Kuzniecky, R.I., 2000. Gray matter heterotopia. Neurology 55, 1603–1608.

Bazelot, M., Simonnet, J., Dinocourt, C., Bruel-Jungerman, E., Miles, R., Fricker, D., Francis, F., 2012. Cellular anatomy, physiology and epileptiform activity in the CA3 region of Dcx knockout mice: A neuronal lamination defect and its consequences. Eur. J. Neurosci. 35, 244–256.

Bear, M.F., Connors, B.W., Paradiso, M.A., 2007. Neuroscience: Exploring the brain, Lippincott Williams & Wilki.

Beerli, P., Edwards, S. V., 2003. When did Neanderthals and modern humans diverge? Evol. Anthropol. Issues, News, Rev. 11, 60–63.

Bentivoglio, M., Mazzarello, P., 1999. The history of radial glia. Brain Res. Bull. 49, 305–315.

Berry, M., Rogers, A.W., 1965. The migration of neuroblasts in the developing cerebral cortex. J. Anat. 99, 691–709.

Bershteyn, M., Nowakowski, T.J., Pollen, A.A., Di Lullo, E., Nene, A., Wynshaw-Boris, A., Kriegstein, A.R., 2017. Human iPSC-derived cerebral organoids model cellular features of lissencephaly and reveal prolonged mitosis of outer radial glia. Cell Stem Cell 20, 435–449.

Betizeau, M., Cortay, V., Patti, D., Pfister, S., Gautier, E., Bellemin-Ménard, A., Afanassieff, M., Huissoud, C., Douglas, R.J., Kennedy, H., Dehay, C., 2013. Precursor diversity and complexity of lineage relationships in the outer subventricular zone of the primate. Neuron 80, 442–457.

Betke, K.M., Rose, K.L., Friedman, D.B., Baucum, A.J., Hyde, K., Schey, K.L., Hamm, H.E., 2014. Differential localization of G protein βγ subunits. Biochemistry 53, 2329–2343.

Birey, F., Andersen, J., Makinson, C.D., Islam, S., Wei, W., Huber, N., Fan, H.C., Metzler, K.R.C., Panagiotakos, G., Thom, N., Rourke, N.A.O., Steinmetz, L.M., Bernstein, J.A., Hallmayer, J., Huguenard, J.R., Paşca, S.P., 2017. Assembly of functional forebrain spheroids from human pluripotent cells. Nature 545, 54–59.

Bizzotto, S., Francis, F., 2015. Morphological and functional aspects of progenitors perturbed in cortical malformations. Front. Cell. Neurosci. 9, 1–10.

Bizzotto, S., Uzquiano, A., Dingli, F., Ershov, D., Houllier, A., Arras, G., Richards, M., Loew, D., Minc, N., Croquelois, A., Houdusse, A., Francis, F., 2017. Eml1 loss impairs apical progenitor spindle length and soma shape in the developing cerebral cortex. Sci. Rep. 7, 1–14.

Bomsel, M., Mostov, K., 1992. Role of heterotrimeric G proteins in polarized membrane transport. J. Cell Sci. 3, 1317–1328.

Bond, J., Roberts, E., Mochida, G.H., Hampshire, D.J., Scott, S., Askham, J.M., Springell, K., Mahadevan, M., Crow, Y.J., Markham, A.F., Walsh, C.A., Geoffrey Woods, C., 2002. ASPM is a major determinant of cerebral cortical size. Nat. Genet. 32, 316–320.

Borrell, V., Götz, M., 2014. Role of radial glial cells in cerebral cortex folding. Curr. Opin. Neurobiol. 27, 39–46.

Borrell, V., Reillo, I., 2012. Emerging roles of neural stem cells in cerebral cortex development and evolution. Dev. Neurobiol. 72, 955–971.

Boyer, L.F., Campbell, B., Larkin, S., Mu, Y., Gage, F.H., 2012. Dopaminergic differentiation of human pluripotent cells. Curr. Protoc. Stem Cell Biol. 1, 1–11.

Brennand, K.J., Simone, A., Jou, J., Gelboin-Burkhart, C., Tran, N., Sangar, S., Li, Y., Mu, Y., Chen, G., Yu, D., McCarthy, S., Sebat, J., Gage, F.H., 2011. Modelling schizophrenia using human induced pluripotent stem cells. Nature 473, 221–225.

Brockington, M., 2001. Mutations in the fukutin-related protein gene (FKRP) identify limb girdle muscular dystrophy 2I as a milder allelic variant of congenital muscular dystrophy MDC1C. Hum. Mol. Genet. 10, 2851–2859.

Broix, L., Jagline, H., Ivanova, E., Drouot, N., Clayton-smith, J., Pagnamenta, A.T., Kay, A., Isidor, B., Louvier, U.W., Poduri, A., Taylor, J.C., Tilly, P., Poirier, K., Saillour, Y., Lebrun, N., Rudolf, G., Muraca, G., Saintpierre, B., 2016. Mutations in the HECT domain of NEDD4L lead to AKT/mTOR pathway deregulation and cause periventricular nodular heterotopia. Nature 48, 1349–1358.

Buchsbaum, I.Y., Cappello, S., 2019. Neuronal migration in the CNS during development and disease: insights from in vivo and in vitro models. Development 146, 1–17.

Buchsbaum, I.Y., Kielkowski, P., Giorgio, G., Neill, A.C.O., Giaimo, R. Di, Kyrousi, C., Khattak, S., Sieber, S.A., Robertson, S.P., Cappello, S., 2020. ECE2 regulates neurogenesis and neuronal migration during human cortical development Isabel. EMBO Rep. 49, 1–24.

Bystron, I., Blakemore, C., Rakic, P., 2008. Development of the human cerebral cortex: Boulder Committee revisited. Nat. Rev. Neurosci. 9, 110–122.

Cakir, B., Xiang, Y., Tanaka, Y., Kural, M.H., Parent, M., Kang, Y.-J., Chapeton, K., Patterson, B., Yuan, Y., He, C.-S., Raredon, M.S.B., Dengelegi, J., Kim, K.-Y., Sun, P., Zhong, M., Lee, S., Patra, P., Hyder, F., Niklason, L.E., Lee, S.-H., Yoon, Y.-S., Park, I.-H., 2019. Engineering of human brain organoids with a functional vascular-like system. Nat. Methods 16, 1169–1175.

Cali, J.J., Balcueva, E.A., Rybalkin, I., Robishaw, J.D., 1992. Selective tissue distribution of G protein γ subunits, including a new form of the γ subunits identified by cDNA cloning. J. Biol. Chem. 267, 24023–24027.

Camp, J.G., Badsha, F., Florio, M., Kanton, S., Gerber, T., Wilsch-Bräuninger, M., Lewitus, E., Sykes, A., Hevers, W., Lancaster, M., Knoblich, J. a, Lachmann, R., Pääbo, S., Huttner, W.B., Treutlein, B., 2015. Human cerebral organoids recapitulate gene expression programs of fetal neocortex development. PNAS 112, 15672–7.

Campbell, K., Götz, M., 2002. Radial glia: multi-purpose cells for vertebrate brain development. Trends Neurosci. 25, 235–238.

Cappello, S., Attardo, A., Wu, X., Iwasato, T., Itohara, S., Wilsch-Brauninger, M., Eilken, H.M., Rieger, M.A., Schroeder, T.T., Huttner, W.B., Brakebusch, C., Gotz, M., 2006. The Rho-GTPase cdc42 regulates neural progenitor fate at the apical surface. Nat. Neurosci. 9, 1099–1107.

Cappello, S., Bohringer, C.R., Bergami, M., Conzelmann, K.K., Ghanem, A., Tomassy, G.S., Arlotta, P., Mainardi, M., Allegra, M., Caleo, M., van Hengel, J., Brakebusch, C., Gotz, M., 2012. A radial glia-specific role of RhoA in double cortex formation. Neuron 73, 911–924.

Cappello, S., Gray, M.J., Badouel, C., Lange, S., Einsiedler, M., Srour, M., Chitayat, D., Hamdan, F.F., Jenkins, Z.A., Morgan, T., Preitner, N., Uster, T., Thomas, J., Shannon, P., Morrison, V., Di Donato, N., Van Maldergem, L., Neuhann, T., Newbury-Ecob, R., Swinkells, M., Terhal, P., Wilson, L.C., Zwijnenburg, P.J., Sutherland-Smith, A.J., Black, M.A., Markie, D., Michaud, J.L., Simpson, M.A., Mansour, S., McNeill, H., Gotz, M., Robertson, S.P., 2013. Mutations in genes encoding the cadherin receptor-ligand pair DCHS1 and FAT4 disrupt cerebral cortical development. Nat. Genet. 45, 1300–1308.

Carabalona, A., Beguin, S., Pallesi-pocachard, E., Buhler, E., Pellegrino, C., Arnaud, K., Hubert, P., Oualha, M., Siffroi, J.P., Khantane, S., Coupry, I., Goizet, C., Gelot, A.B., Represa, A., Cardoso, C., 2012. A glial origin for periventricular nodular heterotopia caused by impaired expression of Filamin-A. Hum. Mol. Genet. 21, 1004–1017.

Chambers, S.M., Fasano, C.A., Papapetrou, E.P., Tomishima, M., Sadelain, M., Studer, L., 2009. Highly efficient neural conversion of human ES and iPS cells by dual inhibition of SMAD signaling. Nat. Biotechnol. 27, 275–280.

Chen, J.F., Zhang, Y., Wilde, J., Hansen, K.C., Lai, F., Niswander, L., 2014. Microcephaly disease gene Wdr62 regulates mitotic progression of embryonic neural stem cells and brain size. Nat. Commun. 5, 1–13.

Cikili-Uytun, M., 2018. Prefrontal Cortex. IntechOpen.

Clapham, D.E., Neer, E.J., 1993. New roles for G-protein (βγ-dimers in transmembrane signalling. Nature 365, 403–406.

Clapham, D.E., Neer, E.J., 1997. G protein beta gamma subunits. Annu. Rev. Pharmacol. Toxicol. 37, 167–203.

Cooper, J.A., Kawauchi, T., Tabata, H., 2004. Molecules and mechanisms that regulate multipolar migration in the intermediate zone 8, 1–11.

Corbo, J.C., Deuel, T.A., Long, J.M., LaPorte, P., Tsai, E., Wynshaw-Boris, A., Walsh, C.A., 2002. Doublecortin is required in mice for lamination of the hippocampus but not the neocortex. J. Neurosci. 22, 7548–7557.

Costa, M.R., Müller, U., 2015. Specification of excitatory neurons in the developing cerebral cortex: Progenitor diversity and environmental influences. Front. Cell. Neurosci. 8, 1–9.

D'Arcangelo, G., Miao, G.G., Chen, S.C., Scares, H.D., Morgan, J.I., Curran, T., 1995. A protein related to extracellular matrix proteins deleted in the mouse mutant reeler. Nature 374, 719–723.

D'Gama, A.M., Geng, Y., Couto, J.A., Martin, B., Boyle, E.A., LaCoursiere, C.M., Hossain, A., Hatem, N.E., Barry, B., Kwiatkowski, D.J., Vinters, H. V, James Barkovich, A., Shendure, J., Mathern, G.W., Walsh, C.A., Poduri, A., designed the study, A., supervised the study AMD, A., Neurol Author manuscript, A., 2015. mTOR pathway mutations cause hemimegalencephaly and focal cortical dysplasia. Ann. Neurol. 77, 720–725.

Daviaud, N., Friedel, R.H., Zou, H., 2018. Vascularization and engraftment of transplanted human cerebral organoids in mouse cortex 5, 1–18.

De Bernabé, D.B.V., Currier, S., Steinbrecher, A., Celli, J., Van Beusekom, E., Van der Zwaag, B., Kayserili, H., Merlini, L., Chitayat, D., Dobyns, W.B., Cormand, B., Lehesjoki, A.E., Cruces, J., Voit, T., Walsh, C.A., Van Bokhoven, H., Brunner, H.G., 2002. Mutations in the O-mannosyltransferase gene POMT1 give rise to the severe neuronal migration disorder Walker-Warburg syndrome. Am. J. Hum. Genet. 71, 1033–1043.

De Juan Romero, C., Borrell, V., 2015. Coevolution of radial glial cells and the cerebral cortex. Glia 63, 1303–1319.

De Sousa, A., Cunha, E., 2012. Hominins and the emergence of the modern human brain. Prog. Brain Res. 195, 293–322.

De Wit, M.C.Y., De Coo, I.F.M., Halley, D.J.J., Lequin, M.H., Mancini, G.M.S., 2009. Movement disorder and neuronal migration disorder due to ARFGEF2 mutation. Neurogenetics 10, 333–336.

Dehay, C., Kennedy, H., 2007. Cell-cycle control and cortical development. Nat. Rev. Neurosci. 8, 438–450.

Dehay, C., Kennedy, H., Kosik, K.S., 2015. The outer subventricular zone and primate-specific cortical complexification. Neuron 85, 683–694.

Del Toro, D., Ruff, T., Cederfjäll, E., Villalba, A., Seyit-Bremer, G., Borrell, V., Klein, R., 2017. Regulation of cerebral cortex folding by controlling neuronal migration via FLRT adhesion molecules. Cell 169, 621–635.

DeMyer, W., 1986. Megalencephaly: Types, clinical syndromes, and management. Pediatr. Neurol. 2, 321–328.

Desikan, R.S., Barkovich, A.J., 2016. Malformations of cortical development. Ann. Neurol. 80, 797–810.

Deuel, T.A.S., Liu, J.S., Corbo, J.C., Yoo, S.Y., Rorke-Adams, L.B., Walsh, C.A., 2006. Genetic interactions between doublecortin and doublecortin-like kinase in neuronal migration and axon outgrowth. Neuron 49, 41–53.

Dezonne, R.S., Sartore, R.C., Nascimento, J.M., Saia-Cereda, V.M., Romão, L.F., Alves-Leon, S.V., de Souza, J.M., Martins-de-Souza, D., Rehen, S.K., Gomes, F.C.A., 2017. Derivation of functional human astrocytes from cerebral organoids. Sci. Rep. 7, 45–91.

Di Matteo, et al, F., 2020. Cystatin B is essential for proliferation and interneuron migration in individuals with EPM1 epilepsy. EMBO Mol. Med. 12, e11419.

Diaz, A.L., Gleeson, J.G., 2009. The molecular and genetic mechanisms of neocortex development. Clin Perinatol 36, 503–512.

Dichter, M.A., Pollard, J., 2006. Cell culture models for studying epilepsy. In: Models of Seizures and Epilepsy. Elsevier Inc., pp. 23–34.

Dies, K.A., Bodell, A., Hisama, F.M., Guo, C.Y., Barry, B., Chang, B.S., Barkovich, A.J., Walsh, C.A., 2013. Schizencephaly: Association with young maternal age, alcohol use, and lack of prenatal care. J. Child Neurol. 28, 198–203.

Dobyns, W.B., Andermann, E., Andermann, F., Czapansky-Beilman, D., Dubeau, F., Dulac, O., Guerrini, R., Hirsch, B., Ledbetter, D.H., Lee, N.S., Motte, J., Pinard, J.M., Radtke, R.A., Ross, M.E., Tampieri, D., Walsh, C.A., Truwit, C.L., 1996. X-linked malformations of neuronal migration. Neurology 47, 331–339.

Dobyns, W.B., Das, S., 1993. PAFAH1B1-Associated Lissencephaly/Subcortical Band Heterotopia. GeneReviews® 1–15.

Dubeau, F., Tampieri, D., Lee, N., Andermann, E., Carpenter, S., Leblanc, R., Olivier, A., Radtke, R., Villemure, J.G., Andermann, F., 1995. Periventricular and subcortical nodular heterotopia. A study of 33 patients. Brain 118, 1273–1287.

Durkee, C.A., Araque, A., 2019. Diversity and specificity of astrocyte–neuron communication. Neuroscience 396, 73–78.

Eiraku, M., Watanabe, K., Matsuo-Takasaki, M., Kawada, M., Yonemura, S., Matsumura, M., Wataya, T., Nishiyama, A., Muguruma, K., Sasai, Y., 2008. Self-organized formation of polarized cortical tissues from ESCs and its active manipulation by extrinsic signals. Cell Stem Cell 3, 519–532.

Ekşioğlu, Y.Z., Scheffer, I.E., Cardenas, P., Knoll, J., DiMario, F., Ramsby, G., Berg, M., Kamuro, K., Berkovic, S.F., Duyk, G.M., Parisi, J., Huttenlocher, P.R., Walsh, C.A., 1996. Periventricular heterotopia: An X-linked dominant epilepsy locus causing aberrant cerebral cortical development. Neuron 16, 77–87.

Elkabetz, Y., Panagiotakos, G., Al Shamy, G., Socci, N.D., Tabar, V., Studer, L., 2008. Human ES cell-derived neural rosettes reveal a functionally distinct early neural stem cell stage. Genes Dev. 22, 152–165.

Emdad, L., D'Souza, S.L., Kothari, H.P., Qadeer, Z.A., Germano, I.M., 2012. Efficient differentiation of human embryonic and induced pluripotent stem cells into functional astrocytes. Stem Cells Dev. 21, 404–410.

Englund, C., Fink, A., Lau, C., Pham, D., Daza, R.A.M., Bulfone, A., Kowalczyk, T., Hevner, R.F., 2005. Pax6, Tbr2, and Tbr1 are expressed sequentially by radial glia, intermediate progenitor cells, and postmitotic neurons in developing neocortex. J. Neurosci. 25, 247–251.

Feng, Y., Chen, M.H., Moskowitz, I.P., Mendonza, A.M., Vidali, L., Nakamura, F., Kwiatkowski, D.J., Walsh, C.A., 2006. Filamin a (FLNA) is required for cell-cell contact in vascular development and cardiac morphogenesis. PNAS 103, 19836–19841.

Ferland, R.J., Batiz, L.F., Neal, J., Lian, G., Bundock, E., Lu, J., Hsiao, Y.C., Diamond, R., Mei, D., Banham, A.H., Brown, P.J., Vanderburg, C.R., Joseph, J., Hecht, J.L., Folkerth, R., Guerrini, R., Walsh, C.A., Rodriguez, E.M., Sheen, V.L., 2009. Disruption of neural progenitors along the ventricular and subventricular zones in periventricular heterotopia. Hum. Mol. Genet. 18, 497–516.

Ferrer, I., Santamaría, J., Alcántara, S., Zújar, M.J., Cinós, C., 1993. Neuronal ectopic masses induced by prenatal irradiation in the rat. Virchows Arch. A Pathol. Anat. Histopathol. 422, 1–6.

Fiddes, I.T., Lodewijk, G.A., Mooring, M., Bosworth, C.M., Ewing, A.D., Mantalas, G.L., Novak, A.M., van den Bout, A., Bishara, A., Rosenkrantz, J.L., Lorig-Roach, R., Field, A.R., Haeussler, M., Russo, L., Bhaduri, A., Nowakowski, T.J., Pollen, A.A., Dougherty, M.L., Nuttle, X., Addor, M.C., Zwolinski, S., Katzman, S., Kriegstein, A., Eichler, E.E., Salama, S.R., Jacobs, F.M.J., Haussler, D., 2018. Human-Specific NOTCH2NL Genes Affect Notch Signaling and Cortical Neurogenesis. Cell 173, 1356-1369.e22.

Fietz, S.A., Kelava, I., Vogt, J., Wilsch-Bräuninger, M., Stenzel, D., Fish, J.L., Corbeil, D., Riehn, A., Distler, W., Nitsch, R., Huttner, W.B., 2010. OSVZ progenitors of human and ferret neocortex are epithelial-like and expand by integrin signaling. Nat. Neurosci. 13, 690–699.

Fietz, S.A., Lachmann, R., Brandl, H., Kircher, M., Samusik, N., Schroder, R., Lakshmanaperumal, N., Henry, I., Vogt, J., Riehn, A., Distler, W., Nitsch, R., Enard, W., Paabo, S., Huttner, W.B., 2012. Transcriptomes of germinal zones of human and mouse fetal neocortex suggest a role of extracellular matrix in progenitor self-renewal. PNAS 109, 11836–11841.

Fish, J.L., Dehay, C., Kennedy, H., Huttner, W.B., 2008. Making bigger brains - The evolution of neural-progenitor-cell division. J. Cell Sci. 121, 2783–2793.

Florio, M., Albert, M., Taverna, E., Namba, T., Brandl, H., Lewitus, E., Haffner, C., Sykes, A., Wong, F.K., Peters, J., Guhr, E., Klemroth, S., Prufer, K., Kelso, J., Naumann, R., Nusslein, I., Dahl, A., Lachmann, R., Paabo, S., Huttner, W.B., 2015. Human-specific gene ARHGAP11B promotes basal progenitor amplification and neocortex expansion. Science 347, 1465–70.

Florio, M., Borrell, V., Huttner, W.B., 2017. Human-specific genomic signatures of neocortical expansion. Curr. Opin. Neurobiol. 42, 33–44.

Florio, M., Heide, M., Pinson, A., Brandl, H., Albert, M., Winkler, S., Wimberger, P., Huttner, W.B., Hiller, M., 2018. Evolution and cell-type specificity of human-specific genes preferentially expressed in progenitors of fetal neocortex. Elife 7, 1–37.

Florio, M., Huttner, W.B., 2014. Neural progenitors, neurogenesis and the evolution of the neocortex. Development 141, 2182–2194.

Fox, J.W., Lamperti, E.D., Ekşioğlu, Y.Z., Hong, S.E., Feng, Y., Graham, D.A., Scheffer, I.E., Dobyns, W.B., Hirsch, B.A., Radtke, R.A., Berkovic, S.F., Huttenlocher, P.R., Walsh, C.A., 1998. Mutations in filamin 1 prevent migration of cerebral cortical neurons in human Periventricular heterotopia. Neuron 21, 1315–1325.

Francis, F., Meyer, G., Fallet-Bianco, C., Moreno, S., Kappeler, C., Socorro, A.C., Tuy, F.P.D., Beldjord, C., Chelly, J., 2006. Human disorders of cortical development: From past to present. Eur. J. Neurosci. 23, 877–893.

Frantz, C., Stewart, K.M., Weaver, V.M., 2010. The extracellular matrix at a glance. J. Cell Sci. 123, 4195–4200.

Friocourt, F., Chédotal, A., 2017. The Robo3 receptor, a key player in the development, evolution, and function of commissural systems. Dev. Neurobiol. 77, 876–890.

Fujii, Y., Ishikawa, N., Kobayashi, Y., Kobayashi, M., Kato, M., 2014. Compound heterozygosity in GPR56 with bilateral frontoparietal polymicrogyria. Brain Dev. 36, 528–531.

Fuster, J.M., 2002. Frontal lobe and cognitive development. J. Neurocytol. 31, 373–385.

Gaitanis, J., Tarui, T., 2018. Nervous System Malformations. Contin. (Minneao Minn) 24, 72–95.

Gal, J.S., Morozov, Y.M., Ayoub, A.E., Chatterjee, M., Rakic, P., Haydar, T.F., 2006. Molecular and morphological heterogeneity of neural precursors in the mouse neocortical proliferative zones. J. Neurosci. 26, 1045–1056.

Gilman, A.G., 1987. G Proteins: Transducers of Receptor-Generated Signals. Annu. Rev. Biochem. 56, 615–649.

Gilmore, E.C., Walsh, C.A., 2013. Genetic causes of microcephaly and lessons for neuronal development. Wiley Interdiscip. Rev. Dev. Biol. 2, 461–478.

Giulietti, M., Vivenzio, V., Piva, F., Principato, G., Bellantuono, C., Nardi, B., 2014. How much do we know about the coupling of G-proteins to serotonin receptors? Mol. Brain 7, 1–15.

Gleeson, J.G., Peter T, L., Flanagan, L.A., Walsh, C.A., 1999. Doublecortin is a microtubule-associated protein and is expressed widely by migrating neurons. Neuron 23, 257–271.

Golan, M.H., Mane, R., Molczadzki, G., Zuckerman, M., Kaplan-Louson, V., Huleihel, M., Perez-Polo, J.R., 2009. Impaired migration signaling in the hippocampus following prenatal hypoxia. Neuropharmacology 57, 511–522.

Götz, M., Huttner, W.B., 2005. The cell biology of neurogenesis. Nat. Rev. Mol. Cell Biol. 6, 777–788.

Götz, M., Stoykova, A., Gruss, P., 1998. Pax6 controls radial glia differentiation in the cerebral cortex. Neuron 21, 1031–1044.

Green, R., Krause, J., Briggs, A., Rasilla Vives, M., Fortea Pérez, F., 2010. A draft sequence of the neandertal genome. Science 328, 710–722.

Gressens, P., Kosofsky, B.E., Evrard, P., 1992. Cocaine-induced disturbances of corticogenesis in the developing murine brain. Neurosci. Lett. 140, 113–116.

Grewal, P.K., Hewitt, J.E., 2003. Glycosylation defects: a new mechanism for muscular dystrophy? Hum. Mol. Genet. 12, R259–R264.

Guerrini, R., Dobyns, W.B., 2014. Malformations of cortical development: clinical features and genetic causes. Lancet Neurol 13, 710–726.

Gunhanlar, N., Shpak, G., van der Kroeg, M., Gouty-Colomer, L.A., Munshi, S.T., Lendemeijer, B., Ghazvini, M., Dupont, C., Hoogendijk, W.J.G., Gribnau, J., de Vrij, F.M.S., Kushner, S.A., 2017. A simplified protocol for differentiation of electrophysiologically mature neuronal networks from human induced pluripotent stem cells. Mol. Psychiatry 1–9.

Gunnersen, J.M., Kim, M.H., Fuller, S.J., De Silva, M., Britto, J.M., Hammond, V.E., Davies, P.J., Petrou, S., Faber, E.S.L., Sah, P., Tan, S.S., 2007. Sez-6 proteins affect dendritic arborization patterns and excitability of cortical pyramidal neurons. Neuron 56, 621–639.

Gunz, P., Neubauer, S., Golovanova, L., Doronichev, V., Maureille, B., Hublin, J.-J., 2012. A uniquely modern human pattern of endocranial development. Insights from a new cranial reconstruction of the Neandertal newborn from Mezmaiskaya. J. Hum. Evol. 62, 300–313.

Gunz, P., Neubauer, S., Maureille, B., Hublin, J.J., 2010. Brain development after birth differs between Neanderthals and modern humans. Curr. Biol. 20, R921–R922.

Gunz, P., Tilot, A.K., Wittfeld, K., Teumer, A., Shapland, C.Y., van Erp, T.G.M., Dannemann, M., Vernot, B., Neubauer, S., Guadalupe, T., Fernández, G., Brunner, H.G., Enard, W., Fallon, J., Hosten, N., Völker, U., Profico, A., Di Vincenzo, F., Manzi, G., Kelso, J., St. Pourcain, B., Hublin, J.J., Franke, B., Pääbo, S., Macciardi, F., Grabe, H.J., Fisher, S.E., 2019. Neandertal introgression sheds light on modern human endocranial globularity. Curr. Biol. 29, 120–127.

Gupta, R., Jung, E., Brunak, S., 2004. Prediction of N-glycosylation sites in human proteins. Prep.

Hansen, D. V., Lui, J.H., Parker, P.R.L., Kriegstein, A.R., 2010. Neurogenic radial glia in the outer subventricular zone of human neocortex. Nature 464, 554–561.

Harris, J.J., Jolivet, R., Attwell, D., 2012. Synaptic energy use and supply. Neuron 75, 762–777.

Hashimoto-Torii, K., Torii, M., Fujimoto, M., Nakai, A., El Fatimy, R., Mezger, V., Ju, M.J., Ishii, S., Chao, S., Brennand, K.J., Gage, F.H., Rakic, P., 2014. Roles of heat shock factor 1 in neuronal response to fetal environmental risks and its relevance to brain disorders. Neuron 82, 560–572.

Haubensak, W., Attardo, A., Denk, W., Huttner, W.B., 2004. Neurons arise in the basal neuroepithelium of the early mammalian telencephalon: A major site of neurogenesis. PNAS 101, 3196–3201.

Heide, M., Haffner, C., Murayama, A., Kurotaki, Y., Shinohara, H., Okano, H., Sasaki, E., Huttner, W.B., 2020. Human-specific ARHGAP11B increases size and folding of primate neocortex in the fetal marmoset. Science 21, 1–9.

Heinzen, E.L., O'Neill, A.C., Zhu, X., Allen, A.S., Bahlo, M., Chelly, J., Chen, M.H., Dobyns, W.B., Freytag, S., Guerrini, R., Leventer, R.J., Poduri, A., Robertson, S.P., Walsh, C.A., Zhang, M., 2018. De novo and inherited private variants in MAP1B in periventricular nodular heterotopia. PLoS Genet. 14, 1–23.

Hendrickson, T.J., Mueller, B.A., Sowell, E.R., Mattson, S.N., Coles, C.D., Kable, J.A., Jones, K.L., Boys, C.J., Lim, K.O., Riley, E.P., Wozniak, J.R., 2017. Cortical gyrification is abnormal in children with prenatal alcohol exposure. NeuroImage Clin. 15, 391–400.

Herculano-Houzel, S., Mota, B., Lent, R., 2006. Cellular scaling rules for rodent brains. Proc. Natl. Acad. Sci. U. S. A. 103, 12138–12143.

Hewavitharana, T., Wedegaertner, P.B., 2012. Non-canonical signaling and localizations of heterotrimeric G proteins. Cell Signal. 24, 25–34.

Hirose, S., Tanaka, Y., Shibata, M., Kimura, Y., Ishikawa, M., Higurashi, N., Yamamoto, T., Ichise, E., Chiyonobu, T., Ishii, A., 2020. Application of induced pluripotent stem cells in epilepsy. Mol. Cell. Neurosci. 108, 103535.

Hirotsune, S., Fleck, M.W., Gambello, M.J., Bix, G.J., Chen, A., Clark, G.D., Ledbetter, D.H., McBain, C.J., Wynshaw-Boris, A., 1998. Graded reduction of Pafah1b1 (Lis1) activity results in neuronal migration defects and early embryonic lethality. Nat. Genet. 19, 333–339.

Hodge, R.D., Bakken, T.E., Miller, J.A., 2019. Conserved cell types with divergent features in human versus mouse cortex. Nature 573, 61–68.

Holloway, R.L., 1981. Volumetric and asymmetry determinations on recent hominid endocasts: Spy I and II, Djebel Ihroud I, and the salè Homo erectus specimens, with some notes on neandertal brain size. Am. J. Phys. Anthropol. 55, 385–393.

Hong, S.E., Shugart, Y.Y., Huang, D.T., Al Shahwan, S., Grant, P.E., Hourihane, J.O.B., Martin, N.D.T., Walsh, C.A., 2000. Autosomal recessive lissencephaly with cerebellar hypoplasia is associated with human RELN mutations. Nat. Genet. 26, 93–96.

Hu, W.F., Chahrour, M.H., Walsh, C.A., 2014. The diverse genetic landscape of neurodevelopmental disorders. Annu. Rev. Genomics Hum. Genet. 15, 195–213.

Hung, L.-Y., Tang, C.-J.C., Tang, T.K., 2000. Protein 4.1 R-135 interacts with a novel centrosomal protein (CPAP) which is associated with the gamma-tubulin complex. Mol. Cell. Biol. 20, 7813–7825.

Hynes, R.O., 2009. Extracellular matrix: not just pretty fibrils. Science 326, 1216–1219.

Iefremova, V., Manikakis, G., Krefft, O., Jabali, A., Weynans, K., Wilkens, R., Marsoner, F., Brändl, B., Müller, F.J., Koch, P., Ladewig, J., 2017. An organoid-based model of cortical development identifies non-cell-autonomous defects in Wnt signaling contributing to Miller-Dieker syndrome. Cell Rep. 19, 50–59.

Im, M.J., Holzhöfer, A., Böttinger, H., Pfeuffer, T., Helmreich, E.J.M., 1988. Interactions of pure βγ-subunits of G-proteins with purified β1-adrenoceptor. FEBS Lett. 227, 225–229.

Ishii, K., Kubo, K.I., Endo, T., Yoshida, K., Benner, S., Ito, Y., Aizawa, H., Aramaki, M., Yamanaka, A., Tanaka, K., Takata, N., Tanaka, K.F., Mimura, M., Tohyama, C., Kakeyama, M., Nakajima, K., 2015. Neuronal heterotopias affect the activities of distant brain areas and lead to behavioral deficits. J. Neurosci. 35, 12432–12445.

Ishii, S., Hashimoto-Torii, K., 2015. Impact of prenatal environmental stress on cortical development. Front. Cell. Neurosci. 9, 1–8.

Ishiuchi, T., Misaki, K., Yonemura, S., Takeichi, M., Tanoue, T., 2009. Mammalian Fat and Dachsous cadherins regulate apical membrane organization in the embryonic cerebral cortex. J. Cell Biol. 185, 959–967.

Iwata, R., Casimir, P., Vanderhaeghen, P., 2020. Mitochondrial dynamics in postmitotic cells regulate neurogenesis. Science 369, 858–862.

Jabaudon, D., Lancaster, M., 2018. Exploring landscapes of brain morphogenesis with organoids. Development 145, 1–4.

Jackson, A.P., Eastwood, H., Bell, S.M., Adu, J., Toomes, C., Carr, I.M., Roberts, E., Hampshire, D.J., Crow, Y.J., Mighell, A.J., Karbani, G., Jafri, H., Rashid, Y., Mueller, R.F., Markham, A.F., Woods, C.G., 2002. Identification of microcephalin, a protein implicated in determining the size of the human brain. Am. J. Hum. Genet. 71, 136–142.

Jansen, A.C., Oostra, A., Desprechins, B., De Vlaeminck, Y., Verhelst, H., Régal, L., Verloo, P., Bockaert, N., Keymolen, K., Seneca, S., De Meirleir, L., Lissens, W., 2011. TUBA1A mutations: From isolated lissencephaly to familial polymicrogyria. Neurology 76, 988–992.

Johnson, M.B., Sun, X., Kodani, A., Borges-Monroy, R., Girskis, K.M., Ryu, S.C., Wang, P.P., Patel, K., Gonzalez, D.M., Woo, Y.M., Yan, Z., Liang, B., Smith, R.S., Chatterjee, M., Coman, D., Papademetris, X., Staib, L.H., Hyder, F., Mandeville, J.B., Grant, P.E., Im, K., Kwak, H., Engelhardt, J.F., Walsh, C.A., Bae, B. Il, 2018. Aspm knockout ferret reveals an evolutionary mechanism governing cerebral cortical size. Nature 556, 370–375.

Ju, X.C., Hou, Q.Q., Sheng, A.L., Wu, K.Y., Zhou, Y., Jin, Y., Wen, T., Yang, Z., Wang, X., Luo, Z.G., 2016. The hominoid-specific gene TBC1D3 promotes generation of basal neural progenitors and induces cortical folding in mice. Elife 5, 1–25.

Kadoshima, T., Sakaguchi, H., Nakano, T., Soen, M., Ando, S., Eiraku, M., Sasai, Y., 2013. Self-organization of axial polarity, inside-out layer pattern, and species-specific progenitor dynamics in human ES cell-derived neocortex. PNAS 110, 20284–20289.

Kandratavicius, L., Alves Balista, P., Lopes-Aguiar, C., Ruggiero, R.N., Umeoka, E.H., Garcia-Cairasco, N., Bueno-Junior, L.S., Leite, J.P., 2014. Animal models of epilepsy: Use and limitations. Neuropsychiatr. Dis. Treat. 10, 1693–1705.

Kanton, S., Boyle, M.J., He, Z., Santel, M., Weigert, A., Sanchís-Calleja, F., Guijarro, P., Sidow, L., Fleck, J.S., Han, D., Qian, Z., Heide, M., Huttner, W.B., Khaitovich, P., Pääbo, S., Treutlein, B., Camp, J.G., 2019. Organoid single-cell genomic atlas uncovers human-specific features of brain development. Nature 574, 418–422.

Karzbrun, E., Kshirsagar, A., Cohen, S.R., Hanna, J.H., Reiner, O., 2018. Human brain organoids on a chip reveal the physics of folding. Nat. Phys. 14, 515–522.

Kawasaki, H., Toda, T., Tanno, K., 2013. In vivo genetic manipulation of cortical progenitors in gyrencephalic carnivores using in utero electroporation. Biol. Open 2, 95–100.

Keays, D.A., Tian, G., Poirier, K., Huang, G.J., Siebold, C., Cleak, J., Oliver, P.L., Fray, M., Harvey, R.J., Molnár, Z., Piñon, M.C., Dear, N., Valdar, W., Brown, S.D.M., Davies, K.E., Rawlins, J.N.P., Cowan, N.J., Nolan, P., Chelly, J., Flint, J., 2007. Mutations in α-tubulin cause abnormal neuronal migration in mice and lissencephaly in humans. Cell 128, 45–57.

Kelava, I., Reillo, I., Murayama, A.Y., Kalinka, A.T., Stenzel, D., Tomancak, P., Matsuzaki, F., Lebrand, C., Sasaki, E., Schwamborn, J.C., Okano, H., Huttner, W.B., Borrell, V., 2012. Abundant occurrence of basal radial glia in the subventricular zone of embryonic neocortex of a lissencephalic primate, the common marmoset callithrix jacchus. Cereb. Cortex 22, 469–481.

Khan, T.A., Revah, O., Gordon, A., Yoon, S.J., Krawisz, A.K., Goold, C., Sun, Y., Kim, C.H., Tian, Y., Li, M.Y., Schaepe, J.M., Ikeda, K., Amin, N.D., Sakai, N., Yazawa, M., Kushan, L., Nishino, S., Porteus, M.H., Rapoport, J.L., Bernstein, J.A., O'Hara, R., Bearden, C.E., Hallmayer, J.F., Huguenard, J.R., Geschwind, D.H., Dolmetsch, R.E., Paşca, S.P., 2020. Neuronal defects in a human cellular model of 22q11.2 deletion syndrome. Nat. Med. 1–11.

Kielar, M., Tuy, F.P., Bizzotto, S., Lebrand, C., de Juan Romero, C., Poirier, K., Oegema, R., Mancini, G.M., Bahi-Buisson, N., Olaso, R., Le Moing, A.G., Boutourlinsky, K., Boucher, D., Carpentier, W., Berquin, P., Deleuze, J.F., Belvindrah, R., Borrell, V., Welker, E., Chelly, J., Croquelois, A., Francis, F., 2014. Mutations in Eml1 lead to ectopic progenitors and neuronal heterotopia in mouse and human. Nat Neurosci 17, 923–933.

Kim, J., Yang, M., Kim, J., Song, L., Lee, S., Son, Y., Kang, S., Bae, C.S., Kim, J.C., Kim, S.H., Shin, T., Wang, H., Moon, C., 2014. Developmental and degenerative modulation of brain-derived neurotrophic factor transcript variants in the mouse hippocampus. Int J Dev Neurosci 38, 68–73.

Klaus, J., Kanton, S., Kyrousi, C., Ayo-Martin, A.C., Di Giaimo, R., Riesenberg, S., O'Neill, A.C., Camp, J.G., Tocco, C., Santel, M., Rusha, E., Drukker, M., Schroeder, M., Götz, M., Robertson, S.P., Treutlein, B., Cappello, S., 2019. Altered neuronal migratory trajectories in human cerebral organoids derived from individuals with neuronal heterotopia. Nat. Med. 25, 561–568.

Kochiyama, T., Ogihara, N., Tanabe, H.C., Kondo, O., Amano, H., Hasegawa, K., Suzuki, H., Ponce De León, M.S., Zollikofer, C.P.E., Bastir, M., Stringer, C., Sadato, N., Akazawa, T., 2018. Reconstructing the Neanderthal brain using computational anatomy. Sci. Rep. 8, 1–9.

Komuro, H., Rakic, P., 1998. Distinct modes of neuronal migration in different domains of developing cerebellar cortex. J. Neurosci. 18, 1478–1490.

Kornack, D.R., Rakic, P., 1998. Changes in cell-cycle kinetics during the development and evolution of primate neocortex. Proc. Natl. Acad. Sci. USA 95, 1242–1246.

Kou, Z., Wu, Q., Kou, X., Yin, C., Wang, H., Zuo, Z., Zhuo, Y., Chen, A., Gao, S., Wang, X., 2015. CRISPR/Cas9-mediated genome engineering of the ferret. Cell Res. 25, 1372–1375.

Kowalczyk, T., Pontious, A., Englund, C., Daza, R.A.M., Bedogni, F., Hodge, R., Attardo, A., Bell, C., Huttner, W.B., Hevner, R.F., 2009. Intermediate neuronal progenitors (basal progenitors) produce pyramidal-projection neurons for all layers of cerebral cortex. Cereb. Cortex 19, 2439–2450.

Krefft, O., Jabali, A., Iefremova, V., Koch, P., Ladewig, J., 2018. Generation of standardized and reproducible forebrain-type cerebral organoids from human induced pluripotent stem cells. J. Vis. Exp. 2018, 56768.

Krencik, R., Weick, J.P., Liu, Y., Zhang, Z., Zhang, S.-C., 2011. Specification of transplantable astroglial subtypes from human pluripotent stem cells. Nat Biotechnol 29, 528–534.

Kriegstein, A.R., Noctor, S., Martínez-cerdeño, V., 2006. Patterns of neural stem and progenitor cell division may underlie evolutionary cortical expansion. Nat. Rev. Neurosci. 7, 883–890.

Kriegstein, A.R., Noctor, S.C., 2004. Patterns of neuronal migration in the embryonic cortex. Trends Neurosci. 27, 392–399.

Krings, M., Stone, A., Schmitz, R.W., Krainitzki, H., Stoneking, M., Pääbo, S., 1997. Neandertal DNA sequences and the origin of modern humans. Cell 90, 19–30.

Krishnaswami, S.R., Grindberg, R. V., Novotny, M., Venepally, P., Lacar, B., Bhutani, K., Linker, S.B., Pham, S., Erwin, J.A., Miller, J.A., Hodge, R., McCarthy, J.K., Kelder, M., McCorrison, J., Aevermann, B.D., Fuertes, F.D., Scheuermann, R.H., Lee, J., Lein, E.S., Schork, N., McConnell, M.J., Gage, F.H., Lasken, R.S., 2016. Using single nuclei for RNA-seq to capture the transcriptome of postmortem neurons. Nat. Protoc. 11, 499–524.

Kuzniecky, R.I., 1994. Magnetic Resonance Imaging in Developmental Disorders of the Cerebral Cortex. Epilepsia 35, S44–S56.

Kuzniecky, R.I., Barkovich, A.J., 2015. Malformations of cortical development and epilepsy. Brain Dev. 23, 2–11.

Kyrousi, C., Cappello, S., 2019. Using brain organoids to study human neurodevelopment, evolution and disease. Wires Dev. Biol. 1–19.

Labelle-Dumais, C., Dilworth, D.J., Harrington, E.P., de Leau, M., Lyons, D., Kabaeva, Z., Manzini, M.C., Dobyns, W.B., Walsh, C.A., Michele, D.E., Gould, D.B., 2011. COL4A1 mutations cause ocular dysgenesis, neuronal localization defects, and myopathy in mice and walker-warburg syndrome in humans. PLoS Genet. 7, e1002062.

Lachmann, A., Xu, H., Krishnan, J., Berger, S.I., Mazloom, A.R., Ma'ayan, A., 2010. ChEA: Transcription factor regulation inferred from integrating genome-wide ChIP-X experiments. Bioinformatics 26, 2438–2444.

Lambert de Rouvroit, C., Goffinet, A.M., 1998. The reeler mouse as a model of brain development. Adv. Anat. Embryol. Cell Biol. 150, 1–106.

Lambert de Rouvroit, C., Goffinet, A.M., 2001. Neuronal Migration. In: Mechanisms of Development. pp. 47–56.

Lancaster, M.A., Knoblich, J.A., 2014. Generation of cerebral organoids from human pluripotent stem cells. Nat. Protoc. 9, 2329–2340.

Lancaster, M.A., Renner, M., Martin, C.-A., Wenzel, D., Bicknell, L.S., Hurles, M.E., Homfray, T., Penninger, J.M., Jackson, A.P., Knoblich, J.A., 2013. Cerebral organoids model human brain development and microcephaly. Nature 501, 373–9.

Laplante, M., Sabatini, D.M., 2012. mTOR signaling in growth control and disease. Cell 149, 247–293.

Latour, Y.L., Yoon, R., Thomas, S.E., Grant, C., Li, C., Sena-Esteves, M., Allende, M.L., Proia, R.L., Tifft, C.J., 2019. Human GLB1 knockout cerebral organoids: A model system for testing AAV9-mediated GLB1 gene therapy for reducing GM1 ganglioside storage in GM1 gangliosidosis. Mol. Genet. Metab. Reports 21, 1–8.

Lee, J., 2017. Malformations of cortical development: Genetic mechanisms and diagnostic approach. Korean J. Pediatr. 60, 1–9.

Lerche, H., Jurkat-Rott, K., Lehmann-Horn, F., 2001. Epilepsy and genetic malformations of the cerebral cortex. Am. J. Med. Genet. - Semin. Med. Genet. 106, 160–173.

Létard, P., Drunat, S., Vial, Y., Duerinckx, S., Ernault, A., Amram, D., Arpin, S., Bertoli, M., Busa, T., Ceulemans, B., Desir, J., Doco-Fenzy, M., Elalaoui, S.C., Devriendt, K., Faivre, L., Francannet, C., Geneviève, D., Gérard, M., Gitiaux, C., Julia, S., Lebon, S., Lubala, T., Mathieu-Dramard, M., Maurey, H., Metreau, J., Nassereddine, S., Nizon, M., Pierquin, G., Pouvreau, N., Rivier-Ringenbach, C., Rossi, M., Schaefer, E., Sefiani, A., Sigaudy, S., Sznajer, Y., Tunca, Y., Guilmin Crepon, S., Alberti, C., Elmaleh-Bergès, M., Benzacken, B., Wollnick, B., Woods, C.G., Rauch, A., Abramowicz, M., El Ghouzzi, V., Gressens, P., Verloes, A., Passemard, S., 2018. Autosomal recessive primary microcephaly due to ASPM mutations: An update. Hum. Mutat. 39, 319–332.

Leventer, R.J., Jansen, A., Pilz, D.T., Stoodley, N., Marini, C., Dubeau, F., Malone, J., Mitchell, L.A., Mandelstam, S., Scheffer, I.E., Berkovic, S.F., Andermann, F., Andermann, E., Guerrini, R., Dobyns, W.B., 2010. Clinical and imaging heterogeneity of polymicrogyria: A study of 328 patients. Brain 133, 1415–1427.

Lewitus, E., Kelava, I., Kalinka, A.T., Tomancak, P., Huttner, W.B., 2014. An Adaptive Threshold in Mammalian Neocortical Evolution. PLoS Biol. 12, e1002000.

Li, R., Sun, L., Fang, A., Li, P., Wu, Q., Wang, X., 2017. Recapitulating cortical development with organoid culture in vitro and modeling abnormal spindle-like (ASPM related primary) microcephaly disease. Protein Cell 8, 823–833.

Li, S., Jin, Z., Koirala, S., Bu, L., Xu, L., Hynes, R.O., Walsh, C.A., Corfas, G., Piao, X., 2008. GPR56 regulates pial basement membrane integrity and cortical lamination. J. Neurosci. 28, 5817–5826.

Li, X., Tao, Yezheng, Bradley, R., Du, Z., Tao, Yunlong, Kong, L., Dong, Y., Jones, J., Yan, Y., Harder, C.R.K., Friedman, L.M., Bilal, M., Hoffmann, B., Zhang, S.C., 2018. Fast generation of functional subtype astrocytes from human pluripotent stem cells. Stem Cell Reports 11, 998–1008.

Lim, W.K., Myung, C.S., Garrison, J.C., Neubig, R.R., 2001. Receptor - G protein γ specificity: γ 11 shows unique potency for A1 adenosine and 5-HT1A receptors. Biochemistry 40, 10532–10541.

Liu, J., Liu, W., Yang, L., Wu, Q., Zhang, H., Fang, A., Li, L., Xu, X., Sun, L., Zhang, J., Tang, F., Wang, X., 2017. The primate-specific gene TMEM14B marks outer radial glia Cells and promotes cortical expansion and folding. Cell Stem Cell 21, 635–649.

Long, H.X., Li, M.Z., Fu, H.Y., 2016. Determination of optimal parameters of MAFFT program based on BAliBASE3.0 database. Springerplus 5, 1–9.

Long, K.R., Huttner, W.B., 2019. How the extracellular matrix shapes neural development. Open Biol. 9, 1–12.

Long, K.R., Newland, B., Florio, M., Kalebic, N., Langen, B., Kolterer, A., Wimberger, P., Huttner, W.B., 2018. Extracellular matrix components HAPLN1, lumican, and collagen I cause hyaluronic acid-dependent folding of the developing human neocortex. Neuron 99, 702–718.

López-Bendito, G., Sánchez-Alcaniz, J.A., Pla, R., Borrell, V., Pico, E., Valdeomilos, M., Marin, O., 2008. Chemokine signaling controls intracortical migration and final distribution of GABAergic interneurons. J. Neurosci. 28, 1613–1624.

Lui, J.H., Hansen, D. V, Kriegstein, A.R., 2011. Development and evolution of the human neocortex. Cell 146, 18–36.

Luo, R., Jeong, S.J., Jin, Z., Strokes, N., Li, S., Piao, X., 2011. G protein-coupled receptor 56 and collagen III, a receptor-ligand pair, regulates cortical development and lamination. PNAS 108, 12925–12930.

Maeta, K., Edamatsu, H., Nishihara, K., Ikutomo, J., Bilasy, S.E., Kataoka, T., 2016. Crucial role of Rapgef2 and Rapgef6, a family of guanine nucleotide exchange factors for Rap1 small GTPase, in formation of apical surface adherens junctions and neural progenitor development in the mouse cerebral cortex. eNeuro 3, 1–17.

Maldergem, L., Wetzburger, C., Verloes, A., Fourneau, C., Gillerot, Y., 2008. Mental retardation with blepharo-naso-facial abnormalities and hand malformations: a new syndrome? Clin. Genet. 41, 22–24.

Mansour, A.A., Gonçalves, J.T., Bloyd, C.W., Li, H., Fernandes, S., Quang, D., Johnston, S., Parylak, S.L., Jin, X., Gage, F.H., 2018. An in vivo model of functional and vascularized human brain organoids. Nat. Biotechnol. 36, 432–441.

Mansour, S., Swinkels, M., Terhal, P.A., Wilson, L.C., Rich, P., Van Maldergem, L., Zwijnenburg, P.J., Hall, C.M., Robertson, S.P., Newbury-Ecob, R., 2012. Van Maldergem syndrome: Further characterisation and evidence for neuronal migration abnormalities and autosomal recessive inheritance. Eur. J. Hum. Genet. 20, 1024–1031.

Mao, Y., Mulvaney, J., Zakaria, S., Yu, T., Morgan, K.M., Allen, S., Basson, M.A., Francis-West, P., Irvine, K.D., 2011. Characterization of a Dchs1 mutant mouse reveals requirements for Dchs1-Fat4 signaling during mammalian development. Development 138, 947–957.

Marin, O., 2003. Cell migration in the Forebrain. Annu. Rev. Neurosci. 25, 441–483.

Marin, O., 2013. Cellular and molecular mechanisms controlling the migration of neocortical interneurons. Eur. J. Neurosci. 1–11.

Marín, O., 2013. Cellular and molecular mechanisms controlling the migration of neocortical interneurons. Eur. J. Neurosci. 38, 2019–2029.

Martens, G., van Loo, K., 2007. Genetic and environmental factors in complex neurodevelopmental disorders. Curr. Genomics 8, 429–444.

Martini, F.J., Valiente, M., Bendito, G.L., Szabó, G., Moya, F., Valdeolmillos, M., Marín, O., 2009. Biased selection of leading process branches mediates chemotaxis during tangential neuronal migration. Development 136, 41–50.

Matsumoto, N., Leventer, R.J., Kuc, J.A., Mewborn, S.K., Dudlicek, L.L., Ramocki, M.B., Pilz, D.T., Mills, P.L., Das, S., Ross, M.E., Ledbetter, D.H., Dobyns, W.B., 2001. Mutation analysis of the DCX gene and genotype/phenotype correlation in subcortical band heterotopia. Eur. J. Hum. Genet. 9, 5–12.

Mattson, S.N., Riley, E.P., 1998. A review of the neurobehavioral deficits in children with fetal alcohol syndrome or prenatal exposure to alcohol. In: Alcoholism: Clinical and Experimental Research. pp. 279–294.

Matys, V., Fricke, E., Geffers, R., Gößling, E., Haubrock, M., Hehl, R., Hornischer, K., Karas, D., Kel, A.E., Kel-Margoulis, O. V., Kloos, D.U., Land, S., Lewicki-Potapov, B., Michael, H., Münch, R., Reuter, I., Rotert, S., Saxel, H., Scheer, M., Thiele, S., Wingender, E., 2003. TRANSFAC®: Transcriptional regulation, from patterns to profiles. Nucleic Acids Res. 31, 374–378.

Matys, V., Kel-Margoulis, O. V., Fricke, E., Liebich, I., Land, S., Barre-Dirrie, A., Reuter, I., Chekmenev, D., Krull, M., Hornischer, K., Voss, N., Stegmaier, P., Lewicki-Potapov, B., Saxel, H., Kel, A.E., Wingender, E., 2006. TRANSFAC and its module TRANSCompel: transcriptional gene regulation in eukaryotes. Nucleic Acids Res. 34, D108–D110.

McCudden, C.R., Hains, M.D., Kimple, R.J., Siderovski, D.P., Willard, F.S., 2005. G-protein signaling: Back to the future. Cell. Mol. Life Sci. 62, 551–577.

McIntire, W.E., 2009. Structural determinants involved in the formation and activation of G protein βγ dimers. NeuroSignals 17, 82–99.

Medina-Cano, D., Ucuncu, E., Nguyen, L.S., Nicouleau, M., Lipecka, J., Bizot, J.C., Thiel, C., Foulquier, F., Lefort, N., Faivre-Sarrailh, C., Colleaux, L., Guerrera, I.C., Cantagrel, V., 2018. High N-glycan multiplicity is critical for neuronal adhesion and sensitizes the developing cerebellum to N-glycosylation defect. Elife 7, 1–27.

Megraw, T.L., Sharkey, J.T., Nowakowski, R.S., 2011. Cdk5rap2 exposes the centrosomal root of microcephaly syndromes. Trends Cell Biol. 21, 470–480.

Mercuri, E., Messina, S., Bruno, C., Mora, M., Pegoraro, E., Comi, G.P., D'Amico, A., Aiello, C., Biancheri, R., Berardinelli, A., Boffi, P., Cassandrini, D., Laverda, A., Moggio, M., Morandi, L., Moroni, I., Pane, M., Pezzani, R., Pichiecchio, A., Pini, A., Minetti, C., Mongini, T., Mottarelli, E., Ricci, E., Ruggieri, A., Saredi, S., Scuderi, C., Tessa, A., Toscano, A., Tortorella, G., Trevisan, C.P., Uggetti, C., Vasco, G., Santorelli, F.M., Bertini, E., 2009. Congenital muscular dystrophies with defective glycosylation of dystroglycan: A population study. Neurology 72, 1802–1809.

Mirzaa, G.M., Campbell, C.D., Solovieff, N., Goold, C.P., Jansen, L.A., Menon, S., Timms, A.E., Conti, V., Biag, J.D., Olds, C., Boyle, E.A., Collins, S., Ishak, G., Poliachik, S.L., Girisha, K.M., Yeung, K.S., Chung, B.H.Y., Rahikkala, E., Gunter, S.A., McDaniel, S.S., Macmurdo, C.F., Bernstein, J.A., Martin, B., Leary, R.J., Mahan, S., Liu, S., Weaver, M., Dorschner, M.O., Jhangiani, S., Muzny, D.M., Boerwinkle, E., Gibbs, R.A., Lupski, J.R., Shendure, J., Saneto, R.P., Novotny, E.J., Wilson, C.J., Sellers, W.R., Morrissey, M.P., Hevner, R.F., Ojemann, J.G., Guerrini, R., Murphy, L.O., Winckler, W., Dobyns, W.B., 2016. Association of MTOR mutations with developmental brain disorders, including megalencephaly, focal cortical dysplasia, and pigmentary mosaicism. JAMA Neurol. 73, 836–845.

Miyata, T., Kawaguchi, A., Okano, H., Ogawa, M., 2001. Asymmetric inheritance of radial glial fibers by cortical neurons. Neuron 31, 727–741.

Miyata, T., Kawaguchi, A., Saito, K., Kawano, M., Muto, T., Ogawa, M., 2004. Asymmetric production of surface-dividing and non-surface-dividing cortical progenitor cells. Development 131, 3133–3145.

Molyneaux, B.J., Arlotta, P., Menezes, J.R.L., Macklis, J.D., 2007. Neuronal subtype specification in the cerebral cortex. Nat. Rev. Neurosci. 8, 427–37.

Moon, A.M., Stauffer, A.M., Schwindinger, W.F., Sheridan, K., Firment, A., Robishaw, J.D., 2014. Disruption of G-Protein y5 subtype causes embryonic lethality in mice. PLoS One 9, e90970.

Moores, C.A., Perderiset, M., Francis, F., Chelly, J., Houdusse, A., Milligan, R.A., 2004. Mechanism of microtubule stabilization by doublecortin. Mol. Cell 14, 833–839.

Mora-Bermúdez, F., Badsha, F., Kanton, S., Camp, J.G., Vernot, B., Köhler, K., Voigt, B., Okita, K., Maricic, T., He, Z., Lachmann, R., Pääbo, S., Treutlein, B., Huttner, W.B., Musacchio, A., 2016. Differences and similarities between human and chimpanzee neural progenitors during cerebral cortex development. Elife 5, 1–24.

Mori, N., Kuwamura, M., Tanaka, N., Hirano, R., Nabe, M., Ibuki, M., Yamate, J., 2012. Ccdc85c encoding a protein at apical junctions of radial glia is disrupted in hemorrhagic hydrocephalus (hhy) mice. Am. J. Pathol. 180, 314–327.

Morishita, R., Shinohara, H., Ueda, H., Kato, K., Asano, T., 1999. High expression of the gamma5 isoform of G protein in neuroepithelial cells and its replacement of the gamma2 isoform during neuronal differentiation in the rat brain. J. Neurochem. 73, 2369–74.

Mormone, E., D'sousa, S., Alexeeva, V., Bederson, M.M., Germano, I.M., 2014. "Footprint-Free" human induced pluripotent stem cell-derived astrocytes for in vivo cell-based therapy. Stem Cells Dev. 23, 2626–2636.

Morris, N.R., Efimov, V.P., Xiang, X., 1998. Nuclear migration, nucleokinesis and lissencephaly. Trends Cell Biol. 8, 467–470.

Muguruma, K., Nishiyama, A., Kawakami, H., Hashimoto, K., Sasai, Y., 2015. Self-Organization of Polarized Cerebellar Tissue in 3D Culture of Human Pluripotent Stem Cells. Cell Rep 10, 537–550.

Mulley, J.C., Iona, X., Hodgson, B., Heron, S.E., Berkovic, S.F., Scheffer, I.E., Dibbens, L.M., 2011. The role of seizure-related SEZ6 as a susceptibility gene in febrile seizures. Neurol. Res. Int. 2011, 1–4.

Nadarajah, B., Brunstrom, J.E., Grutzendler, J., Wong, R.O.L., Pearlman, A.L., 2001. Two modes of radial migration in early development of the cerebral cortex. Nat. Neurosci. 4, 143–150.

Nadarajah, B., Parnavelas, J.G., 2002. Modes of neuronal migration in the developing cerebral cortex. Nat. Rev. Neurosci. 3, 423–432.

Nakahashi, M., Sato, N., Yagishita, A., Ota, M., Saito, Y., Sugai, K., Sasaki, M., Natsume, J., Tsushima, Y., Amanuma, M., Endo, K., 2009. Clinical and imaging characteristics of localized megalencephaly: A retrospective comparison of diffuse hemimegalencephaly and multilobar cortical dysplasia. Neuroradiology 51, 821–830.

Namba, T., Dóczi, J., Pinson, A., Xing, L., Kalebic, N., Wilsch-Bräuninger, M., Long, K.R., Vaid, S., Lauer, J., Bogdanova, A., Borgonovo, B., Shevchenko, A., Keller, P., Drechsel, D., Kurzchalia, T., Wimberger, P., Chinopoulos, C., Huttner, W.B., 2020. Human-Specific ARHGAP11B Acts in Mitochondria to Expand Neocortical Progenitors by Glutaminolysis. Neuron 105, 867-881.e9.

Neubauer, S., Hublin, J.J., Gunz, P., 2018. The evolution of modern human brain shape. Sci. Adv. 4, eaao5961.

Neuhann, T.M., Müller, D., Hackmann, K., Holzinger, S., Schrock, E., Di Donato, N., 2012. A further patient with van Maldergem syndrome. Eur. J. Med. Genet. 55, 423–428.

Nicholas, A.K., Swanson, E.A., Cox, J.J., Karbani, G., Malik, S., Springell, K., Hampshire, D., Ahmed, M., Bond, J., Di Benedetto, D., Fichera, M., Romano, C., Dobyns, W.B., Woods, C.G., 2009. The molecular landscape of ASPM mutations in primary microcephaly. J. Med. Genet. 46, 249–253.

Nikola S. Dzhindzhev, Quan D. Yu, Kipp Weiskopf, George Tzolovsky, Ines Cunha-Ferreira, Maria Riparbelli, Ana Rodrigues-Martins, Monica Bettencourt-Dias2, Giuliano Callaini, David M. Glover, 2010. Asterless is a scaffold for the onset of centriole assembly. Nature 467, 714–721.

Nobrega-Pereira, S., Marin, O., 2009. Transcriptional Control of Neuronal Migration in the Developing Mouse Brain. Cereb. Cortex 19, 107–113.

Noctor, S.C., Martinez-Cerdeño, V., Ivic, L., Kriegstein, A.R., 2004. Cortical neurons arise in symmetric and asymmetric division zones and migrate through specific phases. Nat. Neurosci. 7, 136–144.

Nonaka-Kinoshita, M., Reillo, I., Artegiani, B., Ángeles Martínez-Martínez, M., Nelson, M., Borrell, V., Calegari, F., 2013. Regulation of cerebral cortex size and folding by expansion of basal progenitors. EMBO J. 32, 1817–1828.

Nowakowski, T.J., Pollen, A.A., Sandoval-Espinosa, C., Kriegstein, A.R., 2016. Transformation of the Radial Glia Scaffold Demarcates Two Stages of Human Cerebral Cortex Development. Neuron 91, 1219–1227.

Nunes, M.L., Carlini, C.R., Marinowic, D., Neto, F.K., Fiori, H.H., Scotta, M.C., Zanella, P.L.Á., Soder, R.B., Da Costa, J.C., 2016. Microcephaly and Zika virus: A clinical and epidemiological analysis of the current outbreak in Brazil. J. Pediatr. (Rio. J). 92, 230–240.

O'Neill, Adam C, Kyrousi, C., Einsiedler, M., Burtscher, I., Drukker, M., Markie, D.M., Kirk, E.P., Götz, M., Robertson, S.P., Cappello, S., Heinrich, C., Represa, A., Francis, F., 2018. Mob2 insufficiency disrupts neuronal migration in the developing cortex. Front. Cell. Neurosci. 12, 1–13.

O'Neill, Adam C., Kyrousi, C., Klaus, J., Leventer, R.J., Kirk, E.P., Fry, A., Pilz, D.T., Morgan, T., Jenkins, Z.A., Drukker, M., Berkovic, S.F., Scheffer, I.E., Guerrini, R., Markie, D.M., Götz, M., Cappello, S., Robertson, S.P., 2018. A primate-specific isoform of PLEKHG6 regulates neurogenesis and neuronal migration. Cell Rep. 25, 2729–2741.

Okamoto, N., Kohmoto, T., Naruto, T., Masuda, K., Imoto, I., 2018. Primary microcephaly caused by novel compound heterozygous mutations in ASPM. Hum. Genome Var. 5, 1–3.

Okita, K., Matsumura, Y., Sato, Y., Okada, A., Morizane, A., Okamoto, S., Hong, H., Nakagawa, M., Tanabe, K., Tezuka, K.I., Shibata, T., Kunisada, T., Takahashi, M., Takahashi, J., Saji, H., Yamanaka, S., 2011. A more efficient method to generate integration-free human iPS cells. Nat. Methods 8, 409–412.

Okonechnikov, K., Golosova, O., Fursov, M., Varlamov, A., Vaskin, Y., Efremov, I., German Grehov, O.G., Kandrov, D., Rasputin, K., Syabro, M., Tleukenov, T., 2012. Unipro UGENE: A unified bioinformatics toolkit. Bioinformatics 28, 1166–1167.

Oliveira Melo, A.S., Malinger, G., Ximenes, R., Szejnfeld, P.O., Alves Sampaio, S., Bispo De Filippis, A.M., 2016. Zika virus intrauterine infection causes fetal brain abnormality and microcephaly: Tip of the iceberg? Ultrasound Obstet. Gynecol. 47, 6–7.

Ortega, J.A., Sirois, C.L., Memi, F., Glidden, N., Zecevic, N., 2017. Oxygen levels regulate the development of human cortical radial glia cells. Cereb. Cortex 27, 3736–3751.

Otani, T., Marchetto, M.C., Gage, F.H., Simons, B.D., Livesey, F.J., 2016. 2D and 3D stem cell models of primate cortical development identify species-specific differences in progenitor behavior contributing to brain size. Cell Stem Cell 18, 467–480.

Pais, F.S.M., Ruy, P. de C., Oliveira, G., Coimbra, R.S., 2014. Assessing the efficiency of multiple sequence alignment programs. Algorithms Mol. Biol. 9, 1–8.

Palm, T., Bolognin, S., Meiser, J., Nickels, S., Träger, C., Meilenbrock, R.-L., Brockhaus, J., Schreitmüller, M., Missler, M., Schwamborn, J.C., 2015. Rapid and robust generation of long-term self-renewing human neural stem cells with the ability to generate mature astroglia OPEN. Nat. Publ. Gr. 5, 1–16.

Pang, T., Atefy, R., Sheen, V., 2008. Malformations of cortical development. Neurologist 14, 181–191.

Parnavelas, J.G., 2000. The origin and migration of cortical neurones: New vistas. Trends Neurosci. 23, 126–131.

Parrini, E., Ramazzotti, A., Dobyns, W.B., Mei, D., Moro, F., Veggiotti, P., Marini, C., Brilstra, E.H., Bernardina, B.D., Goodwin, L., Bodell, A., Jones, M.C., Nangeroni, M., Palmeri, S., Said, E., Sander, J.W., Striano, P., Takahashi, Y., Van Maldergem, L., Leonardi, G., Wright, M., Walsh, C.A., Guerrini, R., 2006. Periventricular heterotopia: Phenotypic heterogeneity and correlation with Filamin a mutations. Brain 129, 1892–1906.

Pasca, A.M., Sloan, S.A., Clarke, L.E., Tian, Y., Makinson, C.D., Huber, N., Kim, C.H., Park, J.Y., O'Rourke, N.A., Nguyen, K.D., Smith, S.J., Huguenard, J.R., Geschwind, D.H., Barres, B.A., Pasca, S.P., 2015. Functional cortical neurons and astrocytes from human pluripotent stem cells in 3D culture. Nat. Methods 12, 671–678.

Pearce, E., Stringer, C., Dunbar, R.I.M., 2013. New insights into differences in brain organization between Neanderthals and anatomically modern humans. Proc. R. Soc. B Biol. Sci. 280, 1–7.

Peñagarikano, O., Abrahams, B.S., Herman, E.I., Winden, K.D., Gdalyahu, A., Dong, H., Sonnenblick, L.I., Gruver, R., Almajano, J., Bragin, A., Golshani, P., Trachtenberg, J.T., Peles, E., Geschwind, D.H., 2011. Absence of CNTNAP2 leads to epilepsy, neuronal migration abnormalities, and core autism-related deficits. Cell 147, 235–246.

Penisson, M., Ladewig, J., Belvindrah, R., Francis, F., 2019. Genes and mechanisms involved in the generation and amplification of basal radial glial cells. Front. Cell. Neurosci. 13, 1–21.

Pereira-Pedro, A.S., Bruner, E., Gunz, P., Neubauer, S., 2020. A morphometric comparison of the parietal lobe in modern humans and Neanderthals. J. Hum. Evol. 142, 1–12.

Pilz, D., 1998. LIS1 and XLIS (DCX) mutations cause most classical lissencephaly, but different patterns of malformation. Hum. Mol. Genet. 7, 2029–2037.

Pilz, G.A., Shitamukai, A., Reillo, I., Pacary, E., Schwausch, J., Stahl, R., Ninkovic, J., Snippert, H.J., Clevers, H., Godinho, L., Guillemot, F., Borrell, V., Matsuzaki, F., Götz, M., 2013. Amplification of progenitors in the mammalian telencephalon includes a new radial glial cell type. Nat. Commun. 4, 1–11.

Pimplikar, S.W., Simons, K., 1993. Role of heterotrimeric G proteins in polarized membrane transport. In: Journal of Cell Science. pp. 27–32.

Pinson, A., Namba, T., Huttner, W.B., 2019. Malformations of human neocortex in development – Their progenitor cell basis and experimental model systems. Front. Cell. Neurosci. 13, 1–13.

Pirozzi, F., Nelson, B., Mirzaa, G.M., 2018. From microcephaly to megalencephaly: determinants of brain size. Dialogues Clin. Neurosci. 20, 267–282.

Polioudakis, D., de la Torre-Ubieta, L., Langerman, J., Elkins, A.G., Shi, X., Stein, J.L., Vuong, C.K., Nichterwitz, S., Gevorgian, M., Opland, C.K., Lu, D., Connell, W., Ruzzo, E.K., Lowe, J.K., Hadzic, T., Hinz, F.I., Sabri, S., Lowry, W.E., Gerstein, M.B., Plath, K., Geschwind, D.H., 2019. A Single-Cell Transcriptomic Atlas of Human Neocortical Development during Mid-gestation. Neuron 103, 785-801.e8.

Pollen, A.A., Nowakowski, T.J., Chen, J., Retallack, H., Sandoval-espinosa, C., Nicholas, C.R., Shuga, J., Liu, S.J., Oldham, C., Diaz, A., Lim, D.A., Leyrat, A.A., West, J.A., Arnold, R., 2016. Molecular identity of human outer radial glia during cortical development. Cell 163, 55–67.

Pollen, A.A., Nowakowski, T.J., Chen, J., Retallack, H., Sandoval-Espinosa, C., Nicholas, C.R., Shuga, J., Liu, S.J., Oldham, M.C., Diaz, A., Lim, D.A., Leyrat, A.A., West, J.A., Kriegstein, A.R., 2015. Molecular identity of human outer radial glia during cortical development. Cell 163, 55–67.

Ponce de León, M.S., Bienvenu, T., Akazawa, T., Zollikofer, C.P.E., 2016. Brain development is similar in Neanderthals and modern humans. Curr. Biol. 26, R665–R666.

Ponce De León, M.S., Golovanova, L., Doronichev, V., Romanova, G., Akazawa, T., Kondo, O., Ishida, H., Zollikofer, C.P.E., 2008. Neanderthal brain size at birth provides insights into the evolution of human life history. PNAS 105, 13764–13768.

Prüfer, K., Racimo, F., Patterson, N., Jay, F., Sankararaman, S., Sawyer, S., Heinze, A., Renaud, G., Sudmant, P.H., De Filippo, C., Li, H., Mallick, S., Dannemann, M., Fu, Q., Kircher, M., Kuhlwilm, M., Lachmann, M., Meyer, M., Ongyerth, M., Siebauer, M., Theunert, C., Tandon, A., Moorjani, P., Pickrell, J., Mullikin, J.C., Vohr, S.H., Green, R.E., Hellmann, I., Johnson, P.L.F., Blanche, H., Cann, H., Kitzman, J.O., Shendure, J., Eichler, E.E., Lein, E.S., Bakken, T.E., Golovanova, L. V., Doronichev, V.B., Shunkov, M. V., Derevianko, A.P., Viola, B., Slatkin, M., Reich, D., Kelso, J., Pääbo, S., 2014. The complete genome sequence of a Neanderthal from the Altai Mountains. Nature 505, 43–49.

Qian, X., Jacob, F., Song, M.M., Nguyen, H.N., Song, H., Ming, G.L., 2018. Generation of human brain region–specific organoids using a miniaturized spinning bioreactor. Nat. Protoc. 13, 565–580.

Qian, X., Nguyen, H.N., Song, M.M., Hadiono, C., Ogden, S.C., Hammack, C., Yao, B., Hamersky, G.R., Jacob, F., Zhong, C., Yoon, K.J., Jeang, W., Lin, L., Li, Y., Thakor, J., Berg, D.A., Zhang, C., Kang, E., Chickering, M., Nauen, D., Ho, C.Y., Wen, Z., Christian, K.M., Shi, P.Y., Maher, B.J., Wu, H., Jin, P., Tang, H., Song, H., Ming, G.L., 2016. Brain-Region-Specific Organoids Using Mini-bioreactors for Modeling ZIKV Exposure. Cell 165, 1238–1254.

Quadrato, G., Nguyen, T., Macosko, E.Z., Sherwood, J.L., Yang, S.M., Berger, D.R., Maria, N., Scholvin, J., Goldman, M., Kinney, J.P., Boyden, E.S., Lichtman, J.W., Williams, Z.M., McCarroll, S.A., Arlotta, P., 2017. Cell diversity and network dynamics in photosensitive human brain organoids. Nature 545, 48–53.

Radmanesh, F., Caglayan, A.O., Silhavy, J.L., Yilmaz, C., Cantagrel, V., Omar, T., Rosti, B., Kaymakcalan, H., Gabriel, S., Li, M., Šestan, N., Bilguvar, K., Dobyns, W.B., Zaki, M.S., Gunel, M., Gleeson, J.G., 2013. Mutations in LAMB1 cause cobblestone brain malformation without muscular or ocular abnormalities. Am. J. Hum. Genet. 92, 468–474.

Rakic, P., 1971. Guidance of neurons migrating to the fetal monkey neocortex. Brain Res. 33, 471–476.

Rakic, P., 1972. Mode of cell migration to the superficial layers of fetal monkey neocortex. J. Comp. Neurol. 145, 61–83.

Rakic, P., 1974. Neurons in Rhesus Monkey visual cortex: Systematic relation between time of origin and eventual disposition. Science 183, 425–427.

Rakic, P., 1978. Neuronal migration and contact guidance in the primate telencephalon. Postgrad. Med. J. 54, 25–40.

Rakic, P., 1995. A small step for the cell, a giant leap for mankind: a hypothesis of neocortical expansion during evolution. Trends Neurosci. 18, 383–388.

Rakic, P., 2003. Elusive radial glial cells: Historical and evolutionary perspective. Glia 43, 19–32.

Rakic, P., 2009. Evolution of the neocortex: A perspective from developmental biology. Nat. Rev. Neurosci. 10, 724–735.

Ramos, R.L., Bai, J., LoTurco, J.J., 2006. Heterotopia formation in rat but not mouse neocortex after RNA interference knockdown of DCX. Cereb. Cortex 16, 1323–1331.

Ramsköld, D., Luo, S., Wang, Y.C., Li, R., Deng, Q., Faridani, O.R., Daniels, G.A., Khrebtukova, I., Loring, J.F., Laurent, L.C., Schroth, G.P., Sandberg, R., 2012. Full-length mRNA-Seq from single-cell levels of RNA and individual circulating tumor cells. Nat. Biotechnol. 30, 777–782.

Ran, F.A., Hsu, P.D., Wright, J., Agarwala, V., Scott, D.A., Zhang, F., 2013. Genome engineering using the CRISPR-Cas9 system. Nat. Protoc. 8, 2281–2308.

Reillo, I., De Juan Romero, C., García-Cabezas, M.Á., Borrell, V., 2011. A Role for intermediate radial glia in the tangential expansion of the mammalian cerebral cortex. Cereb. Cortex 21, 1674–1694.

Riesenberg, S., Maricic, T., 2018. Targeting repair pathways with small molecules increases precise genome editing in pluripotent stem cells. Nat. Commun. 9, 1–9.

Rivière, J., Mirzaa, G.M., Roak, B.J.O., Beddaoui, M., Conway, R.L., St-onge, J., Schwartzentruber, J.A., Karen, W., Nikkel, S.M., Worthylake, T., Sullivan, C.T., Ward, T.R., Butler, H.E., Kramer, N.A., Albrecht, B., Armour, C.M., 2013. De novo germline and postzygotic mutations in AKT3, PIK3R2 and PIK3CA cause a spectrum of related megalencephaly syndromes. Nat. Genet. 44, 934–940.

Rock, R., Schrauth, S., Gessler, M., 2005. Expression of mouse dchs1, fjx1, and fat-j suggests conservation of the planar cell polarity pathway identified in Drosophila. Dev. Dyn. 234, 747–755.

Rodenas-Cuadrado, P., Ho, J., Vernes, S.C., 2014. Shining a light on CNTNAP2: Complex functions to complex disorders. Eur. J. Hum. Genet. 22, 171–178.

Rolfe, D.F.S., Brown, G.C., 1997. Cellular energy utilization and molecular origin of standard metabolic rate in mammals. Physiol. Rev. 77, 731–758.

Romero, D.M., Bahi-Buisson, N., Francis, F., 2018. Genetics and mechanisms leading to human cortical malformations. Semin. Cell Dev. Biol. 76, 33–75.

Rosas, A., Ríos, L., Estalrrich, A., Liversidge, H., García-Tabernero, A., Huguet, R., Cardoso, H., Bastir, M., Lalueza-Fox, C., De La Rasilla, M., Dean, C., 2017. The growth pattern of Neandertals, reconstructed from a juvenile skeleton from El Sidrón (Spain). Science 357, 1282–1287.

Roth, G., Dicke, U., 2005. Evolution of the brain and intelligence. Trends Cogn. Sci. 9, 250–257.

Roybon, L., Lamas, N.J., Garcia, A.D., Yang, E.J., Sattler, R., Lewis, V.J., Kim, Y.A., Kachel, C.A., Rothstein, J.D., Przedborski, S., Wichterle, H., Henderson, C.E., 2013. Human stem cell-derived spinal cord astrocytes with defined mature or reactive phenotypes. Cell Rp 4, 1035–1048.

Saburi, S., Hester, I., Fischer, E., Pontoglio, M., Eremina, V., Gessler, M., Quaggin, S.E., Harrison, R., Mount, R., McNeill, H., 2008. Loss of Fat4 disrupts PCP signaling and oriented cell division and leads to cystic kidney disease. Nat. Genet. 40, 1010–1015.

Sakaguchi, H., Kadoshima, T., Soen, M., Narii, N., Ishida, Y., Ohgushi, M., Takahashi, J., Eiraku, M., Sasai, Y., 2015. Generation of functional hippocampal neurons from self-organizing human embryonic stem cell-derived dorsomedial telencephalic tissue. Nat. Commun. 6, 1–11.

Sasaki, E., Suemizu, H., Shimada, A., Hanazawa, K., Oiwa, R., Kamioka, M., Tomioka, I., Sotomaru, Y., Hirakawa, R., Eto, T., Shiozawa, S., Maeda, T., Ito, M., Ito, R., Kito, C., Yagihashi, C., Kawai, K., Miyoshi, H., Tanioka, Y., Tamaoki, N., Habu, S., Okano, H., Nomura, T., 2009. Generation of transgenic non-human primates with germline transmission. Nature 459, 523–527.

Sauer, F.C., 1935. Mitosis in the neural tube. J. Comp. Neurol. 62, 377–405.

Scherer, C., Schuele, S., Minotti, L., Chabardes, S., Hoffmann, D., Kahane, P., 2005. Intrinsic epileptogenicity of an isolated periventricular nodular heterotopia. Neurology 65, 495–496.

Schindelin, J., Arganda-Carreras, I., Frise, E., Kaynig, V., Longair, M., Pietzsch, T., Preibisch, S., Rueden, C., Saalfeld, S., Schmid, B., Tinevez, J.Y., White, D.J., Hartenstein, V., Eliceiri, K., Tomancak, P., Cardona, A., 2012. Fiji: An open-source platform for biological-image analysis. Nat. Methods 9, 676–682.

Schmid, M.-T., Weinandy, F., Wilsch-BrÃ¤uninger, M., Huttner, W.B., Cappello, S., GÃ¶tz, M., 2014. The role of Î±-E-catenin in cerebral cortex development: radial glia specific effect on neuronal migration. Front. Cell. Neurosci. 8, 1–10.

Schwindinger, W.F., Giger, K.E., Betz, K.S., Stauffer, A.M., Sunderlin, E.M., Sim-Selley, L.J., Selley, D.E., Bronson, S.K., Robishaw, J.D., 2004. Mice with deficiency of G protein 3 are lean and have seizures. Mol. Cell. Epilepsy 24, 7758–7768.

Scott, H., Panin, V.M., 2014. N-Glycosylation in regulation of the nervous system. In: Advances in Neurobiology. NIH Public Access, pp. 367–394.

Sekine, K., Honda, T., Kawauchi, T., Kubo, K.-I., Nakajima, K., 2011. The outermost region of the developing cortical plate is crucial for both the switch of the radial migration mode and the Dab1-dependent “Inside-Out” lamination in the neocortex. J. Neurosci. 31, 9426–9439.

Shaltouki, A., Peng, J., Liu, Q., Rao, M.S., Zeng, X., 2013. Efficient generation of astrocytes from human pluripotent stem cells in defined conditions. Stem Cells 31, 941–952.

Shao, Q., Herrlinger, S., Yang, S.L., Lai, F., Moore, J.M., Brindley, M.A., Chen, J.F., 2016. Zika virus infection disrupts neurovascular development and results in postnatal microcephaly with brain damage. Development 143, 4127–4136.

Sharma, P., Mesci, P., Carromeu, C., McClatchy, D.R., Schiapparelli, L., Yates, J.R., Muotri, A.R., Cline, H.T., 2019. Exosomes regulate neurogenesis and circuit assembly. PNAS 116, 16086–16094.

Sheen, V.L., Ganesh, V.S., Topcu, M., Sebire, G., Bodell, A., Hill, R.S., Grant, P.E., Shugart, Y.Y., Imitola, J., Khoury, S.J., Guerrini, R., Walsh, C.A., 2004. Mutations in ARFGEF2 implicate vesicle trafficking in neural progenitor proliferation and migration in the human cerebral cortex. Nat. Genet. 36, 69–76.

Shi, L., Luo, X., Jiang, J., Chen, Y., Liu, C., Hu, T., Li, M., Lin, Q., Li, Y., Huang, J., Wang, H., Niu, Y., Shi, Y., Styner, M., Wang, J., Lu, Y., Sun, X., Yu, H., Ji, W., Su, B., 2019. Transgenic rhesus monkeys carrying the human MCPH1 gene copies show human-like neoteny of brain development. Natl. Sci. Rev. 6, 480–493.

Shi, Y., Kirwan, P., Livesey, F.J., 2012a. Directed differentiation of human pluripotent stem cells to cerebral cortex neurons and neural networks. Nat. Protoc. 7, 1836–1846.

Shi, Y., Kirwan, P., Smith, J., Robinson, H.P.C., Livesey, F.J., 2012b. Human cerebral cortex development from pluripotent stem cells to functional excitatory synapses. Nat. Neurosci. 15, 477–486.

Shitamukai, A., Konno, D., Matsuzaki, F., 2011. Oblique radial glial divisions in the developing mouse neocortex induce self-renewing progenitors outside the germinal zone that resemble primate outer subventricular zone progenitors. J. Neurosci. 31, 3683–3695.

Silbereis, J.C., Pochareddy, S., Zhu, Y., Li, M., Sestan, N., 2016. The cellular and molecular landscapes of the developing human central nervous system. Neuron 89, 248–268.

Sing, A., Tsatskis, Y., Fabian, L., Hester, I., Rosenfeld, R., Serricchio, M., Yau, N., Shanbhag, R., Jurisicova, A., Brill, J.A. a, McQuibban, G.A.A., Bietenhader, M., Shanbhag, R., Jurisicova, A., Brill, J.A. a, McQuibban, G.A.A., McNeill, H., 2014. The atypical cadherin Fat directly regulates mitochondrial function and metabolic state. Cell 158, 1293–1308.

Sloan, S.A., Andersen, J., Paşca, A.M., Birey, F., Paşca, S.P., 2018. Generation and assembly of human brain region–specific three-dimensional cultures. Nat. Protoc. 13, 2062–2085.

Sloan, S.A., Darmanis, S., Huber, N., Khan, T., Birey, F., Caneda, C., Reimer, R., Quake, S.R., Barres, B.A., Paşca, S.P., 2017. Human astrocyte maturation captured in 3D cerebral cortical spheroids derived from pluripotent stem cells. Neuron 95, 779–790.

Smart, I.H.M., 2002. Unique Morphological Features of the Proliferative Zones and Postmitotic Compartments of the Neural Epithelium Giving Rise to Striate and Extrastriate Cortex in the Monkey. Cereb. Cortex 12, 37–53.

Smrcka, A. V, 2008. G protein βγ subunits: Central mediators of G protein-coupled receptor signaling. Cell. Mol. Life Sci. 65, 2191–2214.

Sofie, L., Bak, L.K., Waagepetersen, H.S., Schousboe, A., Michael D., N., 2012. Primary cultures of astrocytes: Their value in understanding astrocytes in health and disease. Physiol. Behav. 37, 2569–2588.

Spiegel, A.M., Weinstein, L.S., 2004. Inherited diseases involving G proteins and G protein–coupled receptors. Annu. Rev. Med. 55, 27–39.

Staerk, J., Dawlaty, M.M., Gao, Q., Maetzel, D., Hanna, J., Sommer, C.A., Mostoslavsky, G., Jaenisch, R., 2010. Reprogramming of human peripheral blood cells to induced pluripotent stem cells. Cell Stem Cell 7, 20–24.

Stafstrom, C.E., Carmant, L., 2015. Seizures and epilepsy: An overview for neuroscientists. Cold Spring Harb. Perspect. Biol. 7, 1–19.

Stagni, F., Giacomini, A., Guidi, S., Ciani, E., Bartesaghi, R., 2015. Timing of therapies for Down syndrome: the sooner, the better. Front. Behav. Neurosci. 9, 1–18.

Stiles, J., Jernigan, T.L., 2010. The basics of brain development. Neuropsychol. Rev. 20, 327–348.

Stutterd, C.A., Leventer, R.J., 2014. Polymicrogyria: A common and heterogeneous malformation of cortical development. Am. J. Med. Genet. Part C Semin. Med. Genet. 166, 227–239.

Sultan, K.T., Brown, K.N., Shi, S.H., 2013. Production and organization of neocortical interneurons. Front. Cell. Neurosci. 7, 1–14.

Suzuki, I.K., Gacquer, D., Van Heurck, R., Kumar, D., Wojno, M., Bilheu, A., Herpoel, A., Lambert, N., Cheron, J., Polleux, F., Detours, V., Vanderhaeghen, P., 2018. Human-Specific NOTCH2NL Genes Expand Cortical Neurogenesis through Delta/Notch Regulation. Cell 173, 1370–1384.

Szklarczyk, D., Morris, J.H., Cook, H., Kuhn, M., Wyder, S., Simonovic, M., Santos, A., Doncheva, N.T., Roth, A., Jensen, L.J., Von Mering, C., 2017. The STRING database in 2017: quality-controlled protein-protein association networks, made broadly accessible. Nucleic Acids Res. 45, D362–D368.

Tabata, H., Nakajima, K., 2003. Multipolar migration: The third mode of radial neuronal migration in the developing cerebral cortex. J. Neurosci. 23, 9996–10001.

Takahashi, K., Yamanaka, S., 2006. Induction of pluripotent stem cells from mouse embryonic and adult fibroblast cultures by defined factors. Cell 126, 663–676.

Takahashi, T., Nowakowski, R.S., Caviness, V.S., 1996. The leaving or Q fraction of the murine cerebral proliferative epithelium: A general model of neocortical neuronogenesis. J. Neurosci. 16, 6183–6196.

Tanaka, T., Serneo, F.F., Higgins, C., Gambello, M.J., Wynshaw-Boris, A., Gleeson, J.G., 2004. Lis1 and doublecortin function with dynein to mediate coupling of the nucleus to the centrosome in neuronal migration. J. Cell Biol. 165, 709–721.

Tang, C.J., Lin, S.Y., Hsu, W.B., Lin, Y.N., Wu, C.T., Lin, Y.C., Chang, C.W., Wu, K.S., Tang, T.K., 2011. The human microcephaly protein STIL interacts with CPAP and is required for procentriole formation. Cell Rep. 30, 4790–4804.

Tang, W.-J., Gilman G., A., 1991. Type-Specific Regulation of Adenylyl Cyclase by G Protein βγ Subunits. Science 254, 1500–1503.

Tassi, L., Colombo, N., Cossu, M., Mai, R., Francione, S., Lo Russo, G., Galli, C., Bramerio, M., Battaglia, G., Garbelli, R., Meroni, A., Spreafico, R., 2005. Electroclinical, MRI and neuropathological study of 10 patients with nodular heterotopia, with surgical outcomes. Brain 128, 321–337.

Taverna, E., Huttner, W.B., 2010. Neural progenitor nuclei IN motion. Neuron 67, 906–914.

Taverna, E., Otz, M., Huttner, W.B., 2014. The cell biology of neurogenesis: Toward an understanding of the development and evolution of the neocortex. Annu. Rev. Cell Dev. Biol 30, 465–502.

Telley, L., Agirman, G., Prados, J., Amberg, N., Fièvre, S., Oberst, P., Bartolini, G., Vitali, I., Cadilhac, C., Hippenmeyer, S., Nguyen, L., Dayer, A., Jabaudon, D., 2019. Temporal patterning of apical progenitors and their daughter neurons in the developing neocortex. Science 364, 1–7.

Thompson, B.L., Levitt, P., Stanwood, G.D., 2009. Prenatal exposure to drugs: effects on brain development and implications for policy and education. Nat. Rev. Neurosci. 10, 303–312.

Thornton, G.K., Woods, C.G., 2009. Primary microcephaly: do all roads lead to Rome? Trends Genet. 25, 501–510.

Tiveron, M.-C., Beurrier, C., Céni, C., Andriambao, N., Combes, A., Koehl, M., Maurice, N., Gatti, E., Abrous, D.N., Kerkerian-Le Goff, L., Pierre, P., Cremer, H., 2016. LAMP5 fine-tunes GABAergic synaptic transmission in defined circuits of the mouse brain. PLoS One 11, 1–19.

Toma, K., Wang, T.C., Hanashima, C., 2016. Encoding and decoding time in neural development. Dev. Growth Differ. 58, 59–72.

Trujillo, C.A., Gao, R., Negraes, P.D., Gu, J., Buchanan, J., Preissl, S., Wang, A., Wu, W., Haddad, G.G., Chaim, I.A., Domissy, A., Vandenberghe, M., Devor, A., Yeo, G.W., Voytek, B., Muotri, A.R., 2019. Complex oscillatory waves emerging from cortical organoids model early human brain network development. Cell Stem Cell 25, 558–569.

Tsai, J.W., Chen, Y., Kriegstein, A.R., Vallee, R.B., 2005. LIS1 RNA interference blocks neural stem cell division, morphogenesis, and motility at multiple stages. J. Cell Biol. 170, 935–945.

Tyler, W.A., Haydar, T.F., 2013. Multiplex genetic fate mapping reveals a novel route of neocortical neurogenesis, which is altered in the Ts65Dn mouse model of down syndrome. J. Neurosci. 158, 5106–5119.

Van den Ameele, J., Tiberi, L., Vanderhaeghen, P., Espuny-Camacho, I., 2014. Thinking out of the dish: what to learn about cortical development using pluripotent stem cells. Trends Neurosci. 37, 334–342.

Van Den Pol, A.N., Mao, G., Yang, Y., Ornaghi, S., Davis, J.N., 2017. Zika virus targeting in the developing brain. J. Neurosci. 37, 2161–2175.

Van Reeuwijk, J., Janssen, M., Van Den Elzen, C., Beltran-Valero De Bernabé, D., Sabatelli, P., Merlini, L., Boon, M., Scheffer, H., Brockington, M., Muntoni, F., Huynen, M.A., Verrips, A., Walsh, C.A., Barth, P.G., Brunner, H.G., Van Bokhoven, H., 2005. POMT2 mutations cause α-dystroglycan hypoglycosylation and Walker-Warburg syndrome. J. Med. Genet. 42, 907–912.

Vasilev, D.S., Dubrovskaya, N.M., Tumanova, N.L., Zhuravin, I.A., 2016. Prenatal hypoxia in different periods of embryogenesis differentially affects cell migration, neuronal plasticity, and rat behavior in postnatal ontogenesis. Front. Neurosci. 10, 1–11.

Velasco, S., Kedaigle, A.J., Simmons, S.K., Nash, A., Rocha, M., Quadrato, G., Paulsen, B., Nguyen, L., Adiconis, X., Regev, A., Levin, J.Z., Arlotta, P., 2019. Individual brain organoids reproducibly form cell diversity of the human cerebral cortex. Nature 570, 523–527.

Vidovic, M., Chen, M.M., Lu, Q.Y., Kalloniatis, K.F., Martin, B.M., Tan, A.H.Y., Lynch, C., Croaker, G.D.H., Cass, D.T., Song, Z.M., 2008. Deficiency in endothelin receptor B reduces proliferation of neuronal progenitors and increases apoptosis in postnatal rat cerebellum. Cell. Mol. Neurobiol. 28, 1129–1138.

Vierbuchen, T., Ostermeier, A., Pang, Z.P., Kokubu, Y., Südhof, T.C., Wernig, M., 2010. Direct conversion of fibroblasts to functional neurons by defined factors. Nature 463, 1035–1041.

Vuillaumier-Barrot, S., Bouchet-Seraphin, C., Chelbi, M., Eude-Caye, A., Charluteau, E., Besson, C., Quentin, S., Devisme, L., Le Bizec, C., Landrieu, P., Goldenberg, A., Maincent, K., Loget, P., Boute, O., Gilbert-Dussardier, B., Encha-Razavi, F., Gonzales, M., Grandchamp, B., Seta, N., 2011. Intragenic rearrangements in LARGE and POMGNT1 genes in severe dystroglycanopathies. Neuromuscul. Disord. 21, 782–790.

Wang, P., Mokhtari, R., Pedrosa, E., Kirschenbaum, M., Bayrak, C., Zheng, D., Lachman, H.M., 2017. CRISPR/Cas9-mediated heterozygous knockout of the autism gene CHD8 and characterization of its transcriptional networks in cerebral organoids derived from iPS cells. Mol. Autism 8, 1–17.

Wang, X., Tsai, J.-W., LaMonica, B., Kriegstein, A.R., 2011. A new subtype of progenitor cell in the mouse embryonic neocortex. Nat. Neurosci. 14, 555–561.

Wass, T.S., Persutte, W.H., Hobbins, J.C., 2001. The impact of prenatal alcohol exposure on frontal cortex development in utero. Am. J. Obstet. Gynecol. 185, 737–742.

Watanabe, M., Buth, J.E., Vishlaghi, N., de la Torre-Ubieta, L., Taxisdis, J., 2017. Self-organized cerebral organoids with human specific features predict effective drugs to combat Zika virus infection. Cell Rep. 21, 517–532.

Wedegaertner, P.B., Wilson, P.T., Bourne, H.R., 1995. Lipid modifications of trimeric G proteins. J. Cell Biol. 270, 503–506.

Wichterle, H., Turnbull, D.H., Nery, S., Fishell, G., Alvarez-Buylla, A., 2001. In utero fate mapping reveals distinct migratory pathways and fates of neurons born in the mammalian basal forebrain. Development 128, 3759–3771.

Wilsch-Bräuninger, M., Florio, M., Huttner, W.B., 2016. Neocortex expansion in development and evolution - from cell biology to single genes. Curr. Opin. Neurobiol. 39, 122–132.

Wodarz, A., Huttner, W.B., 2003. Asymmetric cell division during neurogenesis in Drosophila and vertebrates. Mech. Dev. 120, 1297–1309.

Wong, M., 2011. Epilepsy in a dish: An in vitro model of epileptogenesis. Epilepsy Curr. 11, 153–154.

Wynshaw-Boris, A., Pramparo, T., Ha Youn, Y., Hirotsune, S., 2010. Lissencephaly: Mechanistic insights from animal models and potential therapeutic strategies. Semin. Cell Dev. Biol. 21, 823–830.

Yamamoto, H., Maruo, T., Majima, T., Ishizaki, H., Tanaka-Okamoto, M., Miyoshi, J., Mandai, K., Takai, Y., 2013. Genetic deletion of afadin causes hydrocephalus by destruction of adherens junctions in radial glial and ependymal cells in the midbrain. PLoS One 8, e80356.

Yamamoto, T., Kato, Y., Kawagucki, M., Shibata, N., Kobayashi, M., 2004. Expression and localization of fukutin, POMGnT1, and POMT1 in the central nervous system: Consideration for functions of fukutin. Med. Electron Microsc. 37, 200–207.

Yingling, J., Youn, Y.H., Darling, D., Toyo-oka, K., Pramparo, T., Hirotsune, S., Wynshaw-Boris, A., 2008. Neuroepithelial stem cell proliferation requires LIS1 for precise spindle orientation and symmetric division. Cell 132, 474–486.

Yu, J., Vodyanik, M.A., Smuga-Otto, K., Antosiewicz-Bourget, J., Frane, J.L., Tian, S., Nie, J., Jonsdottir, G.A., Ruotti, V., Stewart, R., Slukvin, I.I., Thomson, J.A., 2007. Induced pluripotent stem cell lines derived from human somatic cells. Science 318, 1917–1920.

Zhang, Y., Pak, C.H., Han, Y., Ahlenius, H., Zhang, Z., Chanda, S., Marro, S., Patzke, C., Acuna, C., Covy, J., Xu, W., Yang, N., Danko, T., Chen, L., Wernig, M., Südhof, T.C., 2013. Rapid single-step induction of functional neurons from human pluripotent stem cells. Neuron 78, 785–798.

Zhong, X., Pfeifer, G.P., Xu, X., 2006. Microcephalin encodes a centrosomal protein. Cell Cycle 5, 457–458.

Zhou, S., Szczesna, K., Ochalek, A., Kobolák, J., Varga, E., Nemes, C., Chandrasekaran, A., Rasmussen, M., Cirera, S., Hyttel, P., Dinnyés, A., Freude, K.K., Avci, H.X., 2016. Neurosphere based differentiation of human IPSC improves astrocyte differentiation. Stem Cells Int. 2016, 1–15.

CHAPTER 9: ACKNOWLEDGEMENTS

Finally, it is time for what I think is the most important part of this thesis. The moment of saying thanks to all the people I have met and have been next to me during this long, exciting, frustrating and challenging journey.

First, to Silvia, for being the best supervisor I could have think of. Thanks a lot for your support, motivational words and for always helping me inside and outside the lab. Those Wednesday meetings were always a refreshment and a motivation to continue working and improving.

I would also like to thank the people that have made the bureaucracy slightly easier in Germany. First, to the IMPRS-TP coordinators, Michael and Bettina, thanks a lot for always being there and helping me find the best solutions. Also, thanks to Heike and Nicole for helping in all the issues related to the institute. Thanks also to Antje that made the last steps of the thesis submission much easier.

I would also like to thank all the member of my thesis advisory committee. Thanks a lot for your words of wisdom and suggestions to improve the quality of my projects. I would also like to thank in advance the committee that will evaluate my thesis.

This thesis contains a lot of work and data that would have not been possible without the help and support from many people. So thanks a lot, to all the collaborators. Matthias and Francesco, thanks a lot for establishing the electrophysiology in organoids and for the analysis that has increased the quality of this work. Thanks a lot, to the people in Binder Lab and to Filippo, that have helped me a lot in the transcriptional analysis of the astroglial cells. Thanks a lot, to Svante and Stephan for the beautiful project you started, and I had the chance to continue.

Thanks a lot, to the members of the C-Lab and Binder Lab. Thanks to Timo, Baerbel, Cinzia and Caro for the wonderful technical support and making things easier in the lab. Thanks a lot also to Monika, for always trying to find a solution to the general problems in the department. Rossella, thanks a lot for always making our experiments together fun and interesting. Thanks for teaching me so much and helping me in the establishment of so many protocols. I really have learnt a lot from you! Thanks also to Francesco and Fabrizia for the wonderful discussion, laughs, and great moments inside and outside the lab. Francesco, special thanks go to you for your enthusiasm in the Ephys work of this thesis. Andrea, even if you were the last one joining the lab it has been great sharing some time with you. Thanks a lot for correcting the English of this thesis.

My Greek girls, Christina and Anthi, thank you for absolutely everything, for your help, support, for listening, for the dinners together. Thanks a lot for this beautiful friendship we have built over these years!

I would also like to thank the members of the science communication group for your enthusiasm and your will to bring sciences and more concretely mental health issues to a young audience.

Thanks Isabel and Christine, for all our beautiful moments in the mountains, girls I will always remember our hikes in the wonderful Bavarian and Austrian Alps. Isabel thanks a lot for always being there even if now hundreds of kilometres separate us, and of course thanks a lot for checking the thesis.

Thanks also to the master students I had the chance to supervise, Alex and Melina. Specially thanks to Melina, for your motivation, your will to improve and the dedication you showed in the 6 months you were in Munich, even if we were in the middle of a pandemic, you worked so hard. Chapter 3 would have not existed if it wasn't for you. Thanks a lot!

Sylvain, thanks for being my buddy, thanks a lot for listening whenever I needed it, thanks a lot for the hikes, our wild camping adventures, our trips together with Fabrizia. You were my first friend here in Munich. I am so happy to still have you by my side.

I would also like to thank some of the people I have met during these four years: Christoph, Jens, Mirzet, Dimitris, Tania, Ezgi, Lucia, Laura, Miriam, Anna, Marta… thanks a lot for everything.

Now let's go to the Spanish speaking audience…

Alazne, Maialen, muchísimas gracias por todo chicas, por ser testigos de nuestra boda, por estar cuando lo necesitábamos, por las comidas, los paseos y los planes.

Juan, gracias por haber venido a Múnich a hacer tu estancia y haber elegido nuestro lab. Gracias porque te he conocido, porque personas como tu hay pocas. Gracias por tu bondad y buen rollo. Esos cuatro meses han sido sin duda de los más bonitos que he vivido en el lab.

Y ahora los de siempre, los que están al pie del cañón, los que nunca defraudan y a pesar de los kilómetros te tienen siempre en mente.

Gracias a mi familia, por el apoyo incondicional, por estar siempre ahí, por tener siempre las palabras adecuadas y los consejos necesario para calmar esta ansiosa cabeza.

Gracias a mi familia gallega, por acogerme como a una más, por cuidarme y protegerme. Gracias por estar siempre pendientes.

Gracias a mis padres, por el amor infinito que me mostráis, por no dudar en darme todo lo que necesitaba y educarme de la mejor manera posible. Gracias por tener siempre las palabras adecuadas para calmar mi alma. Gracias por aguantarme en mis peores momentos, por levantarme cuando lo necesitaba, por ser mi apoyo y compartir mis alegrías como si fuesen vuestras, porque esto no habría sido posible sin vosotros. Gracias por ser un ejemplo para seguir, por enseñarme a relativizar y enseñarme como es compartir la vida con la persona que tú has decidido. Gracias por todas las oportunidades que me habéis dado. Gracias por ser los mejores padres del mundo.

También gracias a los amigos de siempre que siguen, y a los que llegaron para quedarse, con los que he crecido y aprendido, María, Iñigo, Alex, Laura. Gracias por abrazarme cada vez que vuelvo como si no hubiese pasado el tiempo, gracias por seguir compartiendo la vida conmigo, por hacerme feliz cada vez que os veo, por estar siempre a pesar de la distancia.

Por supuesto, gracias a la cuadrilla, al mejor grupo de amigas que una pueda tener, gracias por estos maravillosos años juntas, por querer venir a Múnich en mitad de una pandemia para darme una sorpresa. Es un orgullo teneros, ver como avanzáis en la vida y encontráis vuestro camino, pero sobre todo es un orgullo acompañaros en ello. Gracias por seguir unidas, por acogerme siempre, por compartir los momentos que importan de verdad. Por nunca defraudar, por siempre tener una palabra de consuelo. Gracias por seguir en mi vida. Orain dela urte asko esan genuen bezala, ez da betidanik, baina betirako.

Por último, Cora, mi compañera de viaje, mi compañera de vida, la mujer más maravillosa que podría haber encontrado, mi mujer. Gracias por aguantarme en mis peores momentos, pero sobre todo gracias porque los mejores son siempre a tu lado. Gracias por ser mi bastón, mi guía y mi timón. Gracias por hacerme mejor persona, por querer compartir tus inquietudes y planes de vida conmigo. Gracias por ser un ejemplo de superación, por haber venido hasta Alemania solo para estar conmigo con todo lo que ello ha implicado. Gracias porque los cambios a tu lado no son tan complicados, gracias por alegrarme los días. Gracias por tu sonrisa y ese brillo en los ojos. Gracias por estar, pero sobre todo gracias por ser. Te amo.

10. APPENDIX

10.1 LIST OF FIGURES

10.2 LIST OF TABLES

10.3 LIST OF ABBREVIATIONS

Abbreviation	Meaning
2D	2 dimensions
3D	3 dimensions
aIP	apical intermediate progenitor
AJ	apical junction
aRG	apical radial glia cells
BFPP	frontoparietal polymicrogyria
bIP	basal intermediate progenitor
BLBP	brain-lipid binding protein
BP	basal progenitor
BrDU	5-bromo-2'-deoxyuridine
bRGs	basal radial glia cell
BSA	bovine serum albumin
CGE	caudal ganglionic eminence
cKI	conditional knockin
cKO	conditional knockout
CPL	cortical plate-like area
D	asparagine
D777N	asparagine to aspartic acid change
DAPI	4,6-diamidino-2 phenylindole
DCX	doublecortin
DMEG	dysplastic megalencephaly
DMSO	dimethyl sulfoxide
DPBS	Dulbecco’s phosphate-buffered saline
dpe	day post electroporation
ds	dachous
DTT	dithiothreitol
EB	embryoid body
ECM	extracellular matrix
EDNRB	endothelin receptor B
EX	embryonic day X
FACS	fluorescence-activated cells sorting
F-ACTIN	fraction of actin contained in fibres
FBS	foetal bovine serum
FCD	focal cortical dysplasia
FDR	False discovery rate
ft	fat
GE	ganglionic eminence
GFAP	glia fibrillary acidic protein
GLAST	astrocyte-specific glutamate transporter
GPCR	G-protein coupled receptor
GPR56	G-protein coupled receptor 56
GWX	gestational week X

GZL	germinal zone-like area
Gγ5/GNG5	G protein subunit gamma 5
HCl	hydrochloric acid
hESC	human stem cell
IC	isotype control
INM	interkinetic nuclear migration
iPSC	induced pluripotent stem cell
iSVZ	inner subventricular zone
IUE	in utero electroporation
IZ	intermediate zone
KCl	potassium chloride
KD	knockdown
KO	knockout
LGE	lateral ganglionic eminence
MAP	microtubule-associated protein
MCD	malformations of cortical development
MCPH	primary recessive microcephaly
MDS	Miller Dieker syndrome
MEA	multi-electrode array
MEG	megalencephaly
MGE	medial ganglionic eminence
min	minutes
ml	millilitre
MPI	max planck institute
ms	milliseconds
MYA	million years ago
MZ	marginal zone
N	aspartic acid
N777D	aspartic acid to asparagine change
NaCl	sodium chloride
NEC	neuroepithelial cell
NGN2	neurogenin-2
NGS	normal goat serum
NMD	neuronal migration disorder
NPC	neural precursor cell
NSC	neural stem cell
ORF	open reading frame
oSVZ	outer subventricular zone
OX	overexpression
PBMC	peripheral blood mononuclear cell
PBS	phosphate-buffered saline
PFA	paraformaldehyde
PH	periventricular heterotopia
PH3	phophohistone H3
PMG	polymicrogyria

pVIMENTIN	phopho vimentin
PVNH	periventricular nodular heterotopia
RELN	reelin
RT	room temperature
RT-PCR	real-time PCR
S100β	Ca2+ binding protein
SAP	subapical progenitor
SBH	subcortical band heterotopia
scRNA-seq	single-cell RNA sequencing
SP	subplate
SPC	short precursor cell
SVZ	subventricular zone
TTX	tetrodotoxin
VL	ventricle-like cavities
VMS	Van Maldergem syndrome
VZ	ventricular zone

10.5 LIST OF PUBLICATIONS

1) GNG5 controls the number of apical and basal progenitors and alters neuronal migration during cortical development.
Ane Cristina Ayo-Martin, Christina Kyrousi, Rossella Di Giaimo, Silvia Cappello.
Frontiers in Molecular Bioscience. 2020.

2) Endocannabinoid signalling in stem cells and cerebral organoids drives differentiation to deep layer projection neurons via CB1 receptors.
Juan Paraiso-Luna, Jose Aguareles, Ricardo Martin, **Ane Cristina Ayo-Martin**, Daniel Garcia-Rincon, Samuel Simon-Sanchez, Adan De Salas-Quiroga, Javier Diaz-Alonso, Elena Garcia-Taboada, Isabel Liste, Jose Sanchez-Prieto, Silvia Cappello, Manuel Guzman, And Ismael Galve-Roperh.
Development. 2020. *Accepted for publication.*

3) Cystatin B is essential for proliferation and interneuron migration in individuals with EPM 1 epilepsy.
Francesco Di Matteo, Fabrizia Pipicelli, Christina Kyrousi, Isabella Tovecci, Eduardo Penna, Marianna Crispino, Angela Chambery, Rosita Russo, **Ane Cristina Ayo-Martin**, Martina Giordano, Anke Hoffmann, Emilio Ciusani, Laura Canafoglia, Magdalena Götz, Rossella Di Giaimo and Silvia Cappello.
EMBO Molecular Medicine. 2020.

4) Altered neuronal migratory trajectories in human cerebral organoids derived from individuals with neuronal heterotopia.
Johannes Klaus, Sabina Kanton, Christina Kyrousi, **Ane Cristina Ayo-Martin**, Rossella Di Giaimo, Stephan Riesenberg , Adam C O'Neill, J Gray Camp, Chiara Tocco, Malgorzata Sante, Ejona Rusha, Micha Drukker, Mariana Schroeder, Magdalena Götz, Stephen P Robertson, Barbara Treutlein and Silvia Cappello.
Nature Medicine. 2019.

5) Hepatitis E virus infects neurons and brains.
Xinying Zhou, Fen Huang, Lei Xu, Zhanmin Lin, Femke M S de Vrij, **Ane Cristina Ayo-Martin**, Mark van der Kroeg, Manzhi Zhao, Yuebang Yin, Wenshi Wang, Wanlu Cao, Yijin Wang, Steven A Kushner, Jean Marie Peron, Laurent Alric, Robert A de Man, Bart C Jacobs, Jeroen J van Eijk, Eleonora M A Aronica, Dave Sprengers, Herold J Metselaar, Chris I de Zeeuw , Harry R Dalton, Nassim Kamar, Maikel P Peppelenbosch and Qiuwei Pan.
Journal of Infectious diseases. 2017.

LMU LUDWIG-MAXIMILIANS-UNIVERSITÄT MÜNCHEN

Dean's Office
Medical Faculty

MMRS MUNICH MEDICAL RESEARCH SCHOOL

Affidavit

Ayo Martín, Ane Cristina

Surname, first name

Kraepelinstraße 2-10

Street

80804, Munich

Zip code, town

Germany

Country

I hereby declare, that the submitted thesis entitled

Unravelling the role of altered genes in human Periventricular Heterotopia

is my own work. I have only used the sources indicated and have not made unauthorised use of services of a third party. Where the work of others has been quoted or reproduced, the source is always given.

I further declare that the submitted thesis or parts thereof have not been presented as part of an examination degree to any other university.

Vigo, 22th of April 2021

Place, date

Ane Cristina Ayo Martín

Signature doctoral candidate

LMU LUDWIG-MAXIMILIANS-UNIVERSITÄT MÜNCHEN

Dean's Office
Medical Faculty

MMRS MUNICH MEDICAL RESEARCH SCHOOL

Confirmation of congruency between printed and electronic version of the doctoral thesis

Ayo Martín, Ane Cristina

Surname, first name

Kraepelinstraße 2-10

Street

80804, Munich

Zip code, town

Germany

Country

I hereby declare that the electronic version of the submitted thesis, entitled

Unravelling the role of altered genes in human Periventricular Heterotopia

is congruent with the printed version both in content and format.

Vigo, 22th of April 2021

Place, date

Ane Cristina Ayo Martín

Signature doctoral candidate